Advances in Astronomy

Gamma-Ray Burst in Swift and Fermi Era

Guest Editor: WeiKang Zheng, Xuefeng Wu, Takanori Sakamoto, Yuji Urata, and Shashi B. Pandey

Gamma-Ray Burst in Swift and Fermi Era

Advances in Astronomy

Gamma-Ray Burst in Swift and Fermi Era

Guest Editors: WeiKang Zheng, Xuefeng Wu,
Takanori Sakamoto, Yuji Urata, and Shashi B. Pandey

Editorial Board

Contents

Hindawi Publishing Corporation
Advances in Astronomy
Volume 2015, Article ID 543624, 1 page
http://dx.doi.org/10.1155/2015/543624

Editorial
Gamma-Ray Burst in Swift and Fermi Era

WeiKang Zheng,[1] Xuefeng Wu,[2] Takanori Sakamoto,[3] Yuji Urata,[4,5] and Shashi B. Pandey[6]

[1]*Department of Astronomy, University of California, Berkeley, CA 94720-3411, USA*
[2]*Purple Mountain Observatory, Chinese Academy of Sciences, Nanjing 210008, China*
[3]*Department of Physics and Mathematics, Aoyama Gakuin University, Sagamihara, Kanagawa 252-5258, Japan*
[4]*Institute of Astronomy, National Central University, Chung-Li 32054, Taiwan*
[5]*Academia Sinica Institute of Astronomy and Astrophysics, Taipei 106, Taiwan*
[6]*Aryabhatta Research Institute of Observational Sciences, Manora Peak, Nainital 263129, India*

Correspondence should be addressed to WeiKang Zheng; zwk@astro.berkeley.edu

Received 5 May 2015; Accepted 5 May 2015

Gamma-ray bursts (GRBs) are short-lived and intense flashes of gamma-rays from space associated with the death/explosion of massive stars and/or compact binaries. Since the discovery of GRBs in 1967 by the Vela satellite, the mystery of their origin has attracted many space missions including *Compton*, *BeppoSAX*, *HETE-2*, *INTEGRAL*, *Swift*, and *Fermi*, resulting in many significant breakthroughs. With the *Swift* mission launched in 2004, followed by *Fermi* in 2008, the study of GRBs is now in a productive and unique period while both of these space satellites are operational. Our understanding of GRB physics has undeniably been revolutionized in the past decade, though it is still far from complete. In this special issue, we have collected reviews and research papers that are closely related to the two missions for studies of GRBs and their afterglows.

To begin with, the review article by A. Pe'er focuses on GRB prompt emission in the high-energy gamma-ray band, and another review article by H. Gao and P. Mészáros summarizes the early-time reverse-shock emission. Both reviews show new observations from *Swift* and *Fermi* in the past few years, and they also present theoretical progress. Two other review articles discuss GRBs beyond the gamma-ray band. The one by Y. Urata et al. summarizes GRB follow-up observations in the submillimeter band and shows the expected outcomes from a new planned Greenland Telescope that operates at submillimeter wavelengths. The other, by K. Asano and K. Murase, reviews theoretical models for non-electromagnetic emission from GRBs, mainly neutrinos and cosmic rays.

A set of three research articles in this special issue focus on specific topics of GRBs. One by Y. Kawakubo et al. studies the spectral lags and their implications from a sample of 40 *Swift* GRBs, while that of S. Dado and A. Dar discusses GRB 130603B and some possible theoretical models. The research article by J.-J. Wei et al. utilizes GRBs and Type Ia supernovae to constrain the Cardassian expansion model and dark energy.

Overall, this volume covers various topics about GRBs, summarizes previous results, presents progress during the *Swift* and *Fermi* mission periods, and describes fresh challenges from the new observations. We hope that GRB researchers find this work useful for their studies and that it helps lead to new results and progress toward solving the mysteries of GRBs.

Acknowledgments

We sincerely thank the authors and referees for all of their efforts as well as the Editorial Board members for publishing this special issue.

WeiKang Zheng
Xuefeng Wu
Takanori Sakamoto
Yuji Urata
Shashi B. Pandey

Hindawi Publishing Corporation
Advances in Astronomy
Volume 2015, Article ID 576093, 12 pages
http://dx.doi.org/10.1155/2015/576093

Research Article

Utilizing the Updated Gamma-Ray Bursts and Type Ia Supernovae to Constrain the Cardassian Expansion Model and Dark Energy

Jun-Jie Wei,[1,2] Qing-Bo Ma,[1,2] and Xue-Feng Wu[1,3,4]

[1] *Purple Mountain Observatory, Chinese Academy of Sciences, Nanjing 210008, China*
[2] *University of Chinese Academy of Sciences, Beijing 100049, China*
[3] *Chinese Center for Antarctic Astronomy, Nanjing 210008, China*
[4] *Joint Center for Particle, Nuclear Physics and Cosmology, Nanjing University-Purple Mountain Observatory, Nanjing 210008, China*

Correspondence should be addressed to Xue-Feng Wu; xfwu@pmo.ac.cn

Received 1 December 2014; Accepted 2 April 2015

Academic Editor: Gary Wegner

We update gamma-ray burst (GRB) luminosity relations among certain spectral and light-curve features with 139 GRBs. The distance modulus of 82 GRBs at $z > 1.4$ can be calibrated with the sample at $z \leq 1.4$ by using the cubic spline interpolation method from the Union2.1 Type Ia supernovae (SNe Ia) set. We investigate the joint constraints on the Cardassian expansion model and dark energy with 580 Union2.1 SNe Ia sample ($z < 1.4$) and 82 calibrated GRBs' data ($1.4 < z \leq 8.2$). In ΛCDM, we find that adding 82 high-z GRBs to 580 SNe Ia significantly improves the constraint on $\Omega_m - \Omega_\Lambda$ plane. In the Cardassian expansion model, the best fit is $\Omega_m = 0.24^{+0.15}_{-0.15}$ and $n = 0.16^{+0.30}_{-0.52}$ (1σ), which is consistent with the ΛCDM cosmology ($n = 0$) in the 1σ confidence region. We also discuss two dark energy models in which the equation of state $w(z)$ is parameterized as $w(z) = w_0$ and $w(z) = w_0 + w_1 z/(1+z)$, respectively. Based on our analysis, we see that our universe at higher redshift up to $z = 8.2$ is consistent with the concordance model within 1σ confidence level.

1. Introduction

In recent years, the combined observations of nearby and distant Type Ia supernovae (SNe Ia) have provided strong evidence for the current accelerated expansion of the universe [1–3]. The cause of the acceleration remains unknown. Many authors suggest that the composition of the universe may consist of an extra component called dark energy, which may explain the acceleration of the universe at the current epoch. For example, the dark energy model with a constant equation of state $P/\rho \equiv w = -1$ is one of the several possible explanations for the acceleration, while other models suggest that dark energy changes with time, and there are many ways to characterize the time variation of dark energy. Here, we adopt a simple model in which the dark energy equation of state can be parameterized by $P/\rho \equiv w(z) = w_0 + w_1 z/(1+z) = w_0 + w_1(1-a)$ [4, 5], where w_0 is constant, w_1 represents the time dependence of dark energy, and $a = 1/(1+z)$ is the scale factor. In addition, models where general relativity is modified can also drive universe acceleration, such as the Cardassian expansion model which is a possible alternative for explaining the acceleration of the universe that invokes no vacuum energy [6].

SNe Ia have been considered a perfect standard candle to measure the geometry and dynamics of the universe. Unfortunately, the farthest SNe Ia detected so far is only at $z = 1.914$ [7]. It is difficult to observe SNe at $z > 2$, even with excellent space-based platforms such as SNAP [8]. And this is quite limiting because much of the most interesting evolution of the universe occurred well before this epoch. Gamma-ray bursts (GRBs) are the most luminous transient events at cosmological distances. Owing to their high luminosities, GRBs can be detected out to very high redshifts [9]. In fact, the farthest burst detected so far is GRB 090423, which is at $z = 8.2$ [10]

(a photometric redshift of 9.4 for GRB 090429B was reported by [11]). Moreover, in contrast to SNe Ia, gamma-ray photons from GRBs are almost immune to dust extinction, so the observed gamma-ray flux is a direct measurement of the prompt emission energy. Hence, GRBs are potentially more promising standard candles than SNe Ia at higher redshifts. The possible use of GRBs as cosmological probes started to become reality after some empirical luminosity relations were discovered. These GRB luminosity relations have been proposed as distance indicators, such as the correlations $\tau_{\rm lag} - L$ [12], $V - L$ [13], $E_p - E_{\rm iso}$ [14], $E_p - L$ [15, 16], $E_p - E_\gamma$ [17], and $\tau_{\rm RT} - L$ [18]. Here the time lag ($\tau_{\rm lag}$) is the time shift between the hard and soft light curves; the luminosity (L) is the isotropic peak luminosity of a GRB; the variability (V) of a burst denotes whether its light curve is spiky or smooth, and V can be obtained by calculating the normalized variance of an observed light curve around a smoothed version of that light curve [13]; (E_p) is the burst frame peak energy in the GRB spectrum; ($E_{\rm iso}$) is the isotropic equivalent gamma-ray energy; (E_γ) is the collimation-corrected gamma-ray energy; and the minimum rise time ($\tau_{\rm RT}$) in the gamma-ray light curve is the shortest time over which the light curve rises by half of the peak flux of the pulse. However, [19] found that the updated $V - L$ correlation was quite scattered. Its intrinsic scatter has been larger than the one that could be expected of a linear relation.

Generally speaking, with these luminosity indicators, one can make use of them as standard candles for cosmological research. For example, [20] constructed the first GRB Hubble diagram based on nine GRBs using two GRB luminosity indicators. With the $E_p - E_\gamma$ relation, [21] placed tight constraints on cosmological parameters and dark energy. Reference [22] used a model-independent multivariable GRB luminosity indicator to constrain cosmological parameters and the transition redshift. Reference [18] made use of five luminosity indicators calibrated with 69 events by assuming two adopted cosmological models to construct the GRB Hubble diagram. Reference [23] suggested that the time variation of the dark energy is small or zero up to $z \sim 6$ using the $E_p - L$ relation. Reference [24] extended the Hubble diagram up to $z = 5.6$ using 63 gamma-ray bursts (GRBs) via $E_p - L$ relation and found that these GRB data were consistent with the concordance model within 2σ level. In a word, a lot of other works in this so-called GRB cosmology field have been published (please see [19, 25] for reviews). However, there is a so-called circularity problem in the calibration of these luminosity relations. Because of the current poor information on low-z GRBs, these luminosity relations necessarily depend on the assumed cosmology. Some authors attempted to circumvent the circularity problem by using a less model-dependent approach, such as the scatter method [26, 27], the luminosity distance method [28], the Bayesian method [29, 30], and the method by fitting relation parameters of GRBs and cosmological parameters simultaneously [31, 32]. However, these statistical approaches still can not avoid the circularity problem completely, because a particular cosmology model is required in doing the joint fitting. This means that the parameters of the calibrated relations are still coupled to the cosmological parameters derived from a given cosmological model.

To solve the circularity problem completely, one should calibrate the GRB relations in a cosmology-independent way. Recently, a new method to calibrate GRBs in a cosmological model-independent way has been presented [33–35]. This method is very similar to the calibration for SNe Ia by measuring Cepheid variables in the same galaxy, and it is free from the circularity problem. Cepheid variables have been regarded as the first-order standard candles for calibrating SNe Ia which are the secondary standard candles. Similarly, if we regard SNe Ia as the first-order standard candles, we can also calibrate GRBs relations with a large number of SNe Ia since objects at the same redshift should have the same luminosity distance in any cosmology. This method is one of the interpolation procedures which obtain the distance moduli of GRBs in the redshift range of SNe Ia by interpolating from SNe Ia data in the Hubble diagram. Then, if we assume that the GRB luminosity relations do not evolve with redshift, we can extend the calibrated luminosity relations to high-z and derive the distance moduli of high-z GRBs. From these obtained distance moduli, we can constrain the cosmological parameters.

In this paper, we will try to determine the cosmological parameters and dark energy using both the updated 139 GRBs and 580 SNe Ia. In Section 2, we will describe the data we will use and our method of calibration. To avoid any assumption on cosmological models, we will use the distance moduli of 580 SNe Ia from the Union2.1 sample to calibrate five GRB luminosity relations in the redshift range of SNe Ia sample ($z < 1.4$). Then, the distance moduli of 82 high-z GRBs ($z > 1.4$) can be obtained from the five calibrated GRB luminosity relations. The joint constraints on the Cardassian expansion model and dark energy with 580 SNe and 82 calibrated GRBs' data whose $z > 1.4$ will be presented in Section 3. Finally, we will summarize our findings and present a brief discussion.

2. Calibrating the Updated Luminosity Relations of GRBs

2.1. Observational Data and Methodology. As mentioned above, we calibrate the updated luminosity relations of GRBs using low-z events whose distance moduli can be obtained by those of Type Ia supernovae. Actually, we use the cosmology-independent calibration method developed by [33–35]. This method is one of the interpolation procedures which use the abundant SNe Ia sample to interpolate the distance moduli of GRBs in the redshift range of SNe Ia sample ($z < 1.4$). More recently, the Supernova Cosmology Project collaboration released their latest SNe Ia dataset known as the Union2.1 sample, which contains 580 SNe detections [36]. Obviously, there are rich SNe Ia data points, and we can make a better interpolation by using this dataset.

Our updated GRB sample includes 139 GRBs with redshift measurements; there are 57 GRBs at $z < 1.4$ and 82 GRBs at $z > 1.4$. This sample is shown in Table 1, which includes the following information for each GRB: (1) its name; (2) the redshift; (3) the bolometric peak flux $P_{\rm bolo}$; (4) the bolometric fluence $S_{\rm bolo}$; (5) the beaming factor $f_{\rm beam}$; (6) the time lag $\tau_{\rm lag}$; (7) the spectral peak energy E_p; and (8) the minimum rise time $\tau_{\rm RT}$. All of these data were obtained from previously

Table 1: Luminosities and luminosity indicators.

GRB	z	$P_{\rm bolo}$ (erg cm^{-2} s^{-1})	$S_{\rm bolo}$ (erg cm^{-2})	$f_{\rm beam}$	$\tau_{\rm lag}$ (s)	E_p (keV)	$\tau_{\rm RT}$ (s)
970228	0.70	$7.30E-06 \pm 4.30E-07$	⋯	⋯	⋯	$115\pm^{38}_{38}$	0.26 ± 0.04
970508	0.84	$3.30E-06 \pm 3.30E-07$	$8.09E-06 \pm 8.10E-07$	0.0795 ± 0.0204	0.50 ± 0.30	$389\pm^{40}_{40}$	0.71 ± 0.06
970828	0.96	$1.00E-05 \pm 1.10E-06$	$1.23E-04 \pm 1.20E-05$	0.0053 ± 0.0014	⋯	$298\pm^{30}_{30}$	0.26 ± 0.07
971214	3.42	$7.50E-07 \pm 2.40E-08$	⋯	⋯	0.03 ± 0.03	$190\pm^{20}_{20}$	0.05 ± 0.02
980613	1.10	$3.00E-07 \pm 8.30E-08$	⋯	⋯	⋯	$92\pm^{42}_{42}$	⋯
980703	0.97	$1.20E-06 \pm 3.60E-08$	$2.83E-05 \pm 2.90E-06$	0.0184 ± 0.0027	0.40 ± 0.10	$254\pm^{25}_{25}$	3.60 ± 0.50
990123	1.61	$1.30E-05 \pm 5.00E-07$	$3.11E-04 \pm 3.10E-05$	0.0024 ± 0.0007	0.16 ± 0.03	$604\pm^{60}_{60}$	⋯
990506	1.31	$1.10E-05 \pm 1.50E-07$	⋯	⋯	0.04 ± 0.02	$283\pm^{30}_{30}$	0.17 ± 0.03
990510	1.62	$3.30E-06 \pm 1.20E-07$	$2.85E-05 \pm 2.90E-06$	0.0021 ± 0.0003	0.03 ± 0.01	$126\pm^{10}_{10}$	0.14 ± 0.02
990705	0.84	$6.60E-06 \pm 2.60E-07$	$1.34E-04 \pm 1.50E-05$	0.0035 ± 0.0010	⋯	$189\pm^{15}_{15}$	0.05 ± 0.02
990712	0.43	$3.50E-06 \pm 2.90E-07$	$1.19E-05 \pm 6.20E-07$	0.0136 ± 0.0034	⋯	$65\pm^{10}_{10}$	⋯
991208	0.71	$2.10E-05 \pm 2.10E-06$	⋯	⋯	⋯	$190\pm^{20}_{20}$	0.32 ± 0.04
991216	1.02	$4.10E-05 \pm 3.80E-07$	$2.48E-04 \pm 2.50E-05$	0.0030 ± 0.0009	0.03 ± 0.01	$318\pm^{30}_{30}$	0.08 ± 0.02
000131	4.50	$7.30E-07 \pm 8.30E-08$	⋯	⋯	⋯	$163\pm^{13}_{13}$	0.12 ± 0.06
000210	0.85	$2.00E-05 \pm 2.10E-06$	⋯	⋯	⋯	$408\pm^{14}_{14}$	0.38 ± 0.06
000911	1.06	$1.90E-05 \pm 1.90E-06$	⋯	⋯	⋯	$986\pm^{100}_{100}$	0.05 ± 0.02
000926	2.07	$2.90E-06 \pm 2.90E-07$	⋯	⋯	⋯	$100\pm^{7}_{7}$	0.05 ± 0.03
010222	1.48	$2.30E-05 \pm 7.20E-07$	$2.45E-04 \pm 9.10E-06$	0.0014 ± 0.0001	⋯	$309\pm^{12}_{12}$	0.12 ± 0.03
010921	0.45	$1.80E-06 \pm 1.60E-07$	⋯	⋯	0.90 ± 0.30	$89\pm^{13.8}_{21.8}$	3.90 ± 0.50
011211	2.14	$9.20E-08 \pm 9.30E-09$	$9.20E-06 \pm 9.50E-07$	0.0044 ± 0.0011	⋯	$59\pm^{8}_{8}$	⋯
020124	3.20	$6.10E-07 \pm 1.00E-07$	$1.14E-05 \pm 1.10E-06$	0.0039 ± 0.0010	0.08 ± 0.05	$87\pm^{12}_{18}$	0.25 ± 0.05
020405	0.70	$7.40E-06 \pm 3.10E-07$	$1.10E-04 \pm 2.10E-06$	0.0060 ± 0.0020	⋯	$364\pm^{90}_{90}$	0.45 ± 0.08
020813	1.25	$3.80E-06 \pm 2.60E-07$	$1.59E-04 \pm 2.90E-06$	0.0012 ± 0.0003	0.16 ± 0.04	$142\pm^{13}_{14}$	0.82 ± 0.10
020903	0.25	$3.40E-08 \pm 8.80E-09$	⋯	⋯	⋯	$2.6\pm^{0.8}_{1.4}$	⋯
021004	2.32	$2.30E-07 \pm 5.50E-08$	$3.61E-06 \pm 8.60E-07$	0.0109 ± 0.0027	0.60 ± 0.40	$80\pm^{22}_{53}$	0.35 ± 0.15
021211	1.01	$2.30E-06 \pm 1.70E-07$	⋯	⋯	0.32 ± 0.04	$46\pm^{6}_{8}$	0.33 ± 0.05
030115	2.50	$3.20E-07 \pm 5.10E-08$	⋯	⋯	0.40 ± 0.20	$83\pm^{22}_{53}$	1.47 ± 0.50
030226	1.98	$2.60E-07 \pm 4.70E-08$	$8.33E-06 \pm 9.80E-07$	0.0034 ± 0.0008	0.30 ± 0.30	$97\pm^{17}_{27}$	0.70 ± 0.20
030323	3.37	$1.20E-07 \pm 6.00E-08$	⋯	⋯	⋯	$44\pm^{26}_{90}$	1.00 ± 0.50
030328	1.52	$1.60E-06 \pm 1.10E-07$	$6.14E-05 \pm 2.40E-06$	0.0020 ± 0.0005	0.20 ± 0.20	$126\pm^{14}_{14}$	⋯
030329	0.17	$2.00E-05 \pm 1.00E-06$	$2.31E-04 \pm 2.00E-06$	0.0049 ± 0.0009	0.14 ± 0.04	$68\pm^{2.2}_{2.3}$	0.66 ± 0.08
030429	2.66	$2.00E-07 \pm 5.40E-08$	$1.13E-06 \pm 1.90E-07$	0.0060 ± 0.0029	⋯	$35\pm^{8}_{12}$	0.90 ± 0.20
030528	0.78	$1.60E-07 \pm 3.20E-08$	⋯	⋯	12.50 ± 0.50	$32\pm^{5}_{4.7}$	0.77 ± 0.20
040924	0.86	$2.60E-06 \pm 2.80E-07$	⋯	⋯	0.30 ± 0.04	$67\pm^{6}_{6}$	0.17 ± 0.02
041006	0.71	$2.50E-06 \pm 1.40E-07$	$1.75E-05 \pm 1.80E-06$	0.0012 ± 0.0003	⋯	$63\pm^{13}_{13}$	0.65 ± 0.16
050126	1.29	$1.10E-07 \pm 1.30E-08$	⋯	⋯	2.10 ± 0.30	$47\pm^{8}_{23}$	3.90 ± 0.80
050318	1.44	$5.20E-07 \pm 6.30E-08$	$3.46E-06 \pm 3.50E-07$	0.0020 ± 0.0006	⋯	$47\pm^{8}_{15}$	0.38 ± 0.05
050319	3.24	$2.30E-07 \pm 3.60E-08$	⋯	⋯	⋯	⋯	0.19 ± 0.04
050401	2.90	$2.10E-06 \pm 2.20E-07$	⋯	⋯	0.10 ± 0.06	$118\pm^{18}_{18}$	0.03 ± 0.01
050406	2.44	$4.20E-08 \pm 1.10E-08$	⋯	⋯	0.64 ± 0.40	$25\pm^{13}_{35}$	0.50 ± 0.30
050408	1.24	$1.10E-06 \pm 2.10E-07$	⋯	⋯	0.25 ± 0.10	⋯	0.25 ± 0.08
050416	0.65	$5.30E-07 \pm 8.50E-08$	⋯	⋯	⋯	$15\pm^{2.7}_{2.3}$	0.51 ± 0.30
050502	3.79	$4.30E-07 \pm 1.20E-07$	⋯	⋯	0.20 ± 0.20	$93\pm^{35}_{55}$	0.40 ± 0.20
050505	4.27	$3.20E-07 \pm 5.40E-08$	$6.20E-06 \pm 8.50E-07$	0.0014 ± 0.0007	⋯	$70\pm^{24}_{140}$	0.40 ± 0.15
050525	0.61	$5.20E-06 \pm 7.20E-08$	$2.59E-05 \pm 1.30E-06$	0.0025 ± 0.0010	0.11 ± 0.02	$81\pm^{1.4}_{1.4}$	0.32 ± 0.03
050603	2.82	$9.70E-06 \pm 6.00E-07$	⋯	⋯	0.03 ± 0.03	$344\pm^{52}_{52}$	0.17 ± 0.02
050802	1.71	$5.00E-07 \pm 7.30E-08$	⋯	⋯	⋯	⋯	0.80 ± 0.20
050820	2.61	$3.30E-07 \pm 5.20E-08$	⋯	⋯	0.70 ± 0.30	$246\pm^{40}_{76}$	2.00 ± 0.50
050824	0.83	$9.30E-08 \pm 3.80E-08$	⋯	⋯	⋯	⋯	11.00 ± 2.00
050904	6.29	$2.50E-07 \pm 3.50E-08$	$2.00E-05 \pm 2.00E-06$	0.0097 ± 0.0024	⋯	$436\pm^{90}_{200}$	0.60 ± 0.20

Table 1: Continued.

GRB	z	$P_{\rm bolo}$ (erg cm^{-2} s^{-1})	$S_{\rm bolo}$ (erg cm^{-2})	$f_{\rm beam}$	$\tau_{\rm lag}$ (s)	E_p (keV)	$\tau_{\rm RT}$ (s)
050908	3.35	$9.80E-08 \pm 1.50E-08$	⋯	⋯	⋯	41^{+5}_{-9}	1.50 ± 0.30
050922	2.20	$2.00E-06 \pm 7.30E-08$	⋯	⋯	0.06 ± 0.02	198^{+22}_{-38}	0.13 ± 0.02
051022	0.80	$1.10E-05 \pm 8.70E-07$	$3.40E-04 \pm 1.20E-05$	0.0029 ± 0.0001	⋯	510^{+20}_{-22}	0.19 ± 0.04
051109	2.35	$7.80E-07 \pm 9.70E-08$	⋯	⋯	⋯	161^{+35}_{-130}	1.30 ± 0.40
051111	1.55	$3.90E-07 \pm 5.80E-08$	⋯	⋯	1.02 ± 0.10	⋯	3.20 ± 1.00
060108	2.03	$1.10E-07 \pm 1.10E-07$	⋯	⋯	⋯	65^{+10}_{-600}	0.40 ± 0.20
060115	3.53	$1.30E-07 \pm 1.60E-08$	⋯	⋯	⋯	62^{+6}_{-19}	0.40 ± 0.20
060116	6.60	$2.00E-07 \pm 1.10E-07$	⋯	⋯	⋯	139^{+36}_{-400}	1.30 ± 0.50
060124	2.30	$1.10E-06 \pm 1.20E-07$	$3.37E-05 \pm 3.40E-06$	0.0021 ± 0.0002	0.08 ± 0.04	237^{+51}_{-76}	0.30 ± 0.10
060206	4.05	$4.40E-07 \pm 1.90E-08$	⋯	⋯	0.10 ± 0.10	75^{+12}_{-12}	1.25 ± 0.25
060210	3.91	$5.50E-07 \pm 2.20E-08$	$1.94E-05 \pm 1.20E-06$	0.0005 ± 0.0001	0.13 ± 0.08	149^{+35}_{-400}	0.50 ± 0.20
060223	4.41	$2.10E-07 \pm 3.70E-08$	⋯	⋯	0.38 ± 0.10	71^{+10}_{-100}	0.50 ± 0.10
060418	1.49	$1.50E-06 \pm 5.90E-08$	⋯	⋯	0.26 ± 0.06	230^{+20}_{-20}	0.32 ± 0.08
060502	1.51	$3.70E-07 \pm 1.60E-07$	⋯	⋯	3.50 ± 0.50	156^{+33}_{-400}	3.10 ± 0.30
060510	4.90	$1.00E-07 \pm 1.70E-08$	⋯	⋯	⋯	95^{+30}_{-60}	⋯
060526	3.21	$2.40E-07 \pm 3.30E-08$	$1.17E-06 \pm 1.70E-07$	0.0034 ± 0.0014	0.13 ± 0.03	25^{+5}_{-5}	0.20 ± 0.05
060604	2.68	$9.00E-08 \pm 1.60E-08$	⋯	⋯	5.00 ± 1.00	40^{+5}_{-5}	0.60 ± 0.20
060605	3.80	$1.20E-07 \pm 5.50E-08$	⋯	⋯	5.00 ± 3.00	169^{+30}_{-200}	2.00 ± 0.50
060607	3.08	$2.70E-07 \pm 8.10E-08$	⋯	⋯	2.00 ± 0.50	120^{+17}_{-190}	2.00 ± 0.20
060707	3.43	$1.53E-07 \pm 2.12E-08$	$3.41E-06 \pm 1.96E-07$	⋯	⋯	63^{+6}_{-13}	⋯
060714	2.71	$2.30E-07 \pm 1.42E-08$	$6.88E-06 \pm 2.47E-07$	⋯	⋯	103^{+16}_{-21}	⋯
060729	0.54	$1.93E-07 \pm 1.30E-08$	$6.43E-06 \pm 3.16E-07$	⋯	⋯	61^{+9}_{-9}	⋯
060814	0.84	$1.83E-06 \pm 4.44E-08$	$4.94E-05 \pm 4.91E-07$	⋯	0.29 ± 0.03	257^{+35}_{-74}	1.65 ± 0.24
060904B	0.70	$4.37E-07 \pm 2.28E-08$	$4.05E-06 \pm 2.17E-07$	⋯	0.36 ± 0.09	80^{+12}_{-770}	1.00 ± 0.16
060908	2.43	$6.69E-07 \pm 3.36E-08$	$7.68E-06 \pm 1.85E-07$	⋯	0.26 ± 0.06	151^{+25}_{-112}	0.52 ± 0.09
060926	3.21	$1.56E-07 \pm 1.22E-08$	$5.47E-07 \pm 3.80E-08$	⋯	1.03 ± 0.11	20^{+11}_{-11}	⋯
060927	5.60	$4.02E-07 \pm 1.54E-08$	$2.37E-06 \pm 8.67E-08$	⋯	0.12 ± 0.04	72^{+7}_{-15}	0.46 ± 0.12
061007	1.26	$7.20E-06 \pm 1.11E-07$	$2.24E-04 \pm 1.72E-06$	⋯	0.11 ± 0.01	399^{+11}_{-12}	0.38 ± 0.02
061110A	0.76	$9.79E-08 \pm 1.35E-08$	$2.71E-06 \pm 1.18E-07$	⋯	⋯	90^{+13}_{-13}	⋯
061110B	3.44	$1.79E-07 \pm 2.66E-08$	$6.12E-06 \pm 3.38E-07$	⋯	0.24 ± 0.36	517^{+53}_{-53}	0.79 ± 0.64
061121	1.31	$8.04E-06 \pm 1.07E-07$	$6.53E-05 \pm 5.76E-07$	⋯	0.03 ± 0.01	606^{+44}_{-55}	0.98 ± 0.19
061222B	3.36	$2.29E-07 \pm 3.15E-08$	$5.01E-06 \pm 2.49E-07$	⋯	⋯	49^{+8}_{-8}	⋯
070110	2.35	$1.12E-07 \pm 1.36E-08$	$4.04E-06 \pm 1.64E-07$	⋯	⋯	110^{+30}_{-30}	⋯
070208	1.17	$1.39E-07 \pm 2.06E-08$	$1.06E-06 \pm 1.46E-07$	⋯	⋯	51^{+10}_{-10}	⋯
070318	0.84	$4.10E-07 \pm 2.12E-08$	$7.34E-06 \pm 2.01E-07$	⋯	⋯	154^{+19}_{-19}	0.72 ± 0.24
070411	2.95	$1.50E-07 \pm 1.31E-08$	$6.29E-06 \pm 2.19E-07$	⋯	⋯	83^{+11}_{-11}	⋯
070506	2.31	$1.67E-07 \pm 1.38E-08$	$5.16E-07 \pm 3.43E-08$	⋯	2.52 ± 0.04	31^{+3}_{-2}	0.12 ± 0.06
070508	0.82	$7.67E-06 \pm 1.18E-07$	$7.26E-05 \pm 6.15E-07$	⋯	0.04 ± 0.01	233^{+7}_{-7}	0.20 ± 0.01
070521	0.55	$2.09E-06 \pm 5.26E-08$	$2.97E-05 \pm 4.00E-07$	⋯	0.04 ± 0.01	222^{+12}_{-16}	0.58 ± 0.06
070529	2.50	$3.32E-07 \pm 5.08E-08$	$7.44E-06 \pm 4.31E-07$	⋯	⋯	180^{+52}_{-52}	⋯
070611	2.04	$1.45E-07 \pm 2.25E-08$	$9.52E-07 \pm 8.44E-08$	⋯	⋯	92^{+30}_{-30}	⋯
070612A	0.62	$2.77E-07 \pm 4.24E-08$	$2.72E-05 \pm 9.37E-07$	⋯	⋯	87^{+17}_{-17}	2.49 ± 1.48
070714B	0.92	$3.24E-06 \pm 1.46E-07$	$8.91E-06 \pm 6.77E-07$	⋯	0.03 ± 0.01	1120^{+230}_{-473}	0.45 ± 0.04
070802	2.45	$6.38E-08 \pm 9.69E-09$	$6.50E-07 \pm 7.05E-08$	⋯	⋯	70^{+25}_{-25}	⋯
070810A	2.17	$2.77E-07 \pm 1.77E-08$	$1.59E-06 \pm 8.43E-08$	⋯	1.09 ± 0.23	44^{+9}_{-9}	0.73 ± 0.22
071003	1.10	$4.71E-06 \pm 1.82E-07$	$6.73E-05 \pm 1.48E-06$	⋯	0.38 ± 0.05	799^{+61}_{-75}	0.88 ± 0.07
071010A	0.98	$1.17E-07 \pm 2.67E-08$	$4.97E-07 \pm 6.05E-08$	⋯	⋯	27^{+10}_{-10}	⋯
071010B	0.95	$9.20E-07 \pm 2.18E-08$	$8.37E-06 \pm 1.16E-07$	⋯	0.84 ± 0.04	52^{+8}_{-6}	1.21 ± 0.03
071031	2.69	$7.08E-08 \pm 8.61E-09$	$2.19E-06 \pm 1.92E-07$	⋯	⋯	24^{+7}_{-7}	⋯

Table 1: Continued.

GRB	z	$P_{\rm bolo}$ (erg cm^{-2} s^{-1})	$S_{\rm bolo}$ (erg cm^{-2})	$f_{\rm beam}$	$\tau_{\rm lag}$ (s)	E_p (keV)	$\tau_{\rm RT}$ (s)
071117	1.33	$2.71E-06 \pm 5.83E-08$	$7.97E-06 \pm 2.02E-07$	⋯	0.60 ± 0.01	278^{+48}_{-143}	0.20 ± 0.02
071122	1.14	$6.76E-08 \pm 2.06E-08$	$1.41E-06 \pm 1.63E-07$	⋯	⋯	73^{+30}_{-30}	⋯
080210	2.64	$2.57E-07 \pm 1.95E-08$	$4.17E-06 \pm 1.41E-07$	⋯	0.53 ± 0.17	73^{+15}_{-15}	0.57 ± 0.44
080310	2.43	$1.83E-07 \pm 1.72E-08$	$5.49E-06 \pm 2.90E-07$	⋯	⋯	28^{+6}_{-6}	0.41 ± 0.55
080319B	0.94	$1.55E-05 \pm 1.91E-07$	$5.25E-04 \pm 3.94E-06$	⋯	0.02 ± 0.01	651^{+8}_{-8}	0.14 ± 0.01
080319C	1.95	$2.22E-06 \pm 7.79E-08$	$1.77E-05 \pm 2.99E-07$	⋯	⋯	307^{+56}_{-85}	0.21 ± 0.12
080330	1.51	$1.33E-07 \pm 1.80E-08$	$8.77E-07 \pm 1.26E-07$	⋯	⋯	20^{+9}_{-9}	⋯
080411	1.03	$1.04E-05 \pm 1.31E-07$	$8.75E-05 \pm 2.01E-07$	⋯	0.21 ± 0.01	259^{+16}_{-21}	0.65 ± 0.01
080413A	2.43	$1.22E-06 \pm 2.65E-08$	$9.86E-06 \pm 1.71E-07$	⋯	0.13 ± 0.03	170^{+24}_{-48}	0.23 ± 0.03
080413B	1.10	$3.17E-06 \pm 8.25E-08$	$8.00E-06 \pm 1.52E-07$	⋯	0.23 ± 0.01	73^{+10}_{-10}	0.50 ± 0.03
080430	0.77	$4.60E-07 \pm 2.15E-08$	$3.01E-06 \pm 1.53E-07$	⋯	0.68 ± 0.08	80^{+15}_{-15}	0.76 ± 0.12
080516	3.20	$2.77E-07 \pm 2.80E-08$	$5.88E-07 \pm 5.50E-08$	⋯	0.15 ± 0.01	66^{+24}_{-24}	⋯
080520	1.55	$8.23E-08 \pm 1.00E-08$	$1.59E-07 \pm 3.00E-08$	⋯	⋯	12^{+5}_{-5}	⋯
080603B	2.69	$7.57E-07 \pm 2.63E-08$	$7.02E-06 \pm 1.78E-07$	⋯	0.08 ± 0.01	85^{+18}_{-55}	0.22 ± 0.03
080605	1.64	$5.99E-06 \pm 1.10E-07$	$4.72E-05 \pm 4.32E-07$	⋯	0.11 ± 0.01	246^{+11}_{-14}	0.22 ± 0.01
080607	3.04	$8.35E-06 \pm 2.42E-07$	$1.00E-04 \pm 0.00E+00$	⋯	0.04 ± 0.01	394^{+33}_{-35}	0.18 ± 0.06
080707	1.23	$1.68E-07 \pm 1.02E-08$	$1.26E-06 \pm 8.87E-08$	⋯	⋯	73^{+20}_{-20}	⋯
080721	2.60	$9.57E-06 \pm 5.01E-07$	$5.99E-05 \pm 3.04E-06$	⋯	0.13 ± 0.05	485^{+36}_{-41}	0.09 ± 0.04
080810	3.35	$9.76E-07 \pm 8.40E-08$	$1.80E-05 \pm 1.30E-06$	⋯	⋯	$313.5^{+73.6}_{-73.6}$	⋯
080913	6.70	$2.31E-07 \pm 4.00E-08$	$1.15E-06 \pm 1.20E-07$	⋯	⋯	$93.1^{+56.1}_{-56.1}$	⋯
080916A	0.69	$1.06E-06 \pm 1.60E-07$	$2.19E-05 \pm 7.30E-06$	⋯	⋯	109^{+9}_{-9}	⋯
081121	2.51	$1.87E-06 \pm 4.80E-07$	$1.73E-05 \pm 3.20E-06$	⋯	⋯	248^{+32}_{-38}	⋯
081222	2.77	$2.62E-06 \pm 3.80E-07$	$1.70E-05 \pm 1.40E-06$	⋯	⋯	134^{+9}_{-9}	⋯
090102	1.55	$3.90E-06 \pm 5.60E-07$	$3.66E-05 \pm 3.40E-06$	⋯	⋯	451^{+58}_{-73}	⋯
090323	3.57	$3.80E-06 \pm 6.90E-07$	$1.48E-04 \pm 2.00E-05$	⋯	⋯	416^{+73}_{-76}	⋯
090328	0.74	$7.28E-06 \pm 5.20E-07$	$1.37E-04 \pm 8.00E-06$	⋯	⋯	653^{+45}_{-45}	⋯
090423	8.20	$3.24E-07 \pm 6.80E-08$	$1.17E-06 \pm 3.20E-07$	⋯	⋯	82^{+15}_{-15}	⋯
090424	0.54	$1.80E-05 \pm 1.20E-06$	$5.85E-05 \pm 2.10E-06$	⋯	⋯	177^{+3}_{-3}	⋯
090516	4.11	$5.93E-07 \pm 3.40E-08$	$1.09E-05 \pm 1.60E-06$	⋯	⋯	$185.6^{+42.5}_{-98.4}$	⋯
090618	0.54	$8.58E-06 \pm 9.60E-07$	$3.39E-04 \pm 2.50E-05$	⋯	⋯	$155.5^{+10.5}_{-11.1}$	⋯
090715B	3.00	$8.96E-07 \pm 2.49E-07$	$1.09E-05 \pm 1.60E-06$	⋯	⋯	134^{+30}_{-56}	⋯
090812	2.45	$2.17E-06 \pm 2.40E-07$	$3.15E-05 \pm 4.10E-06$	⋯	⋯	572^{+159}_{-251}	⋯
090902B	1.82	$2.72E-05 \pm 3.00E-07$	$3.78E-04 \pm 3.00E-06$	⋯	⋯	775^{+11}_{-11}	⋯
090926	2.11	$1.82E-05 \pm 3.00E-07$	$1.51E-04 \pm 7.70E-06$	⋯	⋯	314^{+4}_{-4}	⋯
090926B	1.24	$5.55E-07 \pm 7.90E-08$	$1.66E-05 \pm 5.00E-07$	⋯	⋯	78.3^{+7}_{-7}	⋯
091018	0.97	$1.82E-06 \pm 8.40E-07$	$4.33E-06 \pm 7.60E-07$	⋯	⋯	19.2^{+11}_{-18}	⋯
091020	1.71	$1.63E-06 \pm 2.00E-07$	$1.68E-05 \pm 3.70E-06$	⋯	⋯	$47.9^{+7.1}_{-7.1}$	⋯
091029	2.75	$2.82E-07 \pm 1.60E-08$	$5.84E-06 \pm 4.70E-07$	⋯	⋯	$61.4^{+17.5}_{-17.5}$	⋯
091127	0.49	$4.03E-06 \pm 1.70E-07$	$2.65E-05 \pm 5.00E-07$	⋯	⋯	36^{+2}_{-2}	⋯
091208B	1.06	$3.47E-06 \pm 6.00E-07$	$7.78E-06 \pm 8.80E-07$	⋯	⋯	$124^{+19.4}_{-20.1}$	⋯

published studies. Before GRB 060607, we take all the data directly from [18]. We adopt the data between GRB 060707 and GRB 080721 from [19]. For those GRBs detected after July 7, 2008, we adopt the data directly from [37]. Applying the interpolation method, we can derive the distance moduli of 57 low-z GRBs and calibrate five GRB luminosity relations with this low-z sample, that is, the $\tau_{\rm lag} - L$ relation, the $E_p - L$ relation, the $E_p - E_\gamma$ relation, the $\tau_{\rm RT} - L$ relation, and the $E_p - E_{\rm iso}$ relation. The isotropic peak luminosity of a burst is calculated by

$$L = 4\pi D_L^2 P_{\rm bolo}, \tag{1}$$

the isotropic equivalent gamma-ray energy is given by

$$E_{\rm iso} = 4\pi D_L^2 S_{\rm bolo} (1+z)^{-1}, \tag{2}$$

Table 2: Best-fitting results.

Relation	a	b	N	r
$\tau_{\rm lag} - L$	52.32 ± 0.03	-1.10 ± 0.05	27	-0.75
$E_p - L$	52.08 ± 0.02	1.60 ± 0.04	55	0.79
$E_p - E_\gamma$	50.57 ± 0.01	1.76 ± 0.03	12	0.95
$\tau_{\rm RT} - L$	52.85 ± 0.03	-1.51 ± 0.06	40	-0.66
$E_p - E_{\rm iso}$	52.81 ± 0.02	1.53 ± 0.04	42	0.73

and the collimation-corrected energy is

$$E_\gamma = E_{\rm iso} f_{\rm beam} = 4\pi D_L^2 S_{\rm bolo} f_{\rm beam} (1+z)^{-1}. \quad (3)$$

Here, D_L is the luminosity distance of the burst, $P_{\rm bolo}$ and $S_{\rm bolo}$ are the bolometric peak flux and fluence of gamma-rays, respectively, while $f_{\rm beam} = (1 - \cos\theta_{\rm jet})$ is the beaming factor, and $\theta_{\rm jet}$ is the jet half-opening angle. We assume each GRB has bipolar jets, and E_γ is the true energy of the bipolar jets.

For convenience, the luminosity relations involved in this paper can be generally written in the power-law forms:

$$\log y = a + b \log x, \quad (4)$$

where a and b are the intercept and slope of the relation, respectively; y is the luminosity (L in units of erg s^{-1}) or energy ($E_{\rm iso}$ or E_γ in units of erg); x is the GRB parameters measured in the rest frame, for example, $\tau_{\rm lag}(1+z)^{-1}/(0.1\,{\rm s})$, $E_p(1+z)/(300\,{\rm keV})$, $E_p(1+z)/(300\,{\rm keV})$, $\tau_{\rm RT}(1+z)^{-1}/(0.1\,{\rm s})$, and $E_p(1+z)/(300\,{\rm keV})$, for the 5 two-variable relations above.

2.2. Calibration. First of all, we obtain the distance moduli of 57 low-z ($z < 1.4$) GRBs by using cubic spline interpolation from the 580 Union2.1 SNe Ia compiled in [36]. The interpolated distance moduli μ of these 57 GRBs and their corresponding errors σ_μ are shown in Figure 1(a). The SNe Ia data are also plotted in Figure 1(a) for comparison. When the cubic spline interpolation is used, the error of the interpolated distance moduli μ for the GRB at redshift z can be calculated by

$$\sigma_\mu = \left[\left(\frac{z_{i+1} - z}{z_{i+1} - z_i} \right)^2 \epsilon_{\mu,i}^2 + \left(\frac{z - z_i}{z_{i+1} - z_i} \right)^2 \epsilon_{\mu,i+1}^2 \right]^{1/2}, \quad (5)$$

where $\epsilon_{\mu,i}$ and $\epsilon_{\mu,i+1}$ are errors of the SNe at nearby redshifts z_i and z_{i+1}, respectively. With D_L in units of Mpc, the predicted distance modulus is defined as

$$\mu = 5 \log (D_L) + 25. \quad (6)$$

Having estimated the distance moduli μ of 57 low-z GRBs in a model-independent way, we can convert μ into luminosity distance D_L by using (6). From (1)–(3) with the corresponding $P_{\rm bolo}$, $S_{\rm bolo}$, and $f_{\rm beam}$, we can calculate L, $E_{\rm iso}$, and E_γ. In Figures 1(b)–1(f), with the interpolation results, we show the five luminosity indicators for these 57 GRBs at $z < 1.4$. For each relation, we perform a linear least-squares fit, taking into account both the x-axis error and the y-axis error. We also measure the scatter of each relation with the distance of the data points from the best-fit line, as done by [38]. The best-fitting results of the intercept a and the slope b with their 1σ uncertainties and the linear correlation coefficients for each relation are summarized in Table 2. The best-fitting results derived by using the interpolation method are carried out with these 57 GRBs at $z < 1.4$. In other words, the results are derived by using data from 27, 55, 12, 40, and 42 GRBs for the $\tau_{\rm lag} - L$, $E_p - L$, $E_p - E_\gamma$, $\tau_{\rm RT} - L$, and $E_p - E_{\rm iso}$ relations, respectively.

Reference [19] found no statistically significant evidence for the redshift evolution of the luminosity relations. If the GRB luminosity relations indeed do not evolve with redshift, we can extend the calibrated luminosity relations to high-z ($z > 1.4$) and derive the luminosity (L) or energy ($E_{\rm iso}$ or E_γ) of each burst at high-z by utilizing the calibrated relations. Therefore, the luminosity distance D_L can be derived from (1)–(3). The uncertainty of the value of the luminosity or energy deduced from each relation is

$$\sigma_{\log y}^2 = \sigma_a^2 + \left(\sigma_b^2 \log x\right)^2 + \left(\frac{b}{\ln 10} \frac{\sigma_x}{x} \right)^2 + \sigma_{\rm int}^2, \quad (7)$$

where σ_a, σ_b, and σ_x are 1σ uncertainties of the intercept a, the slope b, and the GRB measurable parameters x and $\sigma_{\rm int}$ is the systematic error in the fitting that accounts for the extra scatter of the luminosity relations. Then, we obtain the distance moduli μ for these 82 GRBs at $z > 1.4$ using (6). The propagated uncertainties will depend on whether $P_{\rm bolo}$ or $S_{\rm bolo}$ are given by

$$\sigma_\mu = \left[\left(\frac{5}{2} \sigma_{\log L} \right)^2 + \left(\frac{5}{2 \ln 10} \frac{\sigma_{P_{\rm bolo}}}{P_{\rm bolo}} \right)^2 \right]^{1/2}, \quad (8)$$

or

$$\sigma_\mu = \left[\left(\frac{5}{2} \sigma_{\log E_{\rm iso}} \right)^2 + \left(\frac{5}{2 \ln 10} \frac{\sigma_{S_{\rm bolo}}}{S_{\rm bolo}} \right)^2 \right]^{1/2},$$

$$\sigma_\mu = \left[\left(\frac{5}{2} \sigma_{\log E_\gamma} \right)^2 + \left(\frac{5}{2 \ln 10} \frac{\sigma_{S_{\rm bolo}}}{S_{\rm bolo}} \right)^2 + \left(\frac{5}{2 \ln 10} \frac{\sigma_{f_{\rm beam}}}{f_{\rm beam}} \right)^2 \right]^{1/2}. \quad (9)$$

Here we ignore the uncertainty of z in our calculations.

After obtaining the distance modulus of each GRB using one of these relations, we use the same method as [18] to calculate the real distance modulus, which is the weighted

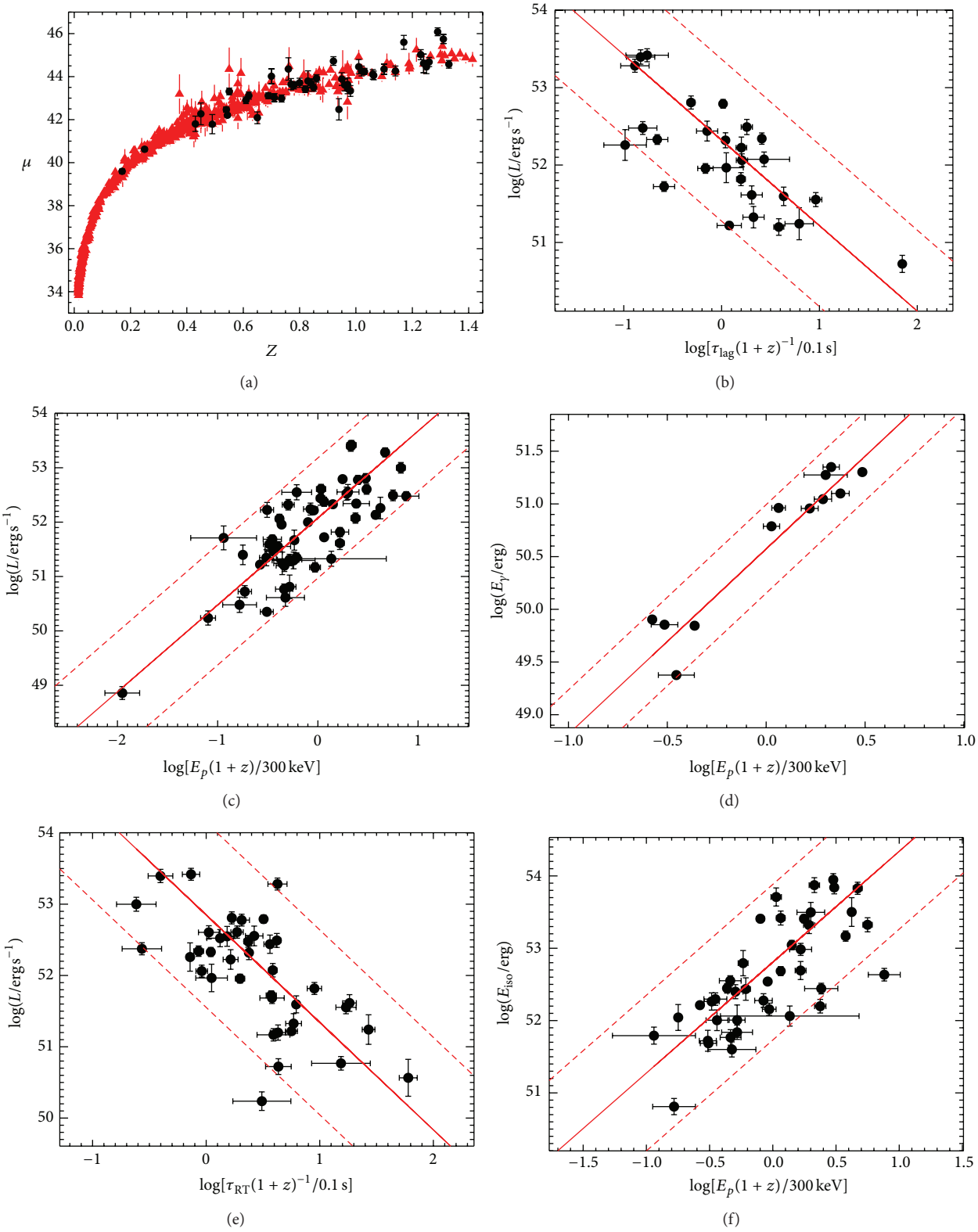

FIGURE 1: (a) The Hubble diagram of 580 SNe Ia (red triangles) and 57 GRBs at $z \leq 1.4$ (black dots) whose distance moduli are derived by using cubic spline interpolation. (b)–(f) The $\tau_{\rm lag} - L$, $E_p - L$, $E_p - E_\gamma$, $\tau_{\rm RT} - L$, and $E_p - E_{\rm iso}$ correlations. The five correlations are calibrated with the sample at $z \leq 1.4$ using cubic spline interpolation. The solid lines show the best-fitting results, while the dashed lines represent their 2σ dispersion around the best fits.

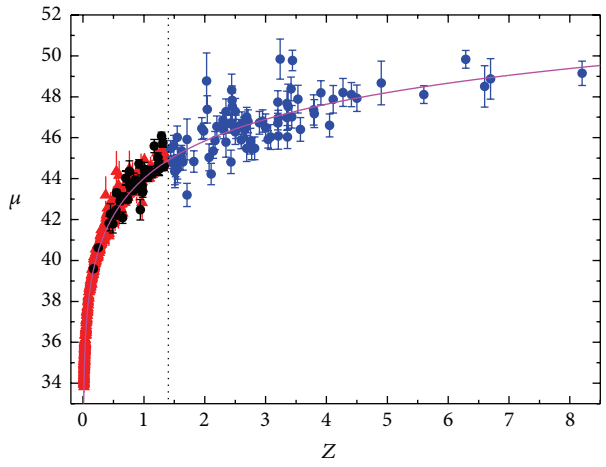

FIGURE 2: Hubble diagram of 580 SNIa (red triangles) and 139 GRBs (dots) obtained using the interpolation method. The 57 GRBs at $z \leq 1.4$ are obtained by interpolating from SNe Ia data (black dots); and the 82 GRBs at $z > 1.4$ (blue dots) are obtained with the five correlations calibrated with the sample at $z \leq 1.4$ using the cubic spline interpolation method. The vertical dotted line represents $z = 1.4$. The solid curve represents the best-fit cosmology for a flat ΛCDM universe: $\Omega_m = 0.29$, $\Omega_\Lambda = 0.71$.

average of all available distance moduli. The real distance modulus for each burst is

$$\mu_{\text{fit}} = \frac{\sum_i \mu_i/\sigma_{\mu_i}^2}{\sum_i \sigma_{\mu_i}^{-2}}, \tag{10}$$

with its corresponding uncertainty $\sigma_{\mu_{\text{fit}}} = (\sum_i \sigma_{\mu_i}^{-2})^{-1/2}$, where the summation runs from 1 to 5 over the relations with available data and μ_i and σ_{μ_i} are the best estimated distance modulus and its corresponding uncertainty from the ith relation.

Figure 2 shows the Hubble diagram from the Union2.1 SNe Ia sample and 139 GRBs. The combined Hubble diagram is consistent with the concordance cosmology. The 57 GRBs at $z < 1.4$ are obtained using interpolation method directly from SNe data. The 82 GRBs at $z > 1.4$ are obtained by utilizing the five relations calibrated with the sample at $z < 1.4$ using the cubic spline interpolation method.

3. Constraints from Supernovae and GRBs

The latest Type Ia SNe dataset known as the Union2.1 sample was recently released by the Supernova Cosmology Project collaboration, which contains 580 SNe detections (see [36]). With luminosity distance $D_L(\xi, z)$ in units of Mpc (where ξ stands for all the cosmological parameters that define the fitted model), the theoretical distance modulus μ_{th} can be calculated by using (6). The likelihood functions can be determined from the χ^2 statistic:

$$\chi^2_{\text{SNe}} = \sum_{i=1}^{N} \frac{[\mu_{\text{th}}(z_i) - \mu_{\text{obs}}(z_i)]^2}{\sigma_{\text{lc}}^2 + \sigma_{\text{ext}}^2 + \sigma_{\text{sample}}^2}, \tag{11}$$

where σ_{lc} is the propagated error from the covariance matrix of the light-curve fit and μ_{obs} is the observational distance modulus. The uncertainties due to host galaxy peculiar velocities, Galactic extinction corrections, and gravitational lensing are included in σ_{ext}, and σ_{sample} is a floating dispersion term containing sample-dependent systematic errors. The confidence regions can be found through marginalizing the likelihood functions over Hubble constant H_0 (i.e., integrating the probability density $p \propto \exp(-\chi^2/2)$ for all values of H_0).

Gamma-ray bursts (GRBs) are the most luminous transient events in the cosmos. Owing to their high luminosity, GRBs can be detected out to the edge of the visible universe, constituting a powerful tool for constructing a Hubble diagram at high-z. We use the above calibration results obtained by using the interpolation methods directly from SNe Ia data. The χ^2 value for the 82 GRBs at $z > 1.4$ is given by

$$\chi^2_{\text{GRB}} = \sum_{i=1}^{N} \frac{[\mu_{\text{th}}(z_i) - \mu_{\text{fit},i}]^2}{\sigma^2_{\mu_{\text{fit},i}}}, \tag{12}$$

where $\mu_{\text{fit},i}$ and $\sigma_{\mu_{\text{fit},i}}$ are the fitted distance modulus and its error for each burst. We also marginalize the nuisance parameter H_0.

Motivated by these significant updates in the observations of SNe Ia and GRBs, it is natural to consider the joint constraints on cosmological parameters and dark energy with the latest observational data. We combine SNe Ia and GRBs by multiplying the likelihood functions. The total χ^2 value is

$$\chi^2_{\text{total}} = \chi^2_{\text{SNe}} + \chi^2_{\text{GRB}}. \tag{13}$$

The best-fitting values of cosmological model are obtained by minimizing χ^2_{total}.

3.1. ΛCDM Model. In a Friedmann-Robertson-Walker (FRW) cosmology with mass density Ω_m and vacuum energy density Ω_Λ, the luminosity distance is given as

$$D_L(z) = \frac{c}{H_0} \frac{(1+z)}{\sqrt{|\Omega_k|}} \cdot \text{sinn}\left\{ |\Omega_k|^{1/2} \int_0^z \frac{dz}{\sqrt{\Omega_m (1+z)^3 + \Omega_\Lambda + \Omega_k (1+z)^2}} \right\}, \tag{14}$$

where c is the speed of light, H_0 is the Hubble constant at the present time, $\Omega_k = 1 - \Omega_m - \Omega_\Lambda$ represents the spatial curvature of the universe, and sinn is sinh when $\Omega_k > 0$ and sin when $\Omega_k < 0$. For a flat universe with $\Omega_k = 0$, (14) simplifies to the form $(1+z)c/H_0$ times the integral. In this ΛCDM model, the transition redshift satisfies

$$z_T = \left(\frac{2\Omega_\Lambda}{\Omega_m}\right)^{1/3} - 1. \tag{15}$$

We use the datasets discussed above to constrain cosmological parameters. In Figure 3(a), we show the confidence

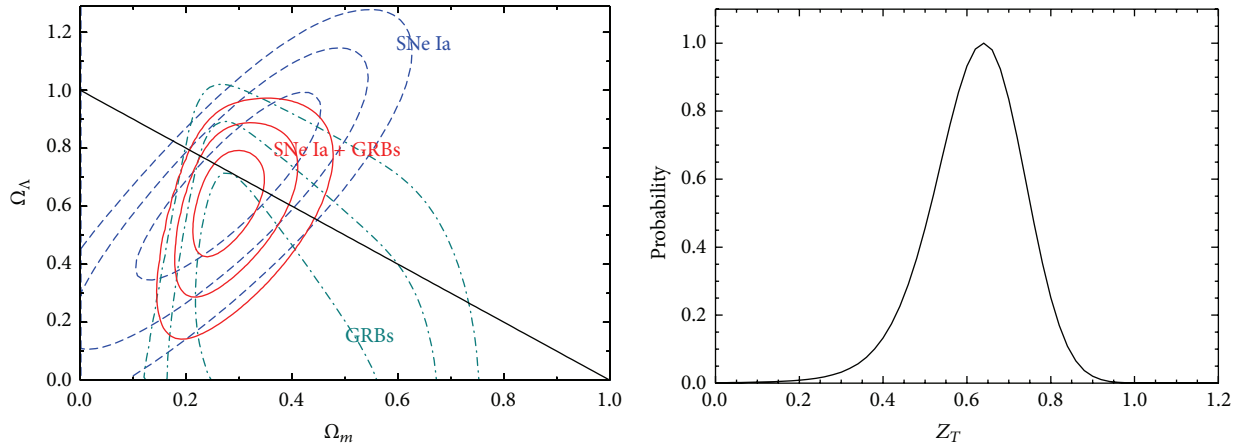

(a) (b)

FIGURE 3: (a) The contour confidence levels of $(\Omega_m, \Omega_\Lambda)$ in the ΛCDM model from the data for 82 GRBs ($z > 1.4$) (dark cyan dash-dotted lines), 580 SNe Ia (blue dashed lines), and 82 GRBs + 580 SNe Ia (red solid lines), respectively. The contours correspond to 1, 2, and 3σ confidence regions. (b) The probability versus the transition redshift derived from the GRB and SNe Ia sample.

regions for $(\Omega_m, \Omega_\Lambda)$ from 82 GRBs (dark cyan dash-dotted lines), 580 SNe Ia (blue dotted lines), and 82 GRBs + 580 SNe Ia (red solid lines), respectively. We can see that adding 82 high redshift GRBs ($z > 1.4$) to 580 SNe Ia ($z < 1.4$) significantly improves the constraint on $\Omega_m - \Omega_\Lambda$ plane. The 1σ confidence region from all the datasets is $(\Omega_m, \Omega_\Lambda) = (0.27^{+0.08}_{-0.06}, 0.62^{+0.18}_{-0.19})$ with $\chi^2_{\min} = 727.01$ for 659 degrees of freedom. Under the assumption of a flat universe (solid line), the contours yield $(\Omega_m, \Omega_\Lambda) = (0.29^{+0.04}_{-0.04}, 0.71^{+0.04}_{-0.04})$. The transition redshift at which the universe switched from deceleration to acceleration phase is $z_T = 0.64^{+0.08}_{-0.14}$ at the 1σ confidence level (Figure 3(b)).

3.2. Cardassian Expansion Model. Reference [6] proposed the Cardassian expansion model as a possible alternative for explaining the acceleration of the universe that invokes no vacuum energy. This model allows an acceleration in a flat, matter-dominated cosmology. If we consider a spatially flat FRW universe, the Friedmann equation is modified as

$$H^2 = \frac{8\pi G}{3}\left(\rho + C\rho^n\right). \tag{16}$$

This modification may arise as a consequence of embedding our observable universe as a (3 + 1)-dimensional brane in extra dimensions or the self-interaction of dark matter. The luminosity distance in this model is given by

$$D_L(z) = cH_0^{-1}(1+z) \cdot \int_0^z dz \left[(1+z)^3 \Omega_m + (1-\Omega_m)(1+z)^{3n}\right]^{-1/2}. \tag{17}$$

Figure 4 shows constraints on Ω_m and n from 1σ to 3σ confidence regions by fitting observational data. The dark cyan dash-dotted lines and blue dashed lines represent the results from 82 GRBs and 580 SNe Ia, respectively. The red solid contours show the constraints from the combination of these data. The best values are $\Omega_m = 0.24^{+0.15}_{-0.15}$ and $n = 0.16^{+0.30}_{-0.52}$ at the 1σ confidence level with $\chi^2_{\min} = 727.31$ for 659 degrees of freedom. This result is consistent with the ΛCDM cosmology ($n = 0$) in the 1σ confidence region.

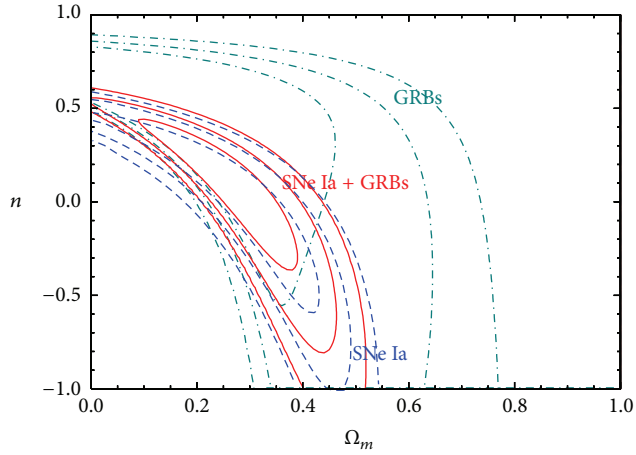

FIGURE 4: The contour confidence levels of (Ω_m, n) in the Cardassian expansion model from the data for 82 GRBs ($z > 1.4$) (dark cyan dash-dotted lines), 580 SNe Ia (blue dashed lines), and 82 GRBs + 580 SNe Ia (red solid lines), respectively. The contours correspond to 1, 2, and 3σ confidence regions.

3.3. $w(z) = w_0$ Model: Constant Equation of State. For the dark energy model with a constant equation of state ($w(z) = w_0$), the luminosity distance for a flat universe is [39]

$$D_L(z) = cH_0^{-1}(1+z) \cdot \int_0^z dz \left[(1+z)^3 \Omega_m + (1-\Omega_m)(1+z)^{3(1+w_0)}\right]^{-1/2}, \tag{18}$$

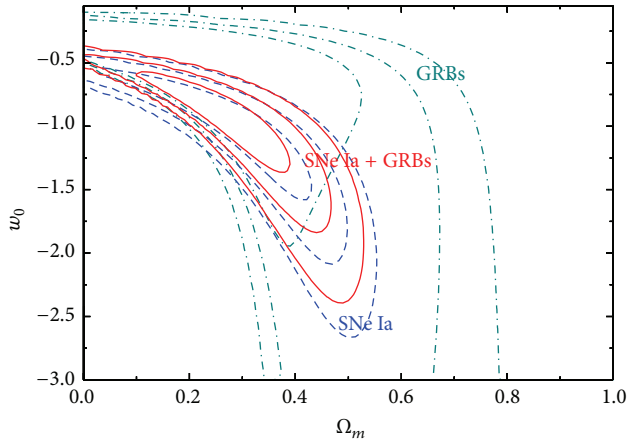

FIGURE 5: Constraints on Ω_m and w_0 from 1σ to 3σ confidence regions with dark energy whose equation state is constant. The contours are derived from GRBs (dark cyan dash-dotted lines), SNe Ia (blue dashed lines), and SNe Ia + GRBs (red solid lines), respectively.

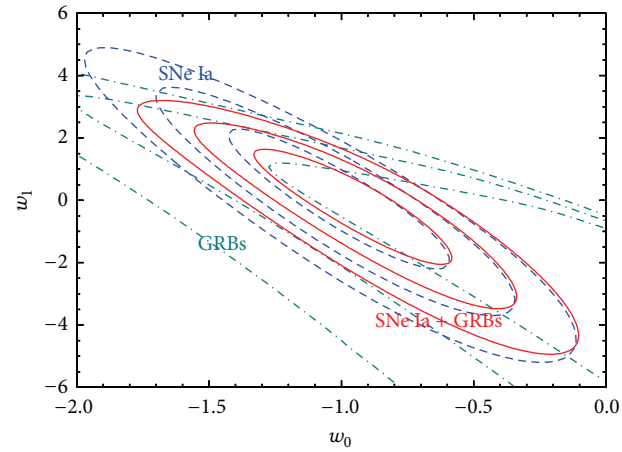

FIGURE 6: Constraints on w_0 and w_1 from 1σ to 3σ confidence regions with dark energy whose equation state is $w(z) = w_0 + w_1 z/(1+z)$. The contours are derived from GRBs (dark cyan dash-dotted lines), SNe Ia (blue dashed lines), and SNe Ia + GRBs (red solid lines), respectively.

and then the likelihood function depends on Ω_m and w_0. Figure 5 shows the likelihood contours on (Ω_m, w_0) plane for GRBs (dark cyan dash-dotted lines), SNe Ia (blue dashed lines), and SNe Ia + GRBs (red solid lines), respectively. The contours correspond to 1, 2, and 3σ confidence regions, respectively. The cosmological parameters with the largest likelihood are $\Omega_m = 0.24^{+0.16}_{-0.14}$ and $w_0 = -0.85^{+0.28}_{-0.51}$ (1σ) with $\chi^2_{\min} = 727.32$ for 659 degrees of freedom. For a prior of $\Omega_m = 0.29$, we obtain $w_0 = -0.95^{+0.14}_{-0.18}$, which is consistent with the cosmological constant (i.e., $w_0 = -1$) in a 1σ confidence region.

3.4. $w(z) = w_0 + w_1 z/(1+z)$ Model: Time-Dependent Equation of State. We next examine models in which dark energy changes with time. As shown above, we adopt a simple model in which the dark energy equation of state can be parameterized by [4, 5]

$$w(z) = w_0 + \frac{w_1 z}{(1+z)}. \tag{19}$$

The ΛCDM model is recovered when $w_0 = -1$ and $w_1 = 0$. In this dark energy model, the luminosity distance is calculated by

$$D_L(z) = cH_0^{-1}(1+z) \cdot \int_0^z dz \left[(1+z)^3 \Omega_m + (1-\Omega_m) \cdot (1+z)^{3(1+w_0+w_1)} e^{-3w_1 z/(1+z)}\right]^{-1/2}. \tag{20}$$

Figure 6 shows the constraints on w_0 versus w_1 from 1σ to 3σ confidence regions. The dark cyan dash-dotted lines and blue dashed lines represent the constraints from 82 GRBs and 580 SNe Ia, respectively. The red solid contours are obtained from the combination of these data. For a prior of $\Omega_m = 0.29$, we find the best dark energy parameters set is $(w_0, w_1) = (-0.96^{+0.39}_{-0.36}, -0.04^{+1.72}_{-1.96})$ at the 1σ confidence level with $\chi^2_{\min} = 727.54/659$. This result is also consistent with the ΛCDM model (i.e., $w_0 = -1$ and $w_1 = 0$) in the 1σ confidence region.

4. Conclusions and Discussion

In this paper, we have updated five GRB luminosity relations ($\tau_{\rm lag} - L$, $E_p - E_{\rm iso}$, $E_p - L$, $E_p - E_\gamma$, and $\tau_{\rm RT} - L$) among certain spectral and light-curve features with the latest 139 GRBs. We find that the five relations indeed exist with the latest GRBs data. To avoid any assumption on cosmological models, we obtained the distance moduli of 57 low-z ($z < 1.4$) GRBs by using cubic spline interpolation from the 580 Union2.1 SNe Ia compiled in [36]. Then, we calibrated the five relations with these 57 low-z GRBs. In order to constrain cosmological models, we extended the five calibrated luminosity relations to high-z and derived the distance moduli of 82 high-z ($z > 1.4$) GRBs.

Motivated by these significant updates of the observational data, we considered the joint constraints on the Cardassian expansion model and dark energy with 580 Union2.1 SNe Ia sample ($z < 1.4$) and 82 calibrated GRBs' data ($1.4 < z \leq 8.2$). In the ΛCDM cosmology, we find that adding 82 high-z GRBs to 580 SNe Ia significantly improves the constraint on $\Omega_m - \Omega_\Lambda$ plane. We obtain $\Omega_m = 0.27^{+0.08}_{-0.06}$ and $\Omega_\Lambda = 0.62^{+0.18}_{-0.19}$ (1σ). For a flat universe, the contours yield $(\Omega_m, \Omega_\Lambda) = (0.29^{+0.04}_{-0.04}, 0.71^{+0.04}_{-0.04})$. The transition redshift at which the universe switched from deceleration to acceleration phase is $z_T = 0.64^{+0.08}_{-0.14}$ (1σ). In the Cardassian expansion model, we obtain $\Omega_m = 0.24^{+0.15}_{-0.15}$ and $n = 0.16^{+0.30}_{-0.52}$ (1σ). This result is consistent with the ΛCDM cosmology ($n = 0$) in the 1σ confidence region, in agreement with the conclusions of [40]. We also fit two dark energy models, including the flat constant w model (i.e.,

$w(z) = w_0$) and the time-dependent w model (i.e., $w(z) = w_0 + w_1 z/(1+z)$). Based on our analysis, it can be seen that our universe at higher redshift up to $z = 8.2$ is consistent with the concordance model ($\Omega_m = 0.27$, $\Omega_\Lambda = 0.73$, $w_0 = -1$, and $w_1 = 0$) within 1σ level. These results suggest that time dependence of the dark energy is small even if it exists.

Since the discoveries of distance indicators of GRBs, these luminosity indicators have been used as standard candles for cosmological research at high redshifts. However, the dispersion of distance indicators is still large, which restricted the precision of distance measurement by GRBs. The large dispersion may be due to the fact that some contamination of the GRB sample is unavoidable and that pure luminosity indicators may never be found for these sources. Of course, it could also be due to the fact that we simply have not yet identified the correct spectral and light-curve features to use for these luminosity relations. On the other hand, it could also be due to the fact that we are inevitably suffering from the systematic errors and intrinsic scatter associated with the data. In order to estimate distance of GRBs more precisely, we should take efforts to investigate possible origins of dispersion of the distance indicators and/or search for more precise distance indicators in the future.

Conflict of Interests

The authors declare that there is no conflict of interests regarding the publication of this paper.

Acknowledgments

This work is partially supported by the National Basic Research Program ("973" Program) of China (Grants 2014CB845800 and 2013CB834900), the National Natural Science Foundation of China (Grants nos. 11322328 and 11373068), the One-Hundred-Talents Program, the Youth Innovation Promotion Association, and the Strategic Priority Research Program "The Emergence of Cosmological Structures" (Grant no. XDB09000000) of the Chinese Academy of Sciences, and the Natural Science Foundation of Jiangsu Province (grant no. BK2012890).

References

[1] S. Perlmutter, G. Aldering, M. Della Valle et al., "Discovery of a supernova explosion at half the age of the Universe," *Nature*, vol. 391, no. 6662, pp. 51–54, 1998.

[2] B. P. Schmidt, N. B. Suntzeff, M. M. Phillips et al., "The high-Z supernova search: measuring cosmic deceleration and global curvature of the universe using type IA supernovae," *The Astrophysical Journal*, vol. 507, no. 1, pp. 46–63, 1998.

[3] A. G. Riess, A. V. Filippenko, P. Challis et al., "Observational evidence from supernovae for an accelerating universe and a cosmological constant," *The Astronomical Journal*, vol. 116, no. 3, pp. 1009–1038, 1998.

[4] M. Chevallier and D. Polarski, "Accelerating universes with scaling dark matter," *International Journal of Modern Physics D*, vol. 10, no. 2, pp. 213–223, 2001.

[5] E. V. Linder, "Exploring the expansion history of the universe," *Physical Review Letters*, vol. 90, no. 9, Article ID 091301, 2003.

[6] K. Freese and M. Lewis, "Cardassian expansion: a model in which the universe is flat, matter dominated, and accelerating," *Physics Letters, Section B: Nuclear, Elementary Particle and High-Energy Physics*, vol. 540, no. 1-2, pp. 1–8, 2002.

[7] D. O. Jones, S. A. Rodney, A. G. Riess et al., "The discovery of the most distant known type Ia supernova at redshift 1.914," *The Astrophysical Journal*, vol. 768, no. 2, article 166, 2013.

[8] M. J. Sholl, M. L. Lampton, G. Aldering et al., "SNAP telescope," *Optical, Infrared, and Millimeter Space Telescopes*, vol. 5487, pp. 1473–1483, 2004.

[9] D. Q. Lamb and D. E. Reichart, "Gamma-ray bursts as a probe of the very high redshift universe," *The Astrophysical Journal*, vol. 536, no. 1, pp. 1–18, 2000.

[10] N. R. Tanvir, D. B. Fox, A. J. Levan et al., "A γ-ray burst at a redshift of z≈ 8.2," *Nature*, vol. 461, no. 7268, pp. 1254–1257, 2009.

[11] A. Cucchiara, A. J. Levan, D. B. Fox et al., "A photometric redshift of $z \sim 9.4$ for GRB 090429B," *The Astrophysical Journal*, vol. 736, article 7, 2011.

[12] J. P. Norris, G. F. Marani, and J. T. Bonnell, "Connection between energy-dependent lags and peak luminosity in gamma-ray bursts," *The Astrophysical Journal*, vol. 534, no. 1, pp. 248–257, 2000.

[13] E. E. Fenimore and E. Ramirez-Ruiz, "Redshifts for 220 BATSE gamma-ray bursts determined by variability and the cosmological consequences," http://arxiv.org/abs/astro-ph/0004176.

[14] L. Amati, F. Frontera, M. Tavani et al., "Intrinsic spectra and energetics of BeppoSAX gamma-ray bursts with known redshifts," *Astronomy & Astrophysics*, vol. 390, no. 1, pp. 81–89, 2002.

[15] D. M. Wei and W. H. Gao, "Are there cosmological evolution trends on gamma-ray burst features?" *Monthly Notices of the Royal Astronomical Society*, vol. 345, no. 3, pp. 743–746, 2003.

[16] D. Yonetoku, T. Murakami, T. Nakamura, R. Yamazaki, A. K. Inoue, and K. Ioka, "Gamma-ray burst formation rate inferred from the spectral peak energy-peak luminosity relation," *The Astrophysical Journal*, vol. 609, no. 2, pp. 935–951, 2004.

[17] G. Ghirlanda, G. Ghisellini, and D. Lazzati, "The collimation-corrected gamma-ray burst energies correlate with the peak energy of their vF_v spectrum," *The Astrophysical Journal*, vol. 616, no. 1, pp. 331–338, 2004.

[18] B. E. Schaefer, "The hubble diagram to redshift >6 from 69 gamma-ray bursts," *The Astrophysical Journal*, vol. 660, no. 1, pp. 16–46, 2007.

[19] F.-Y. Wang, S. Qi, and Z.-G. Dai, "The updated luminosity correlations of gamma-ray bursts and cosmological implications," *Monthly Notices of the Royal Astronomical Society*, vol. 415, no. 4, pp. 3423–3433, 2011.

[20] B. E. Schaefer, "Gamma-ray burst Hubble diagram to z = 4.5," *The Astrophysical Journal Letters*, vol. 583, no. 2, pp. L67–L70, 2003.

[21] Z. G. Dai, E. W. Liang, and D. Xu, "Constraining Ω_M and dark energy with gamma-ray bursts," *The Astrophysical Journal Letters*, vol. 612, no. 2, pp. L101–L104, 2004.

[22] E. Liang and B. Zhang, "Model-independent multivariable gamma-ray burst luminosity indicator and its possible cosmological implications," *The Astrophysical Journal*, vol. 633, no. 2, pp. 611–623, 2005.

[23] Y. Kodama, D. Yonetoku, T. Murakami, S. Tanabe, R. Tsutsui, and T. Nakamura, "Gamma-ray bursts in $1.8 < z < 5.6$ suggest that the time variation of the dark energy is small," *Monthly Notices of the Royal Astronomical Society*, vol. 391, no. 1, pp. L1–L4, 2008.

[24] R. Tsutsui, T. Nakamura, D. Yonetoku et al., "Constraints on ω_0 and ω_a of dark energy from high-redshift gamma-ray bursts," *Monthly Notices of the Royal Astronomical Society: Letters*, vol. 394, no. 1, pp. L31–L35, 2009.

[25] J.-J. Wei, X.-F. Wu, and F. Melia, "The gamma-ray burst hubble diagram and its implications for cosmology," *The Astrophysical Journal*, vol. 772, no. 1, article 43, 2013.

[26] G. Ghirlanda, G. Ghisellini, D. Lazzati, and C. Firmani, "Gamma-ray bursts: new rulers to measure the universe," *The Astrophysical Journal Letters*, vol. 613, no. 1, pp. L13–L16, 2004.

[27] G. Ghirlanda, G. Ghisellini, C. Firmani, L. Nava, F. Tavecchio, and D. Lazzati, "Cosmological constraints with GRBs: homogeneous medium vs. wind density profile," *Astronomy and Astrophysics*, vol. 452, no. 3, pp. 839–844, 2006.

[28] E. Liang and B. Zhang, "Calibration of gamma-ray burst luminosity indicators," *Monthly Notices of the Royal Astronomical Society*, vol. 369, no. 1, pp. L37–L41, 2006.

[29] C. Firmani, G. Ghisellini, G. Ghirlanda, and V. Avila-Reese, "A new method optimized to use gamma-ray bursts as cosmic rulers," *Monthly Notices of the Royal Astronomical Society: Letters*, vol. 360, no. 1, pp. L1–L15, 2005.

[30] F. Y. Wang and Z. G. Dai, "Constraining the cosmological parameters and transition redshift with gamma-ray bursts and supernovae," *Monthly Notices of the Royal Astronomical Society*, vol. 368, no. 1, pp. 371–378, 2006.

[31] L. Amati, C. Guidorzi, F. Frontera et al., "Measuring the cosmological parameters with the $E_{p,i}$–E_{iso} correlation of gamma-ray bursts," *Monthly Notices of the Royal Astronomical Society*, vol. 391, no. 2, pp. 577–584, 2008.

[32] H. Li, M. Su, Z. Fan, Z. Dai, and X. Zhang, "Constraints on dark energy models including gamma ray bursts," *Physics Letters B*, vol. 658, no. 4, pp. 95–100, 2008.

[33] N. Liang, W. K. Xiao, Y. Liu, and S. N. Zhang, "A cosmology-independent calibration of gamma-ray burst luminosity relations and the hubble diagram," *The Astrophysical Journal*, vol. 685, no. 1, pp. 354–360, 2008.

[34] H. Wei and S.-N. Zhang, "Reconstructing the cosmic expansion history up to redshift z=6.29 with the calibrated gamma-ray bursts," *The European Physical Journal C*, vol. 63, no. 1, pp. 139–147, 2009.

[35] H. Wei, "Observational constraints on cosmological models with the updated long gamma-ray bursts," *Journal of Cosmology and Astroparticle Physics*, vol. 2010, no. 8, article 20, 2010.

[36] N. Suzuki, D. Rubin, C. Lidman et al., "The *hubble space telescope* cluster supernova survey. V. Improving the dark-energy constraints above z > 1 and building an early-type-hosted supernova sample," *The Astrophysical Journal*, vol. 746, no. 1, article 85, 2012.

[37] D. Yonetoku, T. Murakami, R. Tsutsui, T. Nakamura, Y. Morihara, and K. Takahashi, "Possible origins of dispersion of the peak energy-brightness correlations of gamma-ray bursts," *Publications of the Astronomical Society of Japan*, vol. 62, no. 6, pp. 1495–1507, 2010.

[38] G. Ghirlanda, G. Ghisellini, C. Firmani, A. Celotti, and Z. Bosnjak, "The peak luminosity-peak energy correlation in gamma-ray bursts," *Monthly Notices of the Royal Astronomical Society*, vol. 360, no. 1, pp. L45–L49, 2005.

[39] A. G. Riess, L.-G. Sirolger, J. Tonry et al., "Type Ia supernova discoveries at $z > 1$ from the *Hubble Space Telescope*: evidence for past deceleration and constraints on dark energy evolution," *The Astrophysical Journal*, vol. 607, no. 2, pp. 665–687, 2004.

[40] C.-J. Feng and X.-Z. Li, "Cardassian universe constrained by latest observations," *Physics Letters B*, vol. 692, no. 2, pp. 152–156, 2010.

Hindawi Publishing Corporation
Advances in Astronomy
Volume 2015, Article ID 907321, 37 pages
http://dx.doi.org/10.1155/2015/907321

Review Article

Physics of Gamma-Ray Bursts Prompt Emission

Asaf Pe'er

Physics Department, University College Cork, Cork, Ireland

Correspondence should be addressed to Asaf Pe'er; a.peer@ucc.ie

Received 5 December 2014; Accepted 30 March 2015

Academic Editor: Dean Hines

In recent years, our understanding of gamma-ray bursts (GRB) prompt emission has been revolutionized, due to a combination of new instruments, new analysis methods, and novel ideas. In this review, I describe the most recent observational results and current theoretical interpretation. Observationally, a major development is the rise of time resolved spectral analysis. These led to (I) identification of a distinguished high energy component, with GeV photons often seen at a delay and (II) firm evidence for the existence of a photospheric (thermal) component in a large number of bursts. These results triggered many theoretical efforts aimed at understanding the physical conditions in the inner jet regions. I highlight some areas of active theoretical research. These include (I) understanding the role played by magnetic fields in shaping the dynamics of GRB outflow and spectra; (II) understanding the microphysics of kinetic and magnetic energy transfer, namely, accelerating particle to high energies in both shock waves and magnetic reconnection layers; (III) understanding how subphotospheric energy dissipation broadens the "Planck" spectrum; and (IV) geometrical light aberration effects. I highlight some of these efforts and point towards gaps that still exist in our knowledge as well as promising directions for the future.

1. Introduction

In spite of an extensive study for nearly a generation, understanding of gamma-ray bursts (GRB) prompt emission still remains an open question. The main reason for this is the nature of the prompt emission phase: the prompt emission lasts typically a few seconds (or less), without repetition and with variable light curve. Furthermore, the spectra vary from burst to burst and do not show any clear feature that could easily be associated with any simple emission model. This is in contrast to the afterglow phase, which lasts much longer, up to years, with (relatively) smooth, well characteristic behavior. These features enable afterglow studies using long term, multiwaveband observations, as well as relatively easy comparison with theories.

Nonetheless, I think it is fair to claim that in recent years understanding of GRB prompt emission has been revolutionized. This follows the launch of *Swift* satellite in 2004 and *Fermi* satellite in 2008. These satellites enable much more detailed studies of the prompt emission, both in the spectral and temporal domains. The new data led to the realization that the observed spectra are composed of several distinctive components. (I) A thermal component identified on top of a nonthermal spectra was observed in a large number of bursts. This component shows a unique temporal behavior. (II) There is evidence that the very high energy (> GeV) part of the spectra evolves differently than the lower energy part and hence is likely to have a separate origin. (III) The sharp cutoff in the light curves of many GRBs observed by *Swift* enables a clear discrimination between the prompt and the afterglow phases.

The decomposition of the spectra into separate components, presumably with different physical origin, enabled an independent study of the properties of each component, as well as study of the complex connection between the different components. Thanks to these studies, we are finally reaching a critical point in which a self-consistent physical picture of the GRB prompt emission, more complete than ever, is emerging. This physical insight is of course a crucial link that connects the physics of GRB progenitor stars with that of their environments.

Many of the ideas gained in these studies are relevant to many other astronomical objects, such as active galactic nuclei (AGNs), X-ray binaries (XRBs), and tidal disruption events (TDEs). All these transient objects share the common

feature of having (trans)relativistic jetted outflows. Therefore, despite the obvious differences, many similarities between various underlying physical processes in these objects and in GRBs are likely to exist. These include the basic questions of jet launching and propagation, as well as the microphysics of energy transfer via magnetic reconnection and particle acceleration to high energies. Furthermore, understanding the physical conditions that exist during the prompt emission phase enables the study of other fundamental questions such as whether GRBs are sources of (ultra-high energy) cosmic rays and neutrinos, as well as the potential of detecting gravitational waves associated with GRBs.

In this review, I will describe the current (December 2014) observational status, as well as the emerging theoretical picture. I will emphasise a major development of recent years, namely, the realization that photospheric emission may play a key role, both directly and indirectly, as part of the observed spectra. I should stress though that in spite of several major observational and theoretical breakthroughs that took place in recent years, our understanding is still far from being complete. I will discuss the gaps that still exist in our knowledge and novel ideas raised in addressing them. I will point to current scientific efforts, which are focused on different, sometimes even perpendicular directions.

The rapid progress in this field is the cause of the fact that in the past decade there have been very many excellent reviews covering various aspects of GRB phenomenology and physics. A partial list includes reviews by Waxman [1], Piran [2], Zhang and Mészáros [3], Mészáros [4], Nakar [5], Zhang [6], Fan and Piran [7], Gehrels et al. [8], Atteia and Boër [9], Gehrels and Mészáros [10], Bucciantini [11], Gehrels and Razzaque [12], Daigne [13], Zhang [14], Kumar and Zhang [15], Berger [16], and Meszaros and Rees [17]. My goal here is not to compete with these reviews, but to highlight some of the recent, partially, still controversial results and developments in this field, as well as pointing into current and future directions which are promising paths.

This review is organized as follows. In Section 2 I discuss the current observational status. I discuss the light curves (Section 2.1), observed spectra (Section 2.2), polarization (Section 2.3), counterparts at high and low energies (Section 2.4), and notable correlations (Section 2.5). I particularly emphasise the different models used today in fitting the prompt emission spectra. Section 3 is devoted to theoretical ideas. To my opinion, the easiest way to understand the nature of GRBs is to follow the various episodes of energy transfer that occur during the GRB evolution. I thus begin by discussing models of GRB progenitors (Section 3.1) that provide the source of energy. This follows by discussing models of relativistic expansion, both "hot" (photon-dominated) (Section 3.2) and "cold" (magnetic-dominated) (Section 3.3). I then discuss recent progress in understanding how dissipation of the kinetic and/or magnetic energy is used in accelerating particles to high-energies (Section 3.4). I complete with the discussion of the final stage of energy conversion, namely, radiative processes by the hot particles as well as the photospheric contribution (Section 3.5), which lead to the observed signal. I conclude with a look into the future in Section 4.

2. Key Observational Properties

2.1. Light Curves. The most notable property of GRB prompt emission light curve is that it is irregular, diverse, and complex. No two gamma-ray bursts light curves are identical, a fact which obviously makes their study challenging. While some GRBs are extremely variable with variability time scale in the millisecond range, others are much smoother. Some have only a single peak, while others show multiple peaks; see Figure 1. Typically, individual peaks are not symmetric but show a "fast rise exponential decay" (FRED) behavior.

The total duration of GRB prompt emission is traditionally defined by the "T_{90}" parameter, which is the time interval in the epoch when 5% and 95% of the total fluence are detected. As thoroughly discussed by Kumar and Zhang [15], this (arbitrary) definition is very subjective, due to many reasons. (1) It depends on the energy range and sensitivity of the different detectors; (2) Different intrinsic light curves: some light curves are very spiky with gaps between the spikes, while others are smooth; (3) no discrimination is made between the "prompt" phase and the early afterglow emission; (4) it does not take into account the difference in redshifts between the bursts, which can be substantial.

In spite of these drawbacks, T_{90} is still the most commonly used parameter in describing the total duration of the prompt phase. While T_{90} is observed to vary between milliseconds and thousands of seconds (the longest to date is GRB111209A, with duration of $\sim 2.5 \times 10^4$ s [18]), from the early 1990s, it was noted that the T_{90} distribution of GRBs is bimodal [19]. About $\lesssim$1/4 of GRBs in the BATSE catalog are "short," with average T_{90} of ~0.2–0.3 s, and roughly 3/4 are "long," with average $T_{90} \approx$ 20–30 s [20]. The boundary between these two distributions is at ~2 s. Similar results are obtained by *Fermi* (see Figure 2), though the subjective definition of T_{90} results in a bit different ratio, where only 17% of *Fermi*-GBM bursts are considered as "short," the rest being long [21–23]. Similar conclusion, though with much smaller sample, and even lesser fraction of short GRBs are observed in the *Swift*-Bat catalog [24] and by *Integral* [25]. These results do not change if instead one uses T_{50} parameter, defined in a similar way.

These results are accompanied by different hardness ratio (the ratio between the observed photon flux at the high and low energy bands of the detector), where short bursts are, on average, harder (higher ratio of energetic photons) than long ones [19]. Other clues for different origin are the association of only the long GRBs with core collapse supernova, of type Ib/c [26–32] which are not found in short GRBs [33]; association of short GRBs to galaxies with little star-formation (as opposed to long GRBs which are found in star forming galaxies), and residing at different locations within their host galaxies than long GRBs [34–41]. Altogether, these results thus suggest two different progenitor classes. However, a more careful analysis reveals a more complex picture with many outliers to these rules (e.g., [42–49]). It is therefore possible, maybe even likely, that the population of short GRBs may have more than a single progenitor

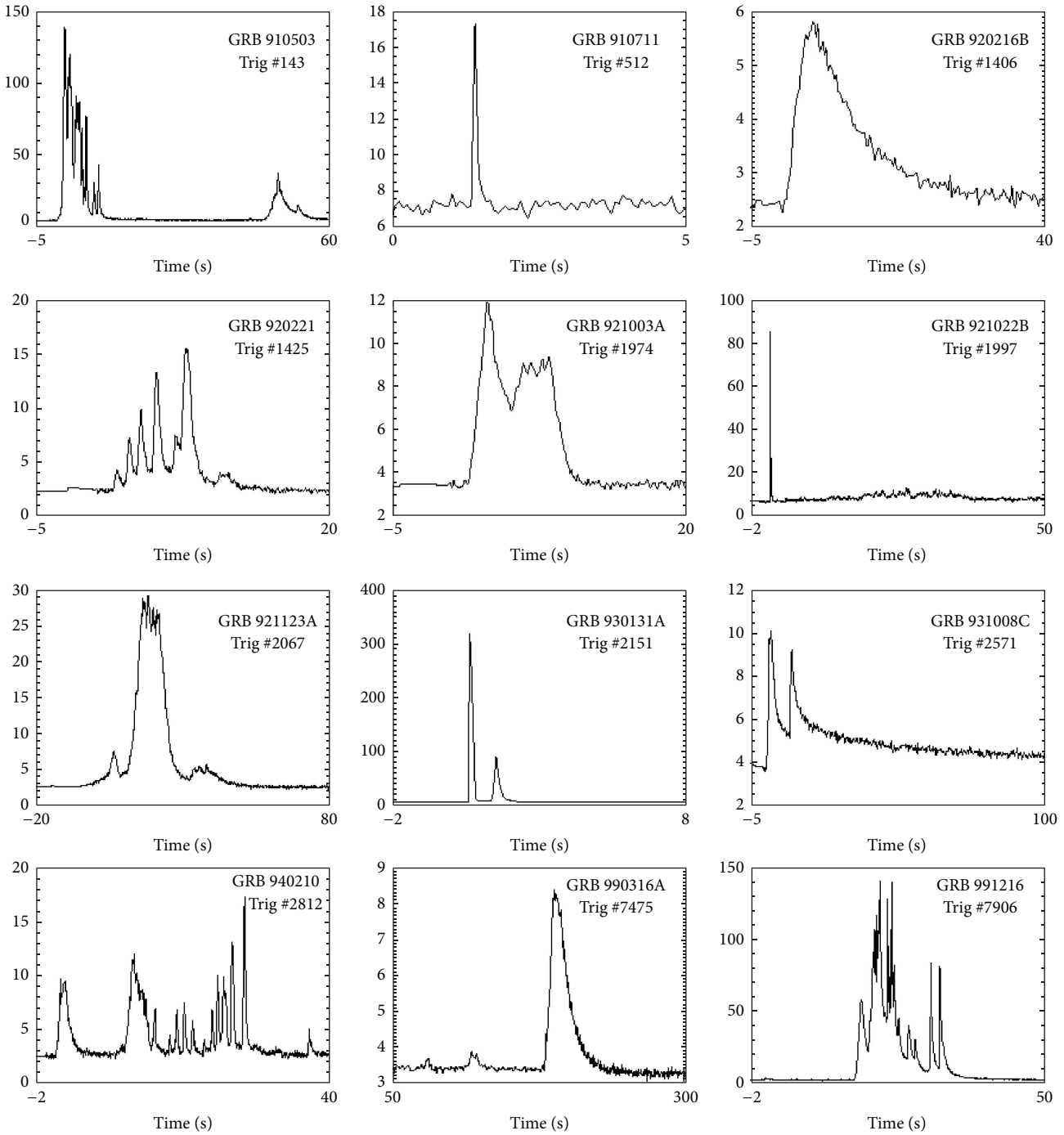

Figure 1: Light curves of 12 bright gamma-ray bursts detected by BATSE. Gamma-ray bursts light curves display a tremendous amount of diversity and few discernible patterns. This sample includes short events and long events (duration ranging from milliseconds to minutes), events with smooth behavior and single peaks, and events with highly variable, erratic behavior with many peaks. Created by Daniel Perley with data from the public BATSE archive (http://gammaray.msfc.nasa.gov/batse/grb/catalog/).

(or physical origin). In addition, there have been several claims for a small, third class of "intermediate" GRBs, with $T_{90} \sim 2$ s [50–53], but this is still controversial (e.g., [48, 54]).

To further add to the confusion, the light curve itself varies with energy band (e.g., Figure 3). One of *Fermi*'s most important results, to my view, is the discovery that the highest energy photons (in the LAT band) are observed to both (I) lag behind the emission at lower energies and (II) last longer. Both these results are seen in Figure 3. Similarly, the width of individual pulses is energy dependent. It was found that the pulse width ω varies with energy, $\omega(E) \propto E^{-\alpha}$ with $\alpha \sim 0.3$–0.4 [55, 56].

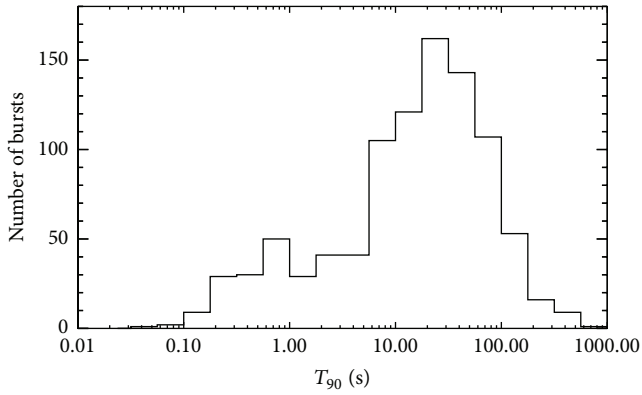

Figure 2: Distribution of GRB durations (T_{90}) of 953 bursts in the *Fermi*-GBM (50–300 keV energy range). Taken from the 2nd *Fermi* catalog, [23]. 159 (17%) of the bursts are "short."

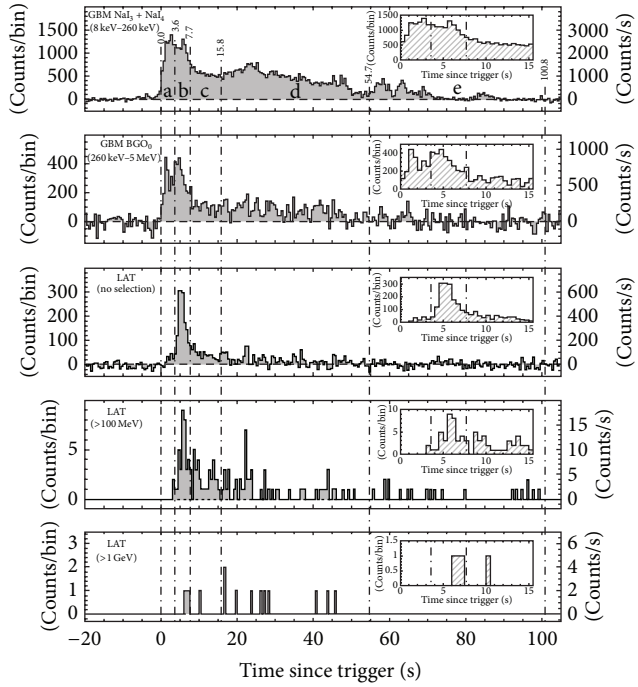

Figure 3: Light curves for GRB 080916C observed with the GBM and the LAT detectors on board the *Fermi* satellite, from lowest to highest energies. The top graph shows the sum of the counts, in the 8 to 260 keV energy band, of two NaI detectors. The second is the corresponding plot for BGO detector 0, between 260 keV and 5 MeV. The third shows all LAT events passing the onboard event filter for gamma-rays. (Insets) Views of the first 15 s from the trigger time. In all cases, the bin width is 0.5 s; the per-second counting rate is reported on the right for convenience. Taken from Abdo et al. [57].

Already in the BATSE era, several bursts were found to have "ultra-long" duration, having T_{90} exceeding ~10^3 s (e.g., [58, 59]). Recently, several additional bursts were found in this category (e.g., GRB 091024A, GRB 101225A, GRB 111209A, GRB 121027A, and GRB 130925A [18, 60–63]), which raise the idea of a new class of GRBs. If these bursts indeed represent a separate class, they may have a different progenitor than that of "regular" long GRBs [62, 64, 65]. However, recent analysis showed that bursts with duration $T_{90} \sim 10^3$ s need not belong to a special population, while bursts with $T_{90} \gtrsim 10^4$ s may belong to a separate population [66, 67]. As the statistics is very low, my view is that this is still an open issue.

2.2. Spectral Properties

2.2.1. A Word of Caution. Since this is a rapidly evolving field, one has to be extra careful in describing the spectra of GRB prompt emission. As I will show below, the observed spectra is, in fact, sensitive to the analysis method chosen. Thus, before describing the spectra, one has to describe the analysis method.

Typically, the spectral analysis is based on analyzing flux integrated over the entire duration of the prompt emission, namely, the spectra is *time-integrated*. Clearly, this is a trade off, as enough photons need to be collected in order to analyze the spectra. For weak bursts this is the only thing one can do. However, there is a major drawback here: use of the time integrated spectra implies that important time-dependent signals could potentially be lost or at least smeared. This can easily lead to the wrong theoretical interpretation.

A second point of caution is the analysis method, which is done by a forward folding technique. This means the following. First, a model spectrum is chosen. Second, the chosen model is convolved with the detector response and compared to the detected counts spectrum. Third, the model parameters are varied in search for the minimal difference between model and data. The outcome is the best fitted parameters within the framework of the chosen model. This analysis method is the only one that can be used, due to the nonlinearity of the detector's response matrix, which makes it impossible to invert.

However, the need to predetermine the fitted model implies that the results are biased by the initial hypothesis. Two different models can fit the data equally well. This fact, which is often being ignored by theoreticians, is important to realize when the spectral fits are interpreted. Key spectral properties such as the energy of the spectral peak put strong constraints on possible emission models. Below I show a few examples of different analysis methods *of the same data* that result in different spectral peak energies, slopes, and so forth and therefore lead to different theoretical interpretations.

2.2.2. The "Band" Model. In order to avoid biases towards a preferred physical emission model, GRB spectra are traditionally fitted with a mathematical function, which is known as the "Band" function (after the late David Band) [68]. This function had become the standard in this field and is often referred to as "Band model." The photon number spectra in this model are given by

$$N_{\rm ph}(E) = A \begin{cases} \left(\dfrac{E}{100\,\text{keV}}\right)^{\alpha} \exp\left(-\dfrac{E}{E_0}\right) & E < (\alpha-\beta)\,E_0 \\ \left[\dfrac{(\alpha-\beta)\,E_0}{100\,\text{keV}}\right]^{\alpha-\beta} \exp(\beta-\alpha) \left(\dfrac{E}{100\,\text{keV}}\right)^{\beta} & E \geq (\alpha-\beta)\,E_0. \end{cases} \quad (1)$$

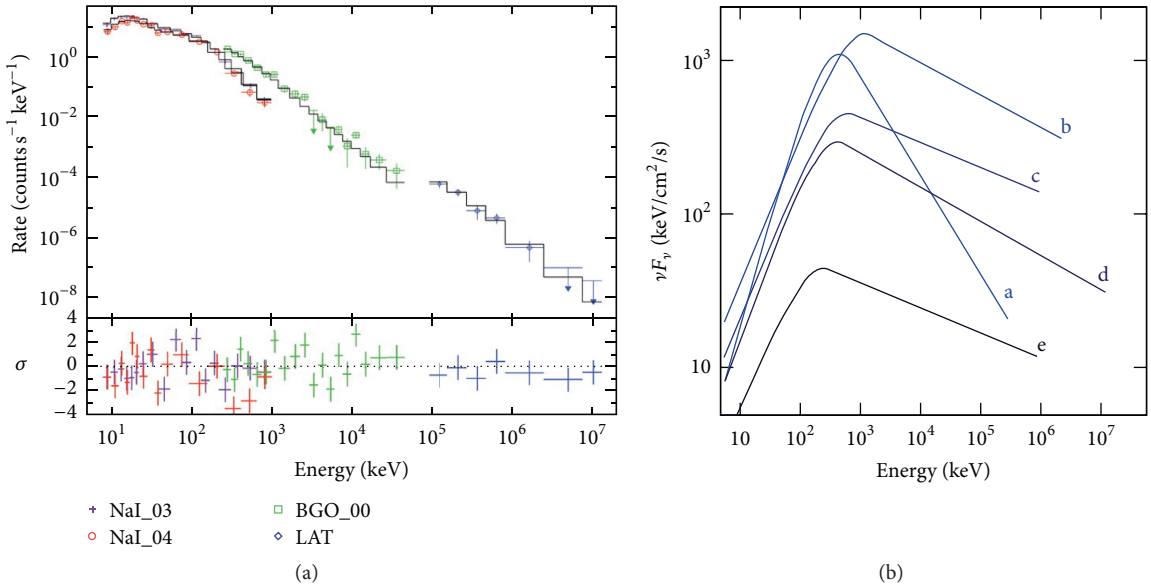

FIGURE 4: Spectra of GRB 080916C at the five time intervals (a–e) defined in Figure 3 are fitted with a "Band" function. (a) Count spectrum for NaI, BGO, and LAT in time bin b. (b) The model spectra in νF_ν units for all five time intervals, in which a flat spectrum would indicate equal energy per decade of photon energy, and the changing shapes show the evolution of the spectrum over time. The "broken power law" figure adopted from Abdo et al. [57].

This model thus has 4 free parameters: low energy spectral slope, α, high energy spectral slope, β, break energy, $\approx E_0$, and an overall normalization, A. It is found that such a simplistic model, which resembles a "broken power law" is capable of providing good fits to many different GRB spectra; see Figure 4 for an example. Thus, this model is by far the most widely used in describing GRB spectra.

Some variations of this model have been introduced in the literature. Examples are single power law (PL), "smooth broken power law" (SBPL), or "Comptonized model" (Comp) (see, e.g., [69–72]). These are very similar in nature and do not, in general, provide a better physical insight.

On the downside, clearly, having only 4 free parameters, this model is unable to capture complex spectral behavior that is known now to exist, such as the different temporal behavior of the high energy emission discussed above. Even more importantly, as will be discussed below, the limited number of free model parameters in this model can easily lead to wrong conclusions. Furthermore, this model, on purpose, is mathematical in nature, and therefore fitting the data with this model does not, by itself, provide any clue about the physical origin of the emission. In order to obtain such an insight, one has to compare the fitted results to the predictions of different theoretical models.

When using the "Band" model to fit a large number of bursts, the distribution of the key model parameters (the low and high energy slopes α and β and the peak energy $E_{\rm peak}$) is shown to be surprisingly narrow (see Figure 5). The spectral properties of the two categories, short and long GRBs, detected by both *BATSE*, *Integral* as well as *Fermi,* are very similar, with only minor differences [25, 69, 71–76]. The low energy spectral slope is roughly in the range $-1.5 < \alpha < 0$, averaging at $\langle\alpha\rangle \simeq -1$. The distribution of the high energy spectral slope peaks at $\langle\beta\rangle \simeq -2$. While typically $\beta < -1.3$, many bursts show a very steep β, consistent with an exponential cutoff. The peak energy averages around $\langle E_{\rm peak}\rangle \simeq 200$ keV, and it ranges from tens keV up to ~MeV (and even higher, in a few rare, exceptional bursts).

As can be seen in Figures 4 and 5, the "Band" fits to the spectra have three key spectral properties. (1) The prompt emission extends to very high energies, $\gtrsim$ MeV. This energy is above the threshold for pair production ($m_e = 0.511$ MeV), which is the original motivation for relativistic expansion of GRB outflows (see below). (2) The "Band" fits do not resemble a "Planck" function, hence the reason why thermal emission, which was initially suggested as the origin of GRB prompt spectra [77, 78], was quickly abandoned and not considered as a valid radiation process for a long time. (3) The values of the free "Band" model parameters, and in particular the value of the low energy spectral slope, α, are not easily fitted with any simply broadband radiative process such as synchrotron or synchrotron self-Compton (SSC). Although in some bursts, synchrotron emission could be used to fit the spectra (e.g., [79–82]), this is not the case in the vast majority of GRBs [83–86]. This was noted already in 1998, with the term "synchrotron line of death" coined by Preece et al. [84], to emphasise the inability of the synchrotron emission model to provide good fits to the spectra of (most) GRBs.

Indeed, these three observational properties introduce a major theoretical challenge, as currently no simple physically motivated model is able to provide convincing explanation to the observed spectra. However, as already discussed above, the "Band" fits suffer from several inherent major drawbacks, and therefore the obtained results must be treated with great care.

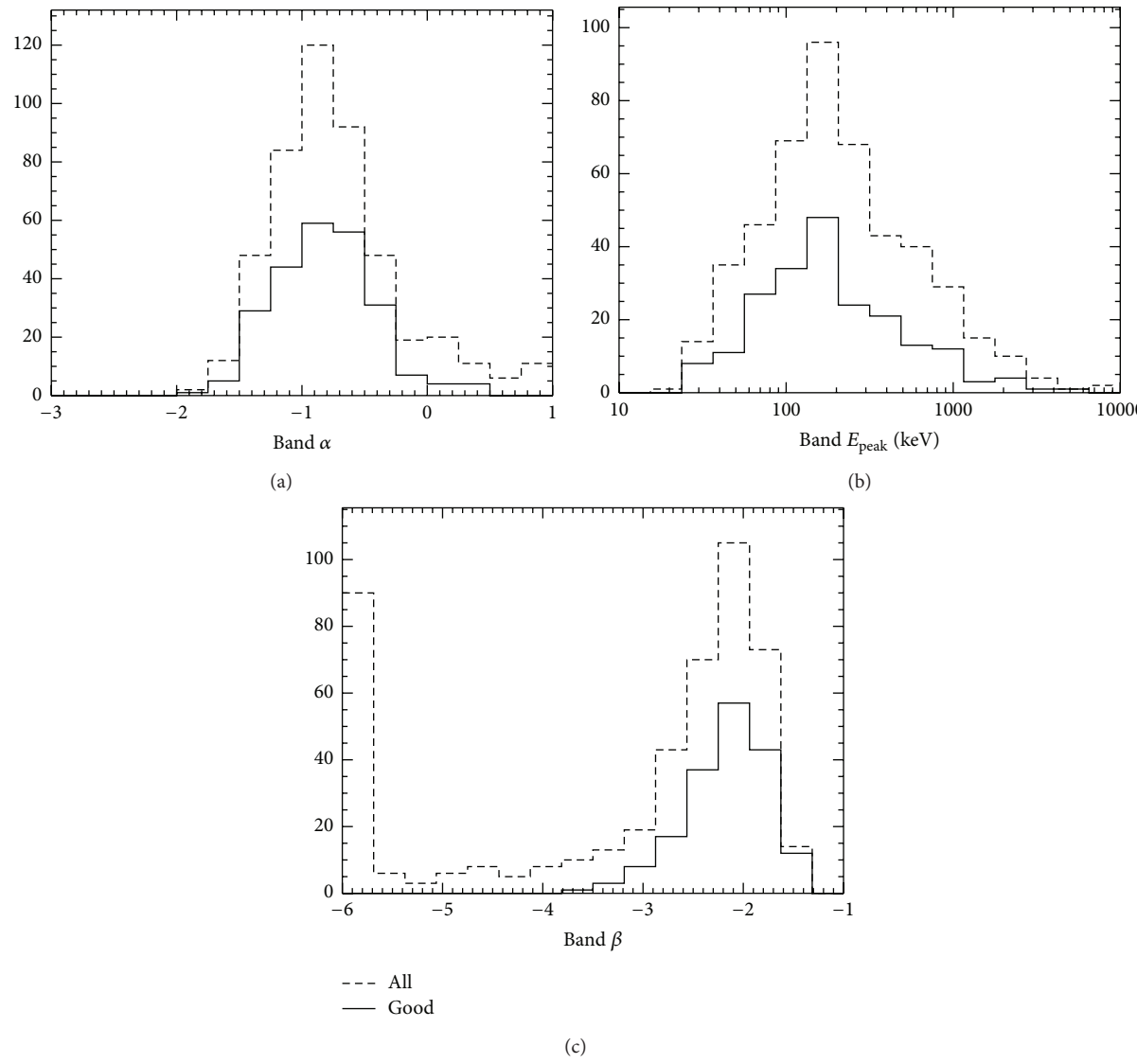

FIGURE 5: Histograms of the distributions of "Band" model free parameters: the low energy slope α (a), peak energy E_{peak} (b), and the high energy slope, β (c). The data represent 3800 spectra derived from 487 GRBs in the first *FERMI*-GBM catalogue. The difference between solid and dashed curves is the goodness of fits, the solid curve represent fits which were done under minimum χ^2 criteria, and the dash curves are for all GRBs in the catalogue. Figure adopted from Goldstein et al. [71].

2.2.3. "Hybrid" Model. An alternative model for fitting the GRB prompt spectra was proposed by Ryde [87, 88]. Being aware of the limitations of the "Band" model, when analyzing BATSE data, Ryde proposed a "hybrid" model that contains a thermal component (a Planck function) and a single power law to fit the nonthermal part of the spectra (presumably, resulting from Comptonization of the thermal photons). Ryde's hybrid model thus contain four free parameters, the same number of free parameters as the "Band" model: two parameters fit the thermal part of the spectrum (temperature and thermal flux) and two fit the nonthermal part. Thus, as opposed to the "Band" model which is mathematical in nature, Ryde's model suggests a physical interpretation to at least part of the observed spectra (the thermal part). An example of the fit is shown in Figure 6.

Clearly, a single power law cannot be considered a valid physical model in describing the nonthermal part of the spectra, as it diverges. Nonetheless, it can be acceptable approximation when considering a limited energy range, as was available when analyzing BATSE data. While the hybrid model was able to provide comparable or even better fits with respect to the "Band" model to several dozens bright GRBs [87–91], it was shown that this model overpredicts the flux at low energies (X-ray range) for many GRBs [92, 93]. This discrepancy, however, can easily be explained by the oversimplification of the use of a single power law as a way to describe the nonthermal spectra both above and below the thermal peak. From a physical perspective, one expects Comptonization to modify the spectra above the thermal peak, but not below it; see discussion below.

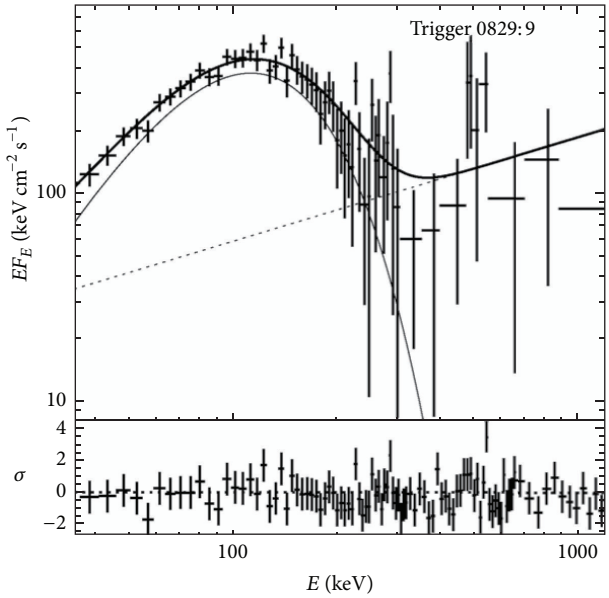

FIGURE 6: A "hybrid" model fit to the spectra of GRB 910927 detected by BATSE. Figure courtesy of Ryde.

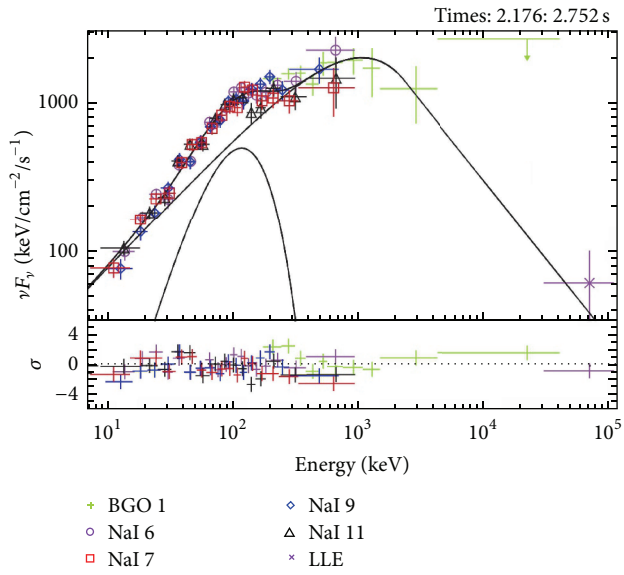

FIGURE 7: The spectra of GRB110721A are best fit with a "Band" model (peaking at $E_{\text{peak}} \sim 1$ MeV) and a blackbody component (having temperature $T \sim 100$ keV). The advantage over using just a "Band" function is evident when looking at the residuals (taken from Iyyani et al. [99]).

As *Fermi* enables a much broader spectral coverage than BATSE, in recent years Ryde's hybrid model could be confronted with data over a broader spectral range. Indeed, it was found that in several bursts (e.g., GRB090510 [94], GRB090902B [95–97], GRB110721A [98, 99], GRB100724B [100], GRB100507 [101], or GRB120323A [102]) the broad-band spectra are best fitted with a combined "Band + thermal" model (see Figure 7). In these fits, the peak of the thermal component is always found to be below the peak energy of the "Band" part of the spectrum. This is consistent with the rising "single power law" that was used in fitting the band-limited nonthermal spectra.

The "Band + thermal" model fits require six free parameters, as opposed to the four free parameters in both the "Band" and in the original "hybrid" models. While this is considered as a drawback, this model has several notable advantages. First, this model does not suffer from the energy divergence of a single power law fit, as in Ryde's original proposal. Second, in comparison with "Band" model fits, it shows significant improvement in quality, both in statistical errors (reduced χ^2), and even more importantly by the behavior of the residuals: when fitting the data with a "Band" function, often the residuals to the fit show a "wiggly" behavior, implying that they are not randomly distributed. This is solved when adding the thermal component to the fits.

Similar to Ryde's original model, fits with "Band + thermal" model can provide a physical explanation to only the thermal part of the spectra; they still do not suggest physical origin to the nonthermal part of the spectra. Nonetheless, the addition of the thermal part implies that the values of the free model parameters used in fitting the nonthermal part, such as the low energy spectral slope (α), as well as the peak energy E_{peak}, are different than the values that would have been obtained by pure "Band" fits (namely, without the thermal component; see [102–105]). In some bursts, the new values obtained are consistent with the predictions of synchrotron theory, suggesting a synchrotron origin of the nonthermal part [106, 107]. However, in many cases this interpretation is insufficient (e.g., [108]); see further discussion below. Another (relatively minor) drawback of these fits is that, from a theoretical perspective, even if a thermal component exists in the spectra, it is expected to have the shape of a gray-body rather than a pure "Planck," due to light aberration (see below).

One therefore concludes that the "Band + thermal" fits which became very popular recently can be viewed as an intermediate step towards full physically motivated fits of the spectra. They contain a mix of a physically motivated part (the thermal part) with an addition mathematical function (the "Band" part) whose physical origin still needs clarification.

As of today, pure "Planck" spectral component is clearly identified in only a very small fraction of bursts. Nonetheless, there is a good reason to believe that it is in fact very ubiquitous and that the main reason it is not clearly identified is due to its distortion. A recent work [109] examined the width of the spectral peak, quantified by W, the ratio of energies that define the full width half maximum (FWHM). The results of an analysis of over 2900 different BATSE and *Fermi* bursts are shown in Figure 8. The smaller W is, the narrower the spectral width is. Imposed on the sample are the line representing the spectral width from a pure "Planck" (black) and a line representing the spectral width for slow cooling synchrotron (red). Fast cooling synchrotron results in much wider spectral width, which would be shown to the far right of this plot. Thus, while virtually all the spectral width is wider than "Planck", over ~80% are narrower than

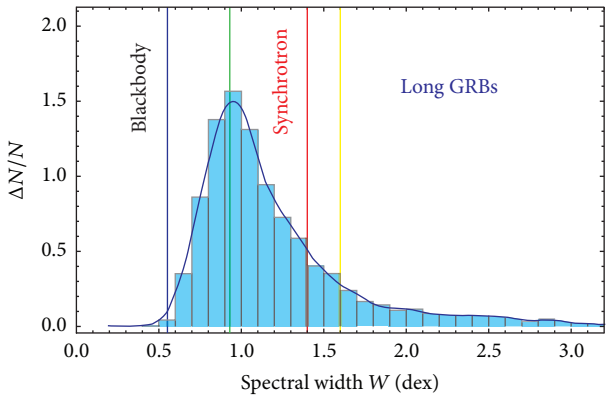

FIGURE 8: Full width half maximum of the spectral peaks of over 2900 bursts fitted with the "Band" function. The narrow most spectra are compatible with a "Planck" spectrum. About ~80% of the spectra are too narrow to be fitted with the (slow cooling) synchrotron emission model (red line). When fast cooling is added, nearly 100% of the spectra are too narrow to be compatible with this model. As it is physically impossible to narrow the broadband synchrotron spectra, these results thus suggest that the spectral peak is due to some widening mechanism of the Planck spectrum, which are therefore pronounced (indirectly) in the vast majority of spectra. Figure taken from Axelsson and Borgonovo [109].

what is allowed by the synchrotron model. On the one hand, "narrowing" a synchrotron spectra is (nearly) impossible. However, there are various ways, which will be discussed below in which pure "Planck" spectra can be broadened. Thus, although "pure" Planck is very rare, these data suggest that broadening of the "Planck" spectra plays a major role in shaping the spectral shape of the vast majority of GRB spectra.

2.2.4. Time Resolved Spectral Analysis. Ryde's original analysis is based on time resolved spectra. The light curve is cut into time bins (having typical duration $\gtrsim$1 s), and the spectra at each time bin are analyzed independently. This approach clearly limits the number of bursts that could be analyzed in this method to only the brightest ones, presumably those showing smooth light curve over several tens of seconds (namely, mainly the long GRBs). However, its great advantage is that it enables detecting temporal evolution in the properties of the fitted parameters, in particular, in the temperature and flux of the thermal component.

One of the key results of the analysis carried by Ryde and Pe'er [89] is the well defined temporal behavior of both the temperature and flux of the thermal component. Both the temperature and flux evolve as a broken power law in time: $T \propto t^{\alpha}$, and $F \propto t^{\beta}$, with $\alpha \simeq 0$ and $\beta \simeq 0.6$ at $t < t_{\rm brk} \approx$ few s, and $\alpha \simeq -0.68$ and $\beta \simeq -2$ at later times (see Figure 9). This temporal behavior was found among all sources in which thermal emission could be identified. It may therefore provide a strong clue about the nature of the prompt emission, in at least those GRBs for which thermal component was identified. To my personal view, these findings may hold the key to understanding the origin of the prompt emission and possibly the nature of the progenitor.

Due to *Fermi*'s much greater sensitivity, time resolved spectral analysis is today in broad use. This enables observing temporal evolution not only of the thermal component, but of other parts of the spectra as well (see, e.g., Figure 4). As an example, a recent analysis of GRB130427A reveals a temporal change in the peak energy during the first 2.5 s of the burst, which could be interpreted as being due to synchrotron origin [110].

2.2.5. Distinguished High Energy Component. Prior to the *Fermi* era, time resolved spectral analysis was very difficult to conduct due to the relatively low sensitivity of the *BATSE* detector, and therefore its use was limited to bright GRBs with smooth light curve. However, *Fermi's* superb sensitivity enables carrying time resolved analysis to many more bursts. One of the findings is the delayed onset of GeV emission with respect to emission at lower energies which is seen in a substantial fraction of LAT bursts (see, e.g., Figure 3). This delayed onset is further accompanied by a long lived emission ($\gtrsim 10^2$ s) and separate light curve [57, 95, 111, 112]. The GeV emission decays as a power law in time, $L_{\rm GeV} \propto t^{-1.2}$ [113–115]. Furthermore, the GeV emission shows smooth decay (see Figure 10). This behavior naturally points towards a separate origin of the GeV and lower energy photons; see discussion below.

Thus, one can conclude that at this point in time (Dec. 2014), evidence exist for three separate components in GRB spectra: (I) a thermal component, peaking typically at ~100 keV; (II) a nonthermal component, whose origin is not fully clear, peaking at $\lesssim$MeV and lacking clear physical picture, fitted with a "Band" function; and (III) a third component, at very high energies ($\gtrsim$100 MeV) showing a separate temporal evolution [75, 105].

Not all three components are clearly identified in all GRBs; in fact, separate evolution of the high energy part is observed in only a handful of GRBs. The fraction of GRBs which show clear evidence for the existence of a thermal component is not fully clear; it seems to depend on the brightness, with bright GRBs more likely to show evidence for a thermal component (up to 50% of bright GRBs show clear evidence for a separate thermal component ([105] and Larsson et. al., in prep.)). Furthermore, this fraction is sensitive to the analysis method. Thus, final conclusions are still lacking.

Even more interestingly, it is not at all clear that the "bump" identified as a thermal component is indeed such; such a bump could have other origins as well (see discussion below). Thus, I think it is fair to claim that we are now in a transition phase: on the one hand, it is clear that fitting the data with a pure "Band" model is insufficient, and thus more complicated models, which are capable of capturing more subtle features of the spectra, are being used. On the other hand, these models are still not fully physically motivated, and thus a full physical insight of the origin of prompt emission is still lacking.

2.3. Polarization. The leading models of the nonthermal emission, namely, synchrotron emission and Compton

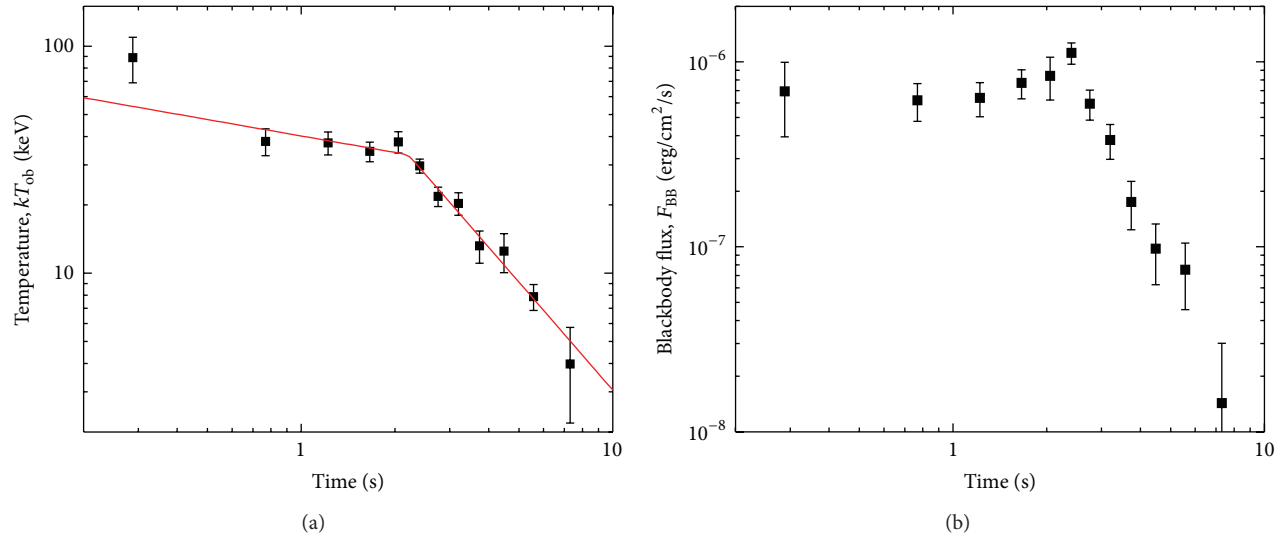

FIGURE 9: (a) The temperature of the thermal component of GRB110721A at different time bins shows a clear "broken power law" with $T(t) \sim t^{-0.25}$ before $t_{brk} \sim 3$ s, and $T(t) \sim t^{-0.67}$ at later times. (b) The flux of the thermal component shows a similar broken power law temporal behavior, with similar break time. At late times, $F_{BB}(t) \propto t^{-2}$. See Ryde and Pe'er [89] for details. Figure courtesy of Ryde.

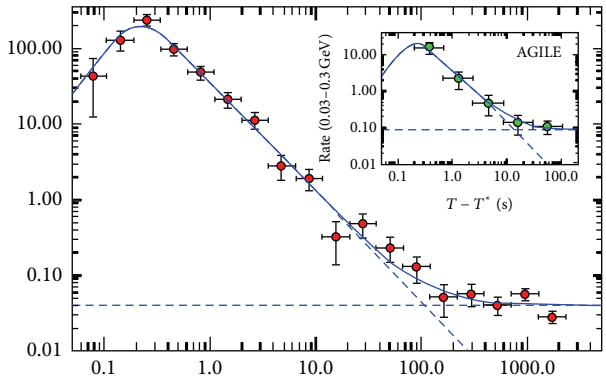

FIGURE 10: Light curve of the emission of GRB090510 above 100 MeV extends to >100 s and can be fitted with a smoothly broken power law. The times are scaled to the time $T^* = 0.6$ s after the GBM trigger. The inset shows the AGILE light curve (energy range 30–300 MeV), extending to much shorter times. Figure taken from Ghirlanda et al. [113].

scattering, both produce highly polarized emission [118]. Nonetheless, due to the spherical assumption, the inability to spatially resolve the sources, and the fact that polarization was initially discovered only during the afterglow phase [119, 120], polarization was initially discussed only in the context of GRB afterglow, but not the prompt phase (e.g., [121–125]).

The first claim of highly linearly polarized prompt emission in a GRB, $\Pi = (80 \pm 20)\%$ in GRB021206 by RHESSI [126], was disputed by a later analysis [127]. A later analysis of BATSE data shows that the prompt emission of GRB930131 and GRB96092 is consistent with having high linear polarization, $\Pi > 35\%$ and $\Pi > 50\%$; though the exact degree of polarization could not be well constrained [128]. Similarly, Kalemci et al. [129], McGlynn et al. [130], and Götz et al. [131] showed that the prompt spectrum of GRB041219a observed by *Integral* is consistent with being highly polarized, but with no statistical significance.

Recently, high linear polarization, $\Pi = (27 \pm 11)\%$ was observed in the prompt phase of GRB 100826a by the GAP instrument on board IKAROS satellite [132]. As opposed to former measurements, the significance level of this measurement is high, 2.9σ. High linear polarization degree was further detected in GRB110301a ($\Pi = 70 \pm 22\%$) with 3.7σ confidence, and in GRB100826a ($\Pi = 84^{+16}_{-28}\%$) with 3.3σ confidence [133].

As of today, there is no agreed theoretical interpretation to the observed spectra (see discussion below). However, different theoretical models predict different levels of polarization, which are correlated with the different spectra. Therefore, polarization measurements have a tremendous potential in shedding new light on the different theoretical models and may hold the key in discriminating between them.

2.4. Emission at Other Wavebands. Clearly, the prompt emission spectra are not necessarily limited to those wavebands that can be detected by existing satellites. Although broadband spectral coverage is important in providing clues to the origin of the prompt emission and the nature of GRBs, due to their random nature and to the short duration, it is extremely difficult to observe the prompt emission without fast, accurate triggering.

As the physical origin of the prompt emission is not fully clear, it is difficult to estimate the flux at wavebands other than observed. Naively, the flux is estimated by interpolating the "Band" function to the required energy (e.g., [134]). However, as discussed above (and proved in the past), this method is misleading, as (1) the "Band" model is a very crude approximation to a more complicated spectra and (2) the values of the "Band" model low and high energy slopes change when new components are added. Thus, it

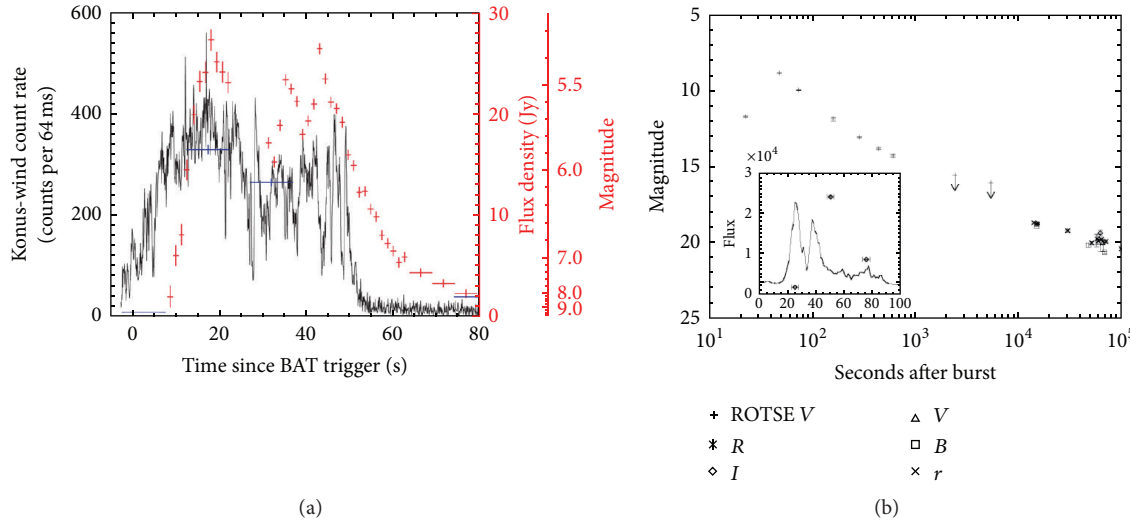

(a) (b)

Figure 11: (a) Gamma-ray light curve (black) and optical data from "Pi in the sky" (blue) and "Tortora" (red) of GRB080319B show how the optical component traces the γ-ray component. Figure taken from Racusin et al. [116]. (b) Gamma-ray and optical light curve of GRB990123 show that the optical light curve lags behind the γ-rays. Figure taken from Akerlof et al. [117].

is of no surprise that early estimates were not matched by observations.

2.4.1. High Energy Counterpart. At high energies, there has been one claim of possible TeV emission associated with GRB970417a [135]. However, since then, no other confirmed detections of high energy photons associated with any GRB prompt emission were reported. Despite numerous attempts, only upper limits on the very high energy flux were obtained by the different detectors (MAGIC [136, 137], MILAGRO (Milagro Collaboration: [138]), HESS [139–141], VERITAS [142], and HAWC [143]).

2.4.2. Optical Counterpart. At lower energies (optic, X), there have been several long GRBs for which a precursor (or a very long prompt emission duration) enabled fast slew of ground based robotic telescopes (and/or Swift XRT and UVOT detectors) to the source during the prompt phase. The first ever detection of optical emission during the prompt phase of a GRB was that of GRB990123 [117]. Other examples of optical detection are GRB041219A [144], GRB060124 [145], GRB 061121 [146], the "naked eye" GRB080319B [116], GRB080603A [147], GRB080928 [148], GRB090727 [149], GRB121217a [150], GRB1304a7A [151], and GRB130925a [152] for a partial list.

The results are diverse. In some cases (e.g., GRB990123), the peak of the optical flux lags behind that of the γ-ray flux, while in other GRBs (e.g., GRB080319B), no lag is observed. This is shown in Figure 11. Similarly, while in some bursts, such as GRB080319B or GRB090727, the optical flux is several orders of magnitude higher than that obtained by direct interpolation of the "Band" function from the X/γ ray band, in other bursts, such as GRB080928, it seems to be fitted well with a broken-power law extending at all energies (see Figure 12). To further add to the confusion, some GRBs show complex temporal and spectral behavior, in which the optical flux and light curve changes its properties (with respect to the X/γ emission) with time. Examples are GRB050820 [153] and GRB110205A [154].

These different properties hint towards different origin of the optical emission. It should be stressed that due to the observational constraints, optical counterparts are observed to date only in very long GRBs, with typical T_{90} of hundreds of seconds (or more). Thus, the optical emission may be viewed as part of the prompt phase, but also as part of the early afterglow; it may result from the reverse shock which takes place during the early afterglow epoch. See further discussion below.

2.5. Correlations. There have been several claims in the past for correlations between various observables of the prompt GRB emission. Clearly, such correlations could potentially be extremely useful in both understanding the origin of the emission, as well as the ability to use GRBs as probes, for example, "standard candles" similar to supernova Ia. However, a word of caution is needed: as already discussed, many of the correlations are based on values of fitted parameters, such as $E_{\rm pk}$, which are sensitive to the fitted model chosen, typically, the "Band" function. As more refined models, such as the addition of a thermal component, can change the peak energy, the claimed correlation may need to be modified. Since final conclusion about the best physically motivated model that can describe the prompt emission spectra has not emerged yet, it is too early to know the modification that may be required to the claimed correlations. Similarly, some of the correlations are based on the prompt emission duration, which is ill-defined.

The first correlation was found between the peak energy (identified as temperature) and luminosity of single pulses within the prompt emission [155]. They found $L \propto E_{\rm peak}^{\alpha}$,

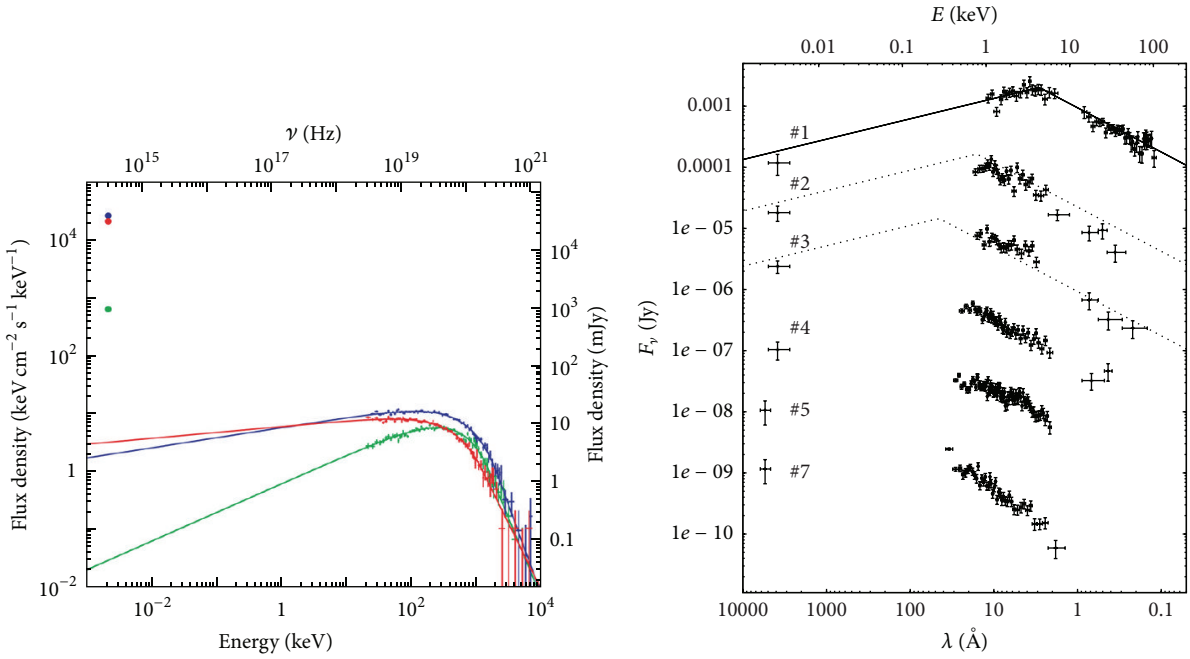

FIGURE 12: (a) The "Pi in the Sky" and Konus-wind flux at 3 time intervals (fitted by a "Band" model) of GRB080319B. The optical flux is 2-3 orders of magnitude above the direct interpolation. Figure taken from Racusin et al. [116]. (b) Combined UVOT and X/γ ray data of GRB080928 at early times are fitted with a broken power law. For this burst, the slope is consistent with having synchrotron origin. Figure taken from Rossi et al. [148].

with $\alpha \sim 1.6$. These results were confirmed by Kargatis et al. [156], though the errors on α were large, as $\alpha \simeq 1.5$–1.7.

A similar correlation between the (redshift corrected) peak energy and the (isotropic equivalent) total gamma-ray energy of different bursts was reported by Amati et al. [157], namely, $E_{\mathrm{peak},z} \propto E^{\alpha}_{\gamma,\mathrm{iso}}$, with $\alpha \sim 0.5$ [157–159]. Here, $E_{\mathrm{peak},z} = E_{\mathrm{peak}}(1+z)$. This became known as the "Amati relation."

The Amati relation has been questioned by several authors, claiming that it is an artifact of a selection effect or biases (e.g., [160–166]). However, counter arguments are that even if such selection effects exist, they cannot completely exclude the correlation [167–171]. To conclude, it seem that current data (and analysis method) do support some correlation, though with wide scatter. This scatter still needs to be understood before the correlation could be used as a tool, for example, for cosmological studies [172, 173].

There are a few other notable correlations that were found in recent years. One is a correlation between the (redshift corrected) peak energy $E_{\mathrm{peak},z}$ and the isotropic luminosity in γ-rays at the peak flux, $L_{\gamma,\mathrm{peak,iso}}$ [174, 175]: $E_{\mathrm{peak},z} \propto L^{0.52}_{\gamma,p,\mathrm{iso}}$. A second correlation is between $E_{\mathrm{peak},z}$ and the geometrically corrected gamma-ray energy, $E_\gamma \simeq (\theta_j^2/2)E_{\gamma,\mathrm{iso}}$, where θ_j is the jet opening angle (inferred from afterglow observations): $E_{\mathrm{peak},z} \propto E_\gamma^{0.7}$ [176]. It was argued that this relation is tighter than the Amati relation; however, it relies on the correct interpretation of breaks in the afterglow light curve to be associated with jet breaks, which can be problematic [177–181].

Several other proposed correlations exist; I refer the reader to Kumar and Zhang [15], for a full list.

3. Theoretical Framework

Perhaps the easiest way to understand the nature of GRBs is to follow the different episodes of energy conversion. Although the details of the energy transfer are still highly debatable, there is a wide agreement, based on firm observational evidence, that there are several key episodes of energy conversion in GRBs. (1) Initially, a large amount of energy, $\sim 10^{53}$ erg or more, is released in a very short time, in a compact region. The source of this energy must be gravitational. (2) Substantial part of this energy is converted into kinetic energy, in the form of relativistic outflow. This is the stage in which GRB jets are formed and accelerated to relativistic velocities. The exact nature of this acceleration process, and in particular the role played by magnetic fields in it, is still not fully clear. (3) Part of this kinetic energy is dissipated and is used in producing the gamma-rays that we observe in the prompt emission. Note that part of the observed prompt emission (the thermal part) may originate directly from photons emitted during the initial explosion; the energy carried by these photons is therefore not initially converted to kinetic form. (4) The remaining of the kinetic energy (still in the form of relativistic jet) runs into the interstellar medium

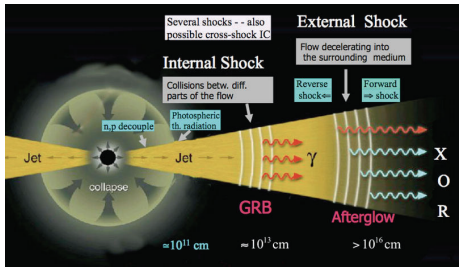

Figure 13: Cartoon showing the basic ingredients of the GRB "fireball" model. (1) The source of energy is a collapse of a massive star (or merger of NS-NS or NS-BH, not shown here). (2) Part of this energy is used in producing the relativistic jet. This could be mediated by hot photons ("fireball"), or by magnetic field. (3) The thermal photons decouple at the photosphere. (4) Part of the jet kinetic energy is dissipated (by internal collisions, in this picture) to produce the observed γ rays. (5) The remaining kinetic energy is deposited into the surrounding medium, heating it and producing the observed afterglow. Cartoon is taken from Meszaros and Rees [17].

(ISM) and heats it, producing the observed afterglow. The kinetic energy is thus gradually converted into heat, and the afterglow gradually fades away. A cartoon showing these basic ingredients in the context of the "fireball" model is shown in Figure 13, adapted from Meszaros and Rees [17].

3.1. Progenitors. The key properties that are required from GRB progenitors are (1) the ability to release a huge amount of energy, $\sim 10^{52}$-10^{53} erg (possibly even larger), within the observed GRB duration of few seconds and (2) the ability to explain the fast time variability observed, $\delta t \gtrsim 10^{-3}$ s, implying (via light crossing time argument) that the energy source must be compact: $R \sim c\delta t \sim 300$ km, namely, of stellar size.

While 20 years ago, over hundred different models were proposed in explaining possible GRB progenitors (see [182]), natural selection (namely, confrontation with observations over the years) led to the survival of two main scenarios. The first is a merger of two neutron stars (NS-NS), or a black hole and a neutron star (BH-NS). The occurrence rate and the expected energy released $\sim GM^2/R \sim 10^{53}$ erg (using $M \sim M_\odot$ and $R \gtrsim R_{\rm sch.}$, the Scharzschild radius of stellar-size black hole) are sufficient for extragalactic GRBs [183–187]. The alternative scenario is the core collapse of a massive star, accompanied by accretion into a black hole ([188–194] and references therein). In this scenario, similar amount of energy, up to $\sim 10^{54}$ erg, may be released by tapping the rotational energy of a Kerr black hole formed in the core collapse and/or the inner layers of the accretion disk.

The observational association of long GRBs to type Ib/c supernova discussed above, as well as the time scale of the collapse event, $\lesssim$1 minute, which is similar to that observed in long GRBs, makes the core collapse, or "collapsar" model, the leading model for explaining long GRBs. The merger scenario, on the other hand, is currently the leading model in explaining short GRBs (see, e.g., discussions in [5, 8, 16]).

3.2. Relativistic Expansion and Kinetic Energy Dissipation: The "Fireball" Model. A GRB event is associated with a catastrophic energy release of a stellar size object. The huge amount of energy, $\sim 10^{52}$-10^{53} erg released in such a short time and compact volume, results in a copious production of neutrinos, antineutrinos (initially in thermal equilibrium) and possible release of gravitational waves. These two, by far the most dominant energy forms are yet not detected. A smaller fraction of the energy (of the order 10^{-3}-10^{-2} of the total energy released) goes into high temperature ($\gtrsim$ MeV) plasma, containing photons, $e^\pm$ pairs, and baryons, known as "fireball" [195]. The fireball may contain a comparable, or even larger amount of magnetic energy, in which case it is Poynting flux dominated [196–201] (some authors use the phrase "cold fireball" in describing magnetically dominated ejecta, as opposed to "hot fireballs"; here, I will simply use the term "fireball" regardless of the fraction of energy stored in the magnetic field).

The scaling laws that govern the expansion of the fireball depend on its magnetization. Thus, one must discriminate between photon-dominated (or magnetically-poor) outflow and magnetic dominated outflow. I discuss in this section the photon-dominated one ("hot fireball"). Magnetic dominated outflow ("cold fireball") will be discussed in the next section (Section 3.3).

3.2.1. Photon Dominated Outflow. Let us consider first photon-dominated outflow. In this model, it is assumed that a large fraction of the energy released during the collapse/merger is converted directly into photons close to the jet core, at radius r_0 (which should be $\gtrsim$ the Schwarzschild radius of the newly formed black hole). The photon temperature is

$$T_0 = \left(\frac{L}{4\pi r_0^2 ca}\right)^{1/4} = 1.2 L_{52}^{1/4} r_{0,7}^{-1/2}\ {\rm MeV}, \qquad (2)$$

where a is the radiation constant, L is the luminosity, and $Q = 10^x Q_x$ in cgs units is used here and below. This temperature is above the threshold for pair production, implying that a large number of $e^\pm$ pairs are created via photon-photon interactions (and justifying the assumption of full thermalization). The observed luminosity is many orders of magnitude above the Eddington luminosity, $L_E = 4\pi GMm_p c/\sigma_T = 1.25 \times 10^{38} (M/M_\odot)\ {\rm erg\ s^{-1}}$, implying that radiation pressure is much larger than self-gravity, and the fireball must expand.

The dynamics of the expected relativistic fireball were first investigated by Goodman [77], Paczynski [78], and Shemi and Piran [202]. The ultimate velocity it will reach depends on the amount of baryons (baryon load) within the fireball [184], which is uncertain. The baryon load can be deduced from observations: as the final expansion kinetic energy cannot exceed the explosion energy, the highest Lorentz factor that can be reached is $\Gamma_{\rm max} = E/Mc^2$. Thus, the fact that GRBs are known to have high bulk Lorentz factors, $\Gamma \gtrsim 10^2$ at later stages (during the prompt and afterglow emission) [203–212], implies that only a small fraction of the baryons in the progenitor star(s) is in fact accelerated and reach relativistic velocities.

3.2.2. Scaling Laws for Relativistic Expansion: Instantaneous Energy Release. The scaling laws for the fireball evolution follow conservation of energy and entropy. Let us assume first that the energy release is "instantaneous," namely, within a shell of size $\delta r \sim r_0$. Thus, the total energy contained within the shell (as seen by an observer outside the expanding shell) is

$$E^{\rm ob} \propto \Gamma(r) V' T'(r)^4 \propto \Gamma(r) r^2 \Gamma(r) r_0 T'(r)^4 = \text{const.} \quad (3)$$

Here, $T'(r)$ is the shell's comoving temperature, and $V' = 4\pi r^2 \delta r'$ is its comoving volume. Note that the first factor of $\Gamma(r)$ is needed in converting the comoving energy to the observed energy, and the second originates from transformation of the shell's width: the shell's comoving width (as measured by a comoving observer within it) is related to its width as measured in the lab frame (r_0) by $\delta r' = \Gamma(r) r_0$.

Starting from the fundamental thermodynamic relation, $dS = (dU + pdV)/T$, one can write the entropy of a fluid component with zero chemical potential (such as photon fluid) in its comoving frame, $S' = V'(u' + p')/T'$. Here, u', p' are the internal energy density and pressure measured in the comoving frame. For photons, $p' = u'/3 \propto T'^4$. Since initially, both the rest mass and energy of the baryons are negligible, the entropy is provided by the photons. Thus, conservation of entropy implies

$$S' \propto V' T'(r)^3 \propto r^2 \Gamma(r) r_0 T'(r)^3 = \text{const.} \quad (4)$$

Dividing (3) and (4), one obtains $\Gamma(r)T'(r) = \text{const}$, from which (using again these equations) one can write the scaling laws of the fireball evolution,

$$\begin{aligned} T'(r) &\propto r^{-1}; \\ \Gamma(r) &\propto r; \\ V'(r) &\propto r^3. \end{aligned} \quad (5)$$

As the shell accelerates, the baryon kinetic energy $\Gamma(r)Mc^2$ increases, until it becomes comparable to the total fireball energy (the energy released in the explosion) at $\Gamma = \Gamma_{\rm max} \simeq \eta$, at radius $r_s \sim \eta r_0$ (assuming that the outflow is still optically thick at r_s, and so the acceleration can continue until this radius). Here, $\eta \equiv E/Mc^2$ is the specific entropy per baryon. Note that during the acceleration phase, the shell's kinetic energy increase comes at the expense of the (comoving) internal energy, as is reflected by the fact that the comoving temperature drops.

Beyond the saturation radius r_s, most of the available energy is in kinetic form, and so the flow can no longer accelerate, and it coasts. The spatial evolution of the Lorentz factor is thus

$$\Gamma(r) = \begin{cases} \left(\dfrac{r}{r_0}\right) & r \lesssim r_s; \\ \eta & r \gtrsim r_s. \end{cases} \quad (6)$$

Equation (4) that describes conservation of (comoving) entropy holds in this regime as well; therefore, in the regime $r > r_s$ one obtains $r^2 T'(r)^3 = \text{const}$, or

$$\begin{aligned} \Gamma(r) &= \eta; \\ T'(r) &\propto r^{-2/3}; \\ V'(r) &\propto r^2. \end{aligned} \quad (7)$$

The observed temperature therefore evolves with radius as

$$T^{\rm ob}(r) = \Gamma(r) T'(r) = \begin{cases} T_0 & r < r_s; \\ T_0 \times \left(\dfrac{r}{r_s}\right)^{-2/3} & r > r_s. \end{cases} \quad (8)$$

3.2.3. Continuous Energy Release. Let us assume next that the energy is released over a longer duration, $t \gg r_0/c$ (as is the case in long GRBs). In this scenario, the progenitor continuously emits energy at a rate L (erg/s), and this emission is accompanied by mass ejected at a rate $\dot{M} = L/\eta c^2$. The analysis carried above is valid for each fluid element separately, provided that E is replaced by L and M by $\dot{M}$, and thus the scaling laws derived above for the evolution of the (average) Lorentz factor and temperature as a function of radius hold. However, there are a few additions to this scenario.

We first note the following [1]. The comoving number density of baryons follows mass conservation:

$$n'_p(r) = \frac{\dot{M}}{4\pi r^2 m_p c \Gamma(r)} = \frac{L}{4\pi r^2 m_p c^3 \eta \Gamma(r)} \quad (9)$$

(assuming spherical explosion). Below r_s, the (comoving) energy density of each fluid element is relativistic, $aT'(r)^4/n'_p m_p c^2 = \eta(r_0/r)$. Thus, the speed of sound in the comoving frame is $c_s \simeq c/\sqrt{3} \sim c$. The time a fluid element takes to expand to radius r, r/c in the observer frame, corresponds to time $t' \sim r/\Gamma c$ in the comoving frame; during this time, sound waves propagate a distance $t' c_s \sim rc/\Gamma c = r/\Gamma$ (in the comoving frame), which is equal to $r/\Gamma^2 = r_0^2/r$ in the observer frame. This implies that at the early stages of the expansion, where $r \gtrsim r_0$, sound waves have enough time to smooth spatial fluctuations on scale $\sim r_0$. On the other hand, regions separated by $\Delta r > r_0$ cannot interact with each other. As a result, fluctuations in the energy emission rate would result in the ejection and propagation of a collection of independent subshells, each having typical thickness r_0.

Each fluid element may have a slightly different density and thus have a slightly different terminal Lorentz factor; the standard assumption is $\delta\Gamma \sim \eta$. This implies a velocity spread $\delta v = v_1 - v_2 \approx c/2\eta^2$, where η is the characteristic value of the terminal Lorentz factor. If such two fluid elements originate within a shell (of initial thickness r_0), spreading between these fluid elements will occur after typical time $t_{\rm spread} = r_0/\delta v$ and at radius (in the observer's frame) [213]

$$r_{\rm spread} = v_2 t_{\rm spread} \simeq c r_0 \left(\frac{2\eta^2}{c}\right) \simeq 2\eta^2 r_0. \quad (10)$$

According to the discussion above, this is also the typical radius where two separate shells will begin to interact (sometimes referred to as the "collision radius", $r_{\rm col}$).

The spreading radius is a factor η larger than the saturation radius. Thus, no internal collisions are expected during the acceleration phase, namely, at $r < r_s$. Below the spreading radius individual shell's thickness (in the observer's frame), δr, is approximately constant and equal to r_0. At larger radii, $r > r_{\rm spread}$, it becomes $\delta r = r\delta v/c \sim r/\eta^2$.

Since the comoving radial width of each shell is $\delta r' = \Gamma \delta r$, it can be written as

$$\delta r' \sim \begin{cases} r_0\Gamma \sim r & r < r_s \\ r_0\eta & r_s < r < r_{\rm spread} \\ \dfrac{r}{\eta} & r > r_{\rm spread}. \end{cases} \tag{11}$$

The comoving volume of each subshell, $V' \propto r^2\delta r'$, is thus

$$V' \propto r^2\delta r' \sim \begin{cases} r^3 & r < r_s \\ r_0\eta & r^2 r_s < r < r_{\rm spread} \\ \dfrac{r^3}{\eta} & r > r_{\rm spread}. \end{cases} \tag{12}$$

3.2.4. Internal Collisions as Possible Mechanism of Kinetic Energy Dissipation. At radii $r > r_{\rm spread} = r_{\rm coll}$, spreading within a single shell, as well as interaction between two consecutive shells, becomes possible. The idea of shell collision was suggested early on [214–218], as a way to dissipate the jet kinetic energy and convert it into the observed radiation.

The key advantages of the internal collision model are (1) its simplicity: it is a very straightforward idea that naturally rises from the discussion above; (2) it is capable of explaining the rapid variability observed; and (3) the internal collisions are accompanied by (internal) shock waves. It is believed that these shock waves are capable of accelerating particles to high energies, via *Fermi* mechanism. The energetic particles, in turn, can emit the high-energy, nonthermal photons observed, for example, via synchrotron emission. Thus, the internal collisions is believed to be an essential part in this energy conversion chain that results in the production of γ-rays.

On the other hand, the main drawbacks of the model are (1) the very low efficiency of energy conversion; (2) by itself, the model does not explain the observed spectra, only suggests a way in which the kinetic energy can be dissipated. In order to explain the observed spectra, one needs to add further assumptions about how the dissipated energy is used in producing the photons (e.g., assumptions about particle acceleration, etc.). Furthermore, as will be discussed in Section 3.5 below, it is impossible to explain the observed spectra within the framework of this model using standard radiative processes (such as synchrotron emission or Compton scattering), without invoking additional assumptions external to it; (3) lack of predictivity: while it does suggest a way of dissipating the kinetic energy, it does not provide many details, such as the time in which dissipations are expected, or the amount of energy that should be dissipated in each collision (only rough limits). Thus, it lacks a predictive power.

The basic assumption is that at radius $r_{\rm coll} = r_{\rm spread}$ two shells collide. This collision dissipates part of the kinetic energy and converts it into photons. The time delay of the produced photons (with respect to a hypothetical photon emitted at the center of expansion and travels directly towards the observer) is

$$\delta t^{\rm ob} \simeq \frac{r_{\rm coll}}{2\eta^2 c} \sim \frac{r_0}{c}, \tag{13}$$

namely, of the same order as the central engine variability time. Thus, this model is capable of explaining the rapid ($\gtrsim$1 ms) variability observed.

On the other hand, this mechanism suffers a severe efficiency problem, as only the differential kinetic energy between two shells can be dissipated. Consider, for example, two shells of masses m_1 and m_2 and initial Lorentz factors Γ_1 and Γ_2 undergoing plastic collision. Conservation of energy and momentum implies that the final Lorentz factor of the combined shell is [217]

$$\Gamma_f \simeq \left(\frac{m_1\Gamma_1 + m_2\Gamma_2}{m_1/\Gamma_1 + m_2/\Gamma_2}\right)^{1/2} \tag{14}$$

(assuming that both $\Gamma_1, \Gamma_2 \gg 1$).

The efficiency of kinetic energy dissipation is

$$\begin{aligned} \eta &= 1 - \frac{(m_1 + m_2)\,\Gamma_f}{m_1\Gamma_1 + m_2\Gamma_2} \\ &\simeq 1 - \frac{m_1 + m_2}{\left(m_1^2 + m_2^2 + m_1 m_2\left(\Gamma_1/\Gamma_2 + \Gamma_2/\Gamma_1\right)\right)^{1/2}}. \end{aligned} \tag{15}$$

Thus, in order to achieve high dissipation efficiency, one ideally requires similar masses, $m_1 \simeq m_2$ and high contrast in Lorentz factors $(\Gamma_1/\Gamma_2) \gg 1$. Such high contrast is difficult to explain within the context of either the "collapsar" or the "merger" progenitor scenarios.

Even under these ideal conditions, the combined shell's Lorentz factor, Γ_f, will be high; therefore the contrast between the Lorentz factors of a newly coming shell and the merged shell in the next collision will not be as high. As a numerical example, if the initial contrast is $(\Gamma_1/\Gamma_2) = 10$, for $m_1 = m_2$ one can obtain high efficiency of $\gtrsim$40%; however, the efficiency of the next collision will drop to ~11%. When considering ensemble of colliding shells under various assumptions of the ejection properties of the different shells, typical values of the global efficiency are of the order of 1%–10% [81, 217, 219–224]. These values are in contrast to observational evidence of a much higher efficiency of kinetic energy conversion during the prompt emission, of the order of tens of percents (~50%), which are inferred by estimating the kinetic energy using afterglow measurements [43, 225–229].

While higher efficiency of energy conversion in internal shocks was suggested by a few authors [230, 231], we point out that these works assumed very large contrast in Lorentz

factors, $(\Gamma_1/\Gamma_2) \gg 10$ for almost all collisions; as discussed above such a scenario is unlikely to be realistic within the framework of the known progenitor models.

I further stress that the efficiency discussed in this section refers only to the efficiency in dissipating the kinetic energy. There are a few more episodes of energy conversion that are required before the dissipated energy is radiated as the observed γ-rays. These include (i) using the dissipated energy to accelerate the radiating particles (likely electrons) to high energies; (ii) converting the radiating particle's energy into photons; and (iii) finally, the detectors being sensitive only over a limited energy band, and thus part of the radiated photons cannot be detected. Thus, over all, the measured efficiency, namely, the energy of the observed γ-ray photons relative to the kinetic energy, is expected to be very low in this model, inconsistent with observations.

An alternative idea for kinetic energy dissipation arises from the possibility that the jet composition may contain a large number of free neutrons. These neutrons, that are produced by dissociation of nuclei by γ-ray photons in the inner regions, decouple from the protons below the photosphere (see below) due to the lower cross section for proton-neutron collision relative to Thomson cross section [232–235]. This leads to friction between protons and neutrons as they have different velocities, which, in turn, results in production of e^+ that follow the decay of pions (which are produced themselves by p-n interactions). These positrons IC scatter the thermal photons, producing γ-ray radiation peaking at ~MeV [236]. A similar result is obtained when nonzero magnetic fields are added, in which case contribution of synchrotron emission becomes comparable to that of scattering the thermal photons [237].

3.2.5. Optical Depth and Photosphere. During the initial stages of energy release, a high temperature, $\gtrsim$ MeV (see (2)) "fireball" is formed. At such high temperature, a large number of $e^{\pm}$ pairs are produced [77, 78, 202]. The photons are scattered by these pairs and cannot escape. However, once the temperature drops to $T' \lesssim 17$ keV, the pairs recombine, and thereafter only a residual number of pairs are left in the plasma [78]. Provided that $\eta \lesssim 10^5$, the density of residual pairs is much less than the density of "baryonic" electrons associated with the protons, $n_e = n_p$. (A large number of pairs may be produced later on, when kinetic energy is dissipated, e.g., by shell collisions). This recombination typically happens at $r < r_s$.

Equation (9) thus provides a good approximation to the number density of both protons and electrons in the plasma. Using this equation, one can calculate the optical depth by integrating the mean free path of photons emitted at radius r. A 1-d calculation (namely, photons emitted on the line of sight) gives [184, 238]

$$\tau = \int_r^{\infty} n'_e \sigma_T \Gamma \left(1-\beta\right) dr' \simeq n'_e \sigma_T \frac{r}{2\Gamma}, \tag{16}$$

where β is the flow velocity and σ_T is Thomson's cross section; the use of this cross section is justified since in the comoving frame, the photon's temperature is $T' = T^{\rm ob}/\Gamma \ll m_e c^2$.

The photospheric radius can be defined as the radius from which $\tau(r_{\rm ph}) = 1$,

$$r_{\rm ph} \simeq \frac{\dot{M}\sigma_T}{8\pi r^2 m_p c \Gamma \eta} = \frac{L\sigma_T}{8\pi m_p c^3 \Gamma \eta^2} \simeq 2\times 10^{11} L_{52}\eta_{2.5}^{-3}\ {\rm cm}. \tag{17}$$

In this calculation, I assumed constant Lorentz factor $\Gamma = \eta$, which is justified for $r_{\rm ph} > r_s$. In the case of fluctuative flow resulting in shells, η represents an average value of the shell's Lorentz factor. Further note that an upper limit on η within the framework of this model is given by the requirement $r_{\rm ph} > r_s \rightarrow \eta < (L\sigma_T/8\pi m_p c^3 r_0) \simeq 10^3 L_{52}^{1/4} r_{0,7}^{-1/4}$. This is because as the photons decouple the plasma at the photosphere, for larger values of η the acceleration cannot continue above $r_{\rm ph}$ [239, 240]. In this scenario, the observed spectra are expected to be (quasi)thermal, in contrast to the observations.

The observed temperature at the photosphere is calculated using (2), (8), and (17),

$$T^{\rm ob} = T_0 \left(\frac{r_{\rm ph}}{r_s}\right)^{-2/3} = \frac{80}{(1+z)} L_{52}^{-5/12} \eta_{2.5}^{8/3} r_{0,7}^{1/6}\ {\rm keV}. \tag{18}$$

Similarly, the observed thermal luminosity, $L_{\rm th}^{\rm ob} \propto r^2\Gamma^2 T'^4 \propto r^0$ at $r < r_s$ and $L_{\rm th}^{\rm ob} \propto r^{-2/3}$ at $r > r_s$ [239]. Thus,

$$\frac{L_{\rm th}}{L} \simeq \left(\frac{r_{\rm ph}}{r_s}\right)^{-2/3} = 6.6\times 10^{-2} L_{52}^{-2/3} \eta_{2.5}^{8/3} r_{0,7}^{2/3}. \tag{19}$$

Note the very strong dependence of the observed temperature and luminosity on η (here, L is the luminosity released in the explosion; the observed luminosity in γ-rays is just a fraction of this luminosity).

The results of (19) show that the energy released as thermal photons may be a few % of the explosion energy. This value is of the same order as the efficiency of the dissipation of kinetic energy via internal shocks. However, as discussed above, only a fraction of the kinetic energy dissipated via internal shocks is eventually observed as photons, while no additional episodes of energy conversion (and losses) are added to the result in (19). Furthermore, the result in (19) is very sensitive to the uncertain value of η, via the ratio of $(r_{\rm ph}/r_s)$: for high η, $r_{\rm ph}$ is close to r_s, reducing the adiabatic losses and increasing the ratio of thermal luminosity. In such a scenario, the internal shocks, if occurring, are likely to take place at $r_{\rm coll} \sim \eta r_s > r_{\rm ph}$, namely, in the optically thin region. I will discuss the consequences of this result in Section 3.5.3 below.

The calculation of the photospheric radius in (17) was generalized by Pe'er [241] to include photons emitted off-axis; in this case, the term "photospheric radius" should be replaced with "photospheric surface," which is the surface of last scattering of photons before they decouple the plasma. Somewhat counterintuitively, for a relativistic ($\Gamma \gg 1$) spherical explosion this surface assumes a parabolic shape, given by Pe'er [241]

$$r_{\rm ph}(\theta) \simeq \frac{R_d}{2\pi}\left(\frac{1}{\Gamma^2} + \frac{\theta^2}{3}\right), \tag{20}$$

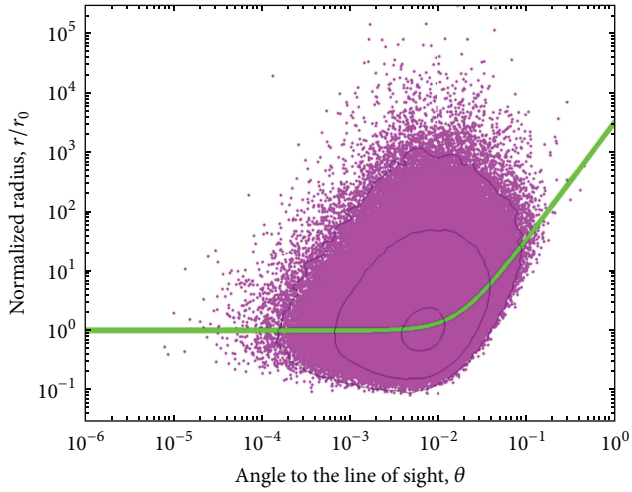

FIGURE 14: The green line represents the (normalized) photospheric radius $r_{\rm ph}$ as a function of the angle to the line of sight, θ, for spherical explosion (see (20)). The red dots represent the last scattering locations of photons ejected in the center of relativistic expanding "fireball" (using a Monte-Carlo simulation). The black lines show contours. Clearly, photons can undergo their last scattering at a range of radii and angles, leading to the concept of "vague photosphere." The observed photospheric signal is therefore smeared both in time and energy. Figure taken from Pe'er [241].

where $R_d \equiv \dot{M}\sigma_T/(4m_p\beta c)$ depends on the mass ejection rate and velocity.

An even closer inspection reveals that photons do not necessarily decouple the plasma at the photospheric surface; this surface of $\tau(r,\theta) = 1$ simply represents a probability of e^{-1} for a photon to decouple the plasma. Instead, the photons have a finite probability of decoupling the plasma at every location in space. This is demonstrated in Figure 14, adopted from [241]. This realization led Beloborodov to coin the term "vague photosphere" [242].

The immediate implication of this nontrivial shape of the photosphere is that the expected radiative signal emerging from the photosphere cannot have a pure "Planck" shape but is observed as a gray-body, due to the different Doppler boosts and different adiabatic energy losses of photons below $r_{\rm ph}$ [241, 243]. This is in fact the relativistic extension of the "limb darkening" effect known from stellar physics. As will be discussed in Section 3.5.4 below, while in spherical outflow only a moderate modification to a pure "Planck" spectra is expected, this effect becomes extremely pronounced when considering more realistic jet geometries and can in fact be used to study GRB jet geometries [244].

3.3. Relativistic Expansion of Magnetized Outflows

3.3.1. The Magnetar Model. A second type of models assumes that the energy released during the collapse (or the merger) is not converted directly into photon-dominated outflow but instead is initially used in producing very strong magnetic fields (Poynting flux dominated plasma). Only at a second stage, the energy stored in the magnetic field is used in both accelerating the outflow to relativistic speeds (jet production and acceleration) as well as heating the particles within the jet.

There are a few motivations for considering this alternative scenario. Observationally, one of the key discoveries of the *Swift* satellite is the existence of a long lasting "plateau" seen in the the early afterglow of GRBs at the X-ray band [227, 245, 246]. This plateau is difficult to explain in the context of jet interaction with the environment but can be explained by continuous central engine activity (though it may be explained by other mechanisms, e.g., reverse shock emission; see [247, 248]). A second motivation is the fact that magnetic fields are long thought to play a major role in jet launching in other astronomical objects, such as AGNs, via the Blandford-Znajek [249] or the Blandford-Payne [250] mechanisms. These mechanisms have been recently tested and validated with state of the art numerical GR-MHD simulations [251–260]; see further explanations in [261]. It is thus plausible that they may play some role in the context of GRBs as well.

The key idea is that the core collapse of the massive star does not form a black hole immediately but instead leads to a rapidly rotating protoneutron star, with a period of ~1 ms, and very strong surface magnetic fields ($B \gtrsim 10^{15}$ G). This is known as the "magnetar" model [197, 262–266]. The maximum energy that can be stored in a rotating neutron star is $\sim 2\times 10^{52}$ erg, and the typical timescale over which this energy can be extracted is ~10 s (for this value of the magnetic field). These values are similar to the values observed in long GRBs. The magnetic energy extracted drives a jet along the polar axis of the neutron star [267–272]. Following this main energy extraction, residual rotational or magnetic energy may continue to power late time flaring or afterglow emission, which may be the origin of the observed X-ray plateau [273].

3.3.2. Scaling Laws for Jet Acceleration in Magnetized Outflows. Extraction of the magnetic energy leads to acceleration of particles to relativistic velocities. The evolution of the hydrodynamic quantities in these Poynting-flux dominated outflow was considered by several authors [274–281]. The scaling laws of the acceleration can be derived by noting that due to the high baryon load ideal MHD limit can be assumed [274].

In this model, there are two parts to the luminosity [275]: a kinetic part, $L_k = \Gamma\dot{M}c^2$, and a magnetic part, $L_M = 4\pi r^2 c\beta(B^2/4\pi)$, where β is the outflow velocity. Thus, $L = L_k + L_M$. Furthermore in this model, throughout most of the jet evolution the dominated component of the magnetic field is the toroidal component, and so $\mathbf{B} \perp \boldsymbol{\beta}$.

An important physical quantity is the magnetization parameter, σ, which is the ratio of Poynting flux to kinetic energy flux:

$$\sigma \equiv \frac{L_M}{L_k} = \frac{B^2}{4\pi\Gamma^2 n m_p c^2}. \tag{21}$$

At the Alfvén radius, r_0 (at $r = r_0$, the flow velocity is equal to the Alfvén speed), the key assumption is that the flow is highly magnetized, and so the magnetization is $\sigma(r_0) \equiv \sigma_0 \gg 1$.

The magnetization plays a similar role to that of the baryon loading in the classical fireball model.

The basic idea is that the magnetic field in the flow changes polarity on a small scale, λ, which is of the order of the light cylinder in the central engine frame ($\lambda \approx 2\pi c/\Omega$), where Ω is the angular frequency of the central engine, either a spinning neutron star or black hole; see [282]. This polarity change leads to magnetic energy dissipation via reconnection process. It is assumed that the dissipation of magnetic energy takes place at a constant rate, that is modeled by a fraction ϵ of the Alfvén speed. As the details of the reconnection process are uncertain, the value of ϵ is highly uncertain. Often a constant value $\epsilon \approx 0.1$ is assumed. This implies that the (comoving) reconnection time is $t'_{\rm rec} \sim \lambda'/\epsilon v'_A$, where v'_A is the (comoving) Alfvén speed, and $\lambda' = \Gamma\lambda$. Since the plasma is relativistic, $v'_A \sim c$, and one finds that $t'_{\rm rec} \propto \Gamma$. In the lab frame, $t_{\rm rec} = \Gamma t'_{\rm rec} \propto \Gamma^2$.

Assuming that a constant fraction of the dissipated magnetic energy is used in accelerating the jet, the rate of kinetic energy increase is therefore given by

$$\frac{dE_k}{dr} \propto \frac{d\Gamma}{dr} \sim \frac{1}{ct_{\rm rec}} \propto \Gamma^{-2}, \tag{22}$$

from which one immediately finds the scaling law $\Gamma(r) \propto r^{1/3}$.

The maximum Lorentz factor that can be achieved in this mechanism is calculated as follows. First, one writes the total luminosity as $L = L_k + L_M = (\sigma_0 + 1)\Gamma_0 \dot{M}c^2$, where Γ_0 is the Lorentz factor of the flow at the Alfvén radius. Second, generalization of the Alfvénic velocity to relativistic speeds [283, 284] reads

$$\gamma_A\beta_A = \frac{B'}{\sqrt{4\pi n m_p c^2}} = \frac{B/\Gamma}{\sqrt{4\pi n m_p c^2}} = \sqrt{\sigma}. \tag{23}$$

By definition of the Alfvénic radius, the flow Lorentz factor at this radius is $\Gamma_0 = \gamma_A \simeq \sqrt{\sigma_0}$ (since at this radius the flow is Poynting-flux dominated, $\sigma_0 \gg 1$). Thus, the mass ejection rate is written as $\dot{M} \approx L/\sigma_0^{3/2}c^2$. As the luminosity is assumed constant throughout the outflow, the maximum Lorentz factor is reached when $L \sim L_k \gg L_M$; namely, $L = \Gamma_{\rm max}\dot{M}c^2$. Thus,

$$\Gamma_{\rm max} \approx \sigma_0^{3/2}. \tag{24}$$

In comparison to the photon-dominated outflow, jet acceleration in the Poynting-flux dominated outflow model is thus much more gradual. The saturation radius is at $r_s = r_0\sigma_0^3 \approx 10^{13.5}\sigma_2^3(\epsilon\Omega)_3^{-1}$ cm. Similar calculations to that presented above show the photospheric radius to be at radius [280]

$$r_{\rm ph} = 6\times 10^{11}\frac{L_{52}^{3/5}}{(\epsilon\Omega)_3^{2/5}\sigma_2^{3/2}}\ {\rm cm}, \tag{25}$$

which is similar (for the values of parameters chosen) to the photospheric radius obtained in the photon-dominated flow. Note that, in this scenario, the photosphere occurs while the flow is still accelerating.

The model described above is clearly very simplistic. In particular, it assumes constant luminosity and constant rate of reconnection along the jet. As such, it is difficult to explain the observed rapid variability in the framework of this model. Furthermore, one still faces the need to dissipate the kinetic energy in order to produce the observed γ-rays. As was shown by several authors [285–287], kinetic energy dissipation via shock waves is much less efficient in Poynting-flow dominated plasma relative to weakly magnetized plasma.

Moreover, even if this is the correct model in describing (even if only approximately) the magnetic energy dissipation rate, it is not known what fraction of the dissipated magnetic energy is used in accelerating the jet (increasing the bulk Lorentz factor) and what fraction is used in heating the particles (increasing their random motion). Lacking clear theoretical model, it is often simply assumed that about half of the dissipated energy is used in accelerating the jet, the other half in heating the particles [288]. Clearly, all these assumptions can be questioned. Despite numerous efforts in recent years in studying magnetic reconnection (e.g., [289–293]) this is still an open issue.

Being aware of these limitations, in recent years several authors have dropped the steady assumption and considered models in which the acceleration of a magnetic outflow occurs over a finite, short duration [294–297]. The basic idea is that variability in the central engine leads to the ejection of magnetized plasma shells that expand due to internal magnetic pressure gradient once they lose causal contact with the source.

One suggestion is that similar to the internal shock model, the shells collide at some radius $r_{\rm coll}$. The collision distort the ordered magnetic field lines entrained in the ejecta. Once reaching a critical point, fast reconnection seeds occur, which induce relativistic MHD turbulence in the interaction regions. This model, known as Internal-Collision-induced Magnetic Reconnection and Turbulence (ICMART) [201], may be able to overcome the low efficiency difficulty of the classical internal shock scenario.

3.4. Particle Acceleration. In order to produce the nonthermal spectra observed, one can in principle consider two mechanisms. The first is emission of radiation via various nonthermal processes, such as synchrotron or Compton. This is the traditional way which is widely considered in the literature. A second way which was discussed only recently is the use of light aberration, to modify the (naively expected) Planck spectrum emitted at the photosphere. The potentials and drawbacks of this second idea will be considered in Section 3.5.4. First, let me consider the traditional way of producing the spectra via nonthermal radiative processes (a photospheric emission cannot explain photons at the GeV range, and thus even if it does play a major role in producing the observed spectra, it is certainly not the only radiative mechanism).

The internal collisions, magnetic reconnection, or possibly other unknown mechanisms dissipate part of the outflow

kinetic energy (within the context of Poynting-flux dominated outflows, it was suggested by Lyutikov and Blandford [200] and Lyutikov [298] that the magnetic energy dissipated may be converted directly into radiating particles, without conversion to kinetic energy first). This dissipated energy, in turn, can be used to heat the particles (increase their random motion) and/or accelerate some fraction of them to a nonthermal distribution. Traditionally, it is also assumed that some fraction of this dissipated energy is used in producing (or enhancing) magnetic fields. Once accelerated, the high energy particles emit the nonthermal spectra.

The most widely discussed mechanism for acceleration of particles is the *Fermi mechanism* [299, 300], which requires particles to cross back and forth a shock wave. Thus, this mechanism is naturally associated with internal shell collisions, where shock waves are expected to form. A basic explanation of this mechanism can be found in the textbook by [301]; For reviews see [302–305]. In this process, the accelerated particle crosses the shock multiple times, and in each crossing its energy increases by a (nearly) constant fraction, $\Delta E/E \sim 1$. This results in a power law distribution of the accelerated particles, $N(E) \propto E^{-S}$ with power law index $S \approx 2.0 - 2.4$ [306–310]. Recent developments in particle-in-cell (PIC) simulations have allowed to model this process from first principles and study it in more detail [311–315]. As can be seen in Figure 15 taken from [313], indeed a power law tail above a low energy Maxwellian in the particle distribution is formed.

The main drawback of the PIC simulations is that due to the numerical complexity of the problem, these simulations can only cover a tiny fraction (~10^{-8}) of the actual emitting region in which energetic particles exist. Thus, these simulations can only serve as guidelines, and the problem is still far from being fully resolved. Regardless of the exact details, it is clear that particle acceleration via the *Fermi* mechanism requires the existence of shock waves and is thus directly related to the internal dynamics of the gas and possibly to the generation of magnetic fields, as mentioned above.

The question of particle acceleration in magnetic reconnection layers has also been extensively addressed in recent years (see [289–293, 316–331] for a partial list of works). The physics of acceleration is somewhat more complicated than in nonmagnetized outflows and may involve several different mechanisms. The basic picture is that the dissipation of the magnetic field occurs in sheets. The first mechanism relies on the realization that within these sheets, there are regions of high electric fields; particles can therefore be accelerated directly by the strong electric fields. A second mechanism is based on instabilities within the sheets that create "magnetic islands" (plasmoids) that are moving close to the Alfvén speed (see Figure 16). Particles can therefore be accelerated via *Fermi* mechanism by scattering between the plasmoids. A third mechanism is based on converging plasma flows towards the current sheets that provide another way of particle acceleration via first order *Fermi* process.

In addition, if the flow is Poynting-flux dominated, particles may also be accelerated in shock waves; however, it was argued that *Fermi*-type acceleration in shock waves

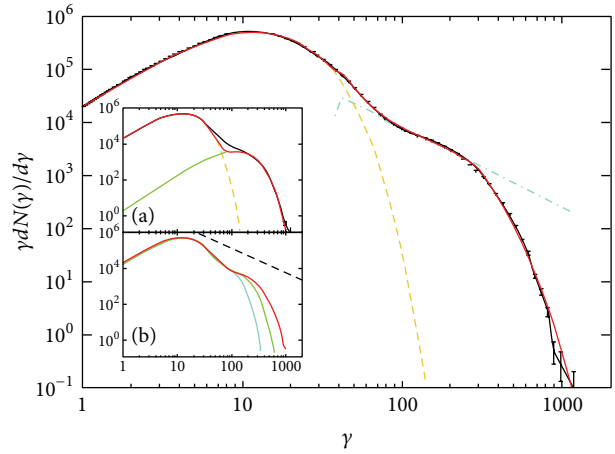

Figure 15: Results of a particle in cell (PIC) simulation shows the particle distribution downstream from the shock (black line). The red line is a fit with a low energy Maxwellian, and a high energy power law, with a high energy exponential cutoff. Subpanel (a) is the fit with a sum of high and low temperature Maxwellians (red line), showing a deficit at intermediate energies; subpanel (b) is the time evolution of a particle spectrum in a downstream slice at three different times. The black dashed line shows a $\gamma^{-2.4}$ power law. Figure taken from Spitkovsky [313].

that may develop in highly magnetized plasma may be inefficient [314, 332]. Thus, while clearly addressing the question of particle acceleration in magnetized outflow is a very active research field, the numerical limitations imply that theoretical understanding of this process and its details (e.g., what fraction of the reconnected energy is being used in accelerating particles, or the energy distribution of the accelerated particles) is still very limited.

Although the power law distribution of particles resulting from *Fermi*-type, or perhaps magnetic-reconnection acceleration is the most widely discussed, we point out that alternative models exist. One such model involves particle acceleration by a strong electromagnetic potential, which can exceed 10^{20} eV close to the jet core [333–335]. The accelerated particles may produce a high energy cascade of electron-positron pairs. Additional model involves stochastic acceleration of particles due to resonant interactions with plasma waves in the black hole magnetosphere [336].

Several authors have also considered the possibility that particles in fact have a relativistic quasi-Maxwellian distribution [337–340]. Such a distribution, with the required temperature (~10^{11}-10^{12} K) may be generated if particles are roughly thermalized behind a relativistic strong shock wave (e.g., [341]). While such a model is consistent with several key observations, it is difficult to explain the very high energy (GeV) emission without invoking very energetic particles, and therefore some type of particle acceleration mechanism must take place as part of the kinetic energy dissipation process.

3.5. Radiative Processes and the Production of the Observed Spectra. Following jet acceleration, kinetic energy dissipation (either via shock waves or via magnetic reconnection),

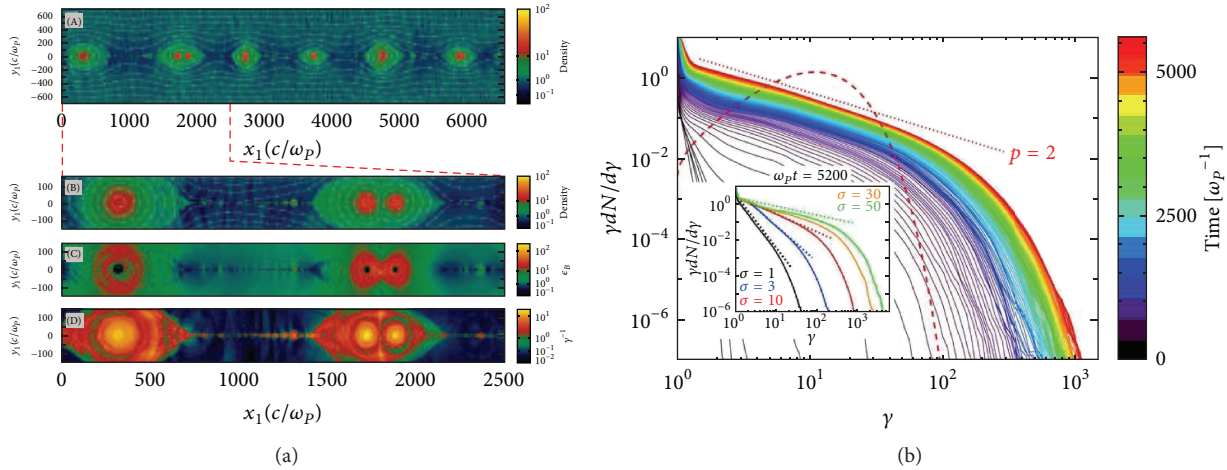

FIGURE 16: Results of an electromagnetic particle in cell (PIC) simulation TRISTAN-MP show the structure of the reconnection layer (a) and the accelerated particle distribution function (b). (a) Structure of the reconnection layer. Shown are the particle densities (A), (B), magnetic energy fraction (C), and mean kinetic energy per particle (D). The plasmoids are clearly seen. (b) Temporal evolution of particle energy spectrum. The spectrum at late times resembles a power law with slope $p = 2$ (dotted red line) and is clearly departed from a Maxwellian. The dependence of the spectrum on the magnetization is shown in the inset. Figure is taken from Sironi and Spitkovsky [330].

and particle acceleration, the final stage of energy conversion must produce the observed spectra. As the γ-ray spectra is both very broad and nonthermal (does not resemble "Planck"), most efforts to date are focused on identifying the relevant radiative processes and physical conditions that enable the production of the observed spectra. The leading radiative models initially discussed are synchrotron emission, accompanied by synchrotron-self Compton at high energies. However, as has already mentioned, it was shown that this model is inconsistent with the data, in particular the low energy spectral slopes.

Various suggestions of ways to overcome this drawback by modifying some of the physical conditions and/or physical properties of the plasma were proposed in the last decade. However, a major revolution occurred with the realization that part of the spectra is thermal. This led to new set of models in which part of the emission originates from below the photosphere (the optically thick region). It should be stressed that only part of the spectrum, but not all of it, is assumed to originate from the photosphere. Thus, in these models as well, there is room for optically thin (synchrotron and IC) emission, originating from a different location. Finally, a few most recent works on light aberration show that the contribution of the photospheric emission may be much broader than previously thought.

3.5.1. Optically Thin Model: Synchrotron. Synchrotron emission is perhaps the most widely discussed model for explaining GRB prompt emission. It has several advantages. First, it has been extensively studied since the 1960s [342, 343] and is the leading model for interpreting nonthermal emission in AGNs, XRBs, and emission during the afterglow phase of GRBs. Second, it is very simple: it requires only two basic ingredients, namely, energetic particles and a strong magnetic field. Both are believed to be produced in shock waves (or magnetic reconnection phase), which tie it nicely to the general "fireball" (both "hot" and "cold") picture discussed above. Third, it is broadband in nature (as opposed, e.g., to the "Planck" spectrum), with a distinctive spectral peak that could be associated with the observed peak energy. Fourth, it provides a very efficient way of energy transfer, as for the typical parameters, energetic electrons radiate nearly 100% of their energy. These properties made synchrotron emission the most widely discussed radiative model in the context of GRB prompt emission (e.g., [79, 80, 213, 214, 218, 344–349] for a very partial list).

Consider a source at redshift z which is moving at velocity $\beta \equiv v/c$ (corresponding Lorentz factor $\Gamma = (1-\beta)^{-1/2}$) at angle θ with respect to the observer. The emitted photons are thus seen with a Doppler boost $\mathscr{D} = [\Gamma(1-\beta\cos\theta)]^{-1}$. Synchrotron emission from electrons having random Lorentz factor $\gamma_{\rm el}$ in a magnetic field B (all in the comoving frame) is observed at a typical energy

$$\epsilon_m^{\rm ob} = \frac{3}{2}\hbar\frac{qB}{m_e c}\gamma_{\rm el}^2\frac{\mathscr{D}}{(1+z)} = 1.75\times10^{-19}B\gamma_{\rm el}^2\frac{\mathscr{D}}{(1+z)}\ \text{erg}. \tag{26}$$

If this model is to explain the peak observed energy, $\epsilon^{\rm ob} \approx 200$ keV with typical Lorentz factor $\mathscr{D} \simeq \Gamma \sim 100$ (relevant for on-axis observer), one obtains a condition on the typical electron Lorentz factor and magnetic field,

$$B\gamma_{\rm el}^2 \simeq 3.6\times10^{10}\left(\frac{1+z}{2}\right)\Gamma_2^{-1}\left(\frac{\epsilon^{\rm ob}}{200\,\text{keV}}\right)G. \tag{27}$$

Thus, both strong magnetic field and very energetic electrons are required in interpreting the observed spectral peak as due to synchrotron emission. Such high values of the electrons

Lorentz factor are not excluded by any of the known models for particle acceleration. High values of the magnetic fields may be present if the outflow is Poynting flux dominated. In the photon-dominated outflow, strong magnetic fields may be generated in shock waves via two stream (Weibel) instabilities [124, 311, 350–353].

One can therefore conclude that the synchrotron model is capable of explaining the peak energy. However, one alarming problem is that the high values of both B and $\gamma_{\rm el}$ required, when expressed as fraction of available thermal energy (the parameters ϵ_e and ϵ_B), are much higher than the (normalized) values inferred from GRB afterglow measurements [354–357]. This is of a concern, since broadband GRB afterglow observations are typically well fitted with the synchrotron model, and the microphysics of particle acceleration and magnetic field generation should be similar in both prompt and afterglow environments (though the forward shock producing the afterglow is initially highly relativistic, while shock waves produced during the internal collisions may be mildly relativistic at most).

The main concern though is the low energy spectral slope. As long as the electrons maintain their energy, the expected synchrotron spectrum below the peak energy is $F_\nu \propto \nu^{1/3}$ (corresponding photon number $N_E \propto E^{-2/3}$) (e.g., [118]). This is roughly consistent with the observed low energy spectral slope, $\langle\alpha\rangle = -1$ (see Section 2.2.2).

However, at these high energies, and with such strong magnetic field, the radiating electrons rapidly cool by radiating their energy on a very short time scale:

$$t'_{\rm cool} = \frac{E}{P} = \frac{\gamma_{\rm el} m_e c^2}{(4/3)\, c\sigma_T \gamma_{\rm el}^2 u_B\, (1+Y)} = \frac{6\pi m_e c}{\sigma_T B^2 \gamma_{\rm el}\, (1+Y)}. \tag{28}$$

Here, $E = \gamma_{\rm el} m_e c^2$ is the electron's energy, P is the radiated power, $u_B \equiv B^2/8\pi$ is the energy density in the magnetic field, σ_T is Thomson's cross section, and Y is Compton parameter. The factor $(1 + Y)$ is added to consider cooling via both synchrotron and Compton scattering.

Using the values obtained in (27), one finds the (comoving) cooling time to be

$$t'_{\rm cool} = 6.0\times 10^{-13} \gamma_{\rm el}^3\, (1+Y)^{-1} \left(\frac{1+z}{2}\right)^{-2} \cdot \Gamma_2^2 \left(\frac{\epsilon^{\rm ob}}{200\,{\rm keV}}\right)^{-2} {\rm s}. \tag{29}$$

This time is to be compared with the comoving dynamical time, $t'_{\rm dyn} \sim R/\Gamma c$. If the cooling time is shorter than the dynamical time, the resulting spectra below the peak are $F_\nu \propto \nu^{-1/2}$ (e.g., [358, 359]), corresponding to $N_E \propto E^{-3/2}$. While values of the power law index *smaller* than $-3/2$, corresponding to shallow spectra, can be obtained by superposition of various emission sites, steeper values cannot be obtained. Thus, the observed low energy spectral slope of ∼85% of the GRBs (see Figure 5) which show α larger than this value ($\langle\alpha\rangle = -1$) cannot be explained by synchrotron emission model. This is the "synchrotron line of death" problem introduced above.

The condition for $t'_{\rm cool} \gtrsim t'_{\rm dyn}$ can be written as

$$\gamma_{\rm el} \gtrsim 3.8\times 10^4 R_{14}^{1/3}\, (1+Y)^{1/3} \left(\frac{1+z}{2}\right)^{2/3} \cdot \Gamma_2^{-1} \left(\frac{\epsilon^{\rm ob}}{200\,{\rm keV}}\right)^{2/3}. \tag{30}$$

The value of the emission radius $R = 10^{14}$ cm is chosen as a representative value that enables variability over time scale $\delta t^{\rm ob} \sim R/\Gamma^2 c \sim 0.3 R_{14}\Gamma_2^{-2}$ s.

Since $\gamma_{\rm el}$ represents the characteristic energy of the radiating electrons, such high values of the *typical* Lorentz factor $\gamma_{\rm el}$ are very challenging for theoretical modeling. However, a much more severe problem is that in this model, under these conditions, the energy content in the magnetic field must be very low (see (27)). In order to explain the observed flux, one must therefore demand high energy content in the electron's component, which is several orders of magnitude higher than that stored in the magnetic field [15, 360, 361]. This, in turn, implies that inverse Compton becomes significant, producing ∼TeV emission component that substantially increase the total energy budget. As was shown by Kumar and McMahon [360], such a scenario can only be avoided if the emission radius is $R \gtrsim 10^{17}$ cm, in which case it is impossible to explain the rapid variability observed. Thus, the overall conclusion is that classical synchrotron emission as a leading radiative process fails to explain the key properties of the prompt emission of the vast majority of GRBs [85, 362].

3.5.2. Suggested Modifications to the Classical Synchrotron Scenario. The basic synchrotron emission scenario thus fails to self-consistently explain both the energy of the spectral peak and the low energy spectral slope. In the past decade there have been several suggestions of ways in which the basic picture might be modified, so that the modified synchrotron emission, accompanied by inverse Compton scattering of the synchrotron photons (synchrotron-self Compton; SSC) would be able to account for these key observations.

The key problem is the fast cooling of the electrons, namely, $t_{\rm cool} < t_{\rm dyn}$. However, in order for the electrons to rapidly cool they must be embedded in a strong magnetic field. The spatial structure of the magnetic field is not clear at all. Thus, it was proposed by Pe'er and Zhang [363] that the magnetic field may decay on a relatively short length scale, and so the electrons would not be able to efficiently cool. This idea had gain interest recently [364, 365]. Its major drawback is the need for high energy budget, as only a small part of the energy stored in the electrons is radiated.

Another idea is that synchrotron self-absorption may produce steep low energy slope below the observed peak [366]. However, this requires unrealistically high magnetic field. Typically, the synchrotron self-absorption frequency is expected at the IR/Optic band (e.g., [118, 367]). Thus, synchrotron self-absorption may be relevant in shaping

the spectrum at the X-rays only under very extreme conditions (e.g., [368]).

Looking into a different parameter space region, it was suggested that the observed peak energy is not due to synchrotron emission, but due to inverse-Compton scattering of the synchrotron photons, which are emitted at much lower energies [369–371]. In these models, the steep low energy spectral slope can result from upscattering of synchrotron self-absorbed photons. However, a careful analysis of this scenario (e.g., [15]) reveals requirements on the emission radius, $R \gtrsim 10^{16}$ cm and optical flux (associated with the synchrotron seed photons) that are inconsistent with observations. Furthermore, a second scattering would lead to substantial TeV flux, resulting in an energy crisis [372, 373]. Thus, this model as well is concluded as not being viable as the leading radiative model during the GRB prompt emission [373].

If the energy density in the photon field is much greater than in the magnetic field, then electron cooling by inverse Compton scattering the low energy photons dominates overcooling by synchrotron radiation. The most energetic electrons cool less efficiently due to the Klein-Nishina (KN) decrease in the scattering cross section. Thus, in this parameter space where KN effect is important, steeper low energy spectral slopes can be obtained [372, 374, 375]. However, even under the most extreme conditions, the steepest slope that can be obtained is no harder than $F_\nu \sim \nu^0$ [374, 376], corresponding to $N_E \propto E^{-1}$, which can explain at most ~50% of the low energy spectral slopes observed. Moreover, very high values of the electron's Lorentz factor, $\gamma_{\rm el} \gtrsim 10^6$ are assumed which challenge theoretical models, as discussed above.

A different proposition was that the heating of the electrons may be slow; namely, the electrons may be continuously heated while radiating their energy as synchrotron photons. This way, the rapid electrons cooling is avoided, and a shallower spectra can be obtained [360, 377–380]. While there is no known mechanism that could continuously heat the electrons as they cross the shock wave and are advected downstream in the classical internal collision scenario, it was proposed that slow heating may result from MHD turbulence down stream of the shock front [380]. Thus this may be an interesting alternative, though currently there are still large gaps in the physics involved in the slow heating process.

Several authors considered the possibility of synchrotron emission from nonisotropic electron distribution [366, 381]. Alternatively, the magnetic field may vary on such a short scale that relativistic electrons transverse deflection is much smaller than the beaming angle [382]. This results in a "jitter" radiation, with different spectral properties than classical synchrotron.

A different suggestion is emission by the hadrons (protons). The key idea is that whatever mechanism that is capable of accelerating electrons to high energies should accelerate protons as well; in fact, the fact that high energy cosmic rays are observed necessitate the existence of such a mechanism, although its details in the context of GRBs are unknown. Many authors have considered possible contribution of energetic protons to the observed spectra (e.g., [383–389]). Energetic proton contribution to the spectrum is both via direct synchrotron emission and also indirectly by photopion production or photopair production.

Clearly, proton acceleration to high energies would imply that GRBs are potentially strong source of both high energy cosmic rays and energetic neutrinos [390–393]. On the other hand, the main drawback of this suggestion is that protons are much less efficient radiators than electrons (as the ratio of proton to electron cross section for synchrotron emission is $\sim (m_e/m_p)^2$). Thus, in order to produce the observed luminosity in γ-rays, the energy content of the protons must be very high, with proton luminosity of ~10^{55}-10^{56} erg s^{-1}. This is at least 3 orders of magnitude higher than the requirement for leptonic models.

3.5.3. Photospheric Emission. As discussed above, photospheric (thermal) emission is an inherent part of both the "hot" and "cold" (magnetized) versions of the fireball model. Thus, it is not surprising that the very early models of cosmological GRBs considered photospheric emission as a leading radiative mechanism [77, 78, 184, 197]. However, following the observational evidence of a nonthermal emission and lacking clear evidence for a thermal component, this idea was abandoned for over a decade.

Renewed interest in this idea began in the early 2000s, with the realization that the synchrotron model, even after being modified, cannot explain the observed spectra. Thus, several authors considered addition of thermal photons to the overall nonthermal spectra, being either dominant [394, 395] or subdominant [239, 240, 396]. Note that as neither the internal collision or the magnetic reconnection models provide clear indication of the location and the amount of dissipated kinetic energy that is later converted into nonthermal radiation, it is impossible to determine the expected ratio of thermal to nonthermal photons from first principles in the framework of these models. Lacking clear observational evidence, it was therefore thought that $r_{\rm ph} \gg r_s$, in which case adiabatic losses lead to strong suppression of the thermal luminosity and temperature (see (18) and (19)).

However, as was pointed out by Pe'er and Waxman [397], in the scenario where $r_{\rm ph} \gg r_s$ it is possible that substantial fraction of kinetic energy dissipation occurs below the photosphere (e.g., in the internal collision scenario, if $r_{\rm coll} < r_{\rm ph}$). In this case, the radiated (nonthermal) photons that are emitted as a result of the dissipation process cannot directly escape but are advected with the flow until they escape at the photosphere. This triggers several events. First, multiple Compton scattering substantially modifies the optically thin (synchrotron) spectra, presumably emitted initially by the heated electrons. Second, the electrons in the plasma rapidly cool, mainly by IC scattering. However, they quickly reach a "quasisteady state," and their distribution becomes quasi-Maxwellian, irrespective of their initial (accelerated) distribution. The temperature of the electrons is determined by balance between heating, both external, and by direct Compton scattering energetic photons, and cooling (adiabatic and radiative) [398]. The photon field is then modified by scattering from this quasi-Maxwellian

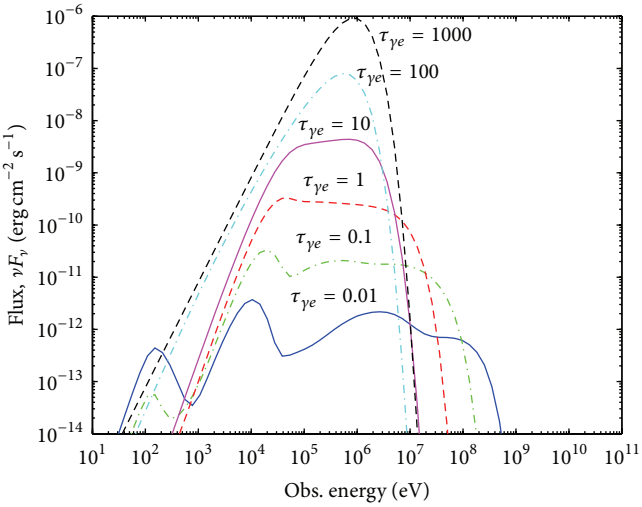

FIGURE 17: Time averaged broadband spectra expected following kinetic energy dissipation at various optical depths. For low optical depth, the two low energy bumps are due to synchrotron emission and the original thermal component, and the high energy bumps are due to inverse Compton phenomenon. At high optical depth, $\tau \geq 100$, a Wien peak is formed at ~10 keV and is blue-shifted to the MeV range by the bulk Lorentz factor ≃100 expected in GRBs. In the intermediate regime, $0.1 < \tau < 100$, a flat energy spectrum above the thermal peak is obtained by multiple Compton scattering. Figure is taken from Pe'er et al. [399].

distribution of electrons. The overall result is a regulation of the spectral peak at ~1 MeV (for dissipation that takes place at moderate optical depth, $\tau \sim$ a few—few tens) and low energy spectral slopes consistent with observations [397].

The addition of the thermal photons that originate from the initial explosion (this term is more pronounced if $r_{ph} \gtrsim r_s$) significantly enhances these effects [399]. The thermal photons serve as seed photons for IC scattering, resulting in rapid cooling of the nonthermal electrons that are heated in the subphotospheric energy dissipation event. As the rapid IC cooling leads to a quasisteady state distribution of the electrons, the outcome is a "two-temperature plasma," with electron temperature higher than the thermal photon temperature, $T_{el} > T_{ph}$. An important result of this model is that the electron temperature is highly regulated and is very weakly sensitive to the model uncertainties; see [398] for details. If the dissipation occurs at intermediate optical depth, $\tau \sim$ a few—few tens, the emerging spectrum has a nearly "top hat" shape (see Figure 17). Below T_{ph} the spectrum is steep, similar to the Rayleigh-Jeans part of the thermal spectrum; in between T_{ph} and T_{el}, a nearly flat energy spectra, $\nu f_\nu \propto \nu^0$ (corresponding $N_E \propto E^{-2}$) is obtained, resulting from multiple Compton scattering; and an exponential cutoff is expected at higher energies.

Interestingly, the spectral slope obtained in the intermediate regime is similar to the obtained high energy spectral slope, $\langle\beta\rangle \sim -2$ (see discussion in Section 2.2.2 and Figure 5). Thus, a simple interpretation is to associate the observed E_{pk} with T_{ph}. However, this is likely a too simplistic interpretation from the following reasons. First, the predicted low energy spectral slopes, being (modified) thermal, are typically *harder* than the observed [104]. Second, in GRB110721A, the peak energy is at ≈15 MeV at early times [98, 99], which is too high to be accounted for by T_{ph} [400, 401]. Moreover, recent analysis of *Fermi* data shows a thermal peak at lower energies than E_{pk} (see, e.g., Figure 7), which is consistent with the interpretation of the thermal peak being associated with T_{ph}. The key result of this model, that $T_{ph} < T_{el}$, is consistent with the observational result of $E_{peak,th} < E_{pk}$, which is applicable to all GRBs in which thermal emission was identified so far. This model thus suggests that E_{pk} may be associated with T_{el}, though it does not exclude synchrotron origin for E_{pk}; see further discussion below.

If the optical depth in which the kinetic energy dissipation takes place is $\tau \gtrsim 100$, the resulting spectra are close to thermal; while if $\tau \lesssim$ a few, the result is a complex spectra, with synchrotron peak, thermal peak, and at least two peaks resulting from IC scattering (see Figure 17). Below the thermal peak, the main contribution is from synchrotron photons that are emitted by the electrons at the quasi steady distribution. Above the thermal peak, multiple IC scattering is the main emission process, resulting in nearly flat energy spectra. Thus, this model naturally predicts different spectral slopes below and above the thermal peak.

Interestingly, the key results of this model do not change if one considers highly magnetized plasma [279, 402–406]. Indeed, as this model of subphotospheric energy dissipation is capable of capturing the key observed features of the prompt emission, it attracted a lot of attention in recent years (e.g., [104, 236, 401, 407–422]).

It should be noted that the above analysis holds for a single dissipation episode. In explaining the complex GRB light curve, multiple such episodes (e.g., internal collisions) are expected. Thus, a variety of observed spectra, which are superposition of the different spectra that are obtained by dissipation at different optical depth, are expected [423].

In spite if this success, this model still suffers two main drawbacks. The first one already discussed is the need to explain low energy spectral slopes that are not as hard as the Rayleigh-Jeans part of a Planck spectra. Further, this model needs to explain the high peak energy (>MeV) observed in some bursts in a self-consistent way. A second drawback is the inability of the subphotospheric dissipation model to explain the very high energy (GeV) emission seen. Such high energy photons must originate from some dissipation above the photosphere.

There are two solutions to these problems. The first is geometric in nature and takes into account the nonspherical nature of GRB jets to explain how low energy spectral slopes are modified. This will be discussed below. The second is the realization that the photospheric emission must be accompanied by at least another one dissipation process that takes place above the photosphere. This conclusion, however, is aligned with both observations of different temporal behavior of the high energy component (see Section 2.2.5), as well as with the basic idea of multiple dissipation episodes, inherent to both the "internal collision" model and to the magnetic reconnection model.

Indeed, in the one case in which detailed modeling was done by considering two emission zones (photosphere and external one), very good fits to the data of GRB090902B were obtained [229]. This fits were done with a fully physically motivated model, which enables determining the physical conditions at both emission zones [229]. This is demonstrated in Figure 18.

3.5.4. Geometrical Broadening. As was already discussed in Section 3.2.5, the definition of the photosphere as the last scattering surface must be modified to incorporate the fact that photons have finite probability of being scattered at every location in space where particles exist. This led to the concept of "vague photosphere" (see Figure 14). The observational consequences of this effect were studied by several authors [236, 241, 242, 244, 424–426]. In spherical explosion case, the effect of the vague photosphere is not large; it somewhat modifies the Rayleigh-Jeans part of the spectrum, to read $F_\nu \propto \nu^{3/2}$ [242]. However, for nonspherical explosion, the effect becomes dramatic.

While the exact geometry of GRB jets, namely, $\Gamma(r, \theta, \phi)$ are unknown, numerical simulations of jets propagating through the stellar core (e.g., [427]) suggest a jet profile of the form $\Gamma(\theta) \sim \Gamma_0/(1 + (\theta/\theta_j)^{2p})$, at least for nonmagnetized outflows. Such a jet profile thus assumes a constant Lorentz factor, $\Gamma \sim \Gamma_0$ for $\theta \lesssim \theta_j$ (the "jet core," or inner jet), and decaying Lorentz factor at larger angles, $\Gamma(\theta) \propto \theta^{-p}$ (outer jet, or jet sheath). As the Lorentz factor is $\Gamma \propto L/\dot{M}$ (Section 3.2.3), such a profile can result from excess of mass load close to the jet edge, by mass collected from the star ($\dot{M} = \dot{M}(\theta)$), or alternatively by angle dependent luminosity.

The scenario of $\dot{M} = \dot{M}(\theta)$ was considered by Lundman et al. [244]. While photospheric emission from the inner parts of the jet results in mild modification to the black body spectrum, photons emitted from the outer jet's photosphere dominate the spectra at low energies (see Figure 19). For narrow jets ($\theta_j\Gamma_0 \lesssim$ few), this leads to flat low energy spectra, $dN/dE \propto E^{-1}$, which is independent on the viewing angle and very weakly dependent on the exact jet profile. This result thus both suggests the possibility that the low energy slopes are in fact part of the photospheric emission and in addition can be used to infer the jet geometry.

A second aspect of the model is that the photospheric emission can be observed to be highly polarized, with up to ≈40% polarization [429, 430]. While IC scattering produces highly polarized light, in spherical models the polarization from different viewing angles cancels. However, this cancellation is incomplete in jet-like models (observed off-axis). While the observed flux by an observer off the jet axis (that can see highly polarized light) is reduced, it is still high enough to be detected [429].

A third unique aspect that results from jet geometry (rather than spherical explosion) is photon energy gain by *Fermi*-like process. As photons are scattered back and forth between the jet core and the sheath, on the average they gain energy. This leads to a high energy power law tail (above the thermal peak) [244, 431]. This again may serve as a new tool in studying jet geometry; though the importance of this effect in determining the high energy spectra of GRBs is still not fully clear (Lundman et. al., in prep.).

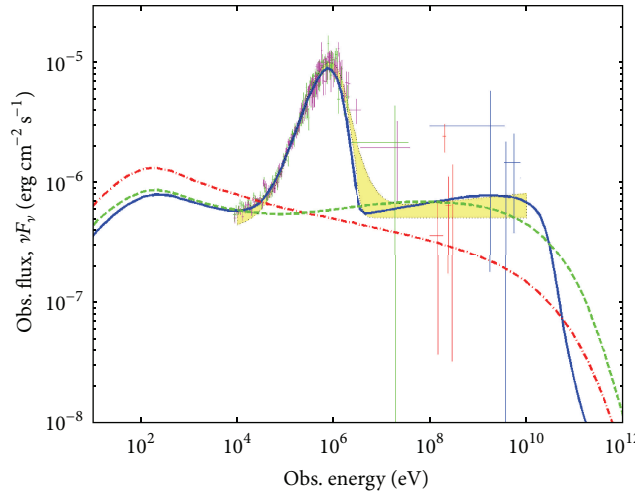

FIGURE 18: Spectral decomposition of GRB090902B (taken at time interval (*c*), 9.6–13.0 seconds after the GBM trigger) enables clear identification of the physical origin of the emission. The dash-dotted (red) curve shows the spectrum that would have been obtained if synchrotron radiation was the only source of emission. The dashed (green) curve shows the resulting spectrum from synchrotron and SSC, and the solid (blue) curve shows the spectrum with the full radiative ingredients (synchrotron, SSC, the ~MeV thermal peak, and Comptonization of the thermal photons). Numerical fits are done using the radiative code developed by Pe'er and Waxman [428]. Figure is taken from Pe'er et al. [229].

3.5.5. A Few Implications of the Photospheric Term. A great advantage of the photospheric emission in its relative simplicity. By definition, the photosphere is the innermost region from which electromagnetic signal can reach the observer. Thus, the properties of the emission site are much more constrained, relative, for example, to synchrotron emission (whose emission radius, magnetic field strength, and particle distribution are not known).

In fact, in the framework of the "hot" fireball model, the (1-d) photospheric radius is a function of only two parameters: the luminosity (which can be measured once the distance is known) and the Lorentz factor (see (17)). The photospheric radius is related to the observed temperature and flux via $r_{\rm ph}/\Gamma \propto (F_{\rm bb}^{\rm ob}/\sigma T^{\rm ob\,4})^{1/4}$, where σ is Stefan's constant, and the extra factor of Γ^{-1} is due to light aberration. Since $r_{\rm ph} \propto L\Gamma^{-3}$, measurements of the temperature and flux in bursts with known redshift enables an independent measurement of Γ, the Lorentz factor at the photosphere [432]. This, in turn, can be used to determine the full dynamical properties of the outflow.

One interesting result is that by using this method it is found that r_0, the size of the jet base is ~$10^{8.5}$ cm, two-three orders of magnitude above the Schwarzschild radius [99, 101, 432, 433]. Interestingly, this result is aligned with recent constraints found by Vurm et al. [416] that showed that the conditions for full thermalization takes place only if

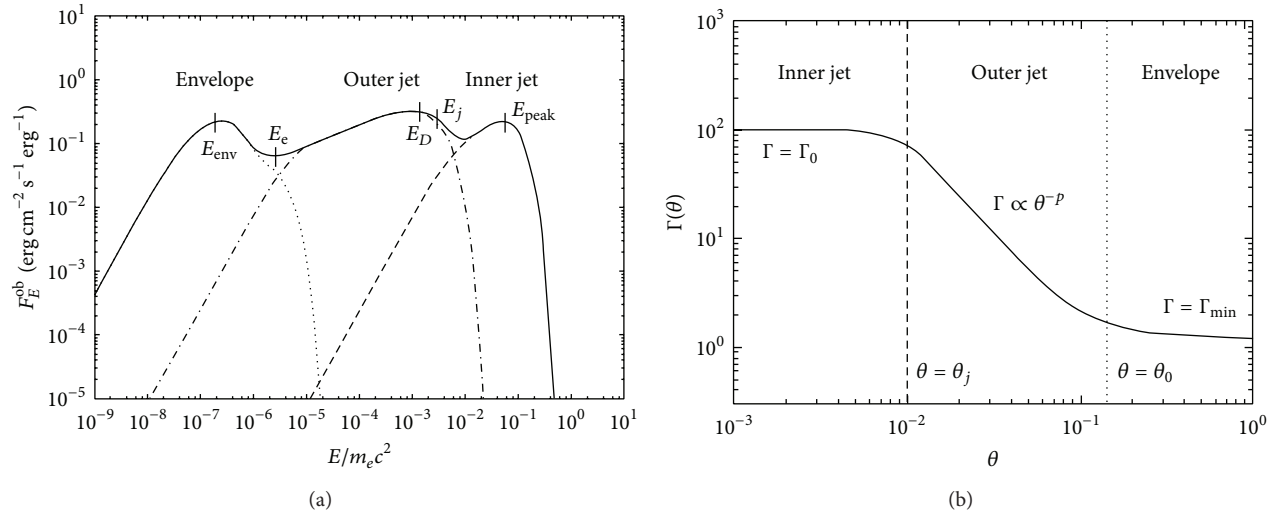

Figure 19: (a) The expected (observed) spectrum from a relativistic, optically thick outflow. The resulting spectra does not resemble the naively expected "Planck" spectrum. Separate integration of the contributions from the inner jet (where $\Gamma \approx \Gamma_0$), outer jet (where Γ drops with angle), and envelope is shown with dashed, dot dashed, and dotted lines, respectively. (b) The assumed jet profile. Figure taken from Lundman et al. [244].

dissipation takes place at intermediate radii, $\sim 10^{10}$ cm, where the outflow Lorentz factor is mild, $\Gamma \sim 10$. Furthermore, this radius of $\sim 10^{8.5}$ cm is a robust radius where jet collimation shock is observed in numerical simulations [427, 434]. These results thus point towards a new understanding of the early phases of jet dynamics.

A second interesting implication is an indirect way of constraining the magnetization of the outflow. It was shown by Zhang and Mészáros [435], Daigne and Mochkovitch [395], and Zhang and Pe'er [436] that for similar parameters, the photospheric contribution in highly magnetized outflows is suppressed. Lack of pronounced thermal component can therefore be used to obtain a lower value on the magnetization parameter, σ [436]. Furthermore, it was recently shown [405] that in fact in the framework of standard magnetic reconnection model, conditions for full thermalization do not exist in the entire region below the photosphere. As a result, the produced photons are upscattered, and the resulting peak of the Wien distribution formed is at $\gtrsim$10 MeV. This again leads to the conclusion that identification of thermal component at energies of $\lesssim$100 keV must imply that the outflow cannot be highly magnetized.

4. Summary and Conclusion

We are currently in the middle of a very exciting epoch in the study of GRB prompt emission. Being very short, random, and nonrepetitive, study of the prompt emission is notoriously difficult. The fact that no two GRBs are similar makes it extremely difficult to draw firm conclusions that are valid for all GRBs. Nonetheless, following the launch of *Swift* and *Fermi*, ample observational and theoretical efforts have been put in understanding the elusive nature of these complex events. I think that it is fair to say that we are finally close to understanding the essence of it.

To my opinion, there are two parts to the revolution that took place in the last few years. The first is the raise of the time-dependent spectral analysis, which enables a distinction between different spectral components that show different temporal evolution. A particularly good example is the temporal behavior of the high energy (GeV) part of the spectrum, that is lagging behind lower energy photons. This temporal distinction enables a separate study of each component and points towards more than a single emission zone. This distinction, in fact, is aligned with the initial assumptions of the "fireball" model, in which internal collisions (or several episodes of magnetic energy dissipation) lead to multiple emission zones.

The second part of the revolution is associated with the identification of a thermal component on top of the nonthermal spectra. For many years, until today, the standard fitting of GRB spectra were and still are carried using a mathematical function, namely, the "Band" model. Being mathematical in nature, this model does not have any "preferred" physical scenario, but its results can be interpreted in more than one way. As a result, it is difficult to obtain a theoretical insight using these fits. As was pointed out over 15 years ago, basic radiative models, such as synchrotron, fail to provide a valid interpretation to the obtained results. Moreover, while a great advantage of this model is its simplicity, here lies also its most severe limitation: being very simply, it is not able to account for many spectral and temporal details, which are likely crucial in understanding the underlying physics of GRBs.

It was only in recent years, with the abandoning of the "Band" model as a sole model for fitting GRB prompt emission data, that rapid progress was enabled. The introduction of thermal emission component played a key role in this revolution. First, it provides a strongly physically motivated explanation to at least part of the spectrum. Second,

the values of the parameters describing the nonthermal part of the spectra are different than the values derived without the addition of a thermal component; this makes it easier to provide a physical interpretation to the nonthermal part. Third, the observed well defined temporal behavior opened a new window into exploring the temporal evolution of the spectra. These observational realizations triggered a wealth of theoretical ideas aimed at explaining both the observed spectral and temporal behaviors.

Currently, there is still no single theoretical model that is accepted by the majority of the community. This is due to the fact that although it is clear that synchrotron emission from optically thin regions cannot account for the vast majority of GRBs, pure thermal component is only rarely observed. Furthermore, clearly the very high energy (GeV band) emission has a nonthermal origin, and therefore even if thermal component does play an important role, there must be additional processes contributing to the high energy part. Moreover, while thermal photons are observed in some GRBs, there are others in which there is no evidence for such a component. Thus, whatever theoretical idea may be used to explain the data, it must be able to explain the diversity observed.

At present epoch, there are three leading suggestions for explaining the variety of the data. The first is that the variety seen is due to different in magnetization. It is indeed a very appealing idea, if it can be proved that the variety of observed spectra depends only on a single parameter. The second type of models consider the different jet geometries and the different observing angles relative to the jet axis. This is a novel approach, never taken before, and as such there is ample of room for continuing research in this direction. The third type of models considers subphotospheric energy dissipation as a way of broadening the "Planck" spectra. The observed spectra in these models thus mainly depend on the details of the dissipation process and in particular the optical depth in which it takes place.

All of these models hold great promise, as they enable not only to identify directly the key ingredients that shape the observed spectra, but also to use observations to directly infer physical properties. These include the jet dynamics, Lorentz factor, geometry (Γ as a function of r, θ, and maybe also ϕ), and even the magnetization. Knowledge of these quantities thus directly reflects on answering basic questions of great interest to astronomy, such as jet launching, composition, and collimation.

Thus, to conclude, my view is that we are in the middle of the "prompt emission revolution." It is too early to claim that we fully understand the prompt emission; indeed, we have reached no consensus yet about many of the key properties, as is reflected by the large number of different ideas. However, we understand various key properties of the prompt emission in a completely different way than only 5–10 years ago. Thus, I believe that another 5–10 years from now there is a good chance that we could get to a conclusive idea about the nature of the prompt emission and would be able to use it as a great tool in studying many other important issues, such as stellar evolution, gravitational waves, and cosmic rays.

Conflict of Interests

The author declares that there is no conflict of interests regarding the publication of this paper.

Acknowledgment

The author would like to thank Felix Ryde for numerous useful discussions.

References

[1] E. Waxman, "Gamma-ray bursts: the underlying model," in *Supernovae and Gamma-Ray Bursters*, K. Weiler, Ed., vol. 598 of *Lecture Notes in Physics*, pp. 393–418, Springer, Berlin, Germany, 2003.

[2] T. Piran, "The physics of gamma-ray bursts," *Reviews of Modern Physics*, vol. 76, no. 4, pp. 1143–1210, 2004.

[3] B. Zhang and P. Mészáros, "Gamma-ray bursts: progress, problems & prospects," *International Journal of Modern Physics A*, vol. 19, no. 15, pp. 2385–2472, 2004.

[4] P. Mészáros, "Gamma-ray bursts," *Reports on Progress in Physics*, vol. 69, no. 8, pp. 2259–2321, 2006.

[5] E. Nakar, "Short-hard gamma-ray bursts," *Physics Reports*, vol. 442, no. 1–6, pp. 166–236, 2007.

[6] B. Zhang, "Gamma-ray bursts in the swift era," *Chinese Journal of Astronomy and Astrophysics*, vol. 7, no. 1, pp. 1–50, 2007.

[7] Y.-Z. Fan and T. Piran, "High-energy γ-ray emission from gamma-ray bursts—before GLAST," *Frontiers of Physics in China*, vol. 3, no. 3, pp. 306–330, 2008.

[8] N. Gehrels, E. Ramirez-Ruiz, and D. B. Fox, "Gamma-ray bursts in the swift era," *Annual Review of Astronomy and Astrophysics*, vol. 47, pp. 567–617, 2009.

[9] J.-L. Atteia and M. Boër, "Observing the prompt emission of GRBs," *Comptes Rendus Physique*, vol. 12, no. 3, pp. 255–266, 2011.

[10] N. Gehrels and P. Mészáros, "Gamma-ray bursts," *Science*, vol. 337, no. 6097, pp. 932–936, 2012.

[11] N. Bucciantini, "Magnetars and gamma ray bursts," in *Proceedings of the IAU Symposium: Death of Massive Stars: Supernovae and Gamma-Ray Bursts*, vol. 279, pp. 289–296, 2012.

[12] N. Gehrels and S. Razzaque, "Gamma-ray bursts in the swift-Fermi era," *Frontiers of Physics*, vol. 8, no. 6, pp. 661–678, 2013.

[13] F. Daigne, "GRB prompt emission and the physics of ultra-relativistic outflows," in *Gamma-Ray Bursts: 15 Years of GRB Afterglows*, A. J. Castro-Tirado, J. Gorosabel, and I. H. Park, Eds., vol. 61 of *Park EAS Publications Series*, pp. 185–191, EAS, 2013.

[14] B. Zhang, "Gamma-ray burst prompt emission," *International Journal of Modern Physics D*, vol. 23, no. 2, Article ID 1430002, 18 pages, 2014.

[15] P. Kumar and B. Zhang, "The physics of gamma-ray bursts and relativistic jets," *Physics Reports*, vol. 561, pp. 1–109, 2015.

[16] E. Berger, "Short-duration gamma-ray bursts," *Annual Review of Astronomy and Astrophysics*, vol. 52, no. 1, pp. 43–105, 2014.

[17] P. Meszaros and M. J. Rees, "Gamma-ray bursts," in *General Relativity and Gravitation: A Centennial Perspective*, A. Ashtekar, B. Berger, J. Isenberg, and M. A. H. MacCallum, Eds., Cambridge University Press, Cambridge, UK, 2014.

[18] B. Gendre, G. Stratta, J. L. Atteia et al., "The ultra-long gamma-ray burst 111209A: the collapse of a blue supergiant?" *The Astrophysical Journal*, vol. 766, no. 1, article 30, 2013.

[19] C. Kouveliotou, C. A. Meegan, G. J. Fishman et al., "Identification of two classes of gamma-ray bursts," *The Astrophysical Journal*, vol. 413, no. 2, pp. 101–104, 1993.

[20] W. S. Paciesas, C. A. Meegan, G. N. Pendleton et al., "The fourth BATSE gamma-ray burst catalog (revised)," *The Astrophysical Journal*, vol. 122, no. 2, pp. 465–495, 1999.

[21] W. S. Paciesas, C. A. Meegan, A. von Kienlin et al., "The Fermi GBM gamma-ray burst catalog: the first two years," *The Astrophysical Journal, Supplement Series*, vol. 199, no. 1, article 18, 2012.

[22] Y. Qin, E.-W. Liang, Y.-F. Liang et al., "A comprehensive analysis of fermi gamma-ray burst data. III. energy-dependent T_{90} distributions of GBM GRBs and instrumental selection effect on duration classification," *The Astrophysical Journal*, vol. 763, no. 1, article 15, 2013.

[23] A. von Kienlin, C. A. Meegan, W. S. Paciesas et al., "The second Fermi GBM gamma-ray burst catalog: the first four years," *The Astrophysical Journal Supplement Series*, vol. 211, no. 1, article 13, 2014.

[24] T. Sakamoto, S. D. Barthelmy, W. H. Baumgartner et al., "The second Swift Burst Alert Telescope gamma-ray burst catalog," *The Astrophysical Journal, Supplement Series*, vol. 195, no. 1, article 2, 2011.

[25] Ž. Bošnjak, D. Götz, L. Bouchet, S. Schanne, and B. Cordier, "The spectral catalogue of INTEGRAL gamma-ray bursts: results of the joint IBIS/SPI spectral analysis," *Astronomy & Astrophysics*, vol. 561, article 25, 2014.

[26] T. J. Galama, P. M. Vreeswijk, J. van Paradijs et al., "An unusual supernova in the error box of the γ-ray burst of 25 April 1998," *Nature*, vol. 395, no. 6703, pp. 670–672, 1998.

[27] J. Hjorth, J. Sollerman, P. Møller et al., "A very energetic supernova associated with the γ-ray burst of 29 March 2003," *Nature*, vol. 423, no. 6942, pp. 847–850, 2003.

[28] K. Z. Stanek, T. Matheson, P. M. Garnavich et al., "Spectroscopic discovery of the supernova 2003dh associated with GRB 030329," *The Astrophysical Journal Letters*, vol. 591, no. 1, pp. L17–L20, 2003.

[29] S. Campana, V. Mangano, A. J. Blustin et al., "The association of GRB 060218 with a supernova and the evolution of the shock wave," *Nature*, vol. 442, no. 7106, pp. 1008–1010, 2006.

[30] E. Pian, P. A. Mazzali, N. Masetti et al., "An optical supernova associated with the X-ray flash XRF 060218," *Nature*, vol. 442, no. 7106, pp. 1011–1013, 2006.

[31] B. E. Cobb, J. S. Bloom, D. A. Perley, A. N. Morgan, S. B. Cenko, and A. V. Filippenko, "Discovery of SN 2009nz associated with GRB 091127," *The Astrophysical Journal Letters*, vol. 718, no. 2, pp. L150–L155, 2010.

[32] R. L. C. Starling, K. Wiersema, A. J. Levan et al., "Discovery of the nearby long, soft GRB100316D with an associated supernova," *Monthly Notices of the Royal Astronomical Society*, vol. 411, no. 4, pp. 2792–2803, 2011.

[33] D. A. Kann, S. Klose, B. Zhang et al., "The afterglows of swift-era gamma-ray bursts. II. Type I GRB versus type II GRB optical afterglows," *Astrophysical Journal*, vol. 734, no. 2, article 96, 2011.

[34] N. Gehrels, C. L. Sarazin, P. T. O'Brien et al., "A short γ-ray burst apparently associated with an elliptical galaxy at redshift z = 0.225," *Nature*, vol. 437, no. 7060, pp. 851–854, 2005.

[35] D. B. Fox, D. A. Frail, P. A. Price et al., "The afterglow of GRB 050709 and the nature of the short-hard γ-ray bursts," *Nature*, vol. 437, no. 7060, pp. 845–850, 2005.

[36] J. S. Villasenor, D. Q. Lamb, G. R. Ricker et al., "Discovery of the short γ-ray burst GRB 050709," *Nature*, vol. 437, no. 7060, pp. 855–858, 2005.

[37] S. D. Barthelmy, G. Chincarini, D. N. Burrows et al., "An origin for short γ-ray bursts unassociated with current star formation," *Nature*, vol. 438, no. 7070, pp. 994–996, 2005.

[38] J. Hjorth, J. Sollerman, J. Gorosabel et al., "GRB 050509B: constraints on short gamma-ray burst models," *The Astrophysical Journal Letters*, vol. 630, no. 2, pp. L117–L120, 2005.

[39] J. S. Bloom, J. X. Prochaska, D. Pooley et al., "Closing in on a short-hard burst progenitor: constraints from early-time optical imaging and spectroscopy of a possible host galaxy of GRB 050509b," *Astrophysical Journal Letters*, vol. 638, no. 1, pp. 354–368, 2006.

[40] E. Troja, A. R. King, P. T. O'Brien, N. Lyons, and G. Cusumano, "Different progenitors of short hard gamma-ray bursts," *Monthly Notices of the Royal Astronomical Society: Letters*, vol. 385, no. 1, pp. L10–L14, 2008.

[41] W. Fong and E. Berger, "The locations of short gamma-ray bursts as evidence for compact object binary progenitors," *Astrophysical Journal*, vol. 776, no. 1, article 18, 2013.

[42] B. Zhang, B.-B. Zhang, E. N.-W. Liang, N. Gehrels, D. N. Burrows, and P. Mészáros, "Making a short gamma-ray burst from a long one: implications for the nature of GRB 060614," *The Astrophysical Journal*, vol. 655, no. 1, pp. L25–L28, 2007.

[43] M. Nysewander, A. S. Fruchter, and A. Pe'Er, "A comparison of the afterglows of short- and long-duration gamma-ray bursts," *The Astrophysical Journal*, vol. 701, no. 1, pp. 824–836, 2009.

[44] B. Zhang, B.-B. Zhang, F. J. Virgili et al., "Discerning the physical origins of cosmological gamma-ray bursts based on multiple observational criteria: the cases of $z = 6.7$ GRB 080913, $z = 8.2$ GRB 090423, and some short/hard GRBs," *The Astrophysical Journal*, vol. 703, no. 2, pp. 1696–1724, 2009.

[45] F. J. Virgili, B. Zhang, P. O'Brien, and E. Troja, "Are all short-hard gamma-ray bursts produced from mergers of compact stellar objects?" *The Astrophysical Journal*, vol. 727, no. 2, 2011.

[46] J. P. Norris, N. Gehrels, and J. D. Scargle, "Heterogeneity in short gamma-ray bursts," *The Astrophysical Journal*, vol. 735, no. 1, article 23, 2011.

[47] E. Berger, "The environments of short-duration gamma-ray bursts and implications for their progenitors," *New Astronomy Reviews*, vol. 55, no. 1-2, pp. 1–22, 2011.

[48] O. Bromberg, E. Nakar, T. Piran, and R. Sari, "Short versus long and collapsars versus non-collapsars: a quantitative classification of gamma-ray bursts," *Astrophysical Journal*, vol. 764, no. 2, article 179, 2013.

[49] W. Fong, E. Berger, R. Chornock et al., "Demographics of the galaxies hosting short-duration gamma-ray bursts," *The Astrophysical Journal*, vol. 769, no. 1, article 56, 2013.

[50] S. Mukherjee, E. D. Feigelson, G. J. Babu, F. Murtagh, C. Fralev, and A. Raftery, "Three types of gamma-ray bursts," *The Astrophysical Journal*, vol. 508, no. 1, pp. 314–327, 1998.

[51] I. Horváth, "A third class of gamma-ray bursts?" *The Astrophysical Journal*, vol. 508, no. 2, pp. 757–759, 1998.

[52] I. Horváth, L. G. Balázs, Z. Bagoly, F. Ryde, and A. Mészáros, "A new definition of the intermediate group of gamma-ray bursts," *Astronomy and Astrophysics*, vol. 447, no. 1, pp. 23–30, 2006.

[53] P. Veres, Z. Bagoly, I. Horváth, A. Mészáros, and L. G. Balázs, "A distinct peak-flux distribution of the third class of gamma-ray bursts: a possible signature of X-ray flashes?" *The Astrophysical Journal*, vol. 725, no. 2, pp. 1955–1964, 2010.

[54] J. Hakkila, T. W. Giblin, R. J. Roiger, D. J. Haglin, W. S. Paciesas, and C. A. Meegan, "How sample completeness affects gamma-ray burst classification," *Astrophysical Journal Letters*, vol. 582, no. 1, pp. 320–329, 2003.

[55] J. P. Norris, J. T. Bonnell, D. Kazanas, J. D. Scarole, J. Hakkila, and T. W. Giblin, "Long-lag, wide-pulse gamma-ray bursts," *The Astrophysical Journal*, vol. 627, no. 1, pp. 324–345, 2005.

[56] E. W. Liang, B. Zhang, P. T. O'Brien et al., "Testing the curvature effect and internal origin of gamma-ray burst prompt emissions and X-ray flares with Swift data," *Astrophysical Journal Letters*, vol. 646, no. 1, pp. 351–357, 2006.

[57] A. A. Abdo, M. Ackermann, M. Arimoto et al., "Fermi observations of high-energy gamma-ray emission from GRB 080916C," *Science*, vol. 323, no. 5922, pp. 1688–1693, 2009.

[58] T. W. Giblin, V. Connaughton, J. van Paradijs et al., "Extended power-law decays in batse gamma-ray bursts: signatures of external shocks," *Astrophysical Journal Letters*, vol. 570, no. 2, pp. 573–587, 2002.

[59] L. Nicastro, J. J. M. In't Zand, L. Amati et al., "Multiwavelength study of the very long GRB 020410," *Astronomy and Astrophysics*, vol. 427, no. 2, pp. 445–452, 2004.

[60] F. J. Virgili, C. G. Mundell, V. Pal'Shin et al., "GRB 091024A and the nature of ultra-long gamma-ray bursts," *Astrophysical Journal*, vol. 778, no. 1, article 54, 2013.

[61] G. Stratta, B. Gendre, J. L. Atteia et al., "The ultra-long GRB 111209A. II. Prompt to afterglow and afterglow properties," *The Astrophysical Journal*, vol. 779, no. 1, article 66, 2013.

[62] A. J. Levan, N. R. Tanvir, R. L. C. Starling et al., "A new population of ultra-long duration gamma-ray bursts," *The Astrophysical Journal*, vol. 781, no. 1, article 13, 2014.

[63] P. A. Evans, R. Willingale, J. P. Osborne et al., "GRB 130925A: an ultralong gamma ray burst with a dust-echo afterglow, and implications for the origin of the ultralong GRBs," *Monthly Notices of the Royal Astronomical Society*, vol. 444, no. 1, pp. 250–267, 2014.

[64] B. Gendre and G. Stratta, "Models and possible progenitors of gamma-ray bursts at the test field of the observations," Proceedings of the Rencontres de Moriond 2013: Very High Energy Phenomena in the Universe session, http://arxiv.org/abs/1305.3194.

[65] D. Nakauchi, K. Kashiyama, Y. Suwa, and T. Nakamura, "Blue supergiant model for ultra-long gamma-ray burst with superluminous-supernova-like bump," *The Astrophysical Journal*, vol. 778, no. 1, article 67, 2013.

[66] B.-B. Zhang, B. Zhang, K. Murase, V. Connaughton, and M. S. Briggs, "How long does a burst burst?" *The Astrophysical Journal*, vol. 787, no. 1, article 66, 2014.

[67] H. Gao and P. Mészáros, "Relation between the intrinsic and observed central engine activity time: implications for ultra-long GRBs," *The Astrophysical Journal*, vol. 802, no. 2, p. 90, 2014.

[68] D. Band, J. Matteson, L. Ford et al., "BATSE observations of gamma-ray burst spectra. I. Spectral diversity," *Astrophysical Journal Letters*, vol. 413, no. 1, pp. 281–292, 1993.

[69] Y. Kaneko, R. D. Preece, M. S. Briggs, W. S. Paciesas, C. A. Meegan, and D. L. Band, "The complete spectral catalog of bright batse gamma-ray bursts," *The Astrophysical Journal, Supplement Series*, vol. 166, no. 1, pp. 298–340, 2006.

[70] L. Nava, G. Ghirlanda, G. Ghisellini, and A. Celotti, "Spectral properties of 438 GRBs detected by *Fermi*/GBM," *Astronomy & Astrophysics*, vol. 530, article 21, 2011.

[71] A. Goldstein, J. M. Burgess, R. D. Preece et al., "The fermi GBM gamma-ray burst spectral catalog: the first two years," *The Astrophysical Journal*, vol. 199, no. 1, article 19, 2012.

[72] A. Goldstein, R. D. Preece, R. S. Mallozzi et al., "The BATSE 5B gamma-ray burst spectral catalog," *Astrophysical Journal*, vol. 208, no. 2, article 21, 2013.

[73] R. D. Preece, M. S. Briggs, R. S. Mallozzi, G. N. Pendleton, W. S. Paciesas, and D. L. Band, "The BATSE gamma-ray Burst spectral catalog. I. High time resolution spectroscopy of bright Bursts using high energy resolution data," *The Astrophysical Journal*, vol. 126, no. 1, pp. 19–36, 2000.

[74] L. Nava, G. Ghirlanda, G. Ghisellini, and A. Celotti, "Fermi/GBM and BATSE gamma-ray bursts: comparison of the spectral properties," *Monthly Notices of the Royal Astronomical Society*, vol. 415, no. 4, pp. 3153–3162, 2011.

[75] B.-B. Zhang, E.-W. Liang, Y.-Z. Fan et al., "A comprehensive analysis of fermi gamma-ray burst data. I. Spectral components and the possible physical origins of LAT/GBM GRBs," *The Astrophysical Journal*, vol. 730, no. 2, article 141, 2011.

[76] D. Gruber, A. Goldstein, V. W. von Ahlefeld et al., "The Fermi GBM gamma-ray burst spectral catalog: four years of data," *Astrophysical Journal, Supplement Series*, vol. 211, no. 1, article 12, 2014.

[77] J. Goodman, "Are gamma-ray bursts optically thick?" *The Astrophysical Journal*, vol. 308, pp. 47–50, 1986.

[78] B. Paczynski, "Gamma-ray bursters at cosmological distances," *The Astrophysical Journal*, vol. 308, pp. L43–L46, 1986.

[79] M. Tavani, "A shock emission model for gamma-ray bursts. II. Spectral properties," *The Astrophysical Journal*, vol. 466, no. 2, pp. 768–778, 1996.

[80] E. Cohen, J. I. Katz, T. Piran, R. Sari, R. D. Preece, and D. L. Band, "Possible evidence for relativistic shocks in gamma-ray bursts," *The Astrophysical Journal*, vol. 488, no. 1, pp. 330–337, 1997.

[81] A. Panaitescu, M. Spada, and P. Mészáros, "Power density spectra of gamma-ray bursts in the internal shock model," *The Astrophysical Journal*, vol. 522, no. 2, pp. L105–L108, 1999.

[82] F. Frontera, L. Amati, E. Costa et al., "Prompt and delayed emission properties of gamma-ray bursts observed with *BeppoSAX*," *The Astrophysical Journal*, vol. 127, no. 1, pp. 59–78, 2000.

[83] B. A. Crider, E. P. Liang, I. A. Smith et al., "Evolution of the low-energy photon spectra in gamma-ray bursts," *Astrophysical Journal Letters*, vol. 479, no. 1, pp. L39–L42, 1997.

[84] R. D. Preece, M. S. Briggs, R. S. Mallozzi, G. N. Pendleton, W. S. Paciesas, and D. L. Band, "The synchrotron shock model confronts a 'Line of death' in the BATSE gamma-ray burst data," *The Astrophysical Journal Letters*, vol. 506, no. 1, pp. L23–L26, 1998.

[85] R. D. Preece, M. S. Briggs, T. W. Gibun et al., "On the consistency of gamma-ray burst spectral indices with the synchrotron shock model," *The Astrophysical Journal*, vol. 581, no. 2, pp. 1248–1255, 2002.

[86] G. Ghirlanda, A. Celotti, and G. Ghisellini, "Extremely hard GRB spectra prune down the forest of emission models," *Astronomy and Astrophysics*, vol. 406, no. 3, pp. 879–892, 2003.

[87] F. Ryde, "The cooling behavior of thermal pulses in gamma-ray bursts," *The Astrophysical Journal*, vol. 614, no. 2, pp. 827–846, 2004.

[88] F. Ryde, "Is thermal emission in gamma-ray bursts ubiquitous?" *The Astrophysical Journal Letters*, vol. 625, no. 2, pp. L95–L98, 2005.

[89] F. Ryde and A. Pe'er, "Quasi-blackbody component and radiative efficiency of the prompt emission of gamma-ray bursts," *Astrophysical Journal Letters*, vol. 702, no. 2, pp. 1211–1229, 2009.

[90] S. McGlynn, S. Foley, B. McBreen et al., "High energy emission and polarisation limits for the *INTEGRAL* burst GRB 061122," *Astronomy & Astrophysics*, vol. 499, no. 2, pp. 465–472, 2009.

[91] J. Larsson, F. Ryde, C. Lundman et al., "Spectral components in the bright, long GRB061007: properties of the photosphere and the nature of the outflow," *Monthly Notices of the Royal Astronomical Society*, vol. 414, no. 3, pp. 2642–2649, 2011.

[92] G. Ghirlanda, Z. Bosnjak, G. Ghisellini, F. Tavecchio, and C. Firmani, "Blackbody components in gamma-ray bursts spectra?" *Monthly Notices of the Royal Astronomical Society*, vol. 379, no. 1, pp. 73–85, 2007.

[93] F. Frontera, L. Amati, R. Farinelli et al., "Comptonization signatures in the prompt emission of gamma-ray bursts," *Astrophysical Journal*, vol. 779, no. 2, article 175, 2013.

[94] M. Ackermann, K. Asano, W. B. Atwood et al., "Fermi observations of GRB 090510: a short-hard gamma-ray burst with an additional, hard power-law component from 10 keV to GeV energies," *The Astrophysical Journal*, vol. 716, no. 2, pp. 1178–1190, 2010.

[95] A. A. Abdo, M. Ackermann, M. Ajello et al., "Fermi observations of GRB 090902B: a distinct spectral component in the prompt and delayed emission," *The Astrophysical Journal Letters*, vol. 706, no. 1, pp. L138–L144, 2009.

[96] F. Ryde, M. Axelsson, B. B. Zhang et al., "Identification and properties of the photospheric emission in GRB090902B," *The Astrophysical Journal Letters*, vol. 709, no. 2, pp. L172–L177, 2010.

[97] F. Ryde, A. Pe'er, T. Nymark et al., "Observational evidence of dissipative photospheres in gamma-ray bursts," *Monthly Notices of the Royal Astronomical Society*, vol. 415, no. 4, pp. 3693–3705, 2011.

[98] M. Axelsson, L. Baldini, G. Barbiellini et al., "GRB110721A: an extreme peak energy and signatures of the photosphere," *Astrophysical Journal Letters*, vol. 757, no. 2, article L31, 2012.

[99] S. Iyyani, F. Ryde, M. Axelsson et al., "Variable jet properties in GRB 110721A: time resolved observations of the jet photosphere," *Monthly Notices of the Royal Astronomical Society*, vol. 433, no. 4, pp. 2739–2748, 2013.

[100] S. Guiriec, V. Connaughton, M. S. Briggs et al., "Detection of a thermal spectral component in the prompt emission of GRB 100724B," *The Astrophysical Journal Letters*, vol. 727, no. 2, article L33, 2011.

[101] G. Ghirlanda, A. Pescalli, and G. Ghisellini, "Photospheric emission throughout grb 100507 detected by fermi," *Monthly Notices of the Royal Astronomical Society*, vol. 432, no. 4, pp. 3237–3244, 2013.

[102] S. Guiriec, F. Daigne, R. Hascoët et al., "Evidence for a photospheric component in the prompt emission of the short GRB 120323a and its effects on the GRB hardness-luminosity relation," *The Astrophysical Journal*, vol. 770, no. 1, article 32, 2013.

[103] R. Basak and A. R. Rao, "Time-resolved spectral study of Fermi gamma-ray bursts having single pulses," *Monthly Notices of the Royal Astronomical Society*, vol. 442, no. 1, pp. 419–427, 2014.

[104] W. Deng and B. Zhang, "Low energy spectral index and E_p evolution of quasi-thermal photosphere emission of gamma-ray bursts," *The Astrophysical Journal*, vol. 785, no. 2, article 112, 2014.

[105] S. Guiriec, C. Kouveliotou, F. Daigne et al., "Towards a better understanding of the GRB phenomenon: a new model for GRB prompt emission and its effects on the new Non55 Thermal $L_{\mathrm{i}}^{\mathrm{NT}}$-$E_{\mathrm{peak,i}}^{\mathrm{rest,NT}}$ relation," http://arxiv.org/abs/1501.07028.

[106] J. M. Burgess, R. D. Preece, V. Connaughton et al., "Time-resolved analysis of fermi gamma-ray bursts with fast- and slow-cooled synchrotron photon models," *The Astrophysical Journal*, vol. 784, no. 1, article 17, 2014.

[107] H.-F. Yu, J. Greiner, H. van Eerten et al., "Synchrotron cooling in energetic gamma-ray bursts observed by the fermi gamma-ray burst monitor," *Astronomy & Astrophysics*, vol. 573, no. 81, 20 pages, 2015.

[108] J. M. Burgess, F. Ryde, and H.-F. Yu, "Taking the band function too far: a tale of two α's," http://arxiv.org/abs/1410.7647.

[109] M. Axelsson and L. Borgonovo, "The width of gamma-ray burst spectra," *Monthly Notices of the Royal Astronomical Society*, vol. 447, no. 4, pp. 3150–3154, 2015.

[110] R. Preece, J. M. Burgess, A. von Kienlin et al., "The first pulse of the extremely bright GRB 130427a: a test lab for synchrotron shocks," *Science*, vol. 343, no. 6166, pp. 51–54, 2014.

[111] A. A. Abdo, M. Ackermann, M. Ajello et al., "A limit on the variation of the speed of light arising from quantum gravity effects," *Nature*, vol. 462, no. 7271, pp. 331–334, 2009.

[112] P. Kumar and R. B. Duran, "External forward shock origin of high-energy emission for three gamma-ray bursts detected by *Fermi*," *Monthly Notices of the Royal Astronomical Society*, vol. 409, no. 1, pp. 226–236, 2010.

[113] G. Ghirlanda, G. Ghisellini, and L. Nava, "The onset of the GeV afterglow of GRB 090510," *Astronomy and Astrophysics*, vol. 510, no. 1, article L7, 2010.

[114] M. Ackermann, M. Ajello, K. Asano et al., "The first Fermi-Lat gamma-ray burst catalog," *Astrophysical Journal, Supplement Series*, vol. 209, no. 1, article 11, 2013.

[115] L. Nava, G. Vianello, N. Omodei et al., "Clustering of LAT light curves: a clue to the origin of high-energy emission in gamma-ray bursts," *Monthly Notices of the Royal Astronomical Society*, vol. 443, no. 4, pp. 3578–3585, 2014.

[116] J. L. Racusin, S. V. Karpov, M. Sokolowski et al., "Broadband observations of the naked-eye γ-ray burst GRB 080319B," *Nature*, vol. 455, no. 7210, pp. 183–188, 2008.

[117] C. Akerlof, R. Balsano, S. Barthelmy et al., "Observation of contemporaneous optical radiation from a γ-ray burst," *Nature*, vol. 398, no. 6726, pp. 400–402, 1999.

[118] G. B. Rybicki and A. P. Lightman, *Radiative Processes in Astrophysics*, 1979.

[119] S. Covino, D. Lazzati, G. Ghisellini et al., "GRB 990510: linearly polarized radiation from a fireball," *Astronomy & Astrophysics*, vol. 348, pp. L1–L4, 1999.

[120] R. A. M. J. Wijers, P. M. Vreeswijk, T. J. Galama et al., "Detection of polarization in the afterglow of GRB 990510 with the ESO very large telescope," *The Astrophysical Journal Letters*, vol. 523, no. 1, pp. L33–L36, 1999.

[121] A. Loeb and R. Perna, "Microlensing of gamma-ray burst afterglows," *The Astrophysical Journal*, vol. 495, no. 2, pp. 597–603, 1998.

[122] A. Gruzinov and E. Waxman, "Gamma-ray burst afterglow: polarization and analytic light curves," *The Astrophysical Journal*, vol. 511, no. 2, pp. 852–861, 1999.

[123] G. Ghisellini and D. Lazzati, "Polarization light curves and position angle variation of beamed gamma-ray bursts," *Monthly Notices of the Royal Astronomical Society*, vol. 309, no. 1, pp. L7–L11, 1999.

[124] M. V. Medvedev and A. Loeb, "Generation of magnetic fields in the relativistic shock of gamma-ray burst sources," *The Astrophysical Journal*, vol. 526, no. 2, pp. 697–706, 1999.

[125] J. Granot and A. Königl, "Linear polarization in gamma-ray bursts: the case for an ordered magnetic field," *The Astrophysical Journal*, vol. 594, no. 2, pp. 83–87, 2003.

[126] W. Coburn and S. E. Boggs, "Polarization of the prompt γ-ray emission from the γ-ray burst of 6 December 2002," *Nature*, vol. 423, no. 6938, pp. 415–417, 2003.

[127] R. E. Rutledge and D. B. Fox, "Re-analysis of polarization in the γ-ray flux of GRB 021206," *Monthly Notices of the Royal Astronomical Society*, vol. 350, no. 4, pp. 1288–1300, 2004.

[128] D. R. Willis, E. J. Barlow, A. J. Bird et al., "Evidence of polarisation in the prompt gamma-ray emission from GRB 930131 and GRB 960924," *Astronomy and Astrophysics*, vol. 439, no. 1, pp. 245–253, 2005.

[129] E. Kalemci, S. E. Boggs, C. Kouveliotou, M. Finger, and M. G. Baring, "Search for polarization from the prompt gamma-ray emission of GRB 041219a with SPI on INTEGRAL," *The Astrophysical Journal*, vol. 169, no. 1, pp. 75–82, 2007.

[130] S. McGlynn, D. J. Clark, A. J. Dean et al., "Polarisation studies of the prompt gamma-ray emission from GRB 041219a using the spectrometer aboard INTEGRAL," *Astronomy and Astrophysics*, vol. 466, no. 3, pp. 895–904, 2007.

[131] D. Götz, P. Laurent, F. Lebrun, F. Daigne, and Ž. Bošnjak, "Variable polarization measured in the prompt emission of GRB 041219a using ibis on board integral," *Astrophysical Journal Letters*, vol. 695, no. 2, pp. L208–L212, 2009.

[132] D. Yonetoku, T. Murakami, S. Gunji et al., "Detection of Gamma-Ray polarization in prompt emission of GRB 100826A," *The Astrophysical Journal*, vol. 743, no. 2, article L30, 2011.

[133] D. Yonetoku, T. Murakami, S. Gunji et al., "Magnetic structures in gamma-ray burst jets probed by gamma-ray polarization," *The Astrophysical Journal Letters*, vol. 758, no. 1, article L1, 2012.

[134] J. Granot, Fermi LAT Collaboration, and GBM Collaboration, "Highlights from Fermi GRB observations," in *Proceedings of the Shocking Universe—Gamma-Ray Bursts and High Energy Shock Phenomena*, Venice, Italy, September 2009, http://arxiv.org/abs/1003.2452.

[135] R. Atkins, W. Benbow, D. Berley et al., "Evidence for TeV emission from GRB 970417a," *Astrophysical Journal Letters*, vol. 533, no. 2, pp. L119–L122, 2000.

[136] J. Albert, E. Aliu, H. Anderhub et al., "Very high energy gamma-ray radiation from the stellar mass black hole binary cygnus X-1," *The Astrophysical Journal Letters*, vol. 665, no. 1, pp. 51–54, 2007.

[137] J. Aleksić, S. Ansoldi, L. A. Antonelli et al., "MAGIC upper limits on the GRB 090102 afterglow," *Monthly Notices of the Royal Astronomical Society*, vol. 437, no. 4, pp. 3103–3111, 2014.

[138] P. M. S. Parkinson and B. L. Dingus, "A search for prompt very high energy emission from satellite-detected gamma-ray bursts using milagro," in *Proceedings of the 30th International Cosmic Ray Conference*, R. Caballero, J. C. D'Olivo, G. Medina-Tanco, L. Nellen, F. A. Sánchez, and J. F. Valdés-Galicia, Eds., vol. 3, pp. 1187–1190, Universidad Nacional Autónoma de México, Yucatán, Mexico, July 2007.

[139] F. Aharonian, A. G. Akhperjanian, U. B. de Almeida et al., "HESS observations of the prompt and afterglow phases of GRB 060602B," *The Astrophysical Journal*, vol. 690, no. 2, pp. 1068–1073, 2009.

[140] F. Aharonian, A. G. Akhperjanian, U. Barres de Almeida et al., "HESS observations of γ-ray bursts in 2003–2007," *Astronomy & Astrophysics*, vol. 495, pp. 505–512, 2009.

[141] H. E. S. S. Collaboration, A. Abramowski, F. Aharonian et al., "Search for TeV gamma-ray emission from GRB 100621A, an extremely bright GRB in X-rays, with H.E.S.S," *Astronomy & Astrophysics*, vol. 565, article A16, 6 pages, 2014.

[142] V. A. Acciari, E. Aliu, T. Arlen et al., "Veritas observations of gamma-ray bursts detected by Swift," *Astrophysical Journal*, vol. 743, no. 1, article 62, 2011.

[143] A. U. Abeysekara, R. Alfaro, C. Alvarez et al., "Search for gamma-rays from the unusually bright GRB 130427A with the HAWC gamma-ray observatory," *The Astrophysical Journal*, vol. 800, no. 2, p. 78, 2015.

[144] C. H. Blake, J. S. Bloom, D. L. Starr et al., "An infrared flash contemporaneous with the -rays of GRB 041219a," *Nature*, vol. 435, no. 7039, pp. 181–184, 2005.

[145] P. Romano, S. Campana, G. Chincarini et al., "Panchromatic study of GRB 060124: from precursor to afterglow," *Astronomy & Astrophysics*, vol. 456, no. 3, pp. 917–927, 2006.

[146] K. L. Page, R. Willingale, J. P. Osborne et al., "GRB 061121: broadband spectral evolution through the prompt and afterglow phases of a bright burst," *The Astrophysical Journal*, vol. 663, no. 2, pp. 1125–1138, 2007.

[147] C. Guidorzi, S. Kobayashi, D. A. Perley et al., "A faint optical flash in dust-obscured GRB 080603A: implications for GRB prompt emission mechanisms," *Monthly Notices of the Royal Astronomical Society*, vol. 417, no. 3, pp. 2124–2143, 2011.

[148] A. Rossi, S. Schulze, S. Klose et al., "The swift/fermi GRB 080928 from 1 eV to 150 keV," *Astronomy & Astrophysics*, vol. 529, article A142, 2011.

[149] D. Kopač, S. Kobayashi, A. Gomboc et al., "GRB 090727 and gamma-ray bursts with early-time optical emission," *Astrophysical Journal*, vol. 772, no. 1, article 73, 2013.

[150] J. Elliott, H.-F. Yu, S. Schmidl et al., "Prompt emission of GRB 121217A from gamma-rays to the near-infrared," *Astronomy & Astrophysics*, vol. 562, article 100, 2014.

[151] A. Maselli, A. Melandri, L. Nava et al., "GRB 130427A: a nearby ordinary monster," *Science*, vol. 343, no. 6166, pp. 48–51, 2014.

[152] J. Greiner, H.-F. Yu, T. Krühler et al., "GROND coverage of the main peak of gamma-ray burst 130925A," *Astronomy & Astrophysics*, vol. 568, p. A75, 2014.

[153] W. T. Vestrand, J. A. Wren, P. R. Wozniak et al., "Energy input and response from prompt and early optical afterglow emission in γ-ray bursts," *Nature*, vol. 442, no. 7099, pp. 172–175, 2006.

[154] W. Zheng, R. F. Shen, T. Sakamoto et al., "Panchromatic observations of the textbook GRB 110205A: constraining physical mechanisms of prompt emission and afterglow," *The Astrophysical Journal*, vol. 751, no. 2, article 90, 2012.

[155] S. V. Golenetskii, E. P. Mazets, R. L. Aptekar, and V. N. Ilyinskii, "Correlation between luminosity and temperature in γ-ray burst sources," *Nature*, vol. 306, no. 5942, pp. 451–453, 1983.

[156] V. E. Kargatis, E. P. Liang, K. C. Hurley, C. Barat, E. Eveno, and M. Niel, "Spectral evolution of gamma-ray bursts detected by the SIGNE experiment. I. Correlation between intensity and spectral hardness," *Astrophysical Journal Letters*, vol. 422, no. 1, pp. 260–268, 1994.

[157] L. Amati, F. Frontera, M. Tavani et al., "Intrinsic spectra and energetics of BeppoSAX gamma-ray bursts with known redshifts," *Astronomy and Astrophysics*, vol. 390, no. 1, pp. 81–89, 2002.

[158] L. Amati, "The $E_{p,i}$-E_{iso} correlation in gamma-ray bursts: updated observational status, re-analysis and main implications," *Monthly Notices of the Royal Astronomical Society*, vol. 372, no. 1, pp. 233–245, 2006.

[159] F. Frontera, L. Amati, C. Guidorzi, R. Landi, and J. In'T Zand, "Broadband time-resolved $E_{p,i}$-L_{iso} correlation in gamma-ray bursts," *The Astrophysical Journal*, vol. 754, no. 2, article 138, 2012.

[160] E. Nakar and T. Piran, "Outliers to the peak energy-isotropic energy relation in gamma-ray bursts," *Monthly Notices of the Royal Astronomical Society*, vol. 360, no. 1, pp. L73–L76, 2005.

[161] D. L. Band and R. D. Preece, "Testing the gamma-ray burst energy relationships," *Astrophysical Journal Letters*, vol. 627, no. 1, pp. 319–323, 2005.

[162] N. R. Butler, D. Kocevski, J. S. Bloom, and J. L. Curtis, "A complete catalog of Swift gamma-ray burst spectra and durations: demise of a physical origin for pre-Swift high-energy correlations," *Astrophysical Journal*, vol. 671, no. 1, pp. 656–677, 2007.

[163] N. R. Butler, D. Kocevski, and J. S. Bloom, "Generalized tests for selection effects in gamma-ray burst high-energy correlations," *Astrophysical Journal Letters*, vol. 694, no. 1, pp. 76–83, 2009.

[164] A. Shahmoradi and R. J. Nemiroff, "The possible impact of gamma-ray burst detector thresholds on cosmological standard candles," *Monthly Notices of the Royal Astronomical Society*, vol. 411, no. 3, pp. 1843–1856, 2011.

[165] A. C. Collazzi, B. E. Schaefer, and J. A. Moree, "The total errors in measuring e peak for gamma-ray bursts," *Astrophysical Journal*, vol. 729, no. 2, article 89, 2011.

[166] D. Kocevski, "On the origin of high-energy correlations in gamma-ray bursts," *The Astrophysical Journal*, vol. 747, no. 2, p. 146, 2012.

[167] G. Ghirlanda, G. Ghisellini, and C. Firmani, "Probing the existence of the E_{peak}-E_{iso} correlation in long gamma ray bursts," *Monthly Notices of the Royal Astronomical Society*, vol. 361, no. 1, pp. L10–L14, 2005.

[168] G. Ghirlanda, L. Nava, G. Ghisellini, C. Firmani, and J. I. Cabrera, "The E_{peak}-E_{iso} plane of long gamma-ray bursts and selection effects," *Monthly Notices of the Royal Astronomical Society*, vol. 387, no. 1, pp. 319–330, 2008.

[169] G. Ghirlanda, G. Ghisellini, L. Nava et al., "The impact of selection biases on the E_{peak}-L_{iso} correlation of gamma-ray bursts," *Monthly Notices of the Royal Astronomical Society*, vol. 422, pp. 2553–2559, 2012.

[170] L. Nava, R. Salvaterra, G. Ghirlanda et al., "A complete sample of bright Swift long gamma-ray bursts: testing the spectral-energy correlations," *Monthly Notices of the Royal Astronomical Society*, vol. 421, no. 2, pp. 1256–1264, 2012.

[171] R. Basak and A. R. Rao, "Pulse-wise Amati correlation in Fermi gamma-ray bursts," *Monthly Notices of the Royal Astronomical Society*, vol. 436, no. 4, pp. 3082–3088, 2013.

[172] F. J. Virgili, Y. Qin, B. Zhang, and E. Liang, "Spectral and temporal analysis of the joint *Swift*/BAT-*Fermi*/GBM GRB sample," *Monthly Notices of the Royal Astronomical Society*, vol. 424, no. 4, pp. 2821–2831, 2012.

[173] V. Heussaff, J.-L. Atteia, and Y. Zolnierowski, "The E_{peak}-E_{iso} relation revisited with fermi GRBs: resolving a long-standing debate?" *Astronomy & Astrophysics*, vol. 557, article 100, 2013.

[174] D. M. Wei and W. H. Gao, "Are there cosmological evolution trends on gamma-ray burst features?" *Monthly Notices of the Royal Astronomical Society*, vol. 345, no. 3, pp. 743–746, 2003.

[175] D. Yonetoku, T. Murakami, T. Nakamura, R. Yamazaki, A. K. Inoue, and K. Ioka, "Gamma-ray burst formation rate inferred from the spectral peak energy-peak luminosity relation," *The Astrophysical Journal*, vol. 609, no. 2, pp. 935–951, 2004.

[176] G. Ghirlanda, G. Ghisellini, and D. Lazzati, "The collimation-corrected gamma-ray burst energies correlate with the peak energy of their νF_ν spectrum," *Astrophysical Journal Letters*, vol. 616, no. 1, pp. 331–338, 2004.

[177] G. Ghisellini, G. Ghirlanda, L. Nava, and C. Firmani, "'Late prompt' emission in gamma-ray bursts?" *Astrophysical Journal*, vol. 658, no. 2, pp. L75–L78, 2007.

[178] E.-W. Liang, J. L. Racusin, B. Zhang, B.-B. Zhang, and D. N. Burrows, "A comprehensive analysis of Swift XRT data. III. Jet break candidates in X-ray and optical afterglow light curves," *The Astrophysical Journal*, vol. 675, no. 1, pp. 528–552, 2008.

[179] D. Kocevski and N. Butler, "Gamma-ray burst energetics in the *Swift* ERA," *The Astrophysical Journal*, vol. 680, no. 1, pp. 531–538, 2008.

[180] J. L. Racusin, E. W. Liang, D. N. Burrows et al., "Jet breaks and energetics of swift gamma-ray burst X-ray afterglows," *The Astrophysical Journal*, vol. 698, no. 1, pp. 43–74, 2009.

[181] G. Ryan, H. van Eerten, A. MacFadyen, and B.-B. Zhang, "Gamma-ray bursts are observed off-axis," *The Astrophysical Journal*, vol. 799, no. 1, article 3, 2015.

[182] R. J. Nemiroff, "A century of gamma ray burst models," *Comments on Astrophysics*, vol. 17, p. 189, 1994.

[183] D. Eichler, M. Livio, T. Piran, and D. N. Schramm, "Nucleosynthesis, neutrino bursts and γ-rays from coalescing neutron stars," *Nature*, vol. 340, no. 6229, pp. 126–128, 1989.

[184] B. Paczyński, "Super-Eddington winds from neutron stars," *Astrophysical Journal*, vol. 363, no. 1, pp. 218–226, 1990.

[185] R. Narayan, T. Piran, and A. Shemi, "Neutron star and black hole binaries in the Galaxy," *Astrophysical Journal Letters*, vol. 379, no. 1, pp. L17–L20, 1991.

[186] P. Mészáros and M. J. Rees, "Tidal heating and mass loss in neutron star binaries: implications for gamma-ray burst models," *The Astrophysical Journal*, vol. 397, no. 2, pp. 570–575, 1992.

[187] R. Narayan, B. Paczyński, and T. Piran, "Gamma-ray bursts as the death throes of massive binary stars," *The Astrophysical Journal*, vol. 395, no. 2, pp. 83–86, 1992.

[188] S. E. Woosley, "Gamma-ray bursts from stellar mass accretion disks around black holes," *The Astrophysical Journal*, vol. 405, no. 1, pp. 273–277, 1993.

[189] B. Paczyński, "Are gamma-ray bursts in star-forming regions?" *The Astrophysical Journal Letters*, vol. 494, no. 1, pp. L45–L48, 1998.

[190] B. Paczyński, "Gamma-ray bursts as hypernovae," in *Proceedings of the 4th Huntsville Gamma-Ray Burst Symposium*, C. A. Meegan, R. D. Preece, and T. M. Koshut, Eds., vol. 428 of *American Institute of Physics Conference Series*, pp. 783–787, Huntsville, Ala, USA, May 1998.

[191] C. L. Fryer, S. E. Woosley, and D. H. Hartmann, "Formation rates of black hole accretion disk gamma-ray bursts," *The Astrophysical Journal*, vol. 526, no. 1, pp. 152–177, 1999.

[192] A. I. MacFadyen and S. E. Woosley, "Collapsars: gamma-ray bursts and explosions in 'failed supernovae'," *Astrophysical Journal Letters*, vol. 524, no. 1, pp. 262–289, 1999.

[193] R. Popham, S. E. Woosley, and C. Fryer, "Hyperaccreting black holes and gamma-ray bursts," *The Astrophysical Journal*, vol. 518, no. 1, pp. 356–374, 1999.

[194] S. E. Woosley and J. S. Bloom, "The supernova-gamma-ray burst connection," *Annual Review of Astronomy and Astrophysics*, vol. 44, pp. 507–556, 2006.

[195] G. Cavallo and M. J. Rees, "A qualitative study of cosmic fireballs and gamma-ray bursts," *Monthly Notices of the Royal Astronomical Society*, vol. 183, no. 3, pp. 359–365, 1978.

[196] V. V. Usov, "On the nature of nonthermal radiation from cosmological gamma-ray bursters," *Monthly Notices of the Royal Astronomical Society*, vol. 267, p. 1035, 1994.

[197] C. Thompson, "A model of gamma-ray bursts," *Monthly Notices of the Royal Astronomical Society*, vol. 270, p. 480, 1994.

[198] J. I. Katz, "Yet another model of gamma-ray bursts," *The Astrophysical Journal*, vol. 490, no. 2, pp. 633–641, 1997.

[199] P. Mészáros and M. J. Rees, "Poynting jets from black holes and cosmological gamma-ray bursts," *Astrophysical Journal Letters*, vol. 482, no. 1, pp. L29–L32, 1997.

[200] M. Lyutikov and R. Blandford, "Gamma ray bursts as electromagnetic outflows," http://arxiv.org/abs/astro-ph/0312347.

[201] B. Zhang and H. Yan, "The internal-collision-induced magnetic reconnection and turbulence (ICMART) model of gamma-ray bursts," *The Astrophysical Journal*, vol. 726, no. 2, p. 90, 2011.

[202] A. Shemi and T. Piran, "The appearance of cosmic fireballs," *Astrophysical Journal*, vol. 365, no. 2, pp. L55–L58, 1990.

[203] J. H. Krolik and E. A. Pier, "Relativistic motion in gamma-ray bursts," *The Astrophysical Journal*, vol. 373, no. 1, pp. 277–284, 1991.

[204] E. E. Fenimore, R. I. Epstein, and C. Ho, "The escape of 100 MeV photons from cosmological gammaray bursts," *Astronomy and Astrophysics Supplement Series*, vol. 97, no. 1, pp. 59–62, 1993.

[205] E. Woods and A. Loeb, "Empirical constraints on source properties and host galaxies of cosmological gamma-ray bursts," *The Astrophysical Journal*, vol. 453, no. 2, pp. 583–595, 1995.

[206] M. G. Baring and A. K. Harding, "The escape of high-energy photons from gamma-ray bursts," *The Astrophysical Journal*, vol. 491, no. 2, pp. 663–686, 1997.

[207] R. Sari and T. Piran, "GRB 990123: the optical flash and the fireball model," *The Astrophysical Journal Letters*, vol. 517, no. 2, pp. L109–L112, 1999.

[208] Y. Lithwick and R. Sari, "Lower limits on Lorentz factors in gamma-ray bursts," *Astrophysical Journal Letters*, vol. 555, no. 1, pp. 540–545, 2001.

[209] B. Zhang, S. Kobayashi, and P. Mészáros, "Gamma-ray burst early optical afterglows: implications for the initial lorentz factor and the central engine," *The Astrophysical Journal*, vol. 595, no. 2, pp. 950–954, 2003.

[210] E. Molinari, S. D. Vergani, D. Malesani et al., "REM observations of GRB060418 and GRB 060607A: the onset of the afterglow and the initial fireball Lorentz factor determination," *Astronomy and Astrophysics*, vol. 469, no. 1, pp. 13–16, 2007.

[211] E.-W. Liang, S.-X. Yi, J. Zhang, H.-J. Lü, and B.-B. Zhang, "Constraining gamma-ray burst initial lorentz factor with the afterglow onset feature and discovery of a tight Γ_0-$E_{\gamma,\mathrm{iso}}$ Correlation," *The Astrophysical Journal*, vol. 725, pp. 2209–2224, 2010.

[212] J. L. Racusin, S. R. Oates, P. Schady et al., "*FERMI* and *Swift* gamma-ray burst afterglow population studies," *The Astrophysical Journal*, vol. 738, no. 2, article 138, 2011.

[213] P. Mészáros, P. Laguna, and M. J. Rees, "Gasdynamics of relativistically expanding gamma-ray burst sources: kinematics, energetics, magnetic fields, and efficiency," *Astrophysical Journal Letters*, vol. 415, no. 1, pp. 181–190, 1993.

[214] B. Paczyński and G. Xu, "Neutrino bursts from gamma-ray bursts," *Astrophysical Journal*, vol. 427, no. 2, pp. 708–713, 1994.

[215] M. J. Rees and P. Mészáros, "Unsteady outflow models for cosmological gamma-ray bursts," *The Astrophysical Journal*, vol. 430, no. 2, pp. L93–L96, 1994.

[216] R. Sari and T. Piran, "Variability in gamma-ray bursts: a clue," *The Astrophysical Journal*, vol. 485, no. 1, pp. 270–273, 1997.

[217] S. Kobayashi, T. Piran, and R. Sari, "Can internal shocks produce the variability in gamma-ray bursts?" *Astrophysical Journal Letters*, vol. 490, no. 1, pp. 92–98, 1997.

[218] F. Daigne and R. Mochkovitch, "Gamma-ray bursts from internal shocks in a relativistic wind: temporal and spectral properties," *Monthly Notices of the Royal Astronomical Society*, vol. 296, no. 2, pp. 275–286, 1998.

[219] R. Mochkovitch, V. Maitia, and R. Marques, "Internal shocks in a relativistic wind as a source for gamma-ray bursts?" *Astrophysics and Space Science*, vol. 231, no. 1-2, pp. 441–444, 1995.

[220] D. Lazzati, G. Ghisellini, and A. Celotti, "Constraints on the bulk Lorentz factor in the internal shock scenario for gamma-ray bursts," *Monthly Notices of the Royal Astronomical Society*, vol. 309, no. 2, pp. L13–L17, 1999.

[221] P. Kumar, "Gamma-ray burst energetics," *The Astrophysical Journal*, vol. 523, no. 2, pp. L113–L116, 1999.

[222] M. Spada, A. Panaitescu, and P. Mészáros, "Analysis of temporal features of gamma-ray bursts in the internal shock model," *The Astrophysical Journal*, vol. 537, no. 2, pp. 824–832, 2000.

[223] D. Guetta, M. Spada, and E. Waxman, "Efficiency and spectrum of internal gamma-ray burst shocks," *The Astrophysical Journal*, vol. 557, no. 1, pp. 399–407, 2001.

[224] A. Maxham and B. Zhang, "Modeling gamma-ray burst X-ray flares within the internal shock model," *The Astrophysical Journal*, vol. 707, no. 2, pp. 1623–1633, 2009.

[225] N. M. Lloyd-Ronning and B. Zhang, "On the kinetic energy and radiative efficiency of gamma-ray bursts," *Astrophysical Journal Letters*, vol. 613, no. 1, pp. 477–483, 2004.

[226] K. Ioka, K. Toma, R. Yamazaki, and T. Nakamura, "Efficiency crisis of swift gamma-ray bursts with shallow X-ray afterglows: prior activity or time-dependent microphysics?" *Astronomy and Astrophysics*, vol. 458, no. 1, pp. 7–12, 2006.

[227] A. Nousek, C. Kouveliotou, D. Grupe et al., "Evidence for a canonical gamma-ray burst afterglow light curve in the Swift XRT data," *The Astrophysical Journal*, vol. 642, no. 1, pp. 389–400, 2006.

[228] B. Zhang, E. Liang, K. L. Page et al., "GRB radiative efficiencies derived from the *Swift* data: GRBs versus XRFs, long versus short," *The Astrophysical Journal*, vol. 655, no. 2, pp. 989–1001, 2007.

[229] A. Pe'er, B.-B. Zhang, F. Ryde, S. Mcglynn, R. D. Preece, and C. Kouveliotou, "The connection between thermal and non-thermal emission in gamma-ray bursts: general considerations and GRB 090902B as a case study," *Monthly Notices of the Royal Astronomical Society*, vol. 420, no. 1, pp. 468–482, 2012.

[230] A. M. Beloborodov, "On the efficiency of internal shocks in gamma-ray bursts," *Astrophysical Journal Letters*, vol. 539, no. 1, pp. L25–L28, 2000.

[231] S. Kobayashi and R. Sari, "Ultraefficient internal shocks," *Astrophysical Journal Letters*, vol. 551, no. 2, pp. 934–939, 2001.

[232] E. V. Derishev and V. V. Kocharovsky, "The neutron component in fireballs of gamma-ray bursts: dynamics and observable imprints," *The Astrophysical Journal*, vol. 521, no. 2, pp. 640–649, 1999.

[233] J. N. Bahcall and P. Mészáros, "5–10 GeV neutrinos from gamma-ray burst fireballs," *Physical Review Letters*, vol. 85, no. 7, pp. 1362–1365, 2000.

[234] P. Mészáros and M. J. Rees, "Multi-GeV neutrinos from internal dissipation in gamma-ray burst fireballs," *The Astrophysical Journal Letters*, vol. 541, no. 1, pp. L5–L8, 2000.

[235] E. M. Rossi, A. M. Beloborodov, and M. J. Rees, "Neutron-loaded outflows in gamma-ray bursts," *Monthly Notices of the Royal Astronomical Society*, vol. 369, no. 4, pp. 1797–1807, 2006.

[236] A. M. Beloborodov, "Collisional mechanism for gamma-ray burst emission," *Monthly Notices of the Royal Astronomical Society*, vol. 407, no. 2, pp. 1033–1047, 2010.

[237] I. Vurm, A. M. Beloborodov, and J. Poutanen, "Gamma-ray bursts from magnetized collisionally heated jets," *The Astrophysical Journal*, vol. 738, no. 1, article 77, 2011.

[238] M. A. Abramowicz, I. D. Novikov, and B. Paczyński, "The appearance of highly relativistic, spherically symmetric stellar winds," *The Astrophysical Journal*, vol. 369, no. 1, pp. 175–178, 1991.

[239] P. Mészáros and M. J. Rees, "Steep slopes and preferred breaks in gamma-ray burst spectra: the role of photospheres and comptonization," *The Astrophysical Journal*, vol. 530, no. 1, pp. 292–298, 2000.

[240] P. Mészáros, E. Ramirez-Ruiz, M. J. Rees, and B. Zhang, "X-ray-rich gamma-ray bursts, photospheres, and variability," *The Astrophysical Journal*, vol. 578, no. 2, pp. 812–817, 2002.

[241] A. Pe'er, "Temporal evolution of thermal emission from relativistically expanding plasma," *The Astrophysical Journal*, vol. 682, no. 1, pp. 463–473, 2008.

[242] A. M. Beloborodov, "Radiative transfer in ultrarelativistic outflows," *The Astrophysical Journal*, vol. 737, no. 2, p. 68, 2011.

[243] A. Pe'er and F. Ryde, "A theory of multicolor blackbody emission from relativistically expanding plasmas," *The Astrophysical Journal*, vol. 732, no. 1, article 49, 2011.

[244] C. Lundman, A. Pe'er, and F. Ryde, "A theory of photospheric emission from relativistic, collimated outflows," *Monthly Notices of the Royal Astronomical Society*, vol. 428, no. 3, pp. 2430–2442, 2013.

[245] B. Zhang, Y. Z. Fan, J. Dyks et al., "Physical processes shaping gamma-ray burst X-ray afterglow light curves: theoretical implications from the swift X-ray telescope observations ," *The Astrophysical Journal*, vol. 642, no. 1, pp. 354–370, 2006.

[246] A. Rowlinson, P. T. O'brien, B. D. Metzger, N. R. Tanvir, and A. J. Levan, "Signatures of magnetar central engines in short GRB light curves," *Monthly Notices of the Royal Astronomical Society*, vol. 430, no. 2, pp. 1061–1087, 2013.

[247] H. van Eerten, "Self-similar relativistic blast waves with energy injection," *Monthly Notices of the Royal Astronomical Society*, vol. 442, no. 4, pp. 3495–3510, 2014.

[248] H. J. van Eerten, "Gamma-ray burst afterglow plateau break time-luminosity correlations favour thick shell models over thin shell models," *Monthly Notices of the Royal Astronomical Society*, vol. 445, no. 3, pp. 2414–2423, 2014.

[249] R. D. Blandford and R. L. Znajek, "Electromagnetic extraction of energy from Kerr black holes," *Monthly Notices of the Royal Astronomical Society*, vol. 179, no. 3, pp. 433–456, 1977.

[250] R. D. Blandford and D. G. Payne, "Hydromagnetic flows from accretion discs and the production of radio jets," *Monthly Notices of the Royal Astronomical Society*, vol. 199, no. 4, pp. 883–903, 1982.

[251] S. S. Komissarov, "Direct numerical simulations of the Blandford-Znajek effect," *Monthly Notices of the Royal Astronomical Society*, vol. 326, no. 3, pp. L41–L44, 2001.

[252] D. L. Meier, S. Koide, and Y. Uchida, "Magnetohydrodynamic production of relativistic jets," *Science*, vol. 291, no. 5501, pp. 84–92, 2001.

[253] J. C. McKinney and C. F. Gammie, "A measurement of the electromagnetic luminosity of a Kerr black hole," *Astrophysical Journal Letters*, vol. 611, no. 2, pp. 977–995, 2004.

[254] S. S. Komissarov, "General relativistic magnetohydrodynamic simulations of monopole magnetospheres of black holes," *Monthly Notices of the Royal Astronomical Society*, vol. 350, no. 4, pp. 1431–1436, 2004.

[255] J. C. McKinney, "Total and jet blandford-znajek power in the presence of an accretion disk," *Astrophysical Journal Letters*, vol. 630, no. 1, pp. L5–L8, 2005.

[256] J. C. McKinney, "General relativistic magnetohydrodynamic simulations of the jet formation and large-scale propagation from black hole accretion systems," *Monthly Notices of the Royal Astronomical Society*, vol. 368, no. 4, pp. 1561–1582, 2006.

[257] S. S. Komissarov, "Multidimensional numerical scheme for resistive relativistic magnetohydrodynamics," *Monthly Notices of the Royal Astronomical Society*, vol. 382, no. 3, pp. 995–1004, 2007.

[258] A. Tchekhovskoy, J. C. McKinney, and R. Narayan, "Simulations of ultrarelativistic magnetodynamic jets from gamma-ray burst engines," *Monthly Notices of the Royal Astronomical Society*, vol. 388, no. 2, pp. 551–572, 2008.

[259] A. Tchekhovskoy, R. Narayan, and J. C. McKinney, "Black hole spin and the radio loud/quiet dichotomy of active galactic nuclei," *The Astrophysical Journal*, vol. 711, no. 1, pp. 50–63, 2010.

[260] A. Tchekhovskoy, R. Narayan, and J. C. Mckinney, "Efficient generation of jets from magnetically arrested accretion on a rapidly spinning black hole," *Monthly Notices of the Royal Astronomical Society: Letters*, vol. 418, no. 1, pp. L79–L83, 2011.

[261] H. C. Spruit, "Theory of magnetically powered jets," in *The Jet Paradigm*, T. Belloni, Ed., vol. 794 of *Lecture Notes in Physics*, p. 233, Springer, Berlin, Germany, 2010.

[262] V. V. Usov, "Millisecond pulsars with extremely strong magnetic fields as a cosmological source of γ-ray bursts," *Nature*, vol. 357, no. 6378, pp. 472–474, 1992.

[263] W. Kluźniak and M. Ruderman, "The central engine of gamma-ray bursters," *The Astrophysical Journal*, vol. 505, no. 2, pp. L113–L117, 1998.

[264] H. C. Spruit, "Gamma-ray bursts from X-ray binaries," *Astronomy & Astrophysics*, vol. 341, pp. L1–L4, 1999.

[265] J. C. Wheeler, I. Yi, P. Höflich, and L. Wang, "Asymmetric supernovae, pulsars, magnetars, and gamma-ray bursts," *The Astrophysical Journal*, vol. 537, no. 2, pp. 810–823, 2000.

[266] T. A. Thompson, P. Chang, and E. Quataert, "Magnetar spin-down, hyperenergetic supernovae, and gamma-ray bursts," *The Astrophysical Journal*, vol. 611, no. 1 I, pp. 380–393, 2004.

[267] D. A. Uzdensky and A. I. MacFadyen, "Magnetar-driven magnetic tower as a model for gamma-ray bursts and asymmetric supernovae," *The Astrophysical Journal*, vol. 669, no. 1, pp. 546–560, 2007.

[268] N. Bucciantini, E. Quataert, J. Arons, B. D. Metzger, and T. A. Thompson, "Relativistic jets and long-duration gamma-ray bursts from the birth of magnetars," *Monthly Notices of the Royal Astronomical Society: Letters*, vol. 383, no. 1, pp. L25–L29, 2008.

[269] N. Bucciantini, E. Quataert, B. D. Metzger, T. A. Thompson, J. Arons, and L. Del Zanna, "Magnetized relativistic jets and long-duration GRBs from magnetar spin-down during core-collapse supernovae," *Monthly Notices of the Royal Astronomical Society*, vol. 396, no. 4, pp. 2038–2050, 2009.

[270] S. S. Komissarov, N. Vlahakis, A. Königl, and M. V. Barkov, "Magnetic acceleration of ultrarelativistic jets in gamma-ray burst sources," *Monthly Notices of the Royal Astronomical Society*, vol. 394, no. 3, pp. 1182–1212, 2009.

[271] N. Globus and A. Levinson, "Loaded magnetohydrodynamic flows in Kerr spacetime," *Physical Review D*, vol. 88, no. 8, Article ID 084046, 2013.

[272] N. Globus and A. Levinson, "Jet formation in GRBs: a semi-analytic model of MHD flow in Kerr geometry with realistic plasma injection," *The Astrophysical Journal*, vol. 796, no. 1, p. 26, 2014.

[273] B. D. Metzger, D. Giannios, T. A. Thompson, N. Bucciantini, and E. Quataert, "The protomagnetar model for gamma-ray bursts," *Monthly Notices of the Royal Astronomical Society*, vol. 413, no. 3, pp. 2031–2056, 2011.

[274] H. C. Spruit, F. Daigne, and G. Drenkhahn, "Large scale magnetic fields and their dissipation in GRB fireballs," *Astronomy and Astrophysics*, vol. 369, no. 2, pp. 694–705, 2001.

[275] G. Drenkhahn, "Acceleration of GRB outflows by Poynting flux dissipation," *Astronomy & Astrophysics*, vol. 387, no. 2, pp. 714–724, 2002.

[276] G. Drenkhahn and H. C. Spruit, "Efficient acceleration and radiation in poynting flux powered GRB outflows," *Astronomy & Astrophysics*, vol. 391, no. 3, pp. 1141–1153, 2002.

[277] N. Vlahakis and A. Königl, "Relativistic magnetohydrodynamics with application to gamma-ray burst outflows. I. Theory and semianalytic trans-alfvénic solutions," *The Astrophysical Journal*, vol. 596, no. 2, pp. 1080–1103, 2003.

[278] D. Giannios, "Spectra of black-hole binaries in the low/hard state: from radio to X-rays," *Astronomy & Astrophysics*, vol. 437, no. 3, pp. 1007–1015, 2005.

[279] D. Giannios, "Prompt emission spectra from the photosphere of a GRB," *Astronomy & Astrophysics*, vol. 457, no. 3, pp. 763–770, 2006.

[280] D. Giannios and H. C. Spruit, "Spectra of Poynting-flux powered GRB outflows," *Astronomy & Astrophysics*, vol. 430, no. 1, pp. 1–7, 2005.

[281] P. Mészáros and M. J. Rees, "GeV emission from collisional magnetized gamma-ray bursts," *Astrophysical Journal Letters*, vol. 733, no. 2, article L40, 2011.

[282] F. V. Coroniti, "Magnetically striped relativistic magnetohydrodynamic winds: the Crab Nebula revisited," *Astrophysical Journal*, vol. 349, no. 2, pp. 538–545, 1990.

[283] A. Lichnerowicz, *Relativistic Hydrodynamics and Magnetohydrodynamics*, Benjamin, 1967.

[284] M. Gedalin, "Linear waves in relativistic anisotropic magnetohydrodynamics," *Physical Review E*, vol. 47, no. 6, pp. 4354–4357, 1993.

[285] B. Zhang and S. Kobayashi, "Gamma-ray burst early afterglows: reverse shock emission from an arbitrarily magnetized ejecta," *The Astrophysical Journal*, vol. 628, no. 1, pp. 315–334, 2005.

[286] P. Mimica, D. Giannios, and M. A. Aloy, "Deceleration of arbitrarily magnetized GRB ejecta: the complete evolution," *Astronomy and Astrophysics*, vol. 494, no. 3, pp. 879–890, 2009.

[287] P. Mimica and M. A. Aloy, "On the dynamic efficiency of internal shocks in magnetized relativistic outflows," *Monthly Notices of the Royal Astronomical Society*, vol. 401, no. 1, pp. 525–532, 2010.

[288] H. C. Spruit and G. D. Drenkhahn, "Magnetically powered prompt radiation and flow acceleration in Grb," in *Gamma-Ray Bursts in the Afterglow Era*, M. Feroci, F. Frontera, N. Masetti, and L. Piro, Eds., vol. 312 of *Astronomical Society of the Pacific Conference Series*, p. 357, 2004.

[289] D. A. Uzdensky and J. C. McKinney, "Magnetic reconnection with radiative cooling. I. Optically thin regime," *Physics of Plasmas*, vol. 18, no. 4, Article ID 042105, 2011.

[290] J. C. McKinney and D. A. Uzdensky, "A reconnection switch to trigger gamma-ray burst jet dissipation," *Monthly Notices of the Royal Astronomical Society*, vol. 419, no. 1, pp. 573–607, 2012.

[291] B. Cerutti, G. R. Werner, D. A. Uzdensky, and M. C. Begelman, "Beaming and rapid variability of high-energy radiation from relativistic pair plasma reconnection," *The Astrophysical Journal*, vol. 754, no. 2, article L33, 2012.

[292] B. Cerutti, G. R. Werner, D. A. Uzdensky, and M. C. Begelman, "Simulations of particle acceleration beyond the classical synchrotron Burnoff limit in magnetic reconnection: an explanation of the Crab flares," *The Astrophysical Journal*, vol. 770, no. 2, article 147, 2013.

[293] G. R. Werner, D. A. Uzdensky, B. Cerutti, K. Nalewajko, and M. C. Begelman, "The extent of power-law energy spectra in collisionless relativistic magnetic reconnection in pair plasmas," http://arxiv.org/abs/1409.8262.

[294] J. Contopoulos, "A simple type of magnetically driven jets: an astrophysical plasma gun," *The Astrophysical Journal*, vol. 450, no. 2, pp. 616–627, 1995.

[295] A. Tchekhovskoy, R. Narayan, and J. C. McKinney, "Magnetohydrodynamic simulations of gamma-ray burst jets: beyond the progenitor star," *New Astronomy*, vol. 15, no. 8, pp. 749–754, 2010.

[296] S. S. Komissarov, N. Vlahakis, and A. Königl, "Rarefaction acceleration of ultrarelativistic magnetized jets in gamma-ray burst sources," *Monthly Notices of the Royal Astronomical Society*, vol. 407, no. 1, pp. 17–28, 2010.

[297] J. Granot, S. S. Komissarov, and A. Spitkovsky, "Impulsive acceleration of strongly magnetized relativistic flows," *Monthly Notices of the Royal Astronomical Society*, vol. 411, no. 2, pp. 1323–1353, 2011.

[298] M. Lyutikov, "The electromagnetic model of gamma-ray bursts," *The New Journal of Physics*, vol. 8, article 119, 2006.

[299] E. Fermi, "On the origin of the cosmic radiation," *Physical Review*, vol. 75, no. 8, pp. 1169–1174, 1949.

[300] E. Fermi, "Galactic magnetic fields and the origin of cosmic radiation," *The Astrophysical Journal*, vol. 119, p. 1, 1954.

[301] M. S. Longair, *High Energy Astrophysics*, Cambridge University Press, Cambridge, UK, 2011.

[302] A. R. Bell, "The acceleration of cosmic rays in shock fronts. I," *Monthly Notices of the Royal Astronomical Society*, vol. 182, pp. 147–156, 1978.

[303] R. D. Blandford and J. P. Ostriker, "Particle acceleration by astrophysical shocks," *The Astrophysical Journal*, vol. 221, pp. 29–32, 1978.

[304] R. Blandford and D. Eichler, "Particle acceleration at astrophysical shocks: a theory of cosmic ray origin," *Physics Reports*, vol. 154, no. 1, pp. 1–75, 1987.

[305] F. C. Jones and D. C. Ellison, "The plasma physics of shock acceleration," *Space Science Reviews*, vol. 58, no. 1, pp. 259–346, 1991.

[306] J. G. Kirk, F. M. Rieger, and A. Mastichiadis, "Particle acceleration and synchrotron emission in blazar jets," *Astronomy and Astrophysics*, vol. 333, no. 2, pp. 452–458, 1998.

[307] J. G. Kirk, A. W. Guthmann, Y. A. Gallant, and A. Achterberg, "Particle acceleration at ultrarelativistic shocks: an eigenfunction method," *The Astrophysical Journal*, vol. 542, no. 1, pp. 235–242, 2000.

[308] D. C. Ellison, S. P. Reynolds, and F. C. Jones, "First-order Fermi particle acceleration by relativistic shocks," *The Astrophysical Journal*, vol. 360, no. 2, pp. 702–714, 1990.

[309] A. Achterberg, Y. A. Gallant, J. G. Kirk, and A. W. Guthmann, "Particle acceleration by ultrarelativistic shocks: theory and simulations," *Monthly Notices of the Royal Astronomical Society*, vol. 328, no. 2, pp. 393–408, 2001.

[310] D. C. Ellison and G. P. Double, "Diffusive shock acceleration in unmodified relativistic, oblique shocks," *Astroparticle Physics*, vol. 22, no. 3-4, pp. 323–338, 2004.

[311] L. O. Silva, R. A. Fonseca, J. W. Tonge, J. M. Dawson, W. B. Mori, and M. V. Medvedev, "Interpenetrating plasma shells: near-equipartition magnetic field generation and nonthermal particle acceleration," *The Astrophysical Journal Letters*, vol. 596, no. 1, pp. L121–L124, 2003.

[312] K.-I. Nishikawa, P. Hardee, G. Richardson, R. Preece, H. Sol, and G. J. Flshman, "Particle acceleration in relativistic jets due to Weibel instability," *The Astrophysical Journal*, vol. 595, no. 1, pp. 555–563, 2003.

[313] A. Spitkovsky, "Particle acceleration in relativistic collisionless shocks: fermi process at last?" *The Astrophysical Journal Letters*, vol. 682, no. 1, pp. L5–L8, 2008.

[314] L. Sironi and A. Spitkovsky, "Particle acceleration in relativistic magnetized collisionless pair shocks: dependence of shock acceleration on magnetic obliquity," *The Astrophysical Journal*, vol. 698, no. 2, pp. 1523–1549, 2009.

[315] T. Haugbølle, "Three-dimensional modeling of relativistic collisionless ion-electron shocks," *The Astrophysical Journal*, vol. 739, no. 2, p. L42, 2011.

[316] M. M. Romanova and R. V. E. Lovelace, "Magnetic field, reconnection, and particle acceleration in extragalactic jets," *Astronomy and Astrophysics*, vol. 262, pp. 26–36, 1992.

[317] S. Zenitani and M. Hoshino, "The generation of nonthermal particles in the relativistic magnetic reconnection of pair plasmas," *The Astrophysical Journal*, vol. 562, no. 1, pp. 63–66, 2001.

[318] M. Lyutikov, "Role of reconnection in AGN jets," *New Astronomy Reviews*, vol. 47, no. 6-7, pp. 513–515, 2003.

[319] C. H. Jaroschek, R. A. Treumann, H. Lesch, and M. Scholer, "Fast reconnection in relativistic pair plasmas: analysis of particle acceleration in self-consistent full particle simulations," *Physics of Plasmas*, vol. 11, no. 3, pp. 1151–1163, 2004.

[320] Y. E. Lyubarsky, "On the relativistic magnetic reconnection," *Monthly Notices of the Royal Astronomical Society*, vol. 358, no. 1, pp. 113–119, 2005.

[321] S. Zenitani and M. Hoshino, "Particle acceleration and magnetic dissipation in relativistic current sheet of pair plasmas," *The Astrophysical Journal*, vol. 670, no. 1, pp. 702–726, 2007.

[322] S. Zenitani and M. Hoshino, "The role of the guide field in relativistic pair plasma reconnection," *The Astrophysical Journal*, vol. 677, no. 1, pp. 530–544, 2008.

[323] Y. Lyubarsky and M. Liverts, "Particle acceleration in the driven relativistic reconnection," *The Astrophysical Journal*, vol. 682, no. 2, pp. 1436–1442, 2008.

[324] L. Yin, W. Daughton, H. Karimabadi, B. J. Albright, K. J. Bowers, and J. Margulies, "Three-dimensional dynamics of collisionless magnetic reconnection in Large-Scale pair plasmas," *Physical Review Letters*, vol. 101, no. 12, Article ID 125001, 2008.

[325] D. Giannios, "UHECRs from magnetic reconnection in relativistic jets," *Monthly Notices of the Royal Astronomical Society: Letters*, vol. 408, no. 1, pp. L46–L50, 2010.

[326] A. Lazarian, G. Kowal, E. Vishniac, and E. D. G. dal Pino, "Fast magnetic reconnection and energetic particle acceleration," *Planetary and Space Science*, vol. 59, no. 7, pp. 537–546, 2011.

[327] W. Liu, H. Li, L. Yin, B. J. Albright, K. J. Bowers, and E. P. Liang, "Particle energization in 3D magnetic reconnection of relativistic pair plasmas," *Physics of Plasmas*, vol. 18, no. 5, Article ID 052105, 2011.

[328] N. Bessho and A. Bhattacharjee, "Fast magnetic reconnection and particle acceleration in relativistic low-density electron-positron plasmas without guide field," *The Astrophysical Journal*, vol. 750, no. 2, article 129, 2012.

[329] D. Kagan, M. Milosavljević, and A. Spitkovsky, "A flux rope network and particle acceleration in three-dimensional relativistic magnetic reconnection," *The Astrophysical Journal*, vol. 774, no. 1, article 41, 2013.

[330] L. Sironi and A. Spitkovsky, "Relativistic reconnection: an efficient source of non-thermal particles," *The Astrophysical Journal Letters*, vol. 783, no. 1, article L21, 2014.

[331] D. A. Uzdensky and A. Spitkovsky, "Physical conditions in the reconnection layer in pulsar magnetospheres," *The Astrophysical Journal*, vol. 780, no. 1, p. 3, 2014.

[332] L. Sironi and A. Spitkovsky, "Particle acceleration in relativistic magnetized collisionless electron-ion shocks," *The Astrophysical Journal*, vol. 726, no. 2, 2011.

[333] R. V. E. Lovelace, "Dynamo model of double radio sources," *Nature*, vol. 262, no. 5570, pp. 649–652, 1976.

[334] R. D. Blandford, "Accretion disc electrodynamics—a model for double radio sources," *Monthly Notices of the Royal Astronomical Society*, vol. 176, no. 3, pp. 465–481, 1976.

[335] A. Neronov, D. V. Semikoz, and I. I. Tkachev, "Ultra-high energy cosmic ray production in the polar cap regions of black hole magnetospheres," *New Journal of Physics*, vol. 11, Article ID 065015, 2009.

[336] C. D. Dermer, J. A. Miller, and H. Li, "Stochastic particle acceleration near accreting black hole," *Astrophysical Journal Letters*, vol. 456, no. 1, pp. 106–118, 1996.

[337] T. W. Jones and P. E. Hardee, "Maxwellian synchrotron sources," *The Astrophysical Journal*, vol. 228, pp. 268–278, 1979.

[338] D. F. Cioffi and T. W. Jones, "Internal Faraday rotation effects in transparent synchrotron sources," *The Astronomical Journal*, vol. 85, pp. 368–375, 1980.

[339] G. Wardziński and A. A. Zdziarski, "Thermal synchrotron radiation and its comptonization in compact X-ray sources," *Monthly Notices of the Royal Astronomical Society*, vol. 314, no. 1, pp. 183–198, 2000.

[340] A. Pe'er and P. Casella, "A model for emission from jets in X-ray binaries: consequences of a single acceleration episode," *The Astrophysical Journal*, vol. 699, no. 2, pp. 1919–1937, 2009.

[341] R. D. Blandford and C. F. McKee, "Radiation from relativistic blast waves in quasars and active galactic nuclei," *Monthly Notices of the Royal Astronomical Society*, vol. 180, no. 3, pp. 343–371, 1977.

[342] V. L. Ginzburg and S. I. Syrovatskii, "Cosmic magneto-bremsstrahlung (synchrotron radiation)," *Annual Review of Astronomy and Astrophysics*, vol. 3, p. 297, 1965.

[343] G. R. Blumenthal and R. J. Gould, "Bremsstrahlung, synchrotron radiation, and compton scattering of high-energy electrons traversing dilute gases," *Reviews of Modern Physics*, vol. 42, no. 2, pp. 237–271, 1970.

[344] M. J. Rees and P. Meszaros, "Relativistic fireballs—energy conversion and time-scales," *Monthly Notices of the Royal Astronomical Society*, vol. 258, pp. 41–43, 1992.

[345] P. Mészáros and M. J. Rees, "Relativistic fireballs and their impact on external matter: models for cosmological gamma-ray bursts," *Astrophysical Journal*, vol. 405, no. 1, pp. 278–284, 1993.

[346] P. Mészáros, M. J. Rees, and H. Papathanassiou, "Spectral properties of blast-wave models of gamma-ray burst sources," *The Astrophysical Journal*, vol. 432, no. 1, pp. 181–193, 1994.

[347] H. Papathanassiou and P. Mészáros, "Spectra of unsteady wind models of gamma-ray bursts," *The Astrophysical Journal*, vol. 471, no. 2, pp. L91–L94, 1996.

[348] R. Sari and T. Piran, "Cosmological gamma-ray bursts: internal versus external shocks," *Monthly Notices of the Royal Astronomical Society*, vol. 287, no. 1, pp. 110–116, 1997.

[349] R. P. Pilla and A. Loeb, "Emission spectra from internal shocks in gamma-ray burst sources," *The Astrophysical Journal*, vol. 494, no. 2, pp. L167–L171, 1998.

[350] E. S. Weibel, "Spontaneously growing transverse waves in a plasma due to an anisotropic velocity distribution," *Physical Review Letters*, vol. 2, no. 3, pp. 83–84, 1959.

[351] J. T. Frederiksen, C. B. Hededal, T. Hauobølle, and Å. Nordlund, "Magnetic field generation in collisionless shocks: pattern growth and transport," *Astrophysical Journal Letters*, vol. 608, no. 1, pp. L13–L16, 2004.

[352] K.-I. Nishikawa, P. Hardee, G. Richardson, R. Preece, H. Sol, and G. J. Fishman, "Particle acceleration and magnetic field generation in electron-positron relativistic shocks," *The Astrophysical Journal*, vol. 622, no. 2, pp. 927–937, 2005.

[353] A. Spitkovsky, "On the structure of relativistic collisionless shocks in electron-ion plasmas," *The Astrophysical Journal Letters*, vol. 673, no. 1, pp. L39–L42, 2008.

[354] R. A. M. J. Wijers, M. J. Rees, and P. Mészáros, "Shocked by GRB 970228: the afterglow of a cosmological fireball," *Monthly Notices of the Royal Astronomical Society*, vol. 288, no. 4, pp. L51–L56, 1997.

[355] A. Panaitescu and P. Kumar, "Properties of relativistic jets in gamma-ray burst afterglows," *The Astrophysical Journal*, vol. 571, no. 2, pp. 779–789, 2002.

[356] R. Santana, R. Barniol Duran, and P. Kumar, "Magnetic fields in relativistic collisionless shocks," *Astrophysical Journal*, vol. 785, no. 1, article 29, 2014.

[357] R. Barniol Duran, "Constraining the magnetic field in GRB relativistic collisionless shocks using radio data," *Monthly Notices of the Royal Astronomical Society*, vol. 442, pp. 3147–3154, 2014.

[358] R. Sari, R. Narayan, and T. Piran, "Cooling timescales and temporal structure of gamma-ray bursts," *The Astrophysical Journal*, vol. 473, no. 1, pp. 204–218, 1996.

[359] R. Sari, T. Piran, and R. Narayan, "Spectra and light curves of gamma-ray burst afterglows," *The Astrophysical Journal Letters*, vol. 497, no. 1, pp. L17–L20, 1998.

[360] P. Kumar and E. McMahon, "A general scheme for modelling γ-ray burst prompt emission," *Monthly Notices of the Royal Astronomical Society*, vol. 384, no. 1, pp. 33–63, 2008.

[361] P. Beniamini and T. Piran, "Constraints on the synchrotron emission mechanism in gamma-ray bursts," *The Astrophysical Journal*, vol. 769, no. 1, article 69, 2013.

[362] G. Ghisellini, A. Celotti, and D. Lazzati, "Constraints on the emission mechanisms of gamma-ray bursts," *Monthly Notices of the Royal Astronomical Society*, vol. 313, no. 1, pp. L1–L5, 2000.

[363] A. Pe'er and B. Zhang, "Synchrotron emission in small-scale magnetic fields as a possible explanation for prompt emission spectra of gamma-ray bursts," *The Astrophysical Journal*, vol. 653, no. 1 I, pp. 454–461, 2006.

[364] X. Zhao, Z. Li, X. Liu, B.-b. Zhang, J. Bai, and P. Mészáros, "Gamma-ray burst spectrum with decaying magnetic field," *The Astrophysical Journal*, vol. 780, no. 1, p. 12, 2014.

[365] Z. L. Uhm and B. Zhang, "Fast-cooling synchrotron radiation in a decaying magnetic field and γ-ray burst emission mechanism," *Nature Physics*, vol. 10, no. 5, pp. 351–356, 2014.

[366] N. M. Lloyd and V. Petrosian, "Synchrotron radiation as the source of gamma-ray burst spectra," *The Astrophysical Journal*, vol. 543, no. 2, pp. 722–732, 2000.

[367] J. Granot, T. Piran, and R. Sari, "The synchrotron spectrum of fast cooling electrons revisited," *The Astrophysical Journal*, vol. 534, no. 2, pp. L163–L166, 2000.

[368] A. Pe'er and E. Waxman, "The high-energy tail of GRB 941017: comptonization of synchrotron self-absorbed photons," *The Astrophysical Journal Letters*, vol. 603, no. 1, pp. L1–L4, 2004.

[369] A. Panaitescu and P. Mészáros, "Gamma-ray bursts from upscattered self-absorbed synchrotron emission," *The Astrophysical Journal Letters*, vol. 544, no. 1, pp. L17–L21, 2000.

[370] C. D. Dermer and M. Böttcher, "Flash heating of circumstellar clouds by gamma-ray bursts," *The Astrophysical Journal Letters*, vol. 534, no. 2, pp. L155–L158, 2000.

[371] B. E. Stern and J. Poutanen, "Gamma-ray bursts from synchrotron self-compton emission," *Monthly Notices of the Royal Astronomical Society*, vol. 352, no. 3, pp. L35–L39, 2004.

[372] E. V. Derishev, V. V. Kocharovsky, and V. V. Kocharovsky, "Physical parameters and emission mechanism in gamma-ray bursts," *Astronomy and Astrophysics*, vol. 372, no. 3, pp. 1071–1077, 2001.

[373] T. Piran, R. Sari, and Y.-C. Zou, "Observational limits on inverse Compton processes in gamma-ray bursts," *Monthly Notices of the Royal Astronomical Society*, vol. 393, no. 4, pp. 1107–1113, 2009.

[374] E. Nakar, S. Ando, and R. Sari, "Klein-Nishina effects on optically thin synchrotron and synchrotron self-compton spectrum," *Astrophysical Journal Letters*, vol. 703, no. 1, pp. 675–691, 2009.

[375] F. Daigne, Ž. Bošnjak, and G. Dubus, "Reconciling observed gamma-ray burst prompt spectra with synchrotron radiation?" *Astronomy and Astrophysics*, vol. 526, article 110, 2011.

[376] R. Barniol Duran, Ž. Bošnjak, and P. Kumar, "Inverse-Compton cooling in Klein-Nishina regime and gamma-ray burst prompt spectrum," *Monthly Notices of the Royal Astronomical Society*, vol. 424, no. 4, pp. 3192–3200, 2012.

[377] G. Ghisellini and A. Celotti, "Quasi-thermal comptonization and gamma-ray bursts," *Astrophysical Journal Letters*, vol. 511, no. 2, pp. L93–L96, 1999.

[378] G. Ghisellini and A. Celotti, "Quasi-thermal comptonization and GRBs," *Astronomy and Astrophysics Supplement Series*, vol. 138, no. 3, pp. 527–528, 1999.

[379] K. Asano and T. Terasawa, "Slow heating model of gamma-ray burst: photon spectrum and delayed emission," *The Astrophysical Journal*, vol. 705, no. 2, pp. 1714–1720, 2009.

[380] K. Murase, K. Asano, T. Terasawa, and P. Mészros, "The role of stochastic acceleration in the prompt emission of gamma-ray bursts: application to hadronic injection," *The Astrophysical Journal*, vol. 746, no. 2, article 164, 2012.

[381] N. M. Lloyd-Ronning and V. Petrosian, "Interpreting the behavior of time-resolved gamma-ray burst spectra," *Astrophysical Journal Letters*, vol. 565, no. 1, pp. 182–194, 2002.

[382] M. V. Medvedev, "Theory of 'jitter' radiation from small-scale random magnetic fields and prompt emission from gamma-ray burst shocks," *The Astrophysical Journal*, vol. 540, no. 2, pp. 704–714, 2000.

[383] M. Böttcher and C. D. Dermer, "High-energy gamma rays from ultra-high-energy cosmic-ray protons in gamma-ray bursts," *Astrophysical Journal Letters*, vol. 499, no. 2, pp. L131–L134, 1998.

[384] T. Totani, "TeV burst of gamma-ray bursts and ultra-high-energy cosmic rays," *The Astrophysical Journal Letters*, vol. 509, no. 2, pp. L81–L84, 1998.

[385] N. Gupta and B. Zhang, "Prompt emission of high-energy photons from gamma ray bursts," *Monthly Notices of the Royal Astronomical Society*, vol. 380, no. 1, pp. 78–92, 2007.

[386] K. Asano, S. Inoue, and P. Mészros, "Prompt high-energy emission from proton-dominated gamma-ray bursts," *Astrophysical Journal Letters*, vol. 699, no. 2, pp. 953–957, 2009.

[387] S. Razzaque, "Synchrotron radiation from ultra-high energy protons and the fermi observations of GRB 080916C," *The Open Astronomy Journal*, vol. 3, no. 1, pp. 150–155, 2010.

[388] K. Asano and P. Mészáros, "Delayed onset of high-energy emissions in leptonic and hadronic models of gamma-ray bursts," *Astrophysical Journal*, vol. 757, no. 2, article 115, 2012.

[389] P. Crumley and P. Kumar, "Hadronic models for Large Area Telescope prompt emission observed in Fermi gamma-ray bursts," *Monthly Notices of the Royal Astronomical Society*, vol. 429, no. 4, pp. 3238–3251, 2013.

[390] M. Milgrom and V. Usov, "Possible association of ultra-high-energy cosmic-ray events with strong gamma-ray bursts," *Astrophysical Journal Letters*, vol. 449, no. 1, pp. L37–L40, 1995.

[391] E. Waxman, "Cosmological gamma-ray bursts and the highest energy cosmic rays," *Physical Review Letters*, vol. 75, no. 3, pp. 386–389, 1995.

[392] E. Waxman and J. Bahcall, "High energy neutrinos from cosmological gamma-ray burst fireballs," *Physical Review Letters*, vol. 78, no. 12, pp. 2292–2295, 1997.

[393] E. Waxman, "High-energy cosmic rays from gamma-ray burst sources: a stronger case," *The Astrophysical Journal*, vol. 606, no. 2, pp. 988–993, 2004.

[394] D. Eichler and A. Levinson, "A compact fireball model of gamma-ray bursts," *The Astrophysical Journal*, vol. 529, no. 1, pp. 146–150, 2000.

[395] F. Daigne and R. Mochkovitch, "The expected thermal precursors of gamma-ray bursts in the internal shock model," *Monthly Notices of the Royal Astronomical Society*, vol. 336, no. 4, pp. 1271–1280, 2002.

[396] M. J. Rees and P. Mészáros, "Dissipative photosphere models of gamma-ray bursts and X-ray flashes," *The Astrophysical Journal*, vol. 628, no. 2, pp. 847–852, 2005.

[397] A. Pe'er and E. Waxman, "Prompt gamma-ray burst spectra: detailed calculations and the effect of pair production," *The Astrophysical Journal*, vol. 613, no. 1, pp. 448–459, 2004.

[398] A. Pe'er, P. Mészáros, and M. J. Rees, "Peak energy clustering and efficiency in compact objects," *The Astrophysical Journal*, vol. 635, no. 1, pp. 476–480, 2005.

[399] A. Pe'er, P. Mészáros, and M. J. Rees, "The observable effects of a photospheric component on GRB and XRF prompt emission spectrum," *The Astrophysical Journal*, vol. 642, no. 2, pp. 995–1003, 2006.

[400] B. Zhang, R.-J. Lu, E.-W. Liang, and X.-F. Wu, "GRB 110721A: photosphere 'death line' and the physical origin of the GRB Band function," *The Astrophysical Journal*, vol. 758, no. 2, article L34, 2012.

[401] P. Veres, B.-B. Zhang, and P. Mészáros, "The extremely high peak energy of GRB 110721A in the context of a dissipative photosphere synchrotron emission model," *The Astrophysical Journal Letters*, vol. 761, no. 2, article L18, 2012.

[402] D. Giannios, "Prompt GRB emission from gradual energy dissipation," *Astronomy and Astrophysics*, vol. 480, no. 2, pp. 305–312, 2008.

[403] D. Giannios, "The peak energy of dissipative gamma-ray burst photospheres," *Monthly Notices of the Royal Astronomical Society*, vol. 422, no. 4, pp. 3092–3098, 2012.

[404] P. Veres and P. Mészáros, "Single- and two-component gamma-ray burst spectra in the *Fermi* GBM-LAT energy range," *The Astrophysical Journal*, vol. 755, no. 1, article 12, 2012.

[405] D. Bégué and A. Pe'er, "Poynting flux dominated jets challenged by their photospheric emission," *The Astrophysical Journal*, vol. 802, no. 2, article 134, 2015.

[406] H. Gao and B. Zhang, "Photosphere emission from a hybrid relativistic outflow with arbitrary dimensionless entropy and magnetization in GRBs," *The Astrophysical Journal*, vol. 801, no. 2, article 103, 2015.

[407] K. Ioka, K. Murase, K. Toma, S. Nagataki, and T. Nakamura, "Unstable GRB photospheres and $e^{\pm}$ annihilation lines," *Astrophysical Journal*, vol. 670, no. 2, pp. L77–L80, 2007.

[408] C. Thompson, P. Mészáros, and M. J. Rees, "Thermalization in relativistic outflows and the correlation between spectral hardness and apparent luminosity in gamma-ray bursts," *The Astrophysical Journal*, vol. 666, no. 2, pp. 1012–1023, 2007.

[409] D. Lazzati, B. J. Morsony, and M. C. Begelman, "Very high efficiency photospheric emission in long-duration γ-ray bursts," *The Astrophysical Journal*, vol. 700, no. 1, pp. 47–50, 2009.

[410] D. Lazzati and M. C. Begelman, "Non-thermal emission from the photospheres of gamma-ray burst outflows. I. High-frequency tails," *The Astrophysical Journal*, vol. 725, no. 1, pp. 1137–1145, 2010.

[411] A. Mizuta, S. Nagataki, and J. Aoi, "Thermal radiation from gamma-ray burst jets," *The Astrophysical Journal*, vol. 732, no. 1, article 26, 2011.

[412] D. Lazzati, B. J. Morsony, and M. C. Begelman, "High-efficiency photospheric emission of long-duration gamma-ray burst jets: the effect of the viewing angle," *The Astrophysical Journal*, vol. 732, no. 1, article 34, 2011.

[413] K. Toma, X.-F. Wu, and P. Mészáros, "Photosphere-internal shock model of gamma-ray bursts: case studies of Fermi/LAT bursts," *Monthly Notices of the Royal Astronomical Society*, vol. 415, no. 2, pp. 1663–1680, 2011.

[414] O. Bromberg, Z. Mikolitzky, and A. Levinson, "Sub-photospheric emission from relativistic radiation mediated shocks in GRBs," *The Astrophysical Journal*, vol. 733, no. 2, p. 85, 2011.

[415] A. Levinson, "Observational signatures of sub-photospheric radiation-mediated shocks in the prompt phase of gamma-ray bursts," *The Astrophysical Journal*, vol. 756, no. 2, article 174, 2012.

[416] I. Vurm, Y. Lyubarsky, and T. Piran, "On thermalization in gamma-ray burst jets and the peak energies of photospheric spectra," *The Astrophysical Journal*, vol. 764, no. 2, article 143, 2013.

[417] A. M. Beloborodov, "Regulation of the spectral peak in gamma-ray bursts," *The Astrophysical Journal*, vol. 764, no. 2, p. 157, 2013.

[418] R. Hascoët, F. Daigne, and R. Mochkovitch, "Prompt thermal emission in gamma-ray bursts," *Astronomy and Astrophysics*, vol. 551, article A124, 2013.

[419] D. Lazzati, B. J. Morsony, R. Margutti, and M. C. Begelman, "Photospheric emission as the dominant radiation mechanism in long-duration gamma-ray bursts," *The Astrophysical Journal*, vol. 765, no. 2, article 103, 2013.

[420] K. Asano and P. Mészáros, "Photon and neutrino spectra of time-dependent photospheric models of gamma-ray bursts," *Journal of Cosmology and Astroparticle Physics*, vol. 2013, no. 9, article 8, 2013.

[421] C. Cuesta-Martinez, M. A. Aloy, P. Mimica, C. Thone, and A. de Ugarte Postigo, "Numerical models of blackbody-dominated gamma-ray bursts. II. Emission properties," *Monthly Notices of the Royal Astronomical Society*, vol. 446, no. 2, pp. 1737–1749, 2015.

[422] A. Chhotray and D. Lazzati, "Gamma-ray burst spectra and spectral correlations from subphotospheric Comptonization," *The Astrophysical Journal*, vol. 802, no. 2, article 132, 2015.

[423] S. Keren and A. Levinson, "Sub-photospheric, radiation-mediated shocks in gamma-ray bursts: multiple shock emission and the band spectrum," *The Astrophysical Journal*, vol. 789, no. 2, p. 128, 2014.

[424] R. Ruffini, I. A. Siutsou, and G. V. Vereshchagin, "A theory of photospheric emission from relativistic outflows," *The Astrophysical Journal*, vol. 772, no. 1, article 11, 2013.

[425] A. G. Aksenov, R. Ruffini, and G. V. Vereshchagin, "Comptonization of photons near the photosphere of relativistic outflows," *Monthly Notices of the Royal Astronomical Society*, vol. 436, no. 1, pp. L54–L58, 2013.

[426] G. V. Vereshchagin, "Physics of nondissipative ultrarelativistic photospheres," *International Journal of Modern Physics. D. Gravitation, Astrophysics, Cosmology*, vol. 23, no. 3, Article ID 1430003, 2014.

[427] W. Zhang, S. E. Woosley, and A. I. MacFadyen, "Relativistic jets in collapsars," *The Astrophysical Journal*, vol. 586, no. 1, pp. 356–371, 2003.

[428] A. Pe'er and E. Waxman, "Time-dependent numerical model for the emission of radiation from relativistic plasma," *The Astrophysical Journal*, vol. 628, no. 2, pp. 857–866, 2005.

[429] C. Lundman, A. Pe'er, and F. Ryde, "Polarization properties of photospheric emission from relativistic, collimated outflows," *Monthly Notices of the Royal Astronomical Society*, vol. 440, no. 4, pp. 3292–3308, 2013.

[430] Z. Chang, H.-N. Lin, and Y. Jiang, "Gamma-ray burst polarization via compton scattering process," *The Astrophysical Journal*, vol. 783, no. 1, p. 30, 2014.

[431] H. Ito, S. Nagataki, M. Ono et al., "Photospheric emission from stratified jets," *The Astrophysical Journal*, vol. 777, no. 1, article 62, 2013.

[432] A. Pe'er, F. Ryde, R. A. M. J. Wijers, P. Mészáros, and M. J. Rees, "A new method of determining the initial size and Lorentz factor of gamma-ray burst fireballs using a thermal emission component," *The Astrophysical Journal*, vol. 664, no. 1, 2007.

[433] J. Larsson, J. L. Racusin, and J. M. Burgess, "Evidence for jet launching close to the black hole in GRB 101219B—a Fermi GRB dominated by thermal emission," *The Astrophysical Journal*, vol. 800, no. 2, article L34, 2015.

[434] A. Mizuta and K. Ioka, "Opening angles of collapsar JETS," *The Astrophysical Journal*, vol. 777, no. 2, article 162, 2013.

[435] B. Zhang and P. Mészáros, "An analysis of gamma-ray burst spectral break models," *The Astrophysical Journal*, vol. 581, no. 2, pp. 1236–1247, 2002.

[436] B. Zhang and A. Pe'er, "Evidence of an initially magnetically dominated outflow in GRB 080916C," *The Astrophysical Journal Letters*, vol. 700, no. 2, pp. L65–L68, 2009.

Hindawi Publishing Corporation
Advances in Astronomy
Volume 2015, Article ID 192383, 16 pages
http://dx.doi.org/10.1155/2015/192383

Review Article

Reverse Shock Emission in Gamma-Ray Bursts Revisited

He Gao and Peter Mészáros

Department of Astronomy and Astrophysics, Department of Physics, Center for Particle and Gravitational Astrophysics, Institute for Gravitation and the Cosmos, 525 Davey Lab, Pennsylvania State University, University Park, PA 16802, USA

Correspondence should be addressed to He Gao; hug18@psu.edu

Received 26 November 2014; Accepted 7 April 2015

Academic Editor: Valery Nakariakov

A generic synchrotron external shock model is the widely preferred paradigm used to interpret the broadband afterglow data of gamma-ray bursts (GRBs), including predicted observable signatures from a reverse shock which have been confirmed by observations. Investigations of the nature of the reverse shock emission can provide valuable insights into the intrinsic properties of the GRB ejecta. Here we briefly review the standard and the extended models of the reverse shock emission, discussing the connection between the theory and observations, including the implications of the latest observational advances.

1. Introduction

Gamma-ray bursts (GRBs), which are the most extreme explosive events in the universe, generally present two phenomenological emission phases: an initial prompt γ-ray emission and a longer-lived broadband afterglow emission. Regardless of the nature of the progenitor and the central engine, the radiation of the GRBs is believed to be caused by the dissipation of the kinetic energy of a relativistic jet which is beamed towards Earth (for reviews, see [1–5]). Although the detailed physics of the prompt γ-ray emission is still uncertain, mainly owing to the poorly understanding composition of the GRB jet (e.g., the degree of magnetization) [6], a generic synchrotron external shock model is the most widely accepted paradigm for interpreting the broadband afterglow data [7–12].

The external shock model is based on a relativistic blastwave theory that describes the interaction between the GRB jet (i.e., the ejecta) and the circumburst medium (for detailed reviews, see [13]). During the interaction, two shocks naturally develop. A long-lived forward shock sweeps up the ambient medium, which gives rise to the long-term broadband afterglow; and a short-lived reverse shock propagates into the GRB ejecta, which can give rise to a short-term optical/IR flash and a radio flare. In the pre-*Swift* era, the forward shock signal was found to successfully represent a large array of late-time afterglow data [14–21], although moderate revisions are sometimes required [13] for the more complicated afterglow behaviors [22–26]. After the launch of NASA's dedicated GRB mission *Swift* [27], unprecedented new information about GRB afterglows was revealed [28–33], especially in the early phases, thanks mainly to the rapid slewing and precise localization capability of its on-board X-Ray Telescope (XRT) [34]. It was found that a number of physical processes are needed to shape the observed lightcurves [30, 31], including, for example, the suggestion that the X-ray afterglow is a superposition of the conventional external shock component and a radiation component that is related to the late central engine activity [4, 29, 30, 35–46]. In any case, the external forward shock still remains the basic theoretical framework to interpret the broadband afterglow signals. It is elegant in its simplicity, since it invokes a limit number of model parameters (e.g., the total energy of the system, the ambient density, and its profile) and has well defined predicted spectral and temporal properties. However, it lacks the ability to study some detailed features of the GRB ejecta, such as the composition, since its radiation comes from the shocked medium rather than the ejecta materials.

The reverse shock, on the other hand, should heat the GRB ejecta within a short period of time, contributing another important aspect to the external shock emission signature. The hydrodynamics of reverse shock propagation in a matter-dominated shell and its corresponding radiation features were studied in great detail [9, 10, 47, 48] prior to

the expected signals being discovered. In the pre-*Swift* era, some cases with very early optical flashes (e.g., GRB 990123 [22]; GRB 021004 [25]; GRB 021211 [26, 49]) or early radio flares [50] were detected, which generally agreed well with the predicted reverse shock emission [51–63].

However, there are also some observations which challenge the simple reverse shock prediction. For instance, the early optical emission of GRB 030418 [64] does not agree with the predicted reverse shock behavior; furthermore, rapid optical follow-up observations for some bursts reveal the so-called "optical flash problem," for example, upper limits of 15 mag were established for specific observed bursts, instead of detecting the expected reverse shock emission [65–68]. In order to better interpret the observational results, the simple reverse shock model was extended to accommodate more realistic conditions than what was initially assumed. For example, the ambient medium might be a stellar wind (or in general have a profile $n \propto r^{-k}$) rather than being a uniform interstellar medium [69–72]; the reverse shock propagation speed might be semirelativistic instead of ultrarelativistic or nonrelativistic [62]; the GRB ejecta might be magnetized, which could enhance the signal when the magnetization is moderate, or completely suppress the signal when magnetization degree is large enough [73–78]; the GRB outflow may carry a good fraction of electron-position pairs or neutrons which could alter the early afterglow behavior [79, 80]; considering a more complicated stratification profile of the ejecta, for example, with a nonuniform Lorentz factor, luminosity, and density, the reverse shock emission could have a richer set of features, including being able to reproduce the canonical X-ray lightcurves as observed by *Swift* as long as the forward shock emission is suppressed [81–86]. Beside these model modifications, some new signatures for reverse shock were also proposed, such as sub-GeV photon flashes and high energy neutrino emission [87, 88] and early X-ray and gamma-ray emission from synchrotron self-Compton (SSC) in the reverse shock region or cross inverse Compton (IC) between the electrons and photons from the forward shock and reverse shock [89, 90], or a polarization signature that offers the possibility to diagnose the structure of the magnetic fields in the GRB ejecta.

Before the launch of *Swift*, the observational data was not ample or detailed enough to comprehensively test these reverse shock models or to study the ejecta properties through the reverse shock signatures. A good sample of early afterglow lightcurves which would allow a detailed study of GRB reverse shocks was one of the expectations from the *Swift* mission [1, 27]. After ten years of successful operation of *Swift*, it is now of great interest to revisit this problem and to see how much progress has been made.

The structure of this review is as follows: we first summarize the models for the reverse shock emission, including the standard synchrotron external shock model in Section 2, and discuss the extended models in Section 3. In Section 4, we illustrate how to identify in practice the reverse shock signals present in the observational data and how to use such signals to study the GRB ejecta properties. The current observational results and their implications are collected in Section 5. We conclude with a brief discussion of the prospects for future reverse shock studies.

2. Standard Modeling of the Reverse Shock Emission

2.1. Model Description. Consider a uniform relativistic coasting shell with rest mass M_0, energy E, initial Lorentz factor $\eta = E/M_0c^2$, and observed width Δ, expanding into the circumburst medium (CBM) described by a density profile $n(r) = Ar^{-k}, 0 \le k < 4$. A pair of shocks will develop, namely, a forward shock propagating into the medium and a reverse shock propagating into the shell. The two shocks and the contact discontinuity separate the system into four regions: (1) the unshocked CBM (called region 1 hereafter), (2) the shocked CBM (region 2), (3) the shocked shell (region 3), and (4) the unshocked shell (region 4). Synchrotron emission is expected from regions 2 and 3, since electrons are accelerated at the shock fronts via the 1st-order Fermi acceleration mechanism and magnetic fields are believed to be generated behind the shocks due to plasma instabilities (for forward shock) [93] or shock compression amplification of the magnetic field carried by the central engine (for reverse shock).

An evaluation of the hydrodynamical and thermodynamical quantities for the regions 2 and 3, namely, γ_i, n_i, p_i and e_i (bulk Lorentz factor, particle number density, pressure, and internal energy density, with i denoting the region number), allows one to straightforwardly calculate the instantaneous synchrotron spectrum at a given epoch, as well as the flux evolution in time (the lightcurve) for a given observed frequency. In doing this, it is customary to introduce parametrizations for the microscopic processes, such as the fractions of the shock energy that go into the electrons and into magnetic fields (ϵ_e and ϵ_B) and the electron spectral index (p). Reference [13] gives detailed examples about such calculations and provides a complete reference for all the analytical synchrotron external shock afterglow models by deriving the temporal and spectral indices of all the models in all spectral regimes. In order to review the reverse shock related features, we give here a brief summary of the dynamical properties of region 3 for various models.

In general, region 3 will evolve through two different phases, that is, before the reverse shock crossing the shell (at T_x) and after the reverse shock crossing. The dynamical solution depends on the relativistic nature of the reverse shock, which can be characterized by the dimensionless parameter $\xi \equiv (l/\Delta)^{1/2}\eta^{-(4-k)/(3-k)}$ [47, 72], where $l = ((3-k)E/4\pi Am_pc^2)^{1/(3-k)}$ is the Sedov length (at which the swept-up medium's rest-mass energy equals the initial energy E of the shell). If $\xi \ll 1$, the reverse shock is ultrarelativistic (thick shell regime), while if $\xi \gg 1$, the reverse shock is Newtonian (thin shell regime). Between these two extreme limits, the reverse shock can be considered semirelativistic when ξ is of the order of unity [62]. Combined with the different (generic) types of CBM, that is, constant density interstellar medium

(ISM) model ($k = 0$), stellar wind model ($k = 2$), and general stratified wind model ($0 \le k < 4$), seven different regimes have been studied in the literature [47, 54, 62, 69–72]. These are (1) thick shell ISM ($\xi \ll 1, n_1 \propto r^0$); (2) thin shell ISM ($\xi \gg 1, n_1 \propto r^0$); (3) thick shell stellar wind ($\xi \ll 1, n_1 \propto r^{-2}$); (4) thin shell stellar wind ($\xi \gg 1, n_1 \propto r^{-2}$); (5) thick shell general stratified wind ($\xi \ll 1, n_1 \propto r^{-k}$); (6) thin shell general stratified wind ($\xi \gg 1, n_1 \propto r^{-k}$); (7) semirelativistic reverse shock ISM ($\xi \sim 1, n_1 \propto r^0$). Below, we summarize the results in the literature for these different regimes.

(1) Thick Shell ISM ($\xi \ll 1, n_1 \propto r^0$) [47, 54]. In this case, the reverse shock crossing time can be estimated as $T_x = \Delta/c$, which is independent of the CBM (applied to all thick shell regimes below). Before T_x, the dynamic variables of region 3 in terms of the observer time $t = r/2c\gamma_3^2$ are

$$\begin{aligned}
\gamma_3 &= \left(\frac{l}{\Delta}\right)^{3/8}\left(\frac{4ct}{\Delta}\right),\\
n_3 &= \frac{8\gamma_3^3 n_1}{\eta} \propto t^{-3/4},\\
p_3 &= \frac{4\gamma_3^2 n_1 m_p c^2}{3} \propto t^{-1/2},\\
N_e &= N_0\frac{ct}{\Delta},
\end{aligned} \tag{1}$$

where $N_0 = E/\eta m_p c^2$ is the total number of electrons in the shell. Since the shocked regions (regions 2 and 3) should be extremely hot, the energy density term is degenerate with the pressure term as $e_3 = 3p_3$.

After T_x, the profile of the shocked medium in region 2 begins to approach the Blandford-McKee (BM) self-similar solution [137, 138]. Since region 3 is located not too far behind region 2, it should roughly fit the BM solution, which is verified numerically as long as the relativistic reverse shock can heat the shell to a relativistic temperature [139]. The BM scaling thus can be applied to the evolution of the shocked shell:

$$\begin{aligned}
\gamma_3 &= \gamma_3(T_x)\left(\frac{t}{T_x}\right)^{-7/16},\\
n_3 &= n_3(T_x)\left(\frac{t}{T_x}\right)^{-13/16},\\
p_3 &= p_3(T_x)\left(\frac{t}{T_x}\right)^{-13/12},\\
N_3 &= N_0.
\end{aligned} \tag{2}$$

Note that the number of the shocked electrons is constant after the shock crossing since no electrons are newly shocked.

(2) Thin Shell ISM ($\xi \gg 1, n_1 \propto r^0$) [47, 54]. In a thin shell case, the reverse shock is too weak to decelerate the shell effectively. T_x can be estimated by the deceleration time of the ejecta (applied to all thin shell regimes below):

$$T_x \simeq t_{\rm dec} = \left[\frac{(3-k)E}{2^{4-k}\pi A m_p \Gamma_0^{8-2k} c^{5-k}}\right]^{1/(3-k)}. \tag{3}$$

Before T_x, the scaling for the dynamic variables of region 3 is given by

$$\begin{aligned}
\gamma_3 &= \eta,\\
n_3 &= 7n_1\eta^2\left(\frac{t}{T_x}\right)^{-3},\\
p_3 &= \frac{4\eta^2 n_1 m_p c^2}{3},\\
N_3 &= N_0\left(\frac{t}{T_x}\right)^{3/2}.
\end{aligned} \tag{4}$$

After T_x, the Lorentz factor of the shocked shell may be assumed to have a general power-law decay behavior $\gamma_3 \propto r^{-g}$ [52, 53]. The dynamical behavior in region 3 may be expressed through the scaling-laws:

$$\begin{aligned}
\gamma_3 &\propto t^{-g/(1+2g)},\\
n_3 &\propto t^{-6(3+g)/7(1+2g)},\\
p_3 &\propto t^{-8(3+g)/7(1+2g)},\\
r &\propto t^{1/(1+2g)},\\
N_{e,3} &\propto t^0.
\end{aligned} \tag{5}$$

For the ISM case, numerical studies showed that the scaling with $g \sim 2$ fits the evolution [53]; for example,

$$\begin{aligned}
\gamma_3 &= \gamma_3(T_x)\left(\frac{t}{T_x}\right)^{-2/5},\\
n_3 &= n_3(T_x)\left(\frac{t}{T_x}\right)^{-6/7},\\
p_3 &= p_3(T_x)\left(\frac{t}{T_x}\right)^{-8/7},\\
N_3 &= N_0.
\end{aligned} \tag{6}$$

(3) Thick Shell Stellar Wind ($\xi \ll 1, n_1 \propto r^{-2}$) [69, 70]. Similar to regime 1, before T_x, we have

$$\begin{aligned}
\gamma_3 &= \frac{1}{\sqrt{2}}\left(\frac{l}{\Delta}\right)^{1/4},\\
n_3 &= \frac{8\sqrt{2}A}{\eta l^{1/4}\Delta^{7/4}}\left(\frac{t}{T_x}\right)^{-2},\\
p_3 &= \frac{8Am_p c^2}{3l^{1/2}\Delta^{3/2}}\left(\frac{t}{T_x}\right)^{-2},\\
N_3 &= N_0\frac{t}{T_x}.
\end{aligned} \tag{7}$$

After T_x, assuming a BM self-similar adiabatic solution for the evolution of the shocked shell [53], the relevant hydrodynamic variables are given by

$$\begin{aligned} \gamma_3 &= \gamma_3(T_x)\left(\frac{t}{T_x}\right)^{-3/8}, \\ n_3 &= n_3(T_x)\left(\frac{t}{T_x}\right)^{-9/8}, \\ p_3 &= p_3(T_x)\left(\frac{t}{T_x}\right)^{-3/2}, \\ N_3 &= N_0. \end{aligned} \tag{8}$$

(4) Thin Shell Stellar Wind ($\xi \gg 1, n_1 \propto r^{-2}$) [71]. In this case, the evolution of the hydrodynamic variables before the time T_x is

$$\begin{aligned} \gamma_3 &= \eta, \\ n_3 &= \frac{7A\eta^6}{l^2}\left(\frac{t}{T_x}\right)^{-3}, \\ p_3 &= \frac{4Am_pc^2\eta^6}{3l^2}\left(\frac{t}{T_x}\right)^{-2}, \\ N_3 &= N_0\left(\frac{t}{T_x}\right)^{1/2}. \end{aligned} \tag{9}$$

After the reverse shock crosses the shell, the scaling law for regime 2 still applies, except $g = 1$; namely,

$$\begin{aligned} \gamma_3 &= \gamma_3(T_x)\left(\frac{t}{T_x}\right)^{-1/3}, \\ n_3 &= n_3(T_x)\left(\frac{t}{T_x}\right)^{-8/7}, \\ p_3 &= p_3(T_x)\left(\frac{t}{T_x}\right)^{-32/21}, \\ N &= N_0. \end{aligned} \tag{10}$$

(5) Thick Shell General Stratified Wind ($\xi \ll 1, n_1 \propto r^{-k}$) [72]. Before the reverse shock crosses the shell, the hydrodynamical evolution of the reverse shock can be characterized by

$$\begin{aligned} \gamma_3 &= \gamma_3(T_x)\left(\frac{t}{T_x}\right)^{-(2-k)/2(4-k)}, \\ n_3 &= n_3(T_x)\left(\frac{t}{T_x}\right)^{-(6+k)/2(4-k)}, \\ p_3 &= p_3(T_x)\left(\frac{t}{T_x}\right)^{-(2+k)/(4-k)}, \\ N_3 &= N_0\frac{t}{T_x}, \end{aligned} \tag{11}$$

where

$$\begin{aligned} \gamma_3(T_x) &= \left[2^k(3-k)(4-k)^{2-k}\right]^{-1/2(4-k)} \\ &\quad\cdot\left(\frac{l}{\Delta}\right)^{(3-k)/2(4-k)}, \\ n_3(T_x) &= \left[2^{24-k}(3-k)^{2k-3}(4-k)^{-(6+k)}\right]^{1/2(4-k)} \\ &\quad\cdot\frac{A}{\eta}\left(l^{(3-2k)(3-k)}\Delta^{k-9}\right)^{1/2(4-k)}, \\ \gamma_{34}(T_x) &= \left[2^{3k-8}(3-k)(4-k)^{2-k}\right]^{1/2(4-k)} \\ &\quad\cdot\eta\left(\frac{l}{\Delta}\right)^{-(3-k)/2(4-k)}, \\ p_3(T_x) &= 3\gamma_{34}(T_x)n_3(T_x)m_pc^2. \end{aligned} \tag{12}$$

After the reverse shock crosses the shell, again with a BM self-similar solution, one gets $\gamma_3 \propto r^{(2k-7)/2}$, $p_3 \propto r^{(4k-26)/3}$, $n_3 \propto r^{(2k-13)/2}$ and $t \propto r/\gamma_3^2 c$. Thus, the hydrodynamic evolution of the reverse shock after crossing the shell is characterized by

$$\begin{aligned} \gamma_3 &= \gamma_3(T_x)\left(\frac{t}{T_x}\right)^{(2k-7)/4(4-k)}, \\ n_3 &= n_3(T_x)\left(\frac{t}{T_x}\right)^{(2k-13)/4(4-k)}, \\ p_3 &= p_3(T_x)\left(\frac{t}{T_x}\right)^{(2k-13)/3(4-k)}, \\ N_3 &= N_0. \end{aligned} \tag{13}$$

(6) Thin Shell General Stratified Wind ($\xi \gg 1, n_1 \propto r^{-k}$) [72]. In this case, before T_x, the hydrodynamic evolution of the reverse shock can be characterized by

$$\begin{aligned} \gamma_3 &= \eta, \\ n_3 &= n_3(T_x)\left(\frac{t}{T_x}\right)^{-3}, \\ p_3 &= p_3(T_x)\left(\frac{t}{T_x}\right)^{-k}, \\ N_3 &= N_0\left(\frac{t}{T_x}\right)^{(3-k)/2}, \end{aligned} \tag{14}$$

where

$$n_3(T_x) = \left[\frac{2^9 7^{6-k}}{3^6 (3-k)^{6-k}}\right]^{1/(3-k)} A^{1-k}\eta^{6/(3-k)},$$
$$\gamma_{34,\Delta} = 1 + \frac{9(3-k)^2}{98}, \quad (15)$$
$$p_3(T_x) = 3(\gamma_{34}(T_x) - 1) n_3(T_x) m_p c^2.$$

After the reverse shock crosses the shell, the scaling law for regime 2 should be still relevant, except that the value of g has not been studied in detail.

(7) Mild Relativistic Reverse Shock ISM ($\xi \sim 1$, $n_1 \propto r^0$) [62]. In this case, a simple analytical solution is no longer achievable. The nature of the reverse shock is determined by ξ and another parameter a, which is the ratio of the Lorentz factor of the shocked matter to η,

$$a \equiv \frac{\gamma_3}{\eta}. \quad (16)$$

Here a can be derived directly from the relativistic jump conditions [47]:

$$\left(\frac{12}{\xi^3} - 1\right) a^4 + 0.5a^3 + a^2 + 0.5a - 1 = 0. \quad (17)$$

The reverse shock reaches the back of the shell at

$$T_x = \frac{\Delta}{c}\left(1 + 0.5\mathcal{N}_t \xi^{3/2}\right), \quad (18)$$

where $\mathcal{N}_t = 1.4$ is a numerical correction factor to the analytic estimates [62]. At this stage,

$$p_r = \frac{4}{3} a^2 \eta^2 n_1 m_p c^2;$$
$$n_r = \xi^3 n_1 \eta^2 \left(\frac{2(a + 1/a)}{3} + 1\right). \quad (19)$$

When $t < T_x$, the dynamical variables of region 3 can be determined by parameterizing all the quantities according to the fraction of the reverse shock crossing the shell, f:

$$\Delta(f) \propto E(f) \propto f,$$
$$\xi(f) \propto f^{-1/3},$$
$$r(f) \propto f^{1/2}, \quad (20)$$
$$t(f) \propto f\left(1 + 0.5\mathcal{N}_t \xi(f)^{3/2}\right).$$

At $t > T_x$, the hydrodynamical evolution becomes almost independent of ξ [53]; therefore, the solutions for the dynamic variables of region 3 become the same as in regime 2.

2.2. Emission Evolution. The instantaneous synchrotron spectrum at a given epoch can be described with three characteristic frequencies ν_a (self-absorption frequency), ν_m, and ν_c (the cooling frequency) and the peak synchrotron flux density $F_{\nu,\max}$ [11]. Based on the dynamical solution for specific situations, one can calculate the temporal evolution of these characteristic parameters and then determine the flux evolution in time (the lightcurve) for a given observed frequency. Since the reverse shock emission is expected to be prominent in the optical band at early stage, here we give a brief description for the morphology of early optical afterglow lightcurves.

It is shown that for reasonable parameter spaces, shortly after (or even during) the prompt emission phase, both forward shock and reverse shock emissions would enter into the "slow cooling" regime ($\nu_c < \nu_m$) [11, 58]. In the following, we will take slow cooling for both reverse and forward shock emissions, so that the shape of the lightcurve essentially depends on the relation between $\nu_m^{r,f}$ and $\nu_{\rm opt}$, where the superscripts r and f represent reverse and forward shock, respectively.

For thin shell case, the evolution of $\nu_m^{r,f}$ reads

$$\nu_m^f \propto t^0 \quad (t < T_x),$$
$$\nu_m^f \propto t^{-3/2} \quad (t > T_x),$$
$$\nu_m^r \propto t^6 \quad (t < T_x), \quad (21)$$
$$\nu_m^r \propto t^{-3/2} \quad (t > T_x).$$

As shown in Figure 1(a), when $\nu_m^{r,f}(T_x)$ is larger than $\nu_{\rm opt}$, $\nu_m^{r,f}$ would cross the optical band once for the forward shock (at t_f) and twice for the reverse shock (at $t_{r,1}$ and $t_{r,2}$). In this case, we have (shown in Figure 1(b))

$$F_\nu^f \propto t^3 \quad (t < T_x),$$
$$F_\nu^f \propto t^{1/2} \quad (T_x < t < t_f),$$
$$F_\nu^f \propto t^{-3(p-1)/4} \quad (t > t_f),$$
$$F_\nu^r \propto t^{(6p-3)/2} \quad (t < t_{r,1}), \quad (22)$$
$$F_\nu^r \propto t^{-1/2} \quad (t_{r,1} < t < t_{r,2}),$$
$$F_\nu^r \propto t^{-(27p+7)/35} \quad (t > t_{r,2}).$$

When $\nu_m^{r,f}(T_x)$ is smaller than $\nu_{\rm opt}$, there is no ν_m crossing and the lightcurves for both shocks peak at T_x. In this case, we have

$$F_\nu^f \propto t^3 \quad (t < T_x),$$
$$F_\nu^f \propto t^{-3(p-1)/4} \quad (t > T_x),$$
$$F_\nu^r \propto t^{(6p-3)/2} \quad (t < T_x), \quad (23)$$
$$F_\nu^r \propto t^{-(27p+7)/35} \quad (t > T_x).$$

Depending on their shapes and relative relations between the forward shock and reverse shock emission, the early optical

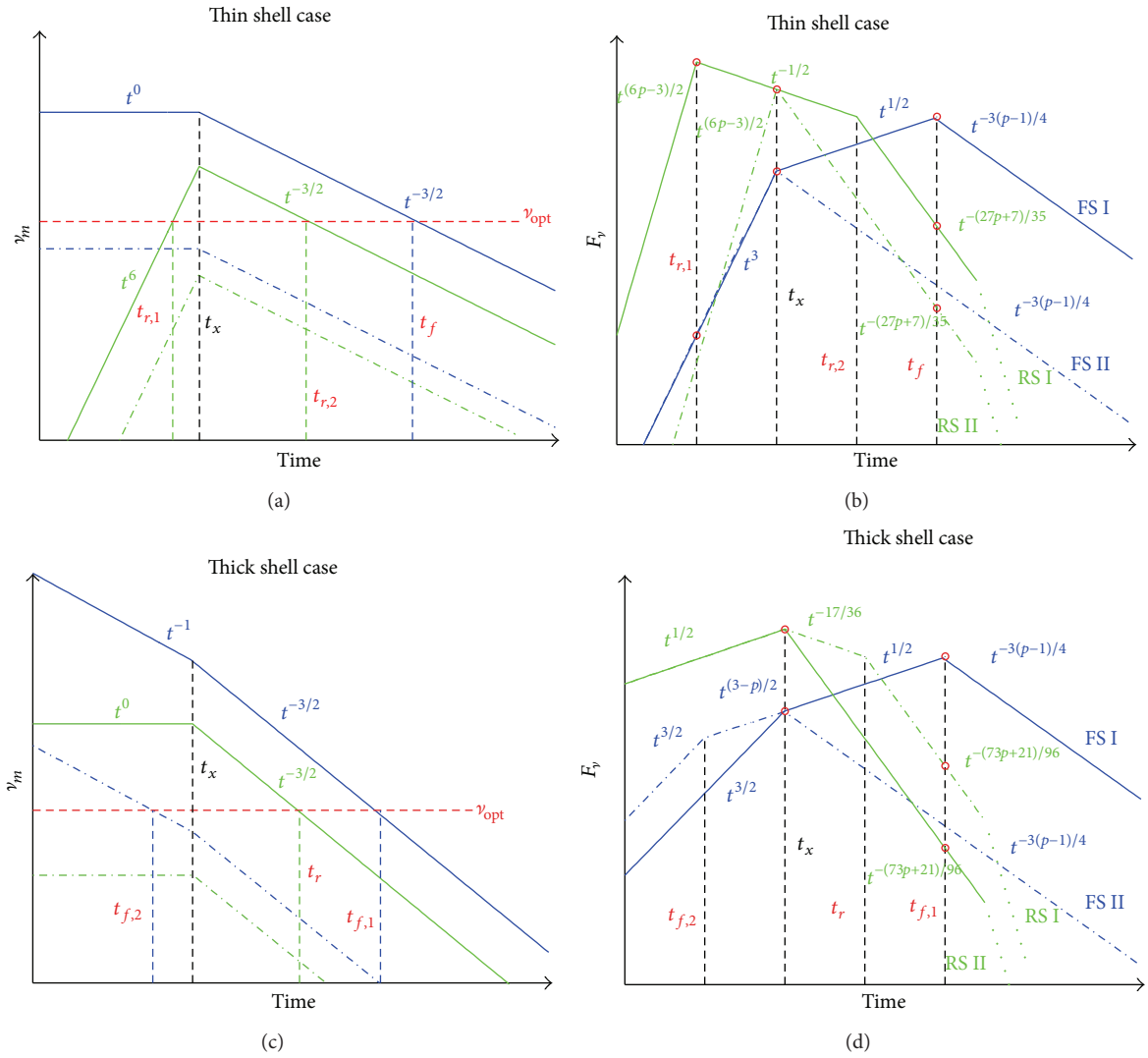

FIGURE 1: Illustration of the ν_m evolution ((a), (c)) and optical lightcurves ((b), (d)) for both forward shock (blue lines) and reverse shock (green lines) emission, from [91]. Red circles on lightcurve indicate the points for comparison in order to categorize the lightcurve types [91].

lightcurves could be distributed into different morphological types; we will discuss this in detail in Section 4.1.

For thick shell case, the evolution of $\nu_m^{r,f}$ reads (shown in Figure 1(c))

$$\begin{aligned}
&\nu_m^f \propto t^{-1} \quad (t < T_x),\\
&\nu_m^f \propto t^{-3/2} \quad (t > T_x),\\
&\nu_m^r \propto t^{0} \quad (t < T_x),\\
&\nu_m^r \propto t^{-3/2} \quad (t > T_x).
\end{aligned} \tag{24}$$

When $\nu_m^{r,f}(T_x)$ is larger than $\nu_{\rm opt}$, $\nu_m^{r,f}$ would cross the optical band once for both forward shock (at $t_{f,1}$) and reverse shock (at t_r). In this case, we have (shown in Figure 1(d))

$$\begin{aligned}
&F_\nu^f \propto t^{3/2} \quad (t < T_x),\\
&F_\nu^f \propto t^{1/2} \quad (T_x < t < t_f),\\
&F_\nu^f \propto t^{-3(p-1)/4} \quad (t > t_f),\\
&F_\nu^r \propto t^{1/2} \quad (t < T_x),\\
&F_\nu^r \propto t^{-17/36} \quad (T_x < t < t_r),\\
&F_\nu^r \propto t^{-(73p+21)/96} \quad (t > t_r).
\end{aligned} \tag{25}$$

When $\nu_m^{r,f}(T_x)$ is smaller than $\nu_{\rm opt}$, there is no ν_m crossing for reverse shock but there is one time crossing for forward shock (at $t_{f,2}$). In this case, we have

$$\begin{aligned}
&F_\nu^f \propto t^{3/2} \quad (t < t_{f,2}),\\
&F_\nu^f \propto t^{(3-p)/2} \quad (t_{f,2} < t < T_x),\\
&F_\nu^f \propto t^{-3(p-1)/4} \quad (t > T_x),
\end{aligned}$$

$$F_\nu^r \propto t^{1/2} \quad (t < T_x),$$
$$F_\nu^r \propto t^{-(73p+21)/96} \quad (t > T_x). \tag{26}$$

3. Extended Models of the Reverse Shock Emission

3.1. Reverse Shock Emission from Magnetized GRB Ejecta. It has been suggested that the GRB ejecta are likely to be magnetized (see [5] for a recent review). Although the degree of magnetization is still unknown, it is usually quantified through the parameter σ, the ratio of the electromagnetic energy flux to the kinetic energy flux. The existence of magnetic fields in the ejecta will influence at least two aspects of the reverse shock characteristics, that is, the hydrodynamical solutions for the shocked shell region and the reverse shock emission level.

Under ideal MHD conditions and with a more accurate approach to account for the modifications in the shock jump conditions when magnetic fields are involved, a rigorous analytical solution for the relativistic 90° shocks was carried out and several interesting conclusions were suggested [73]:

(i) A strong reverse shock still exists in the high-σ regime, as long as the shock is relativistic. For typical GRB parameters, the reverse shock could form when σ is as high as several tens or even hundreds, which is supported numerically by solving the one-dimensional Riemann problem for the deceleration of an arbitrarily magnetized relativistic flow [77].

(ii) The dynamical evolution of region 3 can be still categorized into the thick and thin shell regimes, except that the pivotal parameter to separate the two regimes now becomes σ. At larger σ-value, the thick shell regime greatly shrinks and the reverse shock emission peak is broadened in the thin shell regime due to the separation of the shock crossing radius and the deceleration radius. Such novel features could be useful for diagnosing the magnetization degree of GRB ejecta.

(iii) The reverse shock emission level should initially increase rapidly as σ increases from below, until reaching a peak around $\sigma \sim 0.1$–1, and decreases steadily when $\sigma > 1$. The decrease of the emission level is caused not only because the reverse shock becomes weaker, but also because the total kinetic energy fraction in the flow gets smaller. Separate investigations of the reverse shock emission powered by mildly magnetized ($\sigma \sim 0.05$–1) GRB ejecta were also carried out numerically [140], and similar results were achieved. In that work [140], both ISM and stellar wind CBMs were considered, and it turns out that, before the reverse shock crosses the ejecta, the relevant R-band emission flux increases rapidly for the ISM medium case, but for the wind case it increases only slightly, which is similar to nonmagnetized scenario. Recently, multiband GRB afterglow lightcurves for magnetized ejecta have been calculated with high-resolution relativistic MHD simulations coupled with a radiative transfer code [75, 76], and it is suggested that, for typical parameters of the ejecta, the emission from the reverse shock peaks at magnetization values $\sigma \sim 0.01$–0.1 of the flow and that it is greatly suppressed for higher σ-values.

(iv) In the high σ-value regime, a sufficient magnetic energy has not yet been transferred to the ISM at the end of the reverse shock crossing, since the magnetic pressure behind the contact discontinuity balances the thermal pressure in the forward shock crossing. The leftover magnetic energy would eventually be injected into the blastwave or dissipate into radiation at some point and provide additional signatures to the afterglow lightcurve [73, 76].

3.2. Reverse Shock Emission from Pair-Rich or Neutron-Fed GRB Ejecta. Beside magnetic fields, other components of the GRB ejecta, if present, could also alter the reverse shock emission features, such as $e^\pm$ pairs and neutrons [26, 88].

The intrinsic GRB spectrum may extend to very high energy, so that the optical depth to γ-γ absorption for the most energetic photons at the high energy end of the spectrum may exceed unity. In this case, intense pair production may occur in the prompt emission phase and $e^\pm$ pairs remain in the fireball, with the same bulk Lorentz factor as the fireball (static in the comoving frame). Since the $e^\pm$ pair will also share energy in the reverse shock, the reverse shock emission spectrum is altered, and the peak is softened to lower frequencies. It turns out that a pair-rich reverse shock gives rise to stronger radiation in the IR band, instead of the optical/UV emission in the case where pair-loading is negligible [26]. The optical afterglow signal may suffer significant dust obscuration since long GRBs are usually expected to occur within star forming regions; observable IR flashes could test this issue, provided that IR detector can be slewed rapidly enough to respond the GRB trigger [26].

It has also been pointed out that GRB ejecta may contain a significant fraction of neutrons [88, 141–143], which would cause much more complex dynamics for the system than in the neutron-free case. In general, the neutron shells (N-ejecta) would freely penetrate through the charged ion shells (I-ejecta) in front of them and would separate from the I-ejecta more and more, while the I-ejecta suffer deceleration from internal shocks. The N-ejecta would decelerate by collecting ambient medium and the mass of fast neutrons would decrease as the result of β-decay. The neutron decay products and the shocked medium will form new ejecta (T-ejecta) that follow behind the N-ejecta and the interactions between these three ejecta would give rise to rich radiation features. For an ISM type medium, the T-ejecta move faster than the I-ejecta, so that the T-ejecta would first interact with the N-ejecta or ambient medium, but the reverse shock emission in this stage would be out-shined by the forward shock emission. Later on, the I-ejecta would catch up the T-ejecta and a prominent bump signature around tens to hundreds of seconds would show up, which is mainly

dominated by the refreshed reverse shock emission. For a stellar wind type medium, I-ejecta would pick up the T-ejecta first and then collide with the N-ejecta and ambient medium. In this case, three components contribute to the final emission, that is, the forward shock emission, the reverse shock emission from the shocked I-ejecta, and the shocked T-ejecta emission. A typical neutron-rich wind-interaction lightcurve is characterized by a prominent early plateau lasting for ~100 s, followed by normal power-law decay [88].

3.3. High Energy Photons and Neutrinos from Reverse Shock. Since the number of heated electrons in region 3 is η (10^2–10^3) times higher than in region 2, a strong synchrotron self-Compton (SSC) emission in region 3 is expected, especially when reverse shock emission is prominent [9, 89, 90, 144]. The SSC emission feature is essentially determined by the random Lorentz factors of the electrons γ_e, since the seed photons mainly are concentrated in the optical band. When γ_e is of the order of 1000 or even higher, the SSC emission from the reverse shock could dominate over the synchrotron and other IC emissions in the energy bands from tens of MeV to tens of GeV, while the cross-IC (and/or the forward shock SSC emissions) becomes increasingly dominant at TeV energy bands [89, 90]. When γ_e is of order 100, if the SSC process dominates the cooling of shocked electrons, the majority of the shock energy would be radiated in the second-order scattering at 10–100 MeV, and the first-order scattering may give rise to X-ray flares in the very early afterglow phase [144]. In this case, the optical flash (due to synchrotron) is highly suppressed.

On the other hand, it has been proposed that when GRBs erupt in a stellar wind, usually the region 2 and region 3 still have overlap with the prompt MeV γ-ray emission site at the reverse shock crossing phase [80, 145]. Such overlapping could lead to significant modifications of the early afterglow emission, since the dominant cooling process for the electrons is likely to be the IC process with the MeV photons [145]. Due to the close overlap of the MeV photon flow and the shocked regions, the newly upscattered high energy photons would be absorbed by the MeV photons to generate $e^{\pm}$ pairs and then rescatter the soft X-rays to power a detectable sub-GeV signal [80]. Other than that, 10^{14} eV neutrino emission is also expected from interactions between shocked protons and the MeV photon flow [80]. Alternatively, high energy neutrinos are also expected from reverse shocks as the GRB jets crossing the stellar envelop, either for choked or for successful relativistic jets [146].

3.4. Long Lasting Reverse Shocks. In the standard model, a uniform distribution of the bulk Lorentz factors in the GRB ejecta is assumed. However, in principle GRB ejecta could have a range of bulk Lorentz factors, so that the inner (lower γ) parts may carry most of the mass or even most of the energy, for example, $\gamma Mc^2 \propto \gamma^{-s+1}$ [83, 147, 148]. In this case, the low Lorentz factor part of the ejecta will catch up with the high Lorentz factor part when the latter is decelerated by the ambient medium; thus, a long-lasting weak reverse shock could develop, until the whole ejecta have been shocked. Analogously to the standard model, this process could also be classified analytically into two cases: the thick shell case and the thin shell case [83], and it turns out that, in the thick shell case, the reverse shock is strong and may give rise to the plateau observed in the early optical and X-ray afterglows [83]. Considering more complicated stratification profiles for the ejecta properties (e.g., Lorentz factor, luminosity, and density), the long lasting reverse shock emission could be endowed with a richer set of features, including reproducing the canonical X-ray lightcurve as observed by *Swift*, as long as the forward shock emission can somehow be suppressed [84, 85].

3.5. Polarization of Reverse Shock Emission. If the GRB ejecta contain large scale ordered magnetic fields, the prompt γ-ray emission and the reverse shock emission should be polarized [149]. However, aside from any instrumental difficulties, making unequivocal polarization determinations that prove this is still challenging [149, 150]. Furthermore, a high degree of linear polarization in the prompt γ-rays is also possible in the presence of a random magnetic field, arguably originating in electromagnetic instabilities that develop at the collisionless shock [151]. In any case, polarization measurements of the reverse shock emission could place strong constraints on the strength and perhaps also the structure of the magnetic field within the GRB outflow. The RINGO detector on the Liverpool Telescope has reported an optical polarization of GRB 090102 ($P = 101\%$) [152] and GRB 060418 ($P < 8\%$) [153], but a larger sample is definitely needed to give general discussion on the properties of GRB outflow [150].

4. Connection between Theory and Observations of the Reverse Shock Emission

4.1. Theory Predictions of Observational Features of Reverse Shocks. According to the standard external shock theory, reverse shocks would mainly contribute to the early optical afterglow (if not suppressed) [13]. For the ISM model, the early optical lightcurve of the reverse shock would increase proportional to t^5 (thin shell case) or $t^{1/2}$ (thick shell case) and then decrease with a general slope $\sim t^{-2}$ [54, 58]. For the wind model, the lightcurve would increase initially with slope $t^{5/2}$ when synchrotron self-absorption becomes important in this case and then rise with slope 1/2 for both thin and thick cases to finally decrease with a slope $\sim t^{-3}$, determined by the angular time delay effect [70].

The morphology of early optical afterglows essentially depends on the relative relation between the forward shock and reverse shock emission. In general, the early optical afterglows for constant density medium model were usually classified into three types (see Figure 2):

(i) Type I: rebrightening. Two peaks emerge in this type of lightcurve. The first peak is dominated by the reverse shock emission, and the rebrightening signature comes from the forward shock emission. The temporal index for the rebrightening depends on

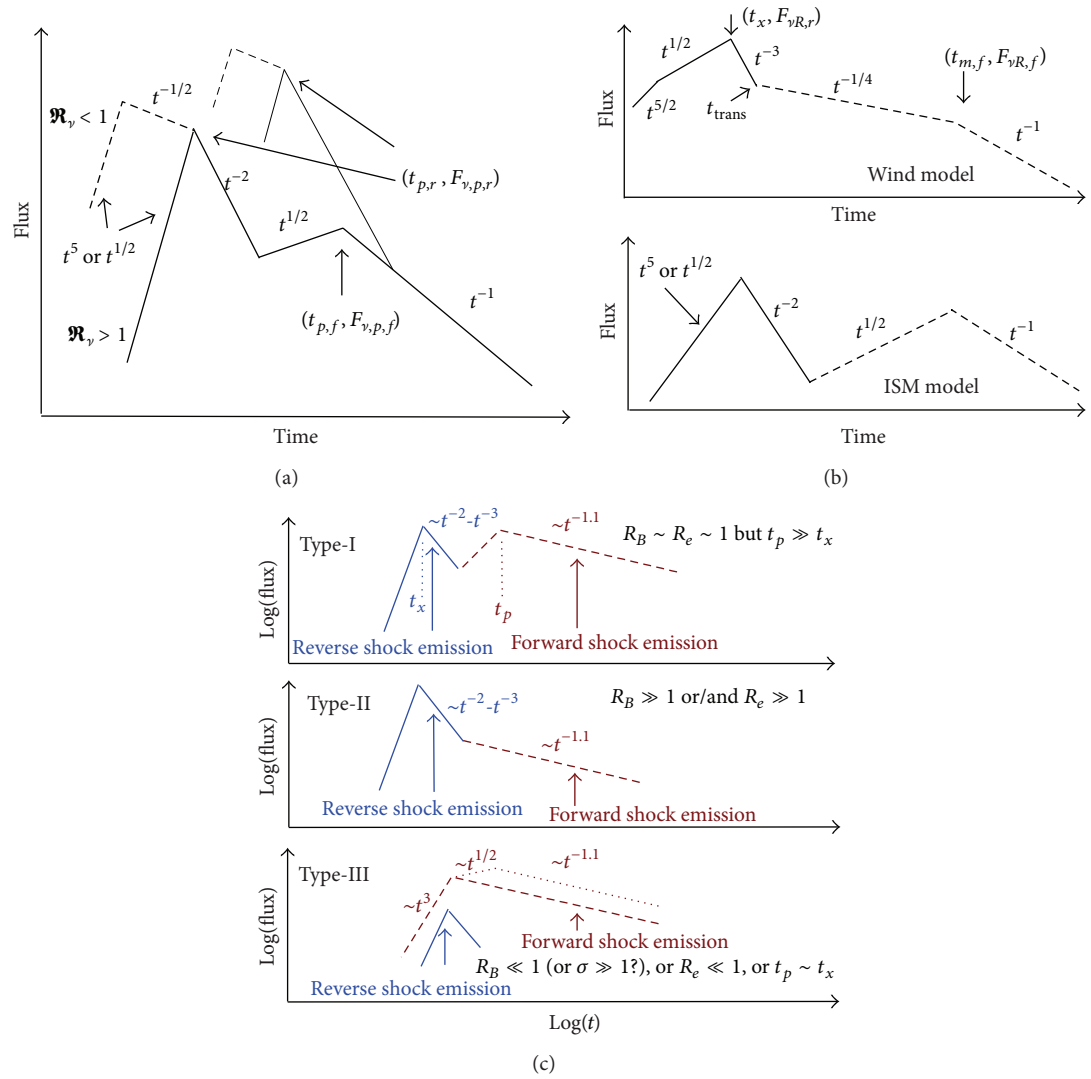

FIGURE 2: Theoretically expected early optical afterglow lightcurves from reverse plus forward shock emission and illustrative diagram of three classified types: (a) from [58]; (b) from [70]; (c) from [92].

the specific forward shock model and the spectral regimes, which are collected in [13].

(ii) Type II: flattening. In this case, the forward shock emission peak is under the reverse shock component, and the decaying part of the forward shock emission shows up later when the reverse shock component is getting fainter more rapidly.

(iii) Type III: no reverse shock component. Two reasons may be responsible for this, one being that the reverse shock component is weak compared with the forward shock emission and the other being that the reverse shock component is completely suppressed for some reason as proposed by some extended models (see Section 3), such as magnetic fields dominating the ejecta [73], $e^{\pm}$ pair effects [26], or SSC process in the reverse shock region [89, 90, 144].

Recently, it is suggested that an insight into the $\nu_m^f(T_x)$ value could lead to strong constraints on relevant afterglow parameters [91], so that the forward shock dominated cases (Type III) should be redefined into two categories:

Type III: forward shock dominated lightcurves without ν_m crossing;

Type IV: forward shock dominated lightcurves with ν_m crossing.

4.2. Identification of Reverse Shock Emission from Observational Data. Based on the theoretically predicted features, once prompt optical observations are obtained, the reverse shock components could be identified with the following procedure:

(1) Compare the first optical observation time t_s and the γ-ray duration T_{90}. If $t_s < T_{90}$, check the variability level of the optical signal. For cases with significant

variability, ascertain the relation between optical variability and γ-ray variability with correlation cross checking method. Bursts with $t_s > T_{90}$ or $t_s < T_{90}$ but with weak variability (or with significant variability but no correlation with γ-ray signal) may be taken as candidates for having a reverse shock signal. It is worth pointing out that variability within a certain level may be explained within the external shock framework, such as invoking density fluctuation, inhomogeneous jets, or neutron decay signatures [88, 154–156]. Information from other observational bands (radio, X-ray, and high energy γ-rays) would be helpful to make a stricter selection between cases.

(2) Fit the optical lightcurve with a multisegment broken power law function. If the initial decay slope of the signal is close to t^{-2} (ISM) or t^{-3} (wind), check whether the following decay or rising slopes are consistent with the forward shock predictions [13] and classify the candidate bursts as one of the four types defined above.

(3) Plot the multiband spectrum of the early afterglow, if possible, and verify if there is evidence for the existence of two components, for example, forward shock component (usually peaks at X-ray) and reverse shock component (usually peaks at optical).

4.3. Constraints on Theoretical Parameters from Observational Results. Valuable results may be expected in the case of bursts where multiband (instead of only X-ray) early afterglow observations are available, especially for the properties of the GRB outflow itself. For cases with identifiable reverse shock component, several important pieces of information, if available, should be useful to constrain model parameters:

(i) Consider the rising and decaying slope of the reverse shock peak. The decaying slope is always in handy since it is the key parameter to identify the reverse shock component. It could be used to differentiate the CBM profile, for example, t^{-2} for ISM and t^{-3} for wind. On the other hand, it is also useful to constrain the electron energy distribution index, p_r, where the subscript r (f) denotes reverse (forward) shock, although the constraint is weak; otherwise, the decay slope would not be general enough for verifying the reverse shock emission. The rising slope of the reverse shock is usually missing from the current data, due to the limited capability of existing facilities (e.g., slewing speed of the dedicated telescopes) and the short-lived nature of the lightcurve rise phase. However, once the rising slope becomes available, not only it is useful for obtaining the CBM profile, but also it is helpful for testing some proposed extended models, such as the neutron-fed outflow model (see details in Section 3).

(ii) The reverse shock peaking time is usually related to the shock crossing time T_x, which is useful to determine the initial physical conditions within the GRB ejecta, specifically its Lorentz factor η and width Δ. But one needs to keep in mind that the first available observational time may not represent the reverse shock peaking time, especially when the rising part of the lightcurve is missing. For those cases, only upper limits could be made for T_x.

(iii) Based on the standard synchrotron external shock model and assigning reasonable ranges of a set of model parameters, one can constrain relevant parameters by fitting the overall observational lightcurve and the broadband spectrum, if available. However, in this approach, too many unknown free parameters are involved, for example, the density of CBM, the isotropic equivalent kinetic energy of the ejecta, the initial Lorentz factor of the ejecta, and especially the microphysics parameters in the shock region ($\epsilon_{e,r}, \epsilon_{e,f}, \epsilon_{B,r}, \epsilon_{e,f}, p_r$, and p_f). Since the observational information is usually not adequate to constrain so many parameters, some *ad hoc* assumptions are commonly used; for instance, the values of the microphysical parameters in the forward and reverse shock region are assumed the same. It is worth pointing out that the relation between $\epsilon_{B,r}$ and $\epsilon_{B,f}$ should be treated carefully, since it is useful for diagnosing the magnetization degree of the initial outflow.

(iv) Beside fitting the overall lightcurves, some important parameters such as the Lorentz factor and the magnetization degree of the initial outflow could also be constrained by working on the "ratios" of the quantities for both shocks, especially at T_x [58, 70]:

$$\begin{aligned} \frac{\nu_{m,r}(T_x)}{\nu_{m,f}(T_x)} &\sim \widehat{\gamma}^{-2}\mathcal{R}_B, \\ \frac{\nu_{c,r}(T_x)}{\nu_{c,f}(T_x)} &\sim \mathcal{R}_B^{-3}, \\ \frac{F_{\nu,m,r}(T_x)}{F_{\nu,m,f}(T_x)} &\sim \widehat{\gamma}\mathcal{R}_B, \end{aligned} \tag{27}$$

where ν_m, ν_c, and $F_{\nu,m}$ are the typical frequency, cooling frequency, and the peak flux for synchrotron spectrum, and

$$\begin{aligned} \widehat{\gamma} &\equiv \frac{\gamma_\times^2}{\eta} = \min\left(\eta, \frac{\gamma_c^2}{\eta}\right), \\ \mathcal{R}_B &\equiv \left(\frac{\epsilon_{B,r}}{\epsilon_{B,f}}\right)^{1/2}, \end{aligned} \tag{28}$$

where γ_c is a critical initial Lorentz factor which divides the thin shell and thick shell regimes [58]. This paradigm provides a straightforward recipe for directly constraining η and $\mathcal{R}_B$ (essentially the magnetization degree of the initial outflow) using early optical afterglow data only. Moreover, the absolute values of the poorly known model parameters related to the shock microphysics (e.g., ϵ_e, p) do not enter the problem, since they largely cancel out once they are assumed to have the same value in both shocks.

Table 1: GRBs with claimed reverse shock signatures and the corresponding references.

Name	References
GRB 990123	[22, 52, 55, 56, 61, 63, 94–105]
GRB 021004	[25, 106]
GRB 021211	[49, 60, 61, 107, 108]
GRB 050525A	[109, 110]
GRB 050904	[111–114]
GRB 060111B	[105, 115]
GRB 060117	[116]
GRB 060908	[117]
GRB 061126	[118, 119]
GRB 080319B	[120–123]
GRB 081007	[124]
GRB 090102	[125, 126]
GRB 090424	[124]
GRB 090902B	[127, 128]
GRB 091024	[129]
GRB 110205A	[130–132]
GRB 130427A	[133–136]

(v) A morphological analysis of the early optical lightcurves can also provide direct model constraints. Given a sample of optical lightcurves with early detections, one can divide them into different categories based on their shapes, then calculate the ratio between each category, and find out the right parameter regimes that can reproduce these ratios with Monte Carlo simulations [91].

(vi) As mentioned above, time variability within certain modest limits in the lightcurve might contain information on some interesting properties, such as external density fluctuations, inhomogeneous jets, or neutron decay signatures.

5. Current Observational Results on Reverse Shock Emission

It has been 15 years since the first prompt optical flash was discovered and was interpreted with a reverse shock model (e.g., GRB 990123 [22, 51, 52]). We have searched the literature since then, finding that 17 GRBs have been claimed to have reverse shock signature (3 in the pre-*Swift* era). The detection rate is much lower than expected. Each of these bursts has been interpreted in great detail. In Table 1, we collect the burst identifiers and their relevant references to the individual studies on those bursts.

Most recently, a comprehensive statistical analysis of reverse shock emission in the optical afterglows of GRBs was carried out [157]. Here we briefly summarize the results as follows:

(i) With stricter criteria, such as requiring redshift measurement, a full sample of 10 GRBs with reverse shock signatures was identified: GRBs 990123, 021004, 021211, 060908, 061126, 080319B, 081007, 090102, 090424, and 130427A. For five of them, a reverse shock component has been firmly confirmed (e.g., GRB 990123 [51], GRB 021211 [25, 59], GRB 061126 [118], GRB 081007 [124], and GRB 130427A [133, 158]). For the remaining five cases, different interpretations (other than the reverse shock emission) can be applicable for the early observational results, due to the lack of good early-time photometric coverage.

(ii) In the sample, GRB 012004 is the only case with a possible Type I lightcurve (in which both reverse and forward shock afterglow lightcurve peaks are observed) and the other nine cases are all with Type II lightcurves (in which the characteristic steep-to-shallow lightcurve evolution is observed).

(iii) Based on the analytic reverse shock plus forward shock model, the physical quantities describing the ejecta and CBM are explored by reproducing the observed optical lightcurves of the sample with Monte Carlo simulations, with the result that the physical properties cover a wide parameter space and do not seem to cluster around any preferential values, which is consistent with previous analyses that concentrated on late time forward shock emission [19, 20].

(iv) It is suggested that GRBs with an identifiable reverse shock component show high magnetization parameter $\mathcal{R}_B \sim \sqrt{2}$–$10^2$. Together with the fact that 9/10 of the cases in the sample belong to Type II, the results are in agreement with the mildly magnetized baryonic jet model of GRBs [73].

6. Summary and Prospects for Reverse Shock Studies

Reverse shock emission is a natural prediction of the standard external shock GRB afterglow model, and it has been firmly confirmed in a small number of cases. Since the reverse shock emission is directly related to the GRB outflow itself, investigating the nature of reverse shock emission would lead to a better understanding of the intrinsic properties of the GRB ejecta, which is essential for constructing a complete picture of the GRB physics.

A theoretical framework for the behavior of the reverse shock emission under various conditions was developed, mostly before the launch of *Swift* (and even before the first relevant discovery of GRB 990123), and expected features were discussed for inferring various intrinsic properties of the GRB ejecta. *Swift* was launched, in part, with hopes to make significant progress on this specific problem. After a decade of highly successful operation, *Swift* indeed has collected a good sample of early afterglow lightcurves to allow detailed studies of GRB reverse shocks. While the size of the sample is still limited, nonetheless, it appears that the number of bursts with confirmed reverse shock components is much lower than the expectation from the standard model.

The mismatch between this theoretical expectation and the observations could be intrinsic or it could be systematically biased due to the limitations of current ground-based observational facilities. If it is intrinsic, the origin of the suppression of the reverse shock emission for most of GRBs would shed new light on the composition problem of GRB jets; for example, most of the jets might be highly magnetized.

Based on current observational results, more reliable results could also be achieved by including more broadband or more specialized information instead of just photometric or spectroscopic optical data. For instance, one could use early radio data or (sub)mm data [159, 160] to search for reverse shock emission signatures [133, 161]; one could identify the reverse shock components and diagnose the structure of the magnetic fields in GRB ejecta via the detection of early time optical polarization [152, 153]; one could estimate the magnetization degree of the GRB jets by comprehensive considering of the γ-ray spectrum [162], the early optical lightcurve type, and special X-ray afterglow features, such as the X-ray plateau due to late magnetic energy injection [73].

At this point, the main problem is that there is still a large fraction of GRBs lacking early optical observations, and a more complete sample is required for firmer conclusions. Some upcoming facilities may help with this issue, such as the Chinese-French mission SVOM [163] and especially its key element, the Ground Wide Angle Cameras (GWACs). The GWACs are an array of wide field of view (about 8000 $\deg^2$, with a sensitivity of about 15 magnitudes at 5 s) optical cameras operating in the optical domain. It will monitor continuously the field covered by the SVOM γ-ray detector ECLAIRs, in order to observe the visible emission of more than 20% of the events, at least 5 minutes before and 15 minutes after the GRB trigger. This and other ground-based facilities may key in making further progress in this field.

Conflict of Interests

The authors declare that there is no conflict of interests regarding the publication of this paper.

Acknowledgment

This work was supported in part by NASA NNX 13AH50G.

References

[1] B. Zhang and P. Mészáros, "Gamma-ray bursts: progress, problems & prospects," *International Journal of Modern Physics A*, vol. 19, no. 15, pp. 2385–2472, 2004.

[2] T. Piran, "Gamma-ray bursts and the fireball model," *Physics Report*, vol. 314, no. 6, pp. 575–667, 1999.

[3] P. Mészros, "Gamma-ray bursts," *Reports on Progress in Physics*, vol. 69, pp. 2259–2322, 2006.

[4] B. Zhang, "Gamma-ray bursts in the swift era," *Chinese Journal of Astronomy and Astrophysics*, vol. 7, no. 1, 2007.

[5] P. Kumar and B. Zhang, "The physics of gamma-ray bursts and relativistic jets," *Physics Reports*, vol. 561, pp. 1–109, 2015.

[6] B. Zhang, "Gamma-ray burst prompt emission," *International Journal of Modern Physics D*, vol. 23, no. 2, Article ID 1430002, 2014.

[7] M. J. Rees and P. Meszaros, "Relativistic fireballs: energy conversion and time-scales," *Monthly Notices of the Royal Astronomical Society*, vol. 258, no. 1, pp. 41P–43P, 1992.

[8] M. J. Rees and P. Mészáros, "Unsteady outflow models for cosmological gamma-ray bursts," *The Astrophysical Journal*, vol. 430, no. 2, pp. L93–L96, 1994.

[9] P. Mészáros and M. J. Rees, "Relativistic fireballs and their impact on external matter: models for cosmological gamma-ray bursts," *Astrophysical Journal Letters*, vol. 405, no. 1, pp. 278–284, 1993.

[10] P. Mészáros and M. J. Rees, "Optical and long-wavelength afterglow from gamma-ray bursts," *Astrophysical Journal Letters*, vol. 476, no. 1, pp. 232–237, 1997.

[11] R. Sari, T. Piran, and R. Narayan, "Spectra and light curves of gamma-ray burst afterglows," *The Astrophysical Journal Letters*, vol. 497, no. 1, pp. L17–L20, 1998.

[12] R. A. Chevalier and Z.-Y. Li, "Wind interaction models for gamma-ray burst afterglows: the case for two types of progenitors," *Astrophysical Journal Letters*, vol. 536, no. 1, pp. 195–212, 2000.

[13] H. Gao, W.-H. Lei, Y.-C. Zou, X.-F. Wu, and B. Zhang, "A complete reference of the analytical synchrotron external shock models of gamma-ray bursts," *New Astronomy Reviews*, vol. 57, no. 6, pp. 141–190, 2013.

[14] R. A. M. J. Wijers, M. J. Rees, and P. Mészáros, "Shocked by GRB 970228: the afterglow of a cosmological fireball," *Monthly Notices of the Royal Astronomical Society*, vol. 288, no. 4, pp. L51–L56, 1997.

[15] E. Waxman, "Gamma-ray-burst afterglow: supporting the cosmological fireball model, constraining parameters, and making predictions," *Astrophysical Journal Letters*, vol. 485, no. 1, pp. L5–L8, 1997.

[16] R. A. M. J. Wijers and T. J. Galama, "Physical parameters of GRB 970508 and GRB 971214 from their afterglow synchrotron emission," *The Astrophysical Journal*, vol. 523, no. 1, pp. 177–186, 1999.

[17] Y. F. Huang, Z. G. Dai, and T. Lu, "A generic dynamical model of gamma-ray burst remnants," *Monthly Notices of the Royal Astronomical Society*, vol. 309, no. 2, pp. 513–516, 1999.

[18] Y. F. Huang, L. J. Gou, Z. G. Dai, and T. Lu, "Overall evolution of jetted gamma-ray burst ejecta," *The Astrophysical Journal*, vol. 543, no. 1, pp. 90–96, 2000.

[19] A. Panaitescu and P. Kumar, "Fundamental physical parameters of collimated gamma-ray burst afterglows," *Astrophysical Journal Letters*, vol. 560, no. 1, pp. L49–L53, 2001.

[20] A. Panaitescu and P. Kumar, "Properties of relativistic jets in gamma-ray burst afterglows," *Astrophysical Journal Letters*, vol. 571, no. 2, pp. 779–789, 2002.

[21] S. A. Yost, F. A. Harrison, R. Sari, and D. A. Frail, "A study of the afterglows of four gamma-ray bursts: constraining the explosion and fireball model," *Astrophysical Journal Letters*, vol. 597, no. 1, pp. 459–473, 2003.

[22] C. Akerlof, R. Balsano, S. Barthelmy et al., "Observation of contemporaneous optical radiation from a γ-ray burst," *Nature*, vol. 398, no. 6726, pp. 400–402, 1999.

[23] F. A. Harrison, J. S. Bloom, D. A. Frail et al., "Optical and radio observations of the afterglow from GRB 990510: evidence for a jet," *Astrophysical Journal Letters*, vol. 523, no. 2, pp. L121–L124, 1999.

[24] E. Berger, S. R. Kulkarni, G. Pooley et al., "A common origin for cosmic explosions inferred from calorimetry of GRB030329," *Nature*, vol. 426, no. 6963, pp. 154–157, 2003.

[25] D. W. Fox, S. Yost, S. R. Kulkarni et al., "Early optical emission from the γ-ray burst of 4 October 2002," *Nature*, vol. 422, no. 6929, pp. 284–286, 2003.

[26] W. Li, A. V. Filippenko, R. Chornock, and S. Jha, "The early light curve of the optical afterglow of GRB 021211," *Astrophysical Journal Letters*, vol. 586, no. 1, pp. L9–L12, 2003.

[27] N. Gehrels, G. Chincarini, P. Giommi et al., "The swift gamma-ray burst mission," *Astrophysical Journal Letters*, vol. 611, no. 2, pp. 1005–1020, 2004.

[28] G. Tagliaferri, M. Goad, G. Chincarini et al., "An unexpectedly rapid decline in the X-ray afterglow emission of long γ-ray bursts," *Nature*, vol. 436, no. 7053, pp. 985–988, 2005.

[29] D. N. Burrows, P. Romano, A. Falcone et al., "Astrophysics: bright X-ray flares in gamma-ray burst afterglows," *Science*, vol. 309, no. 5742, pp. 1833–1835, 2005.

[30] B. Zhang, Y. Z. Fan, J. Dyks et al., "Physical processes shaping gamma-ray burst X-ray afterglow light curves: theoretical implications from the swift X-ray telescope observations," *The Astrophysical Journal*, vol. 642, no. 1, pp. 354–370, 2006.

[31] J. A. Nousek, C. Kouveliotou, D. Grupe et al., "Evidence for a canonical gamma-ray burst afterglow light curve in the swift XRT data," *The Astrophysical Journal*, vol. 642, no. 1, pp. 389–400, 2006.

[32] P. T. O'Brien, R. Willingale, J. Osborne et al., "The early X-ray emission from GRBs," *Astrophysical Journal Letters*, vol. 647, no. 2, pp. 1213–1237, 2006.

[33] P. A. Evans, A. P. Beardmore, K. L. Page et al., "Methods and results of an automatic analysis of a complete sample of Swift-XRT observations of GRBs," *Monthly Notices of the Royal Astronomical Society*, vol. 397, no. 3, pp. 1177–1201, 2009.

[34] D. N. Burrows, J. E. Hill, J. A. Nousek et al., "The wift X-ray telescope," *Space Science Reviews*, vol. 120, no. 3-4, pp. 165–195, 2005.

[35] Y. Z. Fan and D. M. Wei, "Late internal-shock model for bright X-ray flares in gamma-ray burst afterglows and GRB 011121," *Monthly Notices of the Royal Astronomical Society: Letters*, vol. 364, no. 1, pp. L42–L46, 2005.

[36] B.-B. Zhang, E. N.-W. Liang, and B. Zhang, "A comprehensive analysis of Swift XRT data. I. Apparent spectral evolution of gamma-ray burst X-ray tails," *Astrophysical Journal*, vol. 666, no. 2 I, pp. 1002–1011, 2007.

[37] E. N.-W. Liang and B.-B. Zhang, "A comprehensive analysis of Swift XRT data. II. Diverse physical origins of the shallow decay segment," *The Astrophysical Journal*, vol. 670, no. 1, pp. 565–583, 2007.

[38] E.-W. Liang, J. L. Racusin, B. Zhang, B.-B. Zhang, and D. N. Burrows, "A comprehensive analysis of Swift XRT data. III. Jet break candidates in X-ray and optical afterglow light curves," *Astrophysical Journal*, vol. 675, no. 1, pp. 528–552, 2008.

[39] E.-W. Liang, H.-J. Lü, S.-J. Hou, B.-B. Zhang, and B. Zhang, "A comprehensive analysis of swift/X-ray telescope data. IV. single power-law decaying light curves versus canonical light curves and implications for a unified origin of X-rays," *Astrophysical Journal Letters*, vol. 707, no. 1, pp. 328–342, 2009.

[40] N. R. Butler and D. Kocevski, "X-ray hardness evolution in GRB afterglows and flares: late-time GRB activity without NH variations," *Astrophysical Journal*, vol. 663, pp. 407–419, 2007.

[41] D. Kocevski, N. Butler, and J. S. Bloom, "Pulse width evolution of late-time X-ray flares in gamma-ray bursts," *Astrophysical Journal*, vol. 667, no. 2 I, pp. 1024–1032, 2007.

[42] G. Chincarini, A. Moretti, P. Romano et al., "The first survey of X-ray flares from gamma-ray bursts observed by Swift: temporal properties and morphology," *Astrophysical Journal*, vol. 671, no. 2, pp. 1903–1920, 2007.

[43] G. Chincarini, J. Mao, R. Margutti et al., "Unveiling the origin of X-ray flares in gamma-ray bursts," *Monthly Notices of the Royal Astronomical Society*, vol. 406, no. 4, pp. 2113–2148, 2010.

[44] R. Margutti, C. Guidorzi, G. Chincarini et al., "Lag-luminosity relation in γ-ray burst X-ray flares: a direct link to the prompt emission," *Monthly Notices of the Royal Astronomical Society*, vol. 406, no. 4, pp. 2149–2167, 2010.

[45] B. Zhang, "Open questions in GRB physics," *Comptes Rendus Physique*, vol. 12, no. 3, pp. 206–225, 2011.

[46] Y. C. Zou, F. Y. Wang, and K. S. Cheng, "Long-term X-ray emission from Swift J1644+57," *Monthly Notices of the Royal Astronomical Society*, vol. 434, no. 4, pp. 3463–3468, 2013.

[47] R. Sari and T. Piran, "Hydrodynamic timescales and temporal structure of gamma-ray bursts," *Astrophysical Journal Letters*, vol. 455, no. 2, pp. L143–L146, 1995.

[48] R. Sari and T. Piran, "Predictions for the very early afterglow and the optical flash," *The Astrophysical Journal*, vol. 520, no. 2, pp. 641–649, 1999.

[49] D. W. Fox, P. A. Price, A. M. Soderberg et al., "Discovery of early optical emission from GRB 021211," *Astrophysical Journal Letters*, vol. 586, no. 1, pp. L5–L8, 2003.

[50] D. A. Frail, S. R. Kulkarni, E. Berger, and M. H. Wieringa, "A complete catalog of radio afterglows: the first five years," *Astronomical Journal*, vol. 125, no. 5, pp. 2299–2306, 2003.

[51] R. Sari and T. Piran, "GRB 990123: the optical flash and the fireball model," *The Astrophysical Journal*, vol. 517, no. 2, pp. L109–L112, 1999.

[52] P. Mészáros and M. J. Rees, "GRB 990123: reverse and internal shock flashes and late afterglow behaviour," *Monthly Notices of the Royal Astronomical Society*, vol. 306, no. 3, pp. L39–L43, 1999.

[53] S. Kobayashi and R. Sari, "Optical flashes and radio flares in gamma-ray burst afterglow: numerical study," *The Astrophysical Journal*, vol. 542, no. 2, pp. 819–828, 2000.

[54] S. Kobayashi, "Light curves of gamma-ray burst optical flashes," *Astrophysical Journal Letters*, vol. 545, no. 2, pp. 807–812, 2000.

[55] X. Y. Wang, Z. G. Dai, and T. Lu, "Intrinsic parameters of GRB 990123 from its prompt optical flash and afterglow," *Monthly Notices of the Royal Astronomical Society*, vol. 319, no. 4, pp. 1159–1162, 2000.

[56] Y. Z. Fan, Z. G. Dai, Y. F. Huang et al., "Optical flash of GRB 990123: constraints on the physical parameters of the reverse shock," *Chinese Journal of Astronomy and Astrophysics*, vol. 2, no. 5, pp. 449–453, 2002.

[57] S. Kobayashi and B. Zhang, "GRB 021004: reverse shock emission," *The Astrophysical Journal Letters*, vol. 582, no. 2, pp. L75–L78, 2003.

[58] B. Zhang, S. Kobayashi, and P. Mészáros, "Gamma-ray burst early optical afterglows: implications for the initial lorentz factor and the central engine," *Astrophysical Journal Letters*, vol. 595, no. 2 I, pp. 950–954, 2003.

[59] D. M. Wei, "The afterglow of GRB 021211: another case of reverse shock emission," *Astronomy and Astrophysics*, vol. 402, pp. L9–L12, 2003.

[60] P. Kumar and A. Panaitescu, "A unified treatment of the gamma-ray burst 021211 and its afterglow," *Monthly Notices of the Royal Astronomical Society*, vol. 346, no. 3, pp. 905–914, 2003.

[61] A. Panaitescu and P. Kumar, "Analysis of two scenarios for the early optical emission of the gamma-ray burst afterglows 990123 and 021211," *Monthly Notices of the Royal Astronomical Society*, vol. 353, no. 2, pp. 511–522, 2004.

[62] E. Nakar and T. Piran, "Early afterglow emission from a reverse shock as a diagnostic tool for gamma-ray burst outflows," *Monthly Notices of the Royal Astronomical Society*, vol. 353, no. 2, pp. 647–653, 2004.

[63] A. M. Soderberg and E. Ramirez-Ruiz, "Flaring up: radio diagnostics of the kinematic, hydrodynamic and environmental properties of gamma-ray bursts," *Monthly Notices of the Royal Astronomical Society*, vol. 345, no. 3, pp. 854–864, 2003.

[64] E. S. Rykoff, D. A. Smith, P. A. Price et al., "The early optical afterglow of GRB 030418 and progenitor mass loss," *The Astrophysical Journal Letters*, vol. 601, no. 2, pp. 1013–1018, 2004.

[65] G. G. Williams, H. S. Park, and R. Porrata, "GRB 991106, LOTIS optical observations," *GRB Coordinates Network*, vol. 437, p. 1, 1999.

[66] A. Klotz and J. L. Atteia, "GRB 030324: TAROT optical observations," *GRB Coordinates Network*, vol. 1961, p. 1, 2003.

[67] K. Torii, "GRB 030528: optical observations at RIKEN," Tech. Rep. 2253:1, GRB Coordinates Network, 2003.

[68] K. Torii, "GRB 030913: optical limit at RIKEN," *GRB Coordinates Network*, vol. 2381, p. 1, 2003.

[69] X. F. Wu, Z. G. Dai, Y. F. Huang, and T. Lu, "Optical flashes and very early afterglows in wind environments," *Monthly Notices of the Royal Astronomical Society*, vol. 342, no. 4, pp. 1131–1138, 2003.

[70] S. Kobayashi and B. Zhang, "Early optical afterglows from wind-type gamma-ray bursts," *Astrophysical Journal Letters*, vol. 597, no. 1, pp. 455–458, 2003.

[71] Y. C. Zou, X. F. Wu, and Z. G. Dai, "Early afterglows in wind environments revisited," *Monthly Notices of the Royal Astronomical Society*, vol. 363, no. 1, pp. 93–106, 2005.

[72] S.-X. Yi, X.-F. Wu, and Z.-G. Dai, "Early afterglows of gamma-ray bursts in a stratified medium with a power-law density distribution," *The Astrophysical Journal*, vol. 776, no. 2, article 120, 2013.

[73] B. Zhang and S. Kobayashi, "Gamma-ray burst early afterglows: reverse shock emission from an arbitrarily magnetized ejecta," *Astrophysical Journal Letters*, vol. 628, no. 1 I, pp. 315–334, 2005.

[74] Y. Z. Fan, D. M. Wei, and C. F. Wang, "The very early afterglow powered by ultra-relativistic mildly magnetized outflows," *Astronomy & Astrophysics*, vol. 424, no. 2, pp. 477–484, 2004.

[75] P. Mimica, D. Giannios, and M. A. Aloy, "Deceleration of arbitrarily magnetized GRB ejecta: the complete evolution," *Astronomy and Astrophysics*, vol. 494, no. 3, pp. 879–890, 2009.

[76] P. Mimica, D. Giannios, and M. A. Aloy, "Multiwavelength afterglow light curves from magnetized gamma-ray burst flows," *Monthly Notices of the Royal Astronomical Society*, vol. 407, no. 4, pp. 2501–2510, 2010.

[77] Y. Mizuno, B. Zhang, B. Giacomazzo et al., "Magnetohydrodynamic effects in propagating relativistic jets: reverse shock and magnetic acceleration," *The Astrophysical Journal Letters*, vol. 690, no. 1, pp. L47–L51, 2009.

[78] R. Harrison and S. Kobayashi, "Magnetization degree of gamma-ray burst fireballs: numerical study," *Astrophysical Journal*, vol. 772, no. 2, article 101, 2013.

[79] Z. Li, Z. G. Dai, T. Lu, and L. M. Song, "Pair loading in gamma-ray burst fireballs and prompt emission from pair-rich reverse shocks," *The Astrophysical Journal*, vol. 599, no. 1 I, pp. 380–386, 2003.

[80] Y. Z. Fan, B. Zhang, and D. M. Wei, "Early photon-shock interaction in a stellar wind: a sub-GeV photon flash and high-energy neutrino emission from long gamma-ray bursts," *The Astrophysical Journal*, vol. 629, no. 1, pp. 334–340, 2005.

[81] F. Genet, F. Daigne, and R. Mochkovitch, "Can the early X-ray afterglow of gamma-ray bursts be explained by a contribution from the reverse shock?" *Monthly Notices of the Royal Astronomical Society*, vol. 381, no. 2, pp. 732–740, 2007.

[82] Z. L. Uhm and A. M. Beloborodov, "On the mechanism of gamma-ray burst afterglows," *The Astrophysical Journal*, vol. 665, no. 2, pp. L93–L96, 2007.

[83] X.-W. Liu, X.-F. Wu, Y.-C. Zou, and T. Lu, "Early afterglows from radially structured outflows and the application to X-ray shallow decays," *Research in Astronomy and Astrophysics*, vol. 9, no. 8, pp. 911–920, 2009.

[84] Z. L. Uhm, "A semi-analytic formulation for relativistic blast waves with a long-lived reverse shock," *The Astrophysical Journal*, vol. 733, no. 2, article 86, 2011.

[85] Z. L. Uhm, B. Zhang, R. Hascoët, F. Daigne, R. Mochkovitch, and I. H. Park, "Dynamics and afterglow light curves of gamma-ray burst blast waves with a long-lived reverse shock," *The Astrophysical Journal*, vol. 761, no. 2, article 147, 2012.

[86] Z. L. Uhm and B. Zhang, "Dynamics and afterglow light curves of gamma-ray burst blast waves encountering a density bump or void," *The Astrophysical Journal*, vol. 789, no. 1, p. 39, 2014.

[87] Z. G. Dai and T. Lu, "Neutrino afterglows and progenitors of gamma-ray bursts," *The Astrophysical Journal*, vol. 551, no. 1, pp. 249–253, 2001.

[88] Y. Z. Fan, B. Zhang, and D. M. Wei, "Early optical afterglow light curves of neutron-fed gamma-ray bursts," *The Astrophysical Journal*, vol. 628, no. 1, pp. 298–314, 2005.

[89] X. Y. Wang, Z. G. Dai, and T. Lu, "Prompt high-energy gamma-ray emission from the synchrotron self-Compton process in the reverse shocks of gamma-ray bursts," *The Astrophysical Journal Letters*, vol. 546, no. 1, pp. L33–L37, 2001.

[90] X. Y. Wang, Z. G. Dai, and T. Lu, "The inverse Compton emission spectra in the very early afterglows of gamma-ray bursts," *Astrophysical Journal Letters*, vol. 556, no. 2, pp. 1010–1016, 2001.

[91] H. Gao, X. G. Wang, P. Mészáros, and B. Zhang, "A morphological analysis of gamma-ray burst early optical afterglows," *The Astrophysical Journal*. Submitted.

[92] Z. P. Jin and Y. Z. Fan, "GRB 060418 and 060607A: the medium surrounding the progenitor and the weak reverse shock emission," *Monthly Notices of the Royal Astronomical Society*, vol. 378, no. 3, pp. 1043–1048, 2007.

[93] M. V. Medvedev and A. Loeb, "Generation of magnetic fields in the relativistic shock of gamma-ray burst sources," *The Astrophysical Journal*, vol. 526, no. 2, pp. 697–706, 1999.

[94] E. Nakar, T. Piran, and R. Sari, "Pure and loaded fireballs in soft gamma-ray repeater giant flares," *Astrophysical Journal Letters*, vol. 635, no. 1, pp. 516–521, 2005.

[95] S. R. Kulkarni, S. G. Djorgovski, S. C. Odewahn et al., "The afterglow, redshift and extreme energetics of the γ-ray burst of 23 January 1999," *Nature*, vol. 398, no. 6726, pp. 389–394, 1999.

[96] T. J. Galama, M. S. Briggs, R. A. M. J. Wijers et al., "The effect of magnetic fields on γ-ray bursts inferred from multi- wavelength

observations of the burst of 23 January 1999," *Nature*, vol. 398, no. 6726, pp. 394–399, 1999.

[97] J. S. Bloom, S. R. Kulkarni, S. G. Djorgovski et al., "The unusual afterglow of the γ-ray burst of 26 March 1998 as evidence for a supernova connection," *Nature*, vol. 401, no. 6752, pp. 453–456, 1999.

[98] E. E. Fenimore, E. Ramirez-Ruiz, and B. Wu, "GRB 990123: evidence that the gamma rays come from a central engine," *The Astrophysical Journal*, vol. 518, no. 2, pp. L73–L76, 1999.

[99] Z. G. Dai and T. Lu, "The afterglow of GRB 990123 and a dense medium," *Astrophysical Journal Letters*, vol. 519, no. 2, pp. L155–L158, 1999.

[100] S. R. Kulkarni, D. A. Frail, R. Sari et al., "Discovery of a radio flare from GRB 990123," *Astrophysical Journal Letters*, vol. 522, no. 2, pp. L97–L100, 1999.

[101] S. Holland, G. Björnsson, J. Hjorth, and B. Thomsen, "The broken light curves of gamma-ray bursts GRB 990123 and GRB 990510," *Astronomy and Astrophysics*, vol. 364, no. 2, pp. 467–478, 2000.

[102] E. Maiorano, N. Masetti, E. Palazzi et al., "The puzzling case of GRB 990123: multiwavelength afterglow study," *Astronomy and Astrophysics*, vol. 438, no. 3, pp. 821–827, 2005.

[103] A. Corsi, L. Piro, E. Kuulkers et al., "The puzzling case of GRB 990123: prompt emission and broad-band afterglow modeling," *Astronomy & Astrophysics*, vol. 438, no. 3, pp. 829–840, 2005.

[104] A. Panaitescu, "Swift gamma-ray burst afterglows and the forward-shock model," *Monthly Notices of the Royal Astronomical Society*, vol. 379, no. 1, pp. 331–342, 2007.

[105] D. M. Wei, "The GRB early optical flashes from internal shocks: application to GRB 990123, GRB 041219a and GRB 060111b," *Monthly Notices of the Royal Astronomical Society*, vol. 374, no. 2, pp. 525–529, 2007.

[106] D. Lazzati, R. Perna, J. Flasher, V. V. Dwarkadas, and F. Fiore, "Time-resolved spectroscopy of GRB 021004 reveals a clumpy extended wind," *Monthly Notices of the Royal Astronomical Society*, vol. 372, no. 4, pp. 1791–1798, 2006.

[107] W. T. Vestrand, K. Borozdin, D. J. Casperson et al., "RAPTOR: closed-Loop monitoring of the night sky and the earliest optical detection of GRB 021211," *Astronomische Nachrichten*, vol. 325, no. 6–8, pp. 549–552, 2004.

[108] M. C. Nysewander, D. E. Reichart, H. S. Park et al., "Early time chromatic variations in the wind-swept medium of GRB 021211 and the faintness of its afterglow," *The Astrophysical Journal*, vol. 651, no. 2, pp. 994–1004, 2006.

[109] L. Shao and Z. G. Dai, "A reverse-shock model for the early afterglow of GRB 050525A," *The Astrophysical Journal*, vol. 633, no. 2, pp. 1027–1030, 2005.

[110] A. J. Blustin, D. Band, S. Barthelmy et al., "Swift panchromatic observations of the bright gamma-ray burst GRB 050525a," *The Astrophysical Journal*, vol. 637, no. 2, pp. 901–913, 2006.

[111] D. M. Wei, T. Yan, and Y. Z. Fan, "The optical flare and afterglow light curve of GRB 050904 at redshift z = 6.29," *The Astrophysical Journal*, vol. 636, no. 2, pp. L69–L72, 2006.

[112] M. Boër, J. L. Atteia, Y. Damerdji, B. Gendre, A. Klotz, and G. Stratta, "Detection of a very bright optical flare from the gamma-ray burst GRB 050904 at redshift 6.29," *The Astrophysical Journal*, vol. 638, no. 2, pp. L71–L74, 2006.

[113] D. A. Kann, N. Masetti, and S. Klose, "The prompt optical/near-infrared flare of GRB 050904: the most luminous transient ever detected," *Astronomical Journal*, vol. 133, no. 3, pp. 1187–1192, 2007.

[114] L.-J. Gou, D. B. Fox, and P. Mészáros, "Modeling GRB 050904: autopsy of a massive stellar explosion at z = 6.29," *Astrophysical Journal*, vol. 668, no. 2, pp. 1083–1102, 2007.

[115] A. Klotz, B. Gendre, G. Stratta et al., "Continuous optical monitoring during the prompt emission of GRB 060111B," *Astronomy & Astrophysics*, vol. 451, no. 3, pp. L39–L42, 2006.

[116] M. Jelínek, M. Prouza, P. Kubánek et al., "The bright optical flash from GRB 060117," *Astronomy & Astrophysics*, vol. 454, no. 3, pp. L119–L122, 2006.

[117] S. Covino, S. Campana, M. L. Conciatore et al., "Challenging gamma-ray burst models through the broadband dataset of GRB 060908," *Astronomy and Astrophysics*, vol. 521, no. 6, article A53, 2010.

[118] A. Gomboc, S. Kobayashi, C. Guidorzi et al., "Multiwavelength analysis of the intriguing GRB 061126: the reverse shock scenario and magnetization," *Astrophysical Journal*, vol. 687, no. 1, pp. 443–455, 2008.

[119] D. A. Perley, J. S. Bloom, N. R. Butler et al., "The troublesome broadband evolution of GRB 061126: does a gray burst imply gray dust?" *The Astrophysical Journal*, vol. 672, no. 1, pp. 449–464, 2008.

[120] J. L. Racusin, S. V. Karpov, M. Sokolowski et al., "Broadband observations of the naked-eye γ-ray burst GRB 080319B," *Nature*, vol. 455, no. 7210, pp. 183–188, 2008.

[121] P. Kumar and A. Panaitescu, "What did we learn from gamma-ray burst 080319B?" *Monthly Notices of the Royal Astronomical Society*, vol. 391, no. 1, pp. L19–L23, 2008.

[122] J. S. Bloom, D. A. Perley, W. Li et al., "Observations of the naked-eye GRB 080319B: implications of nature's brightest explosion," *The Astrophysical Journal*, vol. 691, no. 1, pp. 723–737, 2009.

[123] S. B. Pandey, A. J. Castro-Tirado, M. Jelínek et al., "Multi-wavelength observations of the GRB 080319B afterglow and the modeling constraints," *Astronomy and Astrophysics*, vol. 504, no. 1, pp. 45–51, 2009.

[124] Z.-P. Jin, S. Covino, M. Della Valle et al., "GRB 081007 and GRB 090424: the surrounding medium, outflows, and supernovae," *Astrophysical Journal*, vol. 774, no. 2, article 114, 2013.

[125] B. Gendre, A. Klotz, E. Palazzi et al., "Testing gamma-ray burst models with the afterglow of GRB 090102," *Monthly Notices of the Royal Astronomical Society*, vol. 405, no. 4, pp. 2372–2380, 2010.

[126] J. Aleksić, S. Ansoldi, L. A. Antonelli et al., "MAGIC upper limits on the GRB 090102 afterglow," *Monthly Notices of the Royal Astronomical Society*, vol. 437, no. 4, pp. 3103–3111, 2014.

[127] S. B. Pandey, C. A. Swenson, D. A. Perley et al., "GRB 090902B: afterglow observations and implications," *Astrophysical Journal Letters*, vol. 714, no. 1, pp. 799–804, 2010.

[128] R.-Y. Liu and X.-Y. Wang, "Modeling the broadband emission of GRB 090902B," *The Astrophysical Journal*, vol. 730, no. 1, article 1, 2011.

[129] D. Gruber, T. Krühler, S. Foley et al., "Fermi /GBM observations of the ultra-long GRB 091024: a burst with an optical flash," *Astronomy and Astrophysics*, vol. 528, article A15, 2011.

[130] W.-H. Gao, "The physical origin of optical flares following GRB 110205A and the nature of the outflow," *Research in Astronomy and Astrophysics*, vol. 11, no. 11, pp. 1317–1326, 2011.

[131] B. Gendre, J. L. Atteia, M. Boër et al., "GRB 110205A: anatomy of a long gamma-ray burst," *The Astrophysical Journal*, vol. 748, no. 1, article no. 59, 2012.

[132] W. Zheng, R. F. Shen, T. Sakamoto et al., "Panchromatic observations of the textbook GRB 110205A: constraining physical

mechanisms of prompt emission and afterglow," *The Astrophysical Journal*, vol. 751, no. 2, article 90, 2012.

[133] T. Laskar, E. Berger, B. A. Zauderer et al., "A reverse shock in GRB 130427A," *The Astrophysical Journal*, vol. 776, no. 2, article 119, 2013.

[134] A. Panaitescu, W. T. Vestrand, and P. Woźniak, "An external-shock model for gamma-ray burst afterglow 130427A," *Monthly Notices of the Royal Astronomical Society*, vol. 436, no. 4, Article ID stt1792, pp. 3106–3111, 2013.

[135] W. T. Vestrand, J. A. Wren, A. Panaitescu et al., "The bright optical flash and afterglow from the gamma-ray burst GRB 130427A," *Science*, vol. 343, no. 6166, pp. 38–41, 2014.

[136] A. J. van der Horst, Z. Paragi, A. G. de Bruyn et al., "A comprehensive radio view of the extremely bright gamma-ray burst 130427A," *Monthly Notices of the Royal Astronomical Society*, vol. 444, no. 4, pp. 3151–3163, 2014.

[137] R. D. Blandford and R. L. Znajek, "Electromagnetic extraction of energy from Kerr black holes," *Monthly Notices of the Royal Astronomical Society*, vol. 179, no. 3, pp. 433–456, 1977.

[138] S. Kobayashi, T. Piran, and R. Sari, "Hydrodynamics of a relativistic fireball: the complete evolution," *The Astrophysical Journal*, vol. 513, no. 2, pp. 669–678, 1999.

[139] R. Sari, T. Piran, and J. P. Halpern, "Jets in gamma-ray bursts," *Astrophysical Journal Letters*, vol. 519, no. 1, pp. L17–L20, 1999.

[140] Y. Z. Fan, D. M. Wei, and B. Zhang, "γ-ray burst internal shocks with magnetization," *Monthly Notices of the Royal Astronomical Society*, vol. 354, no. 4, pp. 1031–1039, 2004.

[141] E. V. Derishev and V. V. Kocharovsky, "The neutron component in fireballs of gamma-ray bursts: dynamics and observable imprints," *Astrophysical Journal Letters*, vol. 521, no. 2, pp. 640–649, 1999.

[142] A. M. Beloborodov, "Nuclear composition of gamma-ray burst fireballs," *Astrophysical Journal Letters*, vol. 588, no. 2, pp. 931–944, 2003.

[143] J. Pruet, S. E. Woosley, and R. D. Huffman, "Nucleosynthesis in gamma-ray burst accretion disks," *The Astrophysical Journal*, vol. 586, no. 2, pp. 1254–1261, 2003.

[144] S. Kobayashi, B. Zhang, P. Mészáros, and D. Burrows, "Inverse compton x-ray flare from gamma-ray burst reverse shock," *Astrophysical Journal*, vol. 655, no. 1, pp. 391–395, 2007.

[145] A. M. Beloborodov, "Optical and GeV-TeV flashes from gamma-ray bursts," *Astrophysical Journal Letters*, vol. 618, no. 1, pp. L13–L16, 2005.

[146] S. Horiuchi and S. Ando, "High-energy neutrinos from reverse shocks in choked and successful relativistic jets," *Physical Review D*, vol. 77, no. 6, Article ID 063007, 2008.

[147] M. J. Rees and P. Mészáros, "Refreshed shocks and afterglow longevity in gamma-ray bursts," *Astrophysical Journal Letters*, vol. 496, no. 1, pp. L1–L4, 1998.

[148] R. Sari and P. Mészáros, "Impulsive and varying injection in gamma-ray burst afterglows," *The Astrophysical Journal*, vol. 535, no. 1, pp. L33–L37, 2000.

[149] D. Lazzati and M. C. Begelman, "Thick fireballs and the steep decay in the early X-ray afterglow of gamma-ray bursts," *The Astrophysical Journal*, vol. 641, no. 2, pp. 972–977, 2006.

[150] S. Kobayashi, "Polarization in very early gamma-ray burst afterglow," *International Journal of Modern Physics: Conference Series*, vol. 8, pp. 220–224, 2012.

[151] A. Sagiv, E. Waxman, and A. Loeb, "Probing the magnetic field structure in gamma-ray bursts through dispersive plasma effects on the afterglow polarization," *The Astrophysical Journal*, vol. 615, no. 1, pp. 366–377, 2004.

[152] I. A. Steele, C. G. Mundell, R. J. Smith, S. Kobayashi, and C. Guidorzi, "Ten per cent polarized optical emission from GRB 090102," *Nature*, vol. 462, no. 7274, pp. 767–769, 2009.

[153] C. G. Mundell, I. A. Steels, R. J. Smith et al., "Early optical polarization of a gamma-ray burst afterglow," *Science*, vol. 315, no. 5820, pp. 1822–1824, 2007.

[154] A. Panaitescu, P. Mészáros, and M. J. Rees, "Multiwavelength afterglows in gamma-ray bursts: Refreshed shock and jet effects," *The Astrophysical Journal*, vol. 503, no. 1, pp. 314–324, 1998.

[155] D. Lazzati, E. Rossi, S. Covino, G. Ghisellini, and D. Malesani, "The afterglow of GRB 021004: surfing on density waves," *Astronomy and Astrophysics*, vol. 396, no. 2, pp. L5–L9, 2002.

[156] K. Ioka, S. Kobayashi, and B. Zhang, "Variabilities of gamma-ray burst afterglows: long-acting engine, anisotropic jet, or many fluctuating regions?" *The Astrophysical Journal*, vol. 631, no. 1, pp. 429–434, 2005.

[157] J. Japelj, D. Kopač, S. Kobayashi et al., "Phenomenology of reverse-shock emission in the optical afterglows of gamma-ray bursts," *The Astrophysical Journal*, vol. 785, no. 2, article 84, 2014.

[158] D. A. Perley, A. J. Levan, N. R. Tanvir et al., "A population of massive, luminous galaxies hosting heavily dust-obscured gamma-ray bursts: implications for the use of GRBs as tracers of cosmic star formation," *The Astrophysical Journal*, vol. 778, no. 2, article 128, 2013.

[159] A. De Ugarte Postigo, A. Lundgren, S. Martín et al., "Pre-ALMA observations of GRBs in the mm/submm range," *Astronomy and Astrophysics*, vol. 538, article A44, 2012.

[160] Y. Urata, K. Huang, K. Asada et al., "A new era of sub-millimeter GRB afterglow follow-ups with the Greenland Telescope," http://arxiv.org/abs/1503.07594.

[161] P. Chandra and D. A. Frail, "A radio-selected sample of gamma-ray burst afterglows," *Astrophysical Journal*, vol. 746, no. 2, article 156, 2012.

[162] H. Gao and B. Zhang, "photosphere emission from a hybrid relativistic outflow with arbitrary dimensionless entropy and magnetization in GRBs," *The Astrophysical Journal*, vol. 801, no. 2, article 103, 2015.

[163] J. Paul, J. Wei, S. Basa, and S.-N. Zhang, "The Chinese-French SVOM mission for gamma-ray burst studies," *Comptes Rendus Physique*, vol. 12, no. 3, pp. 298–308, 2011.

Hindawi Publishing Corporation
Advances in Astronomy
Volume 2015, Article ID 460293, 5 pages
http://dx.doi.org/10.1155/2015/460293

Research Article

GRB 130603B: No Compelling Evidence for Neutron Star Merger

Shlomo Dado and Arnon Dar

Physics Department, Technion, 32000 Haifa, Israel

Correspondence should be addressed to Arnon Dar; arnon@physics.technion.ac.il

Received 22 September 2014; Accepted 3 February 2015

Academic Editor: WeiKang Zheng

The near infrared (NIR) flare/rebrightening in the afterglow of the short hard gamma ray burst (SHB) 130603B measured with the Hubble Space Telescope (HST) and an alleged late-time X-ray excess were interpreted as possible evidence of a neutron star merger origin of SHBs. However, the X-ray afterglow that was measured with the Swift XRT and Newton XMM has the canonical behaviour of a synchrotron afterglow produced by a highly relativistic jet. The H-band flux observed with HST 9.41 days after burst is that expected from the measured late-time X-ray afterglow. The late-time flare/rebrightening of the NIR-optical afterglow of SHB 130603B could have been produced also by jet collision with an interstellar density bump. Moreover, SHB plus a kilonova can be produced also by the collapse of a compact star (neutron star, strange star, or quark star) to a more compact object due to cooling, loss of angular momentum, or mass accretion.

1. Introduction

Stripped envelope supernova explosions and neutron star mergers in close binaries were originally suggested by Goodman et al. [1] as possible sources of cosmological gamma ray bursts. However, their proposed underlying mechanism—a spherical fireball produced by neutrino-antineutrino annihilation into electron positron pairs beyond the surface of the collapsing/merging star—turned out not to be powerful enough to produce GRBs observable at very large cosmological distances as indicated from analysis of the first 153 GRBs observed with the Burst and Transient Source Experiment aboard the Compton Gamma Ray Observatory [2], which was launched in 1991. Consequently, Shaviv and Dar proposed [3] that highly relativistic jets of ordinary matter are probably ejected in such events and produce narrowly collimated GRBs by inverse Compton scattering of circumstellar light. They also suggested that short GRBs may also be produced by highly relativistic jets ejected in the phase transition of compact stars, such as neutron stars, strange stars, and quark stars, into more compact objects due to mass accretion or to cooling and loss of angular momentum via winds and radiation. After the discovery of GRB afterglows, Dar [4] proposed that they are highly beamed synchrotron radiation emitted by these highly relativistic jets in their collision with the interstellar matter.

By now, there is convincing evidence that long duration GRBs and their afterglows are produced mostly by highly relativistic jets launched in stripped envelope supernova explosions (mainly of type Ic), but, despite the enormous observational efforts, the origin of short duration GRBs remains unknown. In fact, the circumstantial evidence that has been claimed to link short hard GRBs (SHBs) with neutron star merger in close binaries, such as their location in both spiral and elliptical galaxies [5, 6] and the distribution of their location offsets relative to the center of their host galaxies, which extends to a distance of 100 kpc [6] and beyond (e.g., SHB 080503 with the lack of a coincident host galaxy down to 28.5 mag in deep Hubble Space Telescope imaging [7]), actually favours a phase transition in a single compact star [8] with a large natal kick velocity over merging neutron stars in neutron star binaries [1] whose velocities are much smaller [9].

A more direct observational evidence that SHBs are produced by neutron stars merger was proposed by Li and Paczynski [10]. These authors suggested that neutron star mergers may create significant quantities of neutron-rich radioactive nuclei whose decay should result in a faint

transient in the days following the burst, a so-called kilonova or macronova.

Recently, the broad band afterglow of the SHB 130603B (Melandri et al. [11] and Golenetskii et al. [12]) that was measured with the Swift X-ray telescope (XRT), Newton XMM, HST, and ground-based optical and radio telescopes was interpreted by Tanvir et al. [13, 14], Berger et al. [15], and Fong et al. [16] as evidence supporting a neutron star merger origin of SHB 130603B. However, in this paper we show that the X-ray afterglow of SHB 130603B, which was measured with Swift XRT (Swift-XRT GRB light-curve repository [17]) and Newton XMM [16], had the canonical behaviour of a synchrotron afterglow produced by a highly relativistic jet propagating in a normal interstellar environment, as predicted by the cannonball model of GRBs [8, 18–20] long before its empirical discovery by Nousek et al. with Swift [21]. This canonical X-ray afterglow does not have a "mysterious late-time X-ray excess" as claimed in [16], and the flux observed in the NIR H-band with HST 9.6 days after burst [13, 14] is that expected from the measured late-time X-ray afterglow. Moreover, a fast decline of a late-time afterglow followed by a rebrightening/flare in the NIR and optical afterglow of a GRB can be produced by a jet colliding with a density bump in the interstellar medium [8], as was observed in several long duration GRBs, such as 030329 [22, 23] and 070311 [24], and SHBs such as 050724 [25] and 080503 [26]. The host galaxy of SHB 130603B at redshift $z = 0.356$ [7], as seen in high-resolution HST imaging, is a perturbed spiral galaxy due to interaction with another galaxy [27]. SHB 130603B was located in one of its tidally disrupted arms [27]. The interaction of the SHB jet with such a bumpy environment may have caused the flare/rebrightening in the NIR afterglow observed with the HST on day 9.41 [13, 14].

Furthermore, a late-time flare/rebrightening of a NIR-optical afterglow of SHB can be produced by either a jet collision with an interstellar density bump or a kilonova. However, SHB plus kilonova can be produced also by collapse of compact stars (neutron star, strange star, or quark star) to a more compact object due to cooling, loss of angular momentum, or mass accretion [3, 8, 28]. The distribution of pulsar velocities has a high velocity component due to single pulsars and a lower velocity component from pulsars in binaries and isolated millisecond pulsars [9]. Hence, single compact stars are more likely than neutron star binaries (neutron stars, neutron star-black hole, and neutron star-white dwarf binaries) to be found at the large observed offsets of several SHBs from the center/disk of their host galaxies or at far away distances where no nearby host candidate was found in very deep searches.

Finally, the star formation within the host, location of SHB 130603B on top of the tidally disrupted arm, strong absorption features, and large line of sight extinction that were observed indicate that the GRB progenitor was probably not far from its birth place [27], untypical of the rather long mean lifetime before neutron star merger due to gravitational wave emission estimated for the known neutron star binaries in our galaxy (see, e.g., [9] for a recent review).

2. The X-Ray Afterglow of SHB 130603B

The conclusion of Fong et al. [16] that the X-ray afterglow of SHB 130603B shows "a mysterious late-time X-ray excess" was based on a standard fireball model analysis of its X-ray afterglow. The standard fireball model, however, predicts that the temporal index α of the afterglow of a conical jet that is parametrized as a smoothly broken power law, $F_\nu \propto t^{-\alpha}\nu^{-\beta}$, increases by $\Delta\alpha_X = 0.75$ across the jet break, independent of the spectral index β_X of the afterglow [20]. The X-ray temporal indices $\alpha_X = 0.35 \pm 0.08$ and $\alpha_X = 1.61 \pm 0.08$ before and after the break, respectively, that were reported in the Swift-XRT GRB Catalogue [17] yield $\Delta\alpha_X = 1.26 \pm 0.11$ ($\alpha_X = 1.75 \pm 0.08$ for the combined data of Swift XRT and Newton XMM yields $\Delta\alpha_X = 1.40 \pm 0.11$), which is at odds with $\Delta\alpha_X \approx 0.75$ expected in the conical fireball model.

In contrast, the X-ray afterglow of SHB 130603B that was measured with Swift XRT [17] and Newton XMM [16] has the canonical behaviour of a normal synchrotron afterglow produced by a highly relativistic jet propagating in a normal interstellar environment of its host galaxy as predicted by the CB model [18] long before the launch of Swift and its empirical discovery by Nousek et al. [21]. It consists of an early plateau phase that follows the fast decline phase of the prompt emission and breaks smoothly into a late-time ($t \gg t_b$) power law decline with a power law index that satisfies the cannonball (CB) model closure relation [19, 20]

$$\alpha_X = \beta_X + \frac{1}{2} = \Gamma_X - \frac{1}{2}, \quad (1)$$

independent of the prebreak power law index, where Γ_X is the photon spectral index of the X-ray afterglow. Using the value $\beta_X = 1.15 \pm 0.11$, which was obtained by de Ugarte Postigo et al. [27] from the Swift-XRT data, the CB model closure relation yields $\alpha_X = 1.65 \pm 0.11$. This value is consistent within errors with the postbreak value $\alpha_X = 1.61 \pm 0.08$ reported for SHB 130603B in the Swift-XRT GRB Catalogue [17].

In the CB model, the canonical light curve of the X-ray afterglow depends only on three parameters [19]: the product $\gamma\theta$ of the bulk motion Lorentz factor of the jet and the viewing angle relative to the direction of motion of the jet, the jet deceleration parameter t_0, and the spectral index p_e of the Fermi accelerated electrons in the jet that satisfies $p_e = 2\beta_X$. CB model fit to the light curve of the 0.3–10 keV X-ray afterglow of SHB 130603B, which was measured with Swift XRT [17] and with Newton XMM assuming the spectral index that was measured with Swift, is shown in Figure 1. The best fit value $p_e = 2.37$ yields $\beta_X = p_e/2 = 1.18$, which is consistent with the late-time photon index $\beta_X + 1 = \Gamma_X = 2.21 \pm 0.18$ reported in the Swift-XRT GRB Catalogue [17]. The two other best fit parameters, $\gamma\theta = 0.55$ and $t_0 = 878$ s, yield a deceleration break (so-called jet break) at $t_b \approx 1500$ s.

Thus, we conclude that there is no evidence for a "mysterious late-time X-ray excess" that was claimed in [16] and was explained by a magnetar contribution to the afterglow emission of SHB 130603B [29, 30].

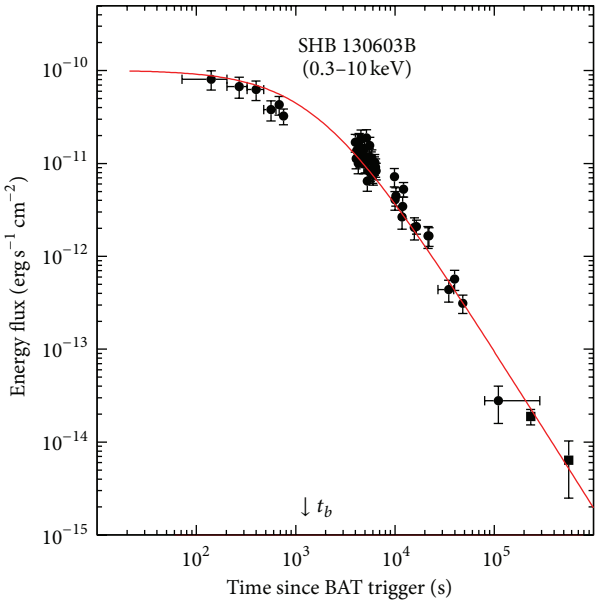

FIGURE 1: Comparison between the light curve of the X-ray afterglow of SHB 130603B, which was measured with Swift XRT [17] and with Newton XMM [16] assuming the spectral index $\beta_X = 1.15$ that was measured with Swift, and a CB model fit.

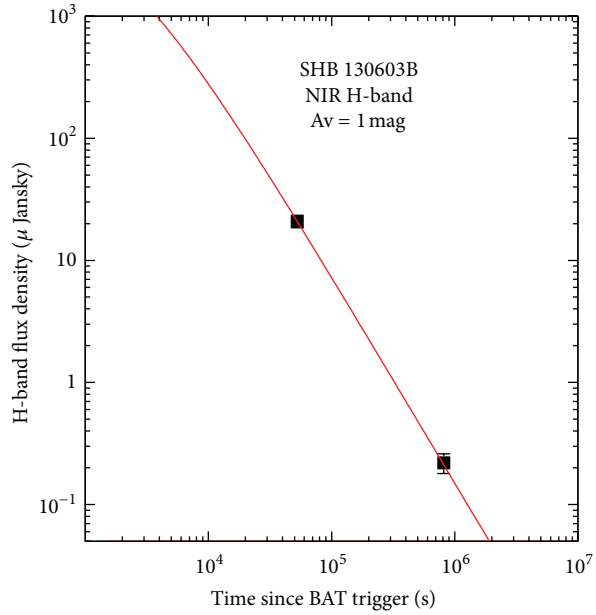

FIGURE 2: Comparison between the observed late-time H-band spectral energy density [14, 15] of SHB 130603B, where the JK-band observations were extrapolated to the H-band and corrected for line of sight extinction [16], and that expected from the CB model fit of the X-ray afterglow shown in Figure 1.

3. The Near Infrared-Optical Afterglow

The conclusion that the NIR-optical afterglow of SHB 130603B provides possible evidence of a macronova/kilonova was based on a rebrightening of the NIR afterglow observed with the Hubble Space Telescope (HST) in the H-band on day 9.41, which is well above that extrapolated from the fast decline of the optical afterglow in the r band during the first day after the break around 0.3 d [15, 16]. However, in the CB model, when the spectral index of the late-time NIR and optical bands is above the spectral break, $\beta_H \approx \beta_X$ and consequently $\alpha_H = \beta_H + 1/2 \approx \alpha_X$. Using the ground-based JK-band observations extrapolated to the H-band [16] and the HST H-band measurement, we obtained the fact that $\alpha_H = 1.69 \pm 0.08$ in the time interval 0.61–9.41 d, which is in agreement, within errors, with the power law index $\alpha_X = 1.68 \pm 0.08$ of the joint late-time Swift-XRT observations [17] and XMM Newton observations [16]. This is shown in Figure 2 where we compare the late-time H-band spectral energy density (SED) of SHB 130603B [14, 15], corrected for line of sight extinction [16], and the SED expected from the CB model fit to the X-ray afterglow.

Moreover, a broken power law best fit to the unabsorbed late-time broad band NIR-optical and Swift X-ray spectrum by de Ugarte Postigo et al. [27] yielded $\beta = 0.65 \pm 0.09$ below a break at $\nu_b = 9.55 \times 10^{15}$ Hz and $\beta_X = 1.15 \pm 0.11$. Using $\lambda = 12.4$ A for 1 keV photons, $\lambda = 16300$ A for H-band photons and $\lambda_{break} = 314$ A; the expected flux ratio of the H and X-ray bands is $F_H/F_{keV} \approx 536 \pm 160$. This ratio is in good agreement within errors with the observed ratio $F_H/F_{keV} = 623 \pm 160$ of the H-band flux measured with HST on day 9.41 after burst and the 1 keV X-ray flux obtained by extrapolating the joint Swift-XRT and Newton XMM 1 keV flux to day 9.41.

The highly relativistic jets of plasmoids (cannonballs) that produce GRBs can encounter a bumpy interstellar medium in the host galaxy. Also, the opacity along the line of sight to the jet in the host can vary significantly due to the "superluminal" motion of the line of sight to the jet in the host galaxy. The collision of a jet with an overdensity bump can produce chromatic rebrightening/flare in the NIR-optical afterglow (e.g., [8, 18]) as was observed in the late-time optical afterglow of several long duration GRBs such as 030329 [22, 23] and 070311 [24] and of SHBs such as 050724 [25] and 080503 [26], while underdensity can cause a fast temporal decline of an afterglow ($\alpha > 2$), as observed in several GRBs (Swift-XRT GRB Catalogue [17]). Such density variations cause spectral and temporal variations in the afterglow, which otherwise has a smooth power law behaviour. After an overdensity or an underdensity, the late-time ($t \gg t_b$) closure relation of the CB model is recovered when the column density as function of distance converges to that of the mean ISM density. This can explain both a fast decline of the NIR-optical afterglow of SHB 130603B after an overdensity followed by an underdensity and a recovery to the normal power law decline like that of the X-ray afterglow.

4. The Macronova-SHB Association

SHBs may be produced by highly relativistic jets launched in the collapse of compact stars (neutron star, strange star, or quark star) to a more compact object due to loss of angular momentum, cooling, or mass accretion [3, 8, 28]. During neutron star mergers, or collapse of compact stars to more compact objects, the crust layers may be stripped

off by very strong outgoing shocks. Neutrino-antineutrino annihilation into electron-positron pairs behind such blown-off layers perhaps can produce a fireball [1] which may accelerate the blown-off crust layers to velocities well above the escape velocity (Li and Paczynski [10]) although the neutrino luminosity, which is well below the "neutrino Eddington luminosity" [28], by itself cannot blow off the crust layers of a compact star.

It is unclear whether a robust r-process occurs in the macronova ejecta, or whether neutrinos drive the composition towards ^{56}Ni dominated composition (e.g., [29]). All together, the total mass of the ejecta, its composition, density, and velocity and their radial and angular distributions are highly uncertain, which makes the predicted signal from an associated macronova [10] very uncertain and unreliable for distinguishing between a phase transition in a single compact star and a merger of compact stars in binaries as the origin of SHBs.

5. Conclusions

Several explanations of the rebrightening of the NIR afterglow of SHB 130603B around 9.41 days after burst have been proposed. These include a macronova/kilonova produced by a neutron star merger in a close binary [15, 16], a millisecond magnetar produced in neutron star merger in close binaries [30, 31], and a late-time flare produced by collision of the SHB jet with an ISM density bump [8, 18].

SHBs plus a minisupernova/macronova/kilonova, however, are not unique to the neutron star merger scenario. They can be produced also in a phase transition/collapse of single compact stars (neutron star, strange star, or quark star) to a more compact object due to cooling, loss of angular momentum, or mass accretion.

The X-ray afterglow that was measured with the Swift XRT and Newton XMM has the expected canonical behaviour of a synchrotron afterglow produced by a highly relativistic jet. Its late-time behaviour does not provide an evidence for a millisecond magnetar as the power-source of the chromatic afterglow of SHB 130603B. The late-time H-band flux observed with HST 9.41 days after burst is that expected from an ordinary synchrotron radiation from a jet that produced the measured late-time X-ray afterglow.

Late-time flare/rebrightening of a NIR-optical afterglow of an SHB can be produced also by jet collision with an interstellar density bump, as seen in several GRBs. The host galaxy of SHB 130603B as seen in high-resolution HST imaging [14, 15] is a perturbed spiral galaxy due to interaction with another galaxy. The GRB was located in a tidally disrupted arm of its host galaxy [27]. The interaction of the GRB jet with such a bumpy environment could produce the flare/rebrightening of the NIR afterglow of the GRB observed with the HST 9.41 days after burst.

The star formation within the host, location of SHB 130603B on top of the tidally disrupted arm, strong absorption features, and large line of sight extinction that were observed indicate that the GRB progenitor was probably not far from its birth place [27], untypical to the usually very long lifetime before neutron star merger due to gravitational wave emission in the known neutron star binaries in our galaxy. Moreover, the failure to detect a host galaxy down to 28.5 mag in deep Hubble Space Telescope imaging searches in the case of, for example, SHB 080503 with a late-time flare/rebrightening [26] suggests a large natal kick velocity of its progenitor, unlikely for compact binaries, but often observed for isolated neutron stars/pulsars [9, 32].

Although radio data and spectroscopy of the late-time afterglow of short hard bursts can provide complementary information on the origin of SHBs [33], the true smoking gun for the neutron star merger in close binaries is the detection of gravitational waves. Unfortunately, this is unlikely to occur before the completion of the new generation of gravity-wave detectors, as the sensitivity of current detectors such as LIGO and Virgo is several orders of magnitude below what would be required to detect a merger at a distance similar to the nearest SHBs with known redshift.

Conflict of Interests

The authors declare that there is no conflict of interests regarding the publication of this paper.

Acknowledgment

The authors thank A. de Ugarte Postigo for useful comments.

References

[1] J. Goodman, A. Dar, and S. Nussinov, "Neutrino annihilation in type II supernovae," *The Astrophysical Journal*, vol. 314, pp. L7–L10, 1987.

[2] C. A. Meegan, G. J. Fishman, R. B. Wilson et al., "Spatial distribution of γ-ray bursts observed by BATSE," *Nature*, vol. 355, no. 6356, pp. 143–145, 1992.

[3] N. J. Shaviv and A. Dar, "Gamma-ray bursts from minijets," *Astrophysical Journal Letters*, vol. 447, no. 2, pp. 863–873, 1995.

[4] A. Dar, "Can fireball models explain gamma-ray bursts?" *Astrophysical Journal Letters*, vol. 500, no. 2, pp. L93–L96, 1998.

[5] E. Nakar, "Short-hard gamma-ray bursts," *Physics Reports*, vol. 442, no. 1–6, pp. 166–236, 2007.

[6] E. Berger, "Short-duration gamma-ray bursts," *Annual Review of Astronomy and Astrophysics*, vol. 51, pp. 43–105, 2014.

[7] D. A. Perley, B. D. Metzger, and J. Granot, "GRB 080503: implications of a naked short gamma-ray burst dominated by extended emission," *The Astrophysical Journal*, vol. 696, pp. 1871–1885, 2009.

[8] S. Dado, A. Dar, and A. de Rújula, "Short hard gamma-ray bursts and their afterglows," *The Astrophysical Journal*, vol. 693, pp. 311–328, 2009.

[9] D. R. Lorimer, "Binary and millisecond pulsars," *Living Reviews in Relativity*, vol. 11, article 8, 2008.

[10] L. X. Li and B. Paczynski, "Transient events from neutron star mergers," *The Astrophysical Journal*, vol. 507, no. 1, pp. L59–L62, 1998.

[11] A. Melandri, W. H. Baumgartner, and D. N. Burrows, "GRB 130603B: swift detection of a bright short burst," *GCN Circulars Archive*, # 14735, 2013.

[12] S. Golenetskii, R. Aptekar, and D. Frederiks, "Konus-wind observation of GRB 130603B," GCN Circulars Archive no. 14771, 2013.

[13] N. R. Tanvir, "GRB 130603B: HST limits on an underlying supernova," *Gamma-Ray Coordination Network (GCN), Circular Archive*, 14893, 2013, http://gcn.gsfc.nasa.gov/gcn/.

[14] N. R. Tanvir, A. J. Levan, A. S. Fruchter et al., "A "kilonova" associated with the short-duration γ-ray burst GRB 130603B," *Nature*, vol. 500, no. 7464, pp. 547–549, 2013.

[15] E. Berger, W. Fong, and R. Chornock, "An r-process kilonova associated with the short-hard GRB 130603B," *The Astrophysical Journal Letters*, vol. 774, no. 2, pp. L23–L26, 2013.

[16] W. Fong, E. Berger, and B. D. Metzger, "Short GRB 130603B: discovery of a jet break in the optical and radio afterglows, and a mysterious late-time X-ray excess," *The Astrophysical Journal*, vol. 780, pp. 118–126, 2014.

[17] P. A. Evans, A. P. Beardmore, K. L. Page et al., "Methods and results of an automatic analysis of a complete sample of Swift-XRT observations of GRBs," *Monthly Notices of the Royal Astronomical Society*, vol. 397, no. 3, pp. 1177–1201, 2009.

[18] S. Dado, A. Dar, and A. de Rújula, "On the optical and X-ray afterglows of gamma ray bursts," *Astronomy and Astrophysics*, vol. 388, no. 3, pp. 1079–1105, 2002.

[19] S. Dado, A. Dar, and A. de Rújula, "The diverse broadband light curves of swift gamma-ray bursts reproduced with the Cannonball model," *The Astrophysical Journal*, vol. 696, no. 1, pp. 994–1020, 2009.

[20] S. Dado and A. Dar, "Conical fireballs, cannonballs, and jet breaks in the afterglows of gamma ray bursts," *Astronomy and Astrophysics*, vol. 558, pp. A115–A121, 2013.

[21] J. A. Nousek, C. Kouveliotou, and D. Grupe, "Evidence for a canonical gamma-ray burst afterglow light curve in the *Swift* XRT Data," *The Astrophysical Journal*, vol. 642, no. 1, pp. 389–400, 2006.

[22] Y. M. Lipkin, E. O. Ofek, A. Gal-Yam et al., "The detailed optical light curve of GRB 030329," *The Astrophysical Journal*, vol. 606, no. 1, pp. 381–394, 2004.

[23] T. Matheson, P. M. Garnavich, and K. Z. Stanek, "Photometry and spectroscopy of GRB 030329 and its sssociated supernova 2003dh: the first two months," *The Astrophysical Journal*, vol. 599, pp. 394–407, 2003.

[24] C. Guidorzi, S. D. Vergani, S. Sazonov et al., "GRB 070311: a direct link between the prompt emission and the afterglow," *Astronomy and Astrophysics*, vol. 474, pp. 793–805, 2007.

[25] D. Malesani, S. Covino, P. D'Avanzo et al., "Multicolor observations of the afterglow of the short/hard GRB 050724," *Astronomy and Astrophysics*, vol. 473, pp. 77–84, 2007.

[26] C. C. Thone, A. de Ugarte Postigo, J. Gorosabel, N. Tanvir, and J. P. U. Fynbo, "GRB 130603B: short GRB afterglow spectrum from GTC," *GCN Circulars Archive*, # 14771, 2013.

[27] A. de Ugarte Postigo, C. C. Thöne, and A. Rowlinson, "Spectroscopy of the short-hard GRB 130603B: the host galaxy and environment of a compact object merger," *Astronomy & Astrophysics*, vol. 563, pp. 62–68, 2013.

[28] A. Dar, B. Kozlovsky, S. Nussinov, and R. Ramaty, "Gamma-ray bursts and cosmic rays from accretion-induced collapse," *The Astrophysical Journal*, vol. 388, pp. 164–170, 1992.

[29] R. Surman, G. C. McLaughlin, M. Ruffert, H.-T. Janka, and W. R. Hix, "r-process nucleosynthesis in hot accretion disk flows from black hole-neutron star mergers," *The Astrophysical Journal Letters*, vol. 679, no. 2, pp. L117–L120, 2008.

[30] B. D. Metzger and A. L. Piro, "Optical and X-ray emission from stable millisecond magnetar formed from merger of binary neutron stars," *Monthly Notices of the Astronomical Royal Society*, vol. 439, pp. 3916–3930, 2014.

[31] Y. Fan, Y.-W. Yu, and D. Xu, "A supramassive magnetar central engine for GRB 130603B," *The Astrophysical Journal*, vol. 779, no. 2, pp. L25–L28, 2013.

[32] G. Hobbs, D. R. Lorimer, A. G. Lyne, and M. Kramer, "A statistical study of 233 pulsar proper motions," *Monthly Notices of the Royal Astronomical Society*, vol. 360, pp. 974–992, 2005.

[33] Z.-P. Jin, D. Xu, and Y.-Z. Fan, "Is the late near-infrared bump in short-hard GRB 130603B due to the Li-Paczynski kilonova?" *The Astrophysical Journal*, vol. 775, pp. L19–L22, 2013.

Hindawi Publishing Corporation
Advances in Astronomy
Volume 2015, Article ID 341018, 12 pages
http://dx.doi.org/10.1155/2015/341018

Research Article

Systematic Spectral Lag Analysis of Swift Known-z GRBs

Yuta Kawakubo,[1] Takanori Sakamoto,[1] Atsumasa Yoshida,[1] and Demos Kazanas[2]

[1]*Department of Physics and Mathematics, Aoyama Gakuin University, 5-10-1 Fuchinobe, Sagamihara, Kanagawa 252-5258, Japan*
[2]*Astrophysics Science Division, NASA/Goddard Space Flight Center, Greenbelt, MD 20771, USA*

Correspondence should be addressed to Yuta Kawakubo; ykawakubo@phys.aoyama.ac.jp

Received 25 December 2014; Revised 12 March 2015; Accepted 3 April 2015

Academic Editor: Wing-Huen Ip

The difference of photon arrival time, which is known as spectral lag, is well known characteristics of gamma-ray bursts (GRBs). In particular, long duration GRBs show a soft lag which means that high energy photons arrive earlier than soft photons. The lag-luminosity relation is the empirical relationship between the isotropic peak luminosity and the spectral lag. We calculated the spectral lags for 40 known redshift GRBs observed by *Swift* addition to the previous 31 GRB samples. We confirmed that most of our samples follow the lag-luminosity relation. However, we noticed that there are some GRBs which show a significant scatter from the relation. We also confirm that the relationship between the break time and the luminosity of the X-ray afterglow (so-called Dainotti relation) extends up to the lag-luminosity relation.

1. Introduction

The time variability and the spectral evolution seen in the prompt emission of gamma-ray bursts (GRBs) are not well understood despite the large data samples collected by various GRB instruments. However, there are some clues to understand temporal and spectral variations seen in the prompt emission. The spectral lag which is known as the difference of an arrival time between high energy photons and low energy photons is one of such clues. It is known that high energy photons arrive earlier than low energy photons for long duration GRBs (hereafter long GRBs) [1, 2], while short duration GRBs (hereafter short GRBs), which have a duration shorter than 2 seconds, have a smaller or a negligible lag than that of long GRBs [3, 4].

There is an empirical relation between a spectral lag and an isotropic peak luminosity which is called lag-luminosity relation [5]. The relation is discovered based on the analysis of only 6 known-z GRBs using the BATSE samples. Recently, Ukwatta et al. [6] calculated the spectral lag for 31 *Swift* known-z GRBs. They found that the *Swift* GRBs follow the lag-luminosity relation with a significant scatter in their samples from the best fit relation.

Many theoretical models suggested explaining the lag-luminosity relation. Salmonson [7] suggests that this relation is caused by the variation in line-of-sight velocity of GRBs. Ioka and Nakamura [8] proposed that an observer's viewing angle to the jet causes this relation, while Schaefer [9] suggested that a lag and a peak luminosity are related to a cooling time of a pulse. Although there are many theoretical models that have been proposed to explain the lag-luminosity relation, physical origin of this relation is still unclear.

On the other hand, Dainotti et al. [10] discovered the empirical relation between an X-ray break time and an X-ray luminosity from the *Swift* X-ray afterglow samples (hereafter Dainotti relation). The break time from a shallow to a normal decay in the X-ray afterglow light curve (e.g., [11]) is anticorrelated with the luminosity at the break time. The theoretical interpretations of this relation include long-term behavior of an external accretion disk [12] and a prior emission model for X-ray plateau phase [13]. Furthermore, Sultana et al. [14] suggested that the lag-luminosity relation at the prompt emission nicely connects to the Dainotti relation found from the X-ray afterglow data. Also, they proposed that both relations might be explained individually by the same kinematic effect, which is viewing the jet at "off-beam" line of sight [8, 15]. If viewing angle is large, an isotropic luminosity and a spectral lag are large in a prompt emission following Ioka and Nakamura [8]. Also, Eichler and Granot [15] proposed that the viewing angle which is slightly larger

than an opening angle makes a long plateau and a low flux emission in an afterglow. Therefore, if this finding is true, we are probably seeing a clear physical connection between the prompt and the afterglow emission. However, since those findings are still based on a small number of GRBs, it is important to investigate using rich GRB samples.

The number of *Swift* known-z GRBs is increasing and becoming large samples. We analyzed additional 40 *Swift* known-z GRBs following the method described in Ukwatta et al. 2010 [6]. Our paper is organized as follows. The analysis method is described in Section 2. The results of analysis and application to the lag-luminosity relation are shown in Section 3. We discussed our results in Section 4. We concluded and summarized our results in Section 5.

2. Method

We calculated a spectral lag following the method described by Ukwatta et al., 2010 [6], using the data of *Swift* Burst Alert Telescope (BAT [16]). First, we made the mask-weighted (background subtracted) light curves using the BAT event data for four energy bands (15–25 keV, 25–50 keV, 50–100 keV, and 100–200 keV). We made 1000 simulated light curves for each energy band. Those simulated light curve bins are calculated by

$$\mathrm{LC}_{\mathrm{sim}}^{\mathrm{bin}} = \mathrm{LC}_{\mathrm{real}}^{\mathrm{bin}} + \xi \mathrm{LC}_{\mathrm{error}}^{\mathrm{bin}}, \tag{1}$$

where ξ is a random number from the standard normal distribution. We calculated cross correlation function (CCF) for all 6 combinations of energy bands and determined spectral lags. We used the Band's CCF formula (Band 1997 [17]) which is expressed as

$$\mathrm{CCF}_{\mathrm{Band}}(d, x, y) = \frac{\sum_{i=\max(1,1-d)}^{\min(N,N-d)} x_i y_{i+d}}{\sqrt{\sum_i x_i^2 \sum_i y_i^2}} \tag{2}$$

for two series x_i and y_i with a delay d, where $i = 0, 1, 2, \ldots, N-1$. We fitted CCF with the Gaussian function to determine the CCF peak for each 1000 CCFs generated from simulated light curves. Then, we made the histogram of the CCF peaks and determined the center value as the best fit value of a lag and its standard deviation as an error of a lag.

To cross-check the validity of our code, we analyzed 5 GRBs whose lags have been reported in Ukwatta et al. 2010 [6]. The results of this cross-check are shown in Figure 1. The figure clearly shows that our lag values are consistent with those of Ukwatta et al. 2010 [6], including the size of the errors.

We selected 229 long GRB samples from *Swift* known-z GRBs between March 2005 and May 2013 at the beginning. Three selections were applied for the initial samples. As the first selection, we selected 198 GRBs of which spectral lags have not been calculated in Ukwatta et al., 2010 [6]. In the second selection, the 92 GRBs are selected based on the peak flux threshold (≥1.5 peak photon flux in the 15–150 keV band). In the third selection, the GRBs which are possible to estimate the peak energy (E_{peak}) using the relationship between E_{peak} and the photon index of the simple power-law fit to the BAT spectral data [18] are selected from the samples. Finally, our samples became 40 GRBs. There are 14 GRBs between 2005 and 2009 which are selected in our samples but not in Ukwatta et al. The difference between our samples and Ukwatta's sample is that our samples include darker GRBs than Ukwatta's samples. Those weak samples are needed in order to confirm the lag-luminosity relation for GRBs which have the low luminosities. The average peak flux of Ukwatta's samples is ~13 counts/sec/cm^2 in 15–150 keV, whereas the averaged peak flux of our 14 GRBs is ~5 counts/sec/cm^2.

We used T_{100} time interval as the time range of the analysis. We examined the time bin of the light curve from 1 ms to 1024 ms and reported the lag as the reliable lag values if the average $\mathrm{CCF}_{\mathrm{max}}$ is greater than ~0.5. This value corresponds to a reasonable signal to noise level in a light curve in this analysis. The validity of the correspondence between a $\mathrm{CCF}_{\mathrm{max}}$ and a signal to noise level is studied in Ukwatta et al. 2010 [6].

Most of the GRB spectra can be fitted by the Band function [19] which has four parameters (normalization, E_{peak}, and power-law photon indices α and β):

$$N(E) = \begin{cases} A\left(\dfrac{E}{100\,\mathrm{keV}}\right)^{\alpha} e^{-(2+\alpha)E/E_{\mathrm{peak}}} & E \le \left(\dfrac{\alpha-\beta}{2+\alpha}\right) E_{\mathrm{peak}} \\ A\left(\dfrac{E}{100\,\mathrm{keV}}\right)^{\beta} \left[\dfrac{(\alpha-\beta)\,E_{\mathrm{peak}}}{(2+\alpha)\,100\,\mathrm{keV}}\right]^{\alpha-\beta} e^{\beta-\alpha} & (\text{otherwise}). \end{cases} \tag{3}$$

We calculated the following equation to determine a normalization A:

$$A = \frac{f_{\mathrm{obs}}}{\int_{15\,\mathrm{keV}}^{150\,\mathrm{keV}} N'(E)\,dE}, \tag{4}$$

where f_{obs} is 1 sec peak photon flux in the 15–150 keV band and N' is $N(E)$ when $A = 1$. The flux in the source flame energy band 1–10000 keV is calculated by

$$f_{\mathrm{obs}}^{\mathrm{new}} = \int_{1.0\,\mathrm{keV}/(1+z)}^{10000\,\mathrm{keV}/(1+z)} N(E)\,E\,dE. \tag{5}$$

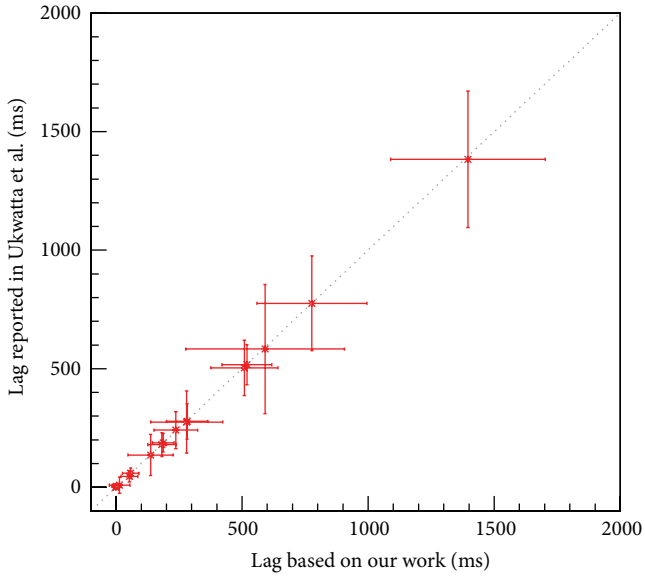

FIGURE 1: The relationship between the lag reported in Ukwatta et al., 2010, and the lag based on our work for common GRBs. The dotted line shows $y = x$.

The isotoropic peak luminosity $L_{\rm iso}$ is

$$L_{\rm iso} = 4\pi d_L^2 f_{\rm obs}^{\rm new}, \tag{6}$$

where d_L is the luminosity distance:

$$d_L = \frac{(1+z)\,c}{H_0} \int_0^z \frac{dz'}{\sqrt{\Omega_M (1+z')^3 + \Omega_L}}, \tag{7}$$

where H_0 is Hubble constant. We assumed that $H_0 = 70\,\mathrm{km\,s^{-1}\,Mpc^{-1}} = 2.268 \times 10^{-18}\,\mathrm{s^{-1}}$, $\Omega_M = 0.27$, $\Omega_L = 0.73$. The error of $L_{\rm iso}$ was estimated by performing the $L_{\rm iso}$ calculations for 1000 times taking into account the uncertainties in spectral parameters. We used reported Band function parameters $E_{\rm peak}$, α, β, flux, and their errors from the BAT analysis (e.g., [20], GCN circulars) as the input parameters. However, if $E_{\rm peak}$, α, and β are not constrained, we estimated $E_{\rm peak}$ from a photon index based on a single power-law fit [18]. In this case, α and β are used from the distributions by BATSE where $\alpha = -0.87 \pm 0.33$ and $\beta = -2.36 \pm 0.31$ [21].

3. Results

We calculated spectral lags for 40 known-z GRBs. Table 1 shows the results of spectral lag analysis and calculation of $L_{\rm iso}$. The columns "LC st" and "LC et" are the start time and the end time of the light curve. The "CCF fit range min" and "CCF fit range max" are the fitting range of the CCF to the Gaussian function. The channel numbers from 1 to 4 correspond to the following energy bands: 15–25 keV, 25–50 keV, 50–100 keV, and 100–200 keV, respectively. We called two pieces of light curve data which are cross-correlated to calculate a lag in the channel numbers. For example, "Lag_{31}" means the lag value obtained by cross-correlating the light curves between the 50–100 keV and the 15–20 keV band. We calculated spectral lags for all 6 combinations. However, if an average of 1000 $\mathrm{CCF}_{\rm max}$ is not larger than ~0.5 in the 1 ms to 1024 ms time binning, we did not report the lags. A few GRBs show the lags which have large errors or negative lags. Since the light curves of those GRBs generally have low statistics, we believe the lags were not measured with a good accuracy.

Figures 2 and 3 shows the relationship between lags and luminosities of 71 known-z *Swift* GRBs based on the BAT data. Table 2 summarized linear correlation coefficients between the lag measured by different combinations of channels and the luminosity. We used a maximum likelihood method which was used to analyze a peak luminosity and variability correlation by Guidorzi et al. 2006 [22]. This method accounts for X and Y errors and samples variance [23]. The parameters are the normalization and index of the power-law and the variance of $L_{\rm iso}$ ($\sigma_{L_{\rm iso}}$). Table 3 shows the results of fittings. In the calculation and fittings, the results of GRB060614A were not used. This is because GRB060614A has smaller lag than that expected from the lag-luminosity relation [24]. The results show that an isotropic peak luminosity negatively correlates with a spectral lag for all combinations of the channels. The best fit power-law index of the lag between the 50–100 keV band and the 15–25 keV band and the luminosity is -0.46 ± 0.04 with logarithm variance $\sigma_{L_{\rm iso}}$ of 0.78. The linear correlation coefficient in this case is −0.40 with sample size of 62 (null probability of 0.2%). Therefore, we concluded that there is a correlation between the lag and the luminosity with the *Swift* GRB samples.

Figure 4 shows the lag-luminosity relation overlaid with the break time and the luminosity of the X-ray afterglow [14]. We used the results of Lag31 for the plot. This is because the lags between consecutive energy bands show low significant values. Also, the sample size of the lags between channel 4 and other channels is small due to a low signal to noise in the light curve of channel 4 in general.

We increased the samples which have both the lag and the luminosity values of the prompt emission, and the X-ray afterglow properties by combining our results and the latest report by Dianotti et al. 2013 [25]. As a result of power-law fitting, best fit parameters are

$$\log\left(L_{\rm iso}\right) = (-1.05 \pm 0.03) \times \log\left(\frac{\mathrm{Lag}_{31}}{(1+z)}\right) + (54.46 \pm 0.11) \tag{8}$$

with $\sigma_{L_{\rm iso}} = 0.82 \pm 0.18$. The correlation coefficient is −0.96 with a sample size of 32. We confirmed that the two relations are connected with a power-law index of −1 as suggested by Sultana et al. 2012 [14], with larger samples.

4. Discussion

Our large known-z samples confirmed that the isotropic luminosity negatively correlates with the spectral lag (Figures 2 and 3). The linear correlation coefficients are between −0.4 and −0.5. These results suggest that the most

Table 1: Summary of spectral lag analysis.

GRB name	Redshift	L_{iso} [erg/s]	LC st [s]	LC et [s]	Time bin [ms]	CCF fit range min [s]	CCF fit range max [s]	LagXX [ms]
050315	1.949	$8.07e+51 \pm 5.11e+51$	−56.108	125.288	256	−10	10	877 ± 528 (Lag21)
					512	−10	10	2458 ± 722 (Lag31)
					512	−10	10	1168 ± 484 (Lag32)
050318	1.44	$4.76e+51 \pm 0.37e+51$	−56.108	125.288	64	−1	1	−2 ± 39 (Lag21)
					64	−1	1	40 ± 50 (Lag31)
					64	−1	1	56 ± 38 (Lag32)
050319	3.14	$2.16e+52 \pm 6.16e+51$	−134.040	28.952	1024	−3	3	22 ± 409 (Lag21)
050505	4.27	$8.50e+52 \pm 2.06e+52$	−10.064	52.492	1024	−20	20	−492 ± 1217 (Lag21)
					1024	−20	20	−371 ± 984 (Lag31)
					1024	−20	20	−298 ± 640 (Lag32)
050802	1.71	$1.11e+52 \pm 4.25e+51$	−2.92	34.08	512	−7	10	545 ± 636 (Lag21)
					512	−7	7	1311 ± 602 (Lag31)
					512	−5	5	575 ± 359 (Lag32)
					1024	−10	10	1467 ± 893 (Lag41)
					1024	−10	10	1261 ± 812 (Lag42)
					1024	−5	5	−93 ± 517 (Lag43)
060502A	1.51	$5.33e+51 \pm 1.80e+51$	−5.644	38.984	128	−20	20	1769 ± 522 (Lag21)
					128	−15	15	3252 ± 549 (Lag31)
					128	−10	20	1371 ± 362 (Lag32)
					512	−10	20	5914 ± 733 (Lag41)
					512	−10	15	3793 ± 574 (Lag42)
					512	−10	15	2577 ± 542 (Lag43)
060614	0.13	$7.87e+49 \pm 5.86e+49$	−1.496	176.472	16	−0.3	0.3	23 ± 15 (Lag21)
					32	−0.5	0.5	78 ± 22 (Lag31)
					32	−0.5	0.5	58 ± 18 (Lag32)
060814	0.84	$4.93e+51 \pm 1.76e+51$	−11.688	218.608	128	−4	4	272 ± 101 (Lag21)
					128	−4	4	495 ± 101 (Lag31)
					128	−4	4	226 ± 79 (Lag32)
					32	−5	5	980 ± 196 (Lag41)
					32	−5	5	674 ± 167 (Lag42)
					32	−4	4	320 ± 152 (Lag43)
060906	3.685	$4.25e+52 \pm 1.30e+52$	−41.796	47.666	512	−30	30	1497 ± 928 (Lag21)
					1024	−30	30	3042 ± 1165 (Lag31)
					1024	−30	30	1111 ± 1091 (Lag32)
060912A	0.94	$6.41e+51 \pm 3.03e+51$	−0.564	6.116	16	−1	1	134 ± 40 (Lag21)
					16	−1	1.5	294 ± 46 (Lag31)
					16	−1	1	130 ± 39 (Lag32)
070508	0.82	$1.86e+52 \pm 1.45e+52$	−13.756	33.112	4	−0.3	0.3	36 ± 8 (Lag21)
					4	−0.3	0.3	58 ± 8 (Lag31)
					2	−0.2	0.2	20 ± 4 (Lag32)
					8	−0.3	0.3	83 ± 14 (Lag41)
					8	−0.2	0.2	39 ± 8 (Lag42)
					8	−0.2	0.2	16 ± 5 (Lag43)

Table 1: Continued.

GRB name	Redshift	L_{iso} [erg/s]	LC st [s]	LC et [s]	Time bin [ms]	CCF fit range min [s]	CCF fit range max [s]	LagXX [ms]
070810A	2.17	$1.03e+52 \pm 3.43e+51$	−3.072	14.264	128	−10	10	509 ± 276 (Lag21)
					256	−10	10	969 ± 404 (Lag31)
					256	−10	10	564 ± 337 (Lag32)
080810	3.35	$5.28e+52 \pm 1.09e+52$	−21.192	111.436	256	−3	3	−49 ± 133 (Lag21)
					256	−3	3	−175 ± 145 (Lag31)
					128	−2	2	−107 ± 99 (Lag32)
					1024	−4	4	97 ± 476 (Lag41)
					512	−2	2	78 ± 266 (Lag42)
					512	−3	3	132 ± 343 (Lag43)
090423	8.0	$2.79e+53 \pm 3.76e+52$	−0.668	11.74	64	−2	2	79 ± 137 (Lag21)
					128	−2	2	132 ± 150 (Lag31)
					128	−3	3	123 ± 227 (Lag32)
090926B	1.24	$5.81e+51 \pm 1.84e+51$	−21.612	130.34	256	−0.7	0.7	47 ± 48 (Lag21)
					256	−0.7	0.7	96 ± 93 (Lag31)
					128	−0.7	0.7	45 ± 22 (Lag32)
091020	1.71	$1.71e+52 \pm 6.21e+51$	−8.476	48.264	64	−10	10	53 ± 266 (Lag21)
					128	−5	5	48 ± 250 (Lag31)
					64	−5	5	−14 ± 163 (Lag32)
					256	−5	5	−413 ± 416 (Lag41)
					256	−5	5	−356 ± 320 (Lag42)
					256	−5	5	−340 ± 323 (Lag43)
091127	0.49034	$5.82e+51 \pm 3.01e+51$	−0.372	7.196	16	−0.3	0.3	17 ± 20 (Lag21)
					16	−0.3	0.3	28 ± 24 (Lag31)
					16	−0.3	0.3	4 ± 22 (Lag32)
					128	−0.3	0.3	26 ± 59 (Lag41)
					64	−0.3	0.3	3 ± 47 (Lag42)
					64	−0.3	0.3	10 ± 57 (Lag43)
100615A	1.398	$1.05e+52 \pm 4.23e+51$	−0.044	47.408	16	−1.5	1.5	202 ± 43 (Lag21)
					32	−1	1.5	408 ± 44 (Lag31)
					16	−1.5	1.5	210 ± 38 (Lag32)
					256	−2	2	620 ± 143 (Lag41)
					256	−2	2	376 ± 132 (Lag42)
					128	−1	1.5	185 ± 101 (Lag43)
100621A	0.542	$2.26e+51 \pm 1.22e+51$	−6.1	204.192	8	−12	3	682 ± 63 (Lag21)
					16	−1	3	1432 ± 85 (Lag31)
					8	−2	3	776 ± 59 (Lag32)

Table 1: Continued.

GRB name	Redshift	L_{iso} [erg/s]	LC st [s]	LC et [s]	Time bin [ms]	CCF fit range min [s]	CCF fit range max [s]	LagXX [ms]
100704A	3.6	$9.03e+52 \pm 1.98e+52$	−62.226	202.304	256	−5	5	599 ± 181 (Lag21)
					256	−3	4	1154 ± 183 (Lag31)
					256	−3	4	735 ± 129 (Lag32)
					1024	−3	5	1576 ± 316 (Lag41)
					512	−3	5	1120 ± 196 (Lag42)
					512	−3	3	425 ± 205 (Lag43)
100728B	2.106	$2.35e+52 \pm 6.89e+51$	−1.744	13.2	256	−2	2	73 ± 294 (Lag21)
					256	−4	3	514 ± 319 (Lag31)
					256	−3	3	183 ± 218 (Lag32)
100814A	1.44	$7.16e+51 \pm 2.53e+51$	−3.204	234.644	128	−3	3	338 ± 189 (Lag21)
					256	−3	4	914 ± 218 (Lag31)
					64	−3	4	920 ± 137 (Lag32)
100906A	1.727	$3.28e+52 \pm 1.42e+52$	−0.192	130.456	16	−1	1	213 ± 64 (Lag21)
					16	−1	1.5	397 ± 71 (Lag31)
					16	−1	1	89 ± 59 (Lag32)
					128	−1.5	3	834 ± 126 (Lag41)
					64	−2.5	2.5	432 ± 98 (Lag42)
					64	−2	2	302 ± 101 (Lag43)
110205A	2.22	$2.27e+52 \pm 6.73e+51$	−129.78	377.232	256	−5	5	−21 ± 194 (Lag21)
					256	−5	5	−18 ± 201 (Lag31)
					256	−2	2	83 ± 126 (Lag32)
110422A	1.77	$1.38e+53 \pm 4.45e+52$	−11.156	40.572	8	−1	1	97 ± 62 (Lag21)
					8	−1	1	166 ± 62 (Lag31)
					4	−0.5	0.5	38 ± 26 (Lag32)
110503A	1.613	$1.25e+53 \pm 3.70e+52$	−6.584	16.296	32	−2	2	272 ± 85 (Lag21)
					32	−1	1.5	456 ± 87 (Lag31)
					16	−1	1.5	293 ± 55 (Lag32)
					128	−1	2	575 ± 131 (Lag41)
					64	−2	3	464 ± 105 (Lag42)
					64	−2	2	99 ± 93 (Lag43)
110715A	0.82	$3.21e+52 \pm 1.26e+52$	−3.144	20.856	2	−1	1	70 ± 16 (Lag21)
					2	−1	1.2	107 ± 17 (Lag31)
					1	−0.5	0.5	41 ± 13 (Lag32)
					8	−0.5	0.7	132 ± 30 (Lag41)
					4	−0.5	0.7	105 ± 19 (Lag42)
					4	−0.5	0.5	52 ± 15 (Lag43)
111008A	4.9898	$3.04e+53 \pm 5.17e+52$	−2.636	72.464	128	−1	1	12 ± 100 (Lag21)
					256	−2	2	113 ± 213 (Lag31)
					128	−1	1	93 ± 114 (Lag32)

Table 1: Continued.

GRB name	Redshift	L_{iso} [erg/s]	LC st [s]	LC et [s]	Time bin [ms]	CCF fit range min [s]	CCF fit range max [s]	LagXX [ms]
111228A	0.71627	$4.21e+51 \pm 2.15e+51$			32	−0.5	0.5	24 ± 22 (Lag21)
					64	−0.5	0.7	60 ± 30 (Lag31)
					64	−0.5	0.5	21 ± 21 (Lag32)
120119A	1.728	$4.95e+52 \pm 1.33e+52$	−13.216	361.888	32	−3	3	476 ± 101 (Lag21)
					32	−3	3	957 ± 123 (Lag31)
					32	−1	1	58 ± 44 (Lag32)
					256	−3	5	1647 ± 209 (Lag41)
					128	−3	3	620 ± 125 (Lag42)
					128	−3	3	240 ± 116 (Lag43)
120326A	1.798	$1.53e+52 \pm 6.46e+51$	−67.9	22.564	32	−3	3	386 ± 81 (Lag21)
					64	−2	4	766 ± 108 (Lag31)
					64	−3	4	367 ± 94 (Lag32)
120327A	2.813	$5.59e+52 \pm 1.35e+52$	−15.788	74.576	128	−1	1.5	144 ± 116 (Lag21)
					128	−2	2.5	247 ± 126 (Lag31)
					64	−1.5	1.5	119 ± 80 (Lag32)
					512	−1.5	2.5	565 ± 238 (Lag41)
					256	−3	4	432 ± 168 (Lag42)
					256	−2	2	244 ± 177 (Lag43)
120712A	4.1745	$1.03e+53 \pm 1.83e+52$	−4.572	16.528	128	−5	5	558 ± 327 (Lag21)
					128	−5	7	809 ± 325 (Lag31)
					64	−1	1	−88 ± 99 (Lag32)
					512	−10	10	1137 ± 757 (Lag41)
					512	−7	7	534 ± 602 (Lag42)
					512	−7	7	352 ± 573 (Lag43)
120802A	3.796	$7.32e+52 \pm 1.73e+52$	−35.680	28.016	128	−3	3	5 ± 156 (Lag21)
					256	−2	3	685 ± 203 (Lag31)
					256	−2	3	504 ± 131 (Lag32)
					1024	−3	4	1231 ± 598 (Lag41)
					1024	−3	4	915 ± 463 (Lag42)
120907A	0.970	$2.58e+51 \pm 1.06e+51$	−0.024	8.136	128	−2	2	129 ± 142 (Lag21)
					256	−1.5	2	196 ± 120 (Lag31)
					256	−1	1	173 ± 124 (Lag32)
121128A	2.20	$7.83e+52 \pm 2.51e+52$	−0.04	41.688	8	−0.5	0.5	18 ± 16 (Lag21)
					16	−0.5	0.5	38 ± 21 (Lag31)
					8	−0.4	0.4	23 ± 10 (Lag32)
					256	−1	1	102 ± 104 (Lag41)
					128	−1	1	96 ± 71 (Lag42)
					128	−0.5	0.5	46 ± 34 (Lag43)

Table 1: Continued.

GRB name	Redshift	L_{iso} [erg/s]	LC st [s]	LC et [s]	Time bin [ms]	CCF fit range min [s]	CCF fit range max [s]	LagXX [ms]
					1024	−20	20	458 ± 1663 (Lag21)
130215A	0.597	$7.22e+50 \pm 3.27e+50$	−5.832	73.384	1024	−20	20	−1235 ± 2013 (Lag31)
					1024	−20	20	−1527 ± 1448 (Lag32)
					64	−10	10	334 ± 274 (Lag21)
130420A	1.297	$5.14e+51 \pm 2.15e+51$	−14.988	188.128	128	−10	10	890 ± 347 (Lag31)
					128	−10	10	515 ± 277 (Lag32)
					256	−3	3	−10 ± 269 (Lag21)
130427B	2.78	$4.13e+52 \pm 1.06e+52$	−0.616	36.808	512	−3	1.5	−279 ± 252 (Lag31)
					256	−3	3	89 ± 204 (Lag32)
					128	−10	10	1522 ± 462 (Lag21)
130514A	3.6	$6.06e+52 \pm 1.23e+52$	−7.088	257.932	256	−10	15	3214 ± 531 (Lag31)
					256	−10	10	1123 ± 400 (Lag32)

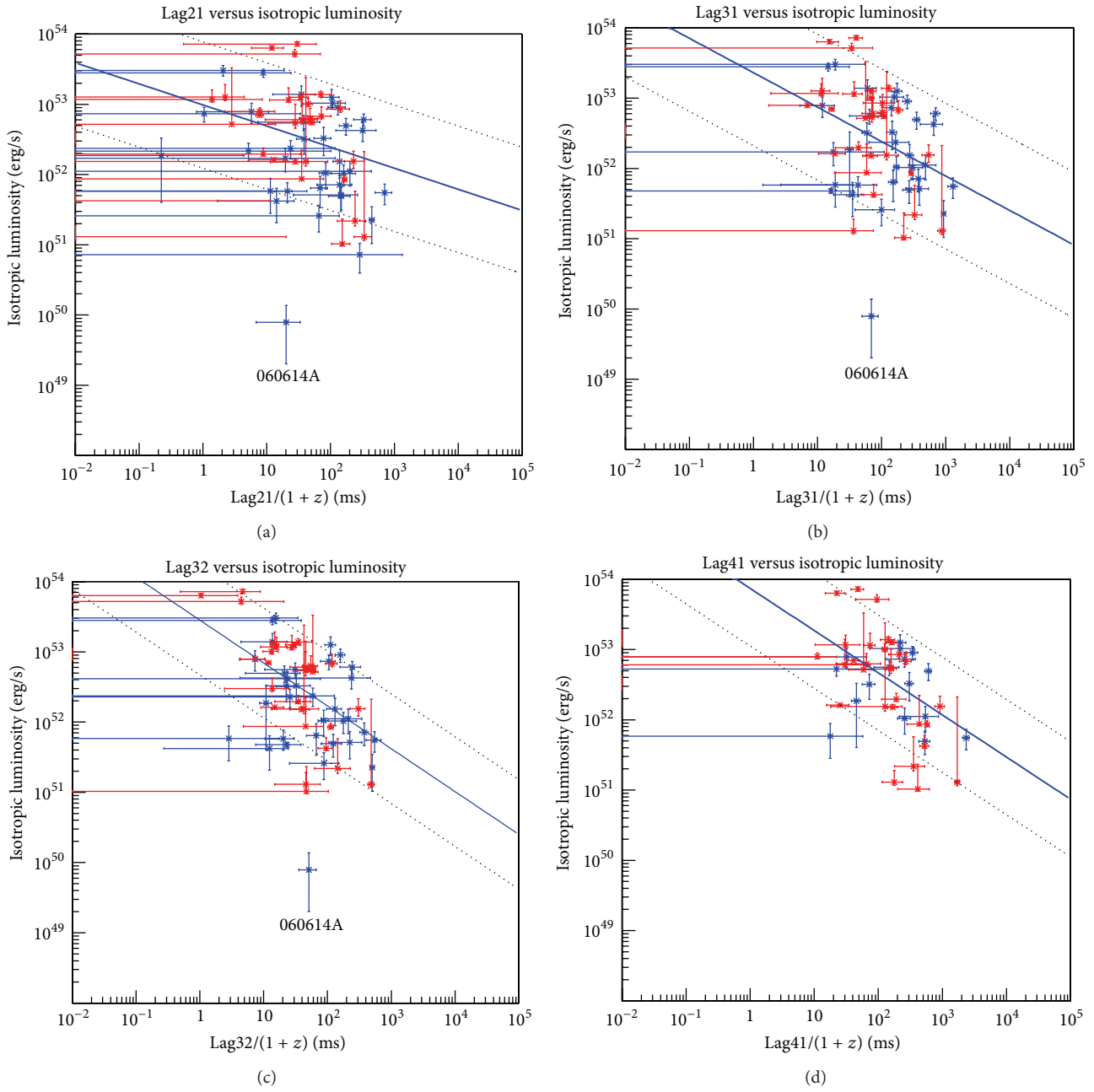

FIGURE 2: The lag versus isotropic peak luminosity. The blue points are our results. The red points are the results which are reported in Ukwatta et al. 2010. The blue lines are best fit values of power-law fitting. The black dotted lines show the region corresponding to variance $\sigma_{L_{\text{iso}}}$. (a) Between 25–50 keV and 15–25 keV, (b) between 50–100 keV and 15–25 keV, (c) between 50–100 keV and 25–50 keV, and (d) between 100–200 keV and 15–25 keV.

of the long GRBs are consistent with the lag-luminosity relation. However, the results of fitting show the samples variance $\sigma_{L_{\text{iso}}}$ between 0.7 and 0.9. This suggests that samples show a significant scatter from the best fit line.

Even if we considered scatter, GRB060614A is far away from the best fit line. Our result confirmed that GRB 060614 is a real outlier to the relation [24].

Combining the fact that the duration itself might not be sufficient enough to distinguish the different classes of GRBs [26], we think multiple aspects of the prompt and the afterglow properties are needed to investigate and classify GRBs appropriately.

We estimated the bulk Lorentz factor Γ from the averaged Lag31 value of ~0.6 seconds following the argument of Lu et al. [27]:

$$\text{lag} = \begin{cases} aE & \text{if } E \le E_s \\ aE_s & \text{if } E \ge E_s, \end{cases} \tag{9}$$

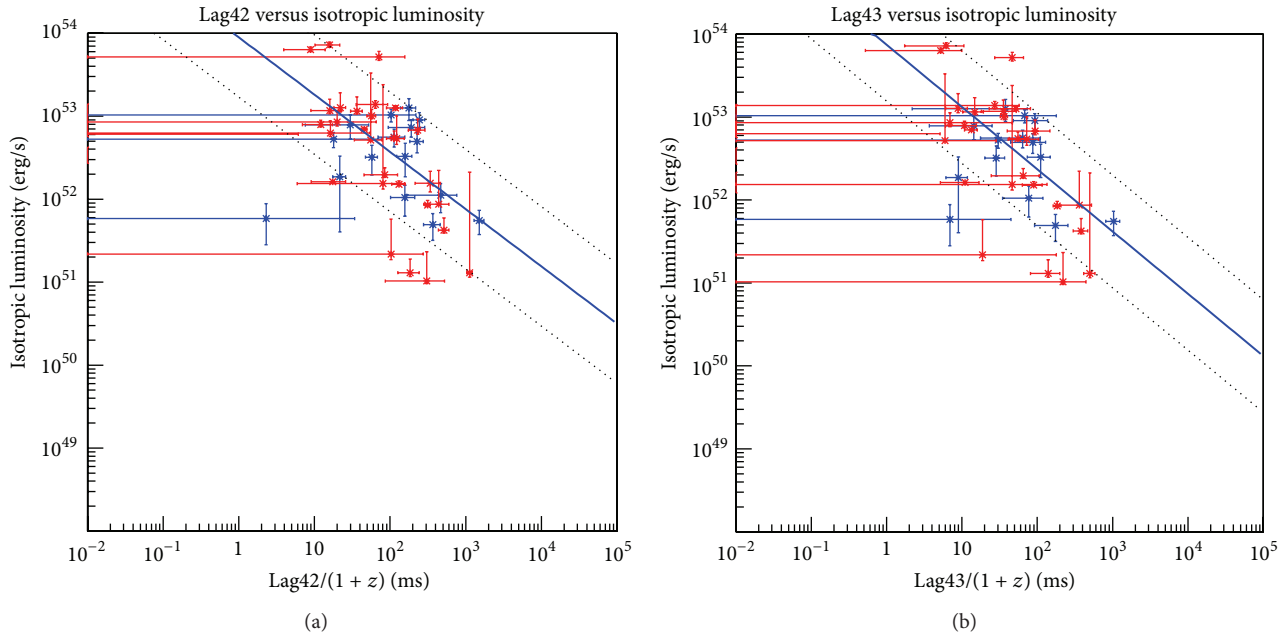

FIGURE 3: The lag versus isotropic peak luminosity. The blue points are our results. The red points are the results which are reported in Ukwatta et al. 2010. The blue lines are best fit values of power-law fitting. The black dotted lines show the region corresponding to variance $\sigma_{L_{\rm iso}}$. (a) Between 100–200 keV and 25–50 keV and (b) between 100–200 keV and 50–100 keV.

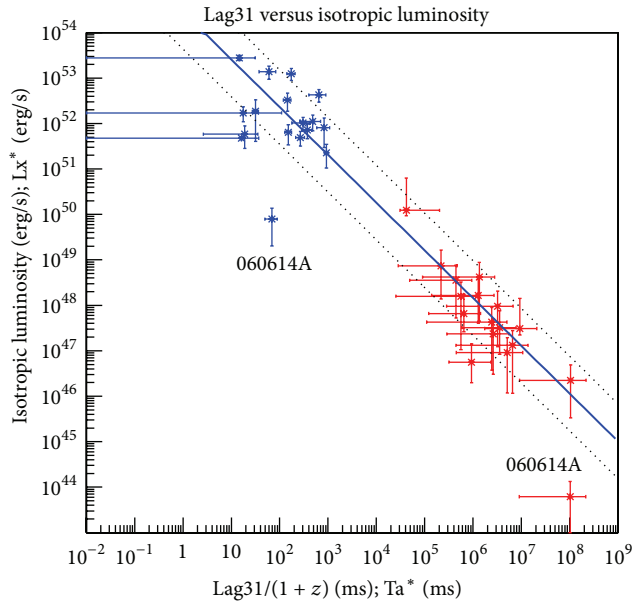

FIGURE 4: The lag between 50–100 keV and 15–25 keV versus isotropic peak luminosity with X-ray break time versus X-ray luminosity. The blue points are lag-luminosity results. The data reported in Dainotti et al. 2013 are shown in red. The blue lines are best fit values of power-law fitting. The black dotted lines show the region corresponding to variance $\sigma_{L_{\rm iso}}$. The correlation coefficient is −0.96 with sample size of 32.

where $E_s = 1.67E_{\rm peak}$ and a is shown by

$$a = 10^{-2.4}\left(\frac{\Gamma}{100}\right)^{-2.8}\ [\text{s/keV}]\,. \tag{10}$$

The bulk Lorentz factor is estimated to be 115 assuming a source frame peak energy $E_{\rm peak}$ of 240 keV (typical observed peak energy of 80 keV for the *Swift* GRBs), a source frame energy E of 75 keV, and redshift of 2.

Figure 4 suggests the clear extension of the lag-luminosity relation to the Dianotti relation. Although the connection of those two relations is still puzzling, this might imply an important clue to understand the physical relationship between the prompt and the X-ray afterglow emission.

Table 2: Correlation coefficient between lag and isotopic luminosity.

Channel XX	Correlation coefficient	Sample size	Null probability
Channel 21	−0.42	61	0.1%
Channel 31	−0.40	62	0.2%
Channel 32	−0.52	62	0.1%
Channel 41	−0.50	45	0.1%
Channel 42	−0.50	45	0.1%
Channel 43	−0.56	41	0.1%

Table 3: Fit parameters.

Channel XX	Best fit	$\sigma_{L_{\rm iso}}$	Sample size
Channel 21	$\log(L_{\rm iso}) = (-0.30 \pm 0.05) \times \log(\mathrm{Lag}_{21}/(1+z)) + (52.99 \pm 0.08)$	0.90 ± 0.12	61
Channel 31	$\log(L_{\rm iso}) = (-0.46 \pm 0.04) \times \log(\mathrm{Lag}_{31}/(1+z)) + (53.37 \pm 0.16)$	0.91 ± 0.12	62
Channel 32	$\log(L_{\rm iso}) = (-0.61 \pm 0.04) \times \log(\mathrm{Lag}_{32}/(1+z)) + (53.45 \pm 0.08)$	0.78 ± 0.10	62
Channel 41	$\log(L_{\rm iso}) = (-0.60 \pm 0.04) \times \log(\mathrm{Lag}_{41}/(1+z)) + (53.87 \pm 0.09)$	0.82 ± 0.13	45
Channel 42	$\log(L_{\rm iso}) = (-0.69 \pm 0.04) \times \log(\mathrm{Lag}_{42}/(1+z)) + (53.95 \pm 0.08)$	0.72 ± 0.12	45
Channel 43	$\log(L_{\rm iso}) = (-0.75 \pm 0.05) \times \log(\mathrm{Lag}_{43}/(1+z)) + (53.87 \pm 0.09)$	0.68 ± 0.13	41

5. Conclusion and Summary

We calculated spectral lags of 40 known-z *Swift* GRBs in addition to the previously calculated 31 GRBs. We found that most of our samples follow the lag-luminosity relation with a scatter of samples. We also confirmed that the negative relation between the break time and the luminosity in the X-ray afterglow extends nicely to the lag-luminosity relation of the prompt emission.

Conflict of Interests

The authors declare that there is no conflict of interests regarding the publication of this paper.

Acknowledgments

The authors would like to thank the anonymous referee for comments and suggestions that materially improved the paper. This work was supported by the *Fermi* Guest Investigator Program and also partially supported by the Grant-in-Aid for Scientific Research KAKENHI Grant no. 24103002.

References

[1] L. X. Cheng, Y. Q. Ma, K. S. Cheng, T. Lu, and Y. Y. Zhou, "The time delay of gamma-ray bursts in the soft energy band," *Astronomy & Astrophysics*, vol. 300, p. 746, 1995.

[2] J. P. Norris, R. J. Nemiroff, J. T. Bonnell et al., "Attributes of pulses in long bright gamma-ray bursts," *The Astrophysical Journal*, vol. 459, p. 393, 1996.

[3] J. P. Norris and J. T. Bonnell, "Short gamma-ray bursts with extended emission," *The Astrophysical Journal*, vol. 643, no. 1, article 266, 2006.

[4] F. Ryde, "Interpretations of gamma-ray burst spectroscopy I. Analytical and numerical study of spectral lags," *Astronomy & Astrophysics*, vol. 429, no. 3, pp. 869–879, 2005.

[5] J. P. Norris, G. F. Marani, and J. T. Bonnell, "Connection between energy-dependent lags and peak luminosity in gamma-ray bursts," *Astrophysical Journal Letters*, vol. 534, no. 1, pp. 248–257, 2000.

[6] T. N. Ukwatta, M. Stamatikos, K. S. Dhuga et al., "Spectral lags and the lag-luminosity relation: an investigation with swift bat gamma-ray bursts," *Astrophysical Journal Letters*, vol. 711, no. 2, pp. 1073–1086, 2010.

[7] J. D. Salmonson, "On the kinematic origin of the luminosity-pulse lag relationship in gamma-ray bursts," *The Astrophysical Journal*, vol. 544, no. 2, pp. L115–L117, 2000.

[8] K. Ioka and T. Nakamura, "Peak luminosity-spectral lag relation caused by the viewing angle of the collimated gamma-ray bursts," *The Astrophysical Journal Letters*, vol. 554, no. 2, pp. L163–L167, 2001.

[9] B. E. Schaefer, "Explaining the gamma−ray burst lag/luminosity relation," *The Astrophysical Journal*, vol. 602, no. 1, pp. 306–311, 2004.

[10] M. G. Dainotti, R. Willingale, S. Capozziello, V. F. Cardone, and M. Ostrowski, "Discovery of a tight correlation for gamma-ray burst afterglows with 'canonical' light curves," *The Astrophysical Journal*, vol. 722, no. 2, pp. L215–L219, 2010.

[11] B. Zhang, Y. Z. Fan, and J. Dyks, "Physical processes shaping gamma-ray burst x-ray afterglow light curves: theoretical implications from the swift x-ray telescope observations," *The Astrophysical Journal*, vol. 642, no. 1, article 354, 2006.

[12] J. K. Cannizzo and N. Gehrels, "A new paradigm for gamma-ray bursts: long-term accretion rate modulation by an external accretion disk," *Astrophysical Journal Letters*, vol. 700, no. 2, pp. 1047–1058, 2009.

[13] R. Yamazaki, "Prior emission model for x-ray plateau phase of gamma-ray burst afterglows," *The Astrophysical Journal Letters*, vol. 690, no. 2, p. L118, 2009.

[14] J. Sultana, D. Kazanas, and K. Fukumura, "Luminosity correlations for gamma-ray bursts and implications for their prompt and afterglow emission mechanisms," *The Astrophysical Journal*, vol. 758, no. 1, p. 32, 2012.

[15] D. Eichler and J. Granot, "The case for anisotropic afterglow efficiency within gamma-ray burst jets," *The Astrophysical Journal*, vol. 641, no. 1, pp. L5–L8, 2006.

[16] S. D. Barthelmy, L. M. Barbier, J. R. Cummings et al., "The burst alert telescope (BAT) on the SWIFT midex mission," *Space Science Reviews*, vol. 120, no. 3-4, pp. 143–164, 2005.

[17] D. L. Band, "Gamma–ray burst spectral evolution through cross–correlations of discriminator light curves," *The Astrophysical Journal*, vol. 486, no. 2, pp. 928–937, 1997.

[18] T. Sakamoto, G. Sato, L. Barbier et al., "E_{peak} estimator for gamma-ray bursts observed by the swift burst alert telescope," *The Astrophysical Journal*, vol. 693, no. 1, pp. 922–935, 2009.

[19] D. L. Band, J. Matteson, L. Ford et al., "BATSE observations of gamma-ray burst spectra. I—spectral diversity," *The Astrophysical Journal*, vol. 413, no. 1, pp. 281–292, 1993.

[20] T. Sakamoto, S. D. Barthelmy, W. H. Baumgartner et al., "The second swift burst alert telescope gamma-ray burst catalog," *The Astrophysical Journal Supplement Series* , vol. 195, no. 1, p. 2, 2011.

[21] Y. Kaneko, R. D. Preece, M. S. Briggs, W. S. Paciesas, C. A. Meegan, and D. L. Band, "The complete spectral catalog of bright BATSE gamma-ray bursts," *The Astrophysical Journal Supplement Series*, vol. 166, no. 1, p. 298, 2006.

[22] C. Guidorzi, F. Frontera, E. Montanari et al., "The slope of the gamma-ray burst variability/peak luminosity correlation," *Monthly Notices of the Royal Astronomical Society*, vol. 371, no. 2, pp. 843–851, 2006.

[23] G. D'Agostini, "Fits, and especially linear fits, with errors on both axes, extra variance of the data points and other complications," http://arxiv.org/abs/physics/0511182.

[24] N. Gehrels, J. P. Norris, S. D. Barthelmy et al., "A new γ-ray burst classification scheme from GRB 060614," *Nature*, vol. 444, no. 7122, pp. 1044–1046, 2006.

[25] M. G. Dainotti, V. Petrosian, J. Singal, and M. Ostrowski, "Determination of the intrinsic luminosity time correlation in the X-ray afterglows of gamma-ray bursts," *The Astrophysical Journal*, vol. 774, no. 2, p. 157, 2013.

[26] B. Zhang, B.-B. Zhang, F. J. Virgili et al., "Discerning the physical origins of cosmological gamma-ray bursts based on multiple observational criteria: the cases of $z = 6.7$ GRB 080913, $z = 8.2$ GRB 090423, and some short/hard GRBs," *The Astrophysical Journal*, vol. 703, no. 2, pp. 1696–1724, 2011.

[27] R.-J. Lu, Y.-P. Qin, Z.-B. Zhang, and T.-F. Yi, "Spectral lags caused by the curvature effect of fireballs," *Monthly Notices of the Royal Astronomical Society*, vol. 367, no. 1, pp. 275–289, 2006.

Hindawi Publishing Corporation
Advances in Astronomy
Volume 2015, Article ID 165030, 12 pages
http://dx.doi.org/10.1155/2015/165030

Review Article

A New Era of Submillimeter GRB Afterglow Follow-Ups with the Greenland Telescope

Yuji Urata,[1,2] Kuiyun Huang,[3] Keiichi Asada,[2] Hiroyuki Hirashita,[2] Makoto Inoue,[2] and Paul T. P. Ho[2,4]

[1]*Institute of Astronomy, National Central University, Chungli 32054, Taiwan*
[2]*Academia Sinica Institute of Astronomy and Astrophysics, Taipei 106, Taiwan*
[3]*Department of Mathematics and Science, National Taiwan Normal University, Linkou District, New Taipei City 24449, Taiwan*
[4]*Harvard-Smithsonian Center for Astrophysics, 60 Garden Street, Cambridge, MA 02138, USA*

Correspondence should be addressed to Yuji Urata; urata@astro.ncu.edu.tw

Received 1 December 2014; Revised 19 March 2015; Accepted 23 March 2015

Academic Editor: Valery Nakariakov

Planned rapid submillimeter (submm) gamma-ray-bursts (GRBs) follow-up observations conducted using the Greenland Telescope (GLT) are presented. The GLT is a 12-m submm telescope to be located at the top of the Greenland ice sheet, where the high altitude and dry weather porvide excellent conditions for observations at submm wavelengths. With its combination of wavelength window and rapid responding system, the GLT will explore new insights on GRBs. Summarizing the current achievements of submm GRB follow-ups, we identify the following three scientific goals regarding GRBs: (1) systematic detection of bright submm emissions originating from reverse shock (RS) in the early afterglow phase, (2) characterization of forward shock and RS emissions by capturing their peak flux and frequencies and performing continuous monitoring, and (3) detections of GRBs at a high redshift as a result of the explosion of first generation stars through systematic rapid follow-ups. The light curves and spectra calculated by available theoretical models clearly show that the GLT could play a crucial role in these studies.

1. Introduction

Gamma-ray bursts (GRBs) are among the most powerful explosions in the universe and are observationally characterized according to intense short flashes mainly in high-energy band (so-called "prompt emission") and long-lasting afterglows observed in X-ray to radio bands. Both types of radiation are sometimes extremely bright and can be observed using small- and middle-aperture optical and near-infrared telescopes (e.g., [1, 2]). Because of their intense luminosity, the highest redshift (z) in the reionization epoch ($z \gtrsim 8$) has been observed and has a high possibility for discovery even at $z > 10$ [2]. Although there are various diversities (long/short duration of prompt γ-ray radiation, X-ray flares associated with X-ray afterglows, and complex temporal evolutions of afterglows), optical afterglow and host galaxy observations indicate that the majority of long-duration GRBs occur as a result of the death of massive stars (e.g., [3]). Thus GRBs are unique and powerful means of observing explosions first generation stars (population III, POP-III). Understanding the diversity of the astrophysical entities that cause GRBs is the subject of ongoing study and represents one of the most prominent inquiries in modern astrophysics.

Using GRBs to investigate the high-z universe requires an understanding of their radiation mechanisms. Confirming the existence of reverse shocks (RS) and ascertaining their typical occurrence conditions are critical. The GRB afterglow is believed to involve a relativistically expanding fireball (e.g., [4]). The Interstellar Medium (ISM) influences the fireball shell after it has accumulated, and considerable energy is transferred from the shell to the ISM. The energy transfer is caused by two shocks: a forward shock (FS) propagating into the ISM and an RS propagating into the shell. Millimeter/submillimeter (mm/submm) observations are the key elements in understanding the emission mechanism of GRB

afterglows. They provide "clean" measurements of source intensity and are unaffected by scintillation and extinction. Hence, studies of submm properties of the afterglow are likely to enrich the understanding of GRB physics.

In this paper, we review the status and achievements of submm afterglow observations in Section 2. In Section 3, we introduce the Greenland Telescope (GLT) project and its advantages for GRB follow-up observations. We also expect the GRB follow-ups in the era of GLT in Section 4. On the basis of these advantages, we establish three scientific goals by introducing the expected light curves and spectra with the expected sensitivity limit of GLT in Section 5. Finally, we summarize this paper in Section 6.

2. Status and Achievements of Submillimeter Afterglow Follow-Ups

Numbers of dedicated follow-up instruments of GRBs and afterglows have been developed in γ-ray, X-ray [5], optical, and near-infrared (e.g. [6–12]). Afterglow observations in X-ray and optical have been adequately covered from very early phase including some fractions of γ-ray prompt phase (e.g., [13–16]). In addition, more than 300 afterglow observations have been made at the cm wavelengths mainly using the Very Large Array (e.g., [17]). However, submm has lagged behind X-ray and optical. Figure 1 shows a schematic summary of achievements in GRB observations according to wavelength and time range. It is obvious that prompt afterglow observations are lacking at submm wavelengths. The numbers of submm-detected events have been limited as summarized in Figures 1 and 2. Figure 2 shows all of afterglow observations in submm bands (230 and 345 GHz) including upper limits. There have been only seven detections and three well-monitored events (GRB030329, GRB100418A, and GRB120326A) in the submm bands. Unlike X-ray and optical observations, afterglow monitoring in the submm band covers only the late phase of GRBs and misses their brightening phases. However, several of these observations, in conjunction with intensive X-ray and optical monitoring, as in the GRB 120326A case [18], have addressed crucial physical properties of afterglow. Hence, submm afterglow observations are crucial for understanding the nature of GRBs. In the following, we briefly summarize three well-monitored submm afterglow cases.

GRB030329. Because of the low redshift ($z = 0.168$) origin and bright optical afterglow (~13 mag at 0.1 days), numerous follow-up observations were conducted at various wavelengths (e.g., [3, 19–31]). The 250-GHz monitoring follow-ups were performed by the MAMBO-2 bolometer array on the IRAM 30-m telescope [32] and the IRAM Plateau de Bure Interferometer (PdBI) [33]. The monitoring observations were conducted from 1.4 to 22.3 days after the burst. The light curve after ~8 days exhibited a simple power-law decay with a decay index of −1.68 [32]. The value was consistent with that determined for the optical decay after ~0.5 days and indicated a common physical effect [34]. These monitoring observations supported the two-component jet model, in which a narrow-angle jet is responsible for the high-energy emission and early optical afterglow; the radio afterglow emission is powered by the wide-angle jet [32, 35].

GRB100418A. The Submillimeter Array (SMA, [36]) was used to observe the submm afterglow from ~16 hours after the burst. Continuous monitoring proceeded until 5 days after the burst, at which point it became undetectable [37]. As shown in Figure 2, the submm light curve exhibited a significant fading (equivalent decay power-law index of ~−1.3) between 1 and 2 days and then exhibited a plateau phase until 4 days. The X-ray and optical light curves showed a late bump peak at $\sim 5 \times 10^4$ s [38].

GRB120326A. The SMA observation provided the fastest detection to date among the seven submm afterglows at 230 GHz (Figure 2). In addition, comprehensive monitoring in the X-ray and optical bands was also performed. These observations revealed that the temporal evolution and spectral properties in the optical bands were consistent with the standard FS synchrotron with jet collimation (6°.7). Furthermore, the X-ray and submm behavior indicated different radiation processes from the optical afterglow as shown in Figure 3. Introducing synchrotron self-inverse Compton radiation from RS is a possible solution that is supported by the detection and slow decay of the afterglow in the submm band. As shown in Figure 4, the light curve exhibited the slow temporal evolution ($\alpha_{\rm submm} = -0.33$) between 4×10^4 and 1×10^5 s; this evolution is consistent with the expected decay index of the RS with the $\nu_{\rm obs} < \nu^{\rm Sync}_{m,\rm RS}$ condition [18]. Here, $\nu_{\rm obs}$ and $\nu^{\rm Sync}_{m,\rm RS}$ are the observing frequency and the characteristic synchrotron frequency of the RS. And because half of the events exhibit similar X-ray and optical properties (e.g., [39–41]) as the current event, GRB120326A constitutes a benchmark requiring additional rapid follow-ups conducted using submm instruments such as the SMA and the Atacama Large Millimeter/submm Array (ALMA).

To enhance afterglow studies, submm monitoring observations from an early phase are required. Although rapid follow-ups have been performed using the SMA, as in the GRB130427A case (beginning 1.6 hours after the burst), these follow-ups have been still limited; specifically, we have failed to detect the GRB130427A afterglow with an insufficient sensitivity (~10 mJy) for detecting the RS component [42–44] caused by poor weather conditions. The ongoing SMA programs have also been suffering from the poor weather conditions of the Mauna Kea site. The condition of the Mauna Kea site for the SMA and the James Clerk Maxwell Telescope (JCMT) is inferior for submm observations comparing with other sites such as the ALMA site. Five out of 13 observations with SMA (average responding time is 11.3 hours) were made under the poor or marginal weather conditions. Hence, weather condition for submm bands is one of the crucial points for the time critical observations. As demonstrated through JCMT observations [45–50], rapid follow-ups can be managed by using existing submm telescopes with suitable follow-up programs and observation system. The typical delay time of JCMT is hours scale (average of 59 min with

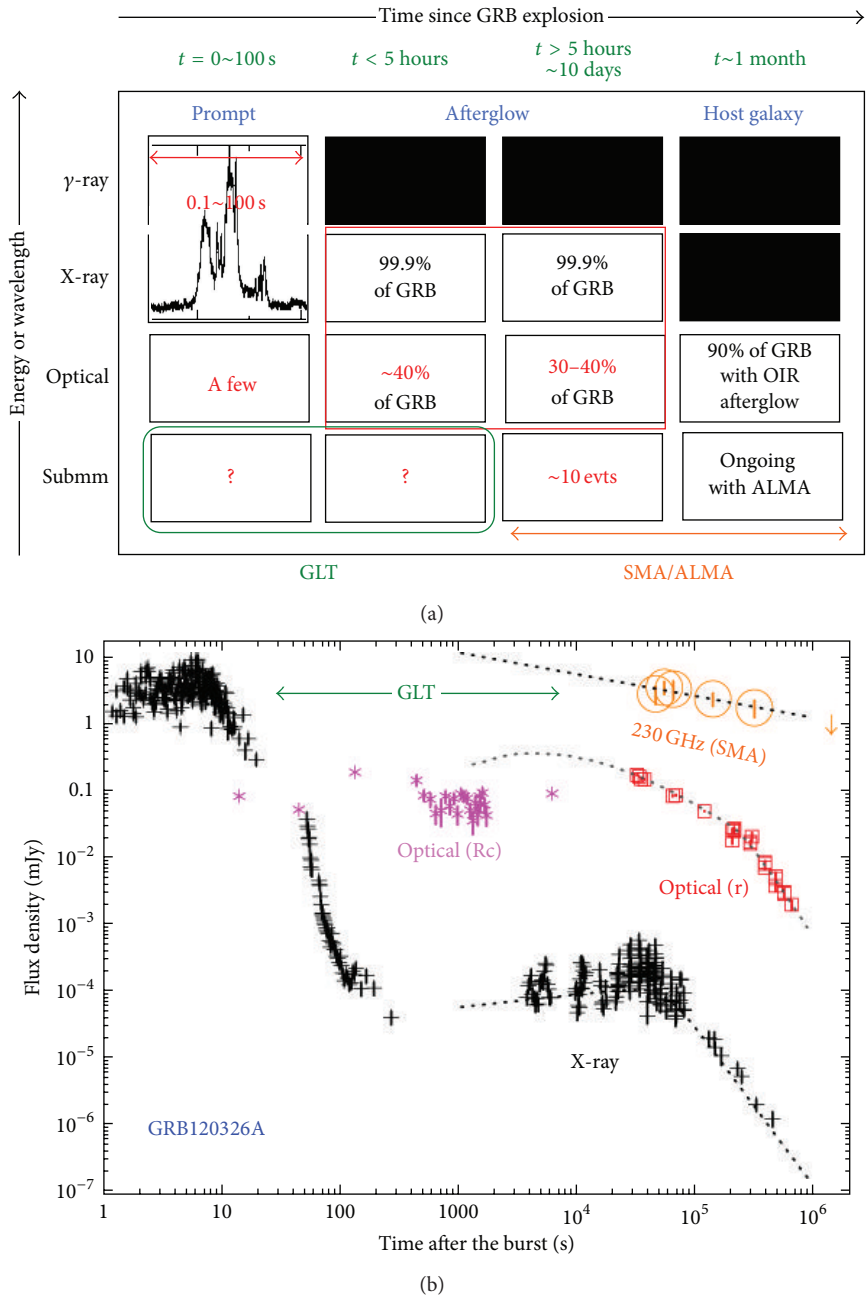

Figure 1: (a) Schematic summary of the GRB observational achievements along with time from the bursts in individual wavelength (from γ-ray to submm). (b) One of actual light curves in X-ray, optical, and submm with the earliest submm detection.

6 GRB observations). Therefore, the succession of the JCMT rapid response system is also desired in the future. In addition, the constructions of dedicated submm telescopes based on these experiences at the better observing site are required to conduct systematic rapid and dense continuous follow-ups (sometimes coordinated with several submm telescopes at the different longitude for covering light curve within a day).

3. Greenland Telescope

The GLT is a state-of-the-art 12-m submm telescope to be located in the Summit Station in Greenland. The aims of the project are establishing a new submm very long baseline interferometer (VLBI) station for the first imaging of shadow of supermassive black holes in M87 [51] and exploring a new terahertz frequency window [52] and time-domain astronomy in submm (e.g., this paper). The expected first light of the GLT will be made in 2017/18.

3.1. Site of the Greenland Telescope. The Summit Station is located on top of the Greenland ice sheet, at 72.5° N and 38.5° W (north of the Arctic Circle) at a 3,200-m altitude. The temperature is extremely low, especially in winter when

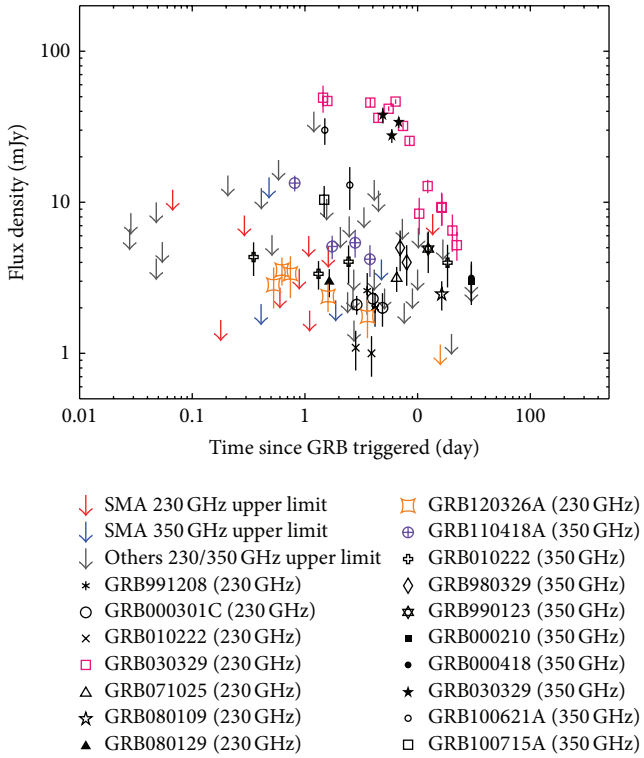

Figure 2: Light curve summary of afterglow observations in submm bands (230 and 345 GHz). Red (230 GHz upper limits), blue (345 GHz upper limits), orange (GRB120326A), and purple (GRB100418A) points were obtained with the SMA. The SMA successfully monitored two of three well-observed submm afterglows, GRB100418A and GRB120326A.

the temperature reaches between −40°C and −60°C (the lowest temperature of −72°C has been recorded). Because of the combination of low temperature and high altitude, considerably low opacity is expected. In 2011, a tipping radiometer at 225 GHz was deployed to Greenland to monitor the sky and weather conditions at the Summit Station and measure opacities from October 2011 to March 2014. The best and the most frequent opacities at 225 GHz were 0.021 and 0.04, respectively [51]. The weather conditions are compatible with those at the ALMA site and significantly better than those of the Manna Kea site [53]. These low opacities and weather conditions are the advantage of the GLT in managing submm and time critical observations including GRB follow-ups with higher sensitivity (or short exposure cycle).

3.2. Planned Instruments and Expected Sensitivities. The GLT will be initially equipped with VLBI receivers at 86, 230, and 345 GHz. Whether large single-dish receivers as second-generation instruments (e.g., submm heterodyne arrays, a THz HEB array, and bolometric spectrometer array) will be installed depends on the scientific merits of the instruments and is still under discussion. For GRB observations, three frequency bands of the VLBI receivers are appropriate and, therefore, the first generation receivers can be used for afterglow observations. The current expected sensitivities of VLBI receivers are 36 and 88 mJy with 1 s integration at 230 and 345 GHz, respectively [54]. These are at least two times better than those of SMA and JCMT. We note that minimum integration time would be less than 0.5 s, since duty cycle for positional switch will be 2 Hz. Longer integration will be achieved as the accumulation of the short integrated data points. Hence, the GLT with the receivers will provide sufficient sensitivities to detect GRB counterparts at the 230 GHz band with shorter exposure (e.g., 3σ limit of 48.3 mJy with 5 s, 10.8 mJy with 100 s, 3.6 mJy with 15 min, and 1.8 mJy with 1 h). This shorter exposure cycle is one of advantages to characterized temporal evolutions of submm afterglows. The field-of-view (FOV) of the receivers will be 25″ and 16″ at 230 and 345 GHz, respectively. These relatively narrow FOV require a tiling observation for covering entire error region determined by hard X-ray instruments (e.g., *Swift*/BAT) or accurate position determination with X-ray afterglows.

We are also planning to install semiautomated responding system for the GRB alerts to manage the rapid GRB follow-ups with secure procedures at the extreme site. We enjoyed the prototype system at the Kiso observatory [23]. The pointing will be started using the position determined by γ-ray instruments and additional adjustment will be made responding to the position of X-ray afterglows. By combination use of this system and site advantages including visibility for targets as shown in Figure 5, we will be able to perform nearly real-time follow-ups for GRBs whose declinations are higher than 30 degrees. A continuous monitoring (nearly video mode) will be managed in the first one day.

4. Expected GRB Follow-Up Observations in the GLT Era

To achieve successful observations, rapid follow-ups using the GLT will be coordinated through *Swift* and the planned Space-based Multiband Astronomical Variable Objects Monitor (SVOM) [55]. One of the obstacles to performing rapid follow-ups of *Swift*-detected GRBs is the poor visibility from ground-based instruments. Although *Swift* has enabled detecting between 100 and 150 events per year, only ~ 10 GRBs per year are observable from the major astronomical observation sites (e.g., Mauna Kea, Chile) without any delay from their γ-ray triggers, because of visibility problems that occur when using ground-based instruments and the random pointing strategy associated with *Swift* observations. According to statistical data in 10 years of *Swift* observations, 10 to 12 events per year could be observed from the early phase of the afterglow by using currently existing telescopes within a 0–3-hour delay by maintaining a proper exposure time (>3-4 hours). The current fraction of total *Swift*/BAT pointing time to around antisun directions (sun hour angle from 9 to 15 hours) is limited to 30–40% [56]. The ideal location of the GLT will enable solving this problem. As shown in Figure 5, GRBs located at a declination higher than 29 degrees will always exhibit an elevation angle higher than 12 degrees over days. Hence, in winter, the GLT will be able to begin rapid GRB follow-ups without any delay

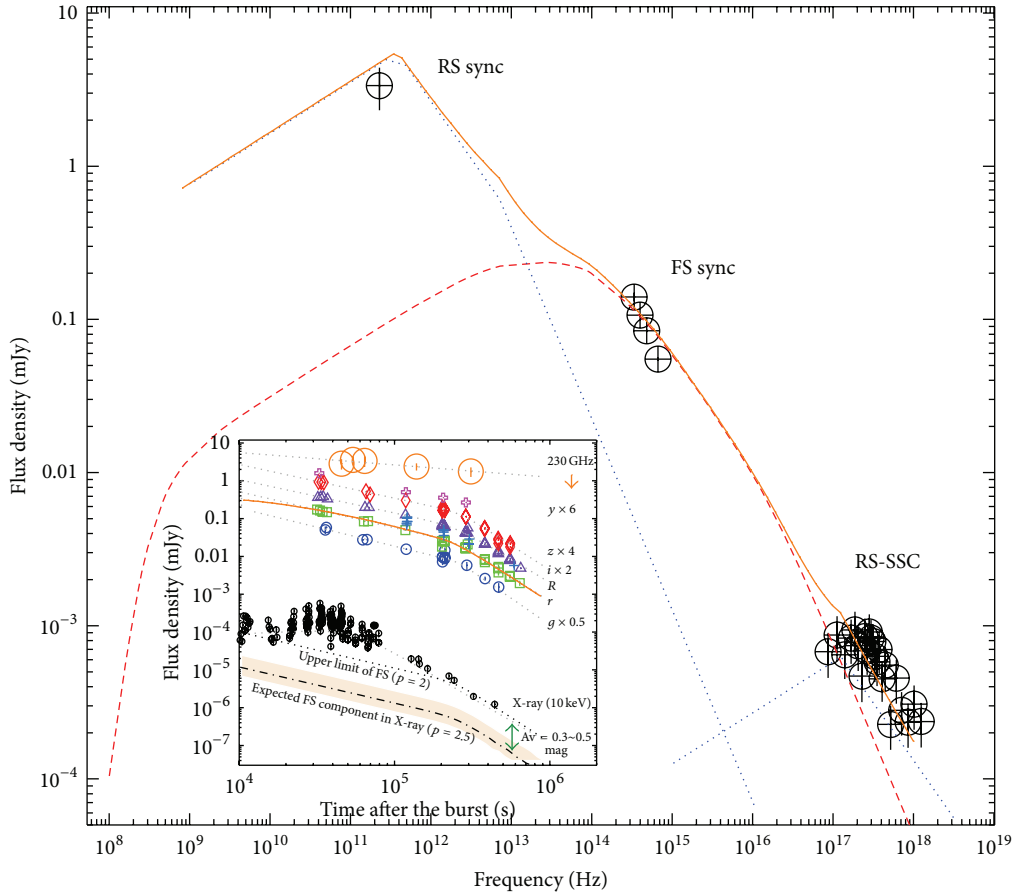

FIGURE 3: Main panel: The spectral energy distribution of GRB120326A at 6.42×10^4 s after the burst [18]. The red dashed line shows the forward shock synchrotron model spectrum calculated using the boxfit code [89] with the same parameters for the best modeling light curve shown in the subpanel. The blue dotted lines show the reverse shock synchrotron radiation and its self-inverse Compton component calculated based on Kobayashi et al. [72] using the observed values and model function for the forward shock component. Subpanel: X-ray, optical, and submm light curves of the GRB120326A afterglow. The grey dotted lines show the best analytical fitted functions described in the text. The orange solid line shows the best modeling function for the r-band light curve obtained with the numerical simulation using boxfit.

caused by unfavorable visibility and perform continuous submm monitoring over days. In addition, these observation conditions are advantageous for observing GRB afterglows that exhibit a rich diversity in various time ranges. In summer, the 86 GHz receiver will be used when weather conditions are unsuitable for observations at 230 and 345 GHz.

SVOM (2020~) will be a timely mission for conducting rapid GLT observations. The GRB detectors will observe antisun directions that enable ground-based instruments to begin follow-ups and continuous long-term monitoring of markedly early cases immediately after receiving GRB alerts. The GRB detection rate of *SVOM* will be ~80 events per year, providing 10 to 20 events per year for rapid GLT follow-ups. In a typical GRB case, X-ray afterglows will be observed immediately through a *SVOM* X-ray telescope (MXT) [57], with the same strategy of X-ray observations of *Swift*. This provides a position accuracy of the counterpart of 2-3″, which is sufficient to cover the position with the FOV of the GLT.

An additional crucial advantage of *SVOM* follow-ups is the capability of detecting X-ray flashes (XRFs) and X-ray-rich GRBs (XRRs) [58] and determining the prompt spectral peak energy E_{peak}. Because of the slightly higher energy range of *Swift*/BAT (15–150 keV), sample collections of XRFs and related rapid follow-ups have been entirely terminated. The E_{peak} estimation of the *Swift*-detected GRBs (mainly XRRs and classical GRBs) has been provided by joint spectrum fittings of *Swift*/BAT and *Suzaku*/WAM [59]. Although spectral parameters of prompt emissions are adequately constrained by these joint fittings (e.g., [60–64]), the number of events is limited. This has caused a stagnation of the study of GRBs with prompt characterization. Because two of the prompt-emission-observing instruments onboard *SVOM*, ECLAIRs [65], and the Gamma Ray Monitor (GRM) [66] will cover the energy bands 4–150 keV and 30–5000 keV, respectively, the E_{peak} for most of *SVOM*-detected GRBs would be determined. In addition, numerous XRRs and XRFs would be detected with the E_{peak} estimation through ECLIAS

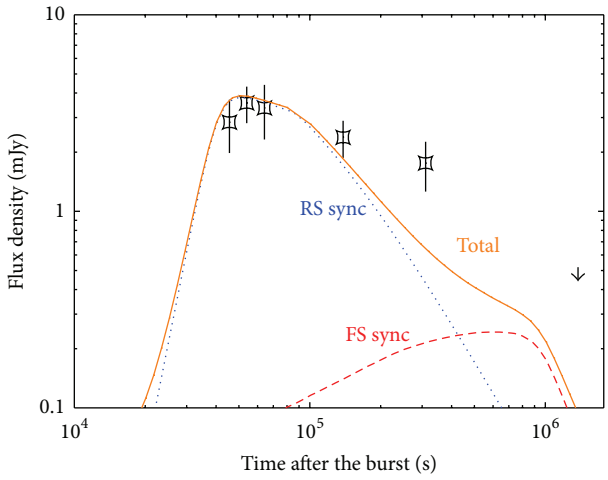

FIGURE 4: Submm light curve of GRB120326A with RS and FS model functions.

and GRM. According to the *HETE-2* observations [58], the numbers of XRFs, XRRs, and GRBs were 16, 19, and 10, respectively. The number of softer events (XRFs/XRRs) was considerably higher than that of classical GRBs. Because the lower-energy coverage of *HETE-2* (2–400 keV) [67] was similar to that of *SVOM*, a high volume of XRF and XRR samples with $E_{\rm peak}$ measurements can be generated. This is likely to enhance the study of the origins of XRRs and XRFs by enabling the determination of their physical parameters. Hence, the GLT will be able to facilitate characterizing prompt and late-phase submm afterglows of all three types of bursts for the first time, providing crucial insights into the nature of XRFs and XRRs.

5. Expected Science Cases

On the basis of the summary of submm afterglow observations and the GLT project, we established the following three scientific goals.

5.1. Systematic Detection of Bright Submm Emissions. It is believed that RSs generate short bright optical flashes (e.g., [13]) and/or intense radio afterglows (e.g., [68]). According to the standard relativistic fireball model, RSs are expected to radiate emissions in the long wavelength bands (optical, infrared, and radio) by executing a synchrotron process in a particularly early afterglow phase (e.g., [69]).

Detecting this brief RS emission and measuring its magnitude would lead to constraints on several crucial parameters of the GRB ejecta, such as its initial Lorentz factor and magnetization [70]. Although RS emission has been detected in the optical wavelength in several GRBs, early optical observations for most GRBs have yielded no evidence of RS emission. The nondetection of RSs in optical bands could be an indicator of a magnetically dominated outflow. Another possible reason for the nondetection is that the typical RS synchrotron frequency is markedly below the optical band (e.g., [71]). Searching for RS emissions in the submm wavelength would test these possibilities. The comparison of early optical and submm temporal evolution would enable studying the composition of the GRB ejecta. If an RS component was regularly detected in GRBs of which the early optical light curve shows no evidence of RS emission, we would be able to claim that GRB ejecta are baryonic in nature. The detection of RS emissions in the submm band of most GRB would support the possibility that GRBs are baryonic flow.

One of the critical problems is that there has been no systematic submm observational study in the early afterglow phase of GRBs. As shown in Figure 1, the number of events that have been observed earlier than 1 day after bursts has remained at 16 for some time. The expected RS light curve for classical GRBs is fainter than 1 mJy at 1 day after bursts and therefore undetectable using currently existing submm telescopes, excpet for ALMA. Figure 6 shows the expected RS light curves based on Kobayashi [69] and Kobayashi et al. [72] with various magnetic energy densities of RS $\epsilon_{B,\rm RS}$ and an initial Lorentz factor Γ_0 in comparison with the GLT sensitivity limit. In most of the cases shown in Figure 6, the RS component faded away before 1×10^5 s (~1 day). Hence, to detect and characterize RS components, rapid (~ min scale) and continuous dense monitoring within 1 day is required. Although some of successful RS observations were made by SMA, CARMA, VLA, and others with their open use framework (e.g. [18, 42–44]), dedicated radio telescopes are strongly desired to make the systematic investigation. In addition, dense monitoring with the same wavelength is required to characterize the RS components, because sparse monitoring, even though rapid detection is included, failed to decode RS and FS components (e.g., [73]). Therefore, the use of the GLT would initiate the era of systematic submm follow-ups.

In Figure 6, cases of low initial Lorentz factors (20, 40) are provided showing XRRs and XRFs that are expected to be detected using the planned GRB satellite SVOM. The origin of the XRFs is not known. However, there are two major models, namely, (1) the failed GRBs or dirty fireball model (e.g., [74]) and (2) the off-axis jet model [75]. According to the dirty fireball model, low-inital-Lorentz-factor ($\Gamma_0 \ll 100$), GRBs produce a lower spectral peak energy $E_{\rm peak}$ in the prompt phase because of $E_{\rm peak} \propto \Gamma_0^4$ dependence, and it is therefore natural to attribute this energy to XRRs and XRFs. The low Lorentz factors substantially delay the RS peak (Figure 6(b)). For the latter model, it is assumed that the viewing angle is considerably larger than the collimation angle of the jet, and the high ratio of X-ray to γ-ray fluence is caused by a relativistic beaming factor when a GRB is observed through off-axis direction. The key observable feature is the achromatic brightening optical afterglow light curves, of which the peak time depends on the viewing angle [76, 77]. Hence, identifying a delayed RS peak through rapid GLT monitoring and the prompt spectral characterization of *SVOM* will confirm and identify the origin of XRFs and XRRs.

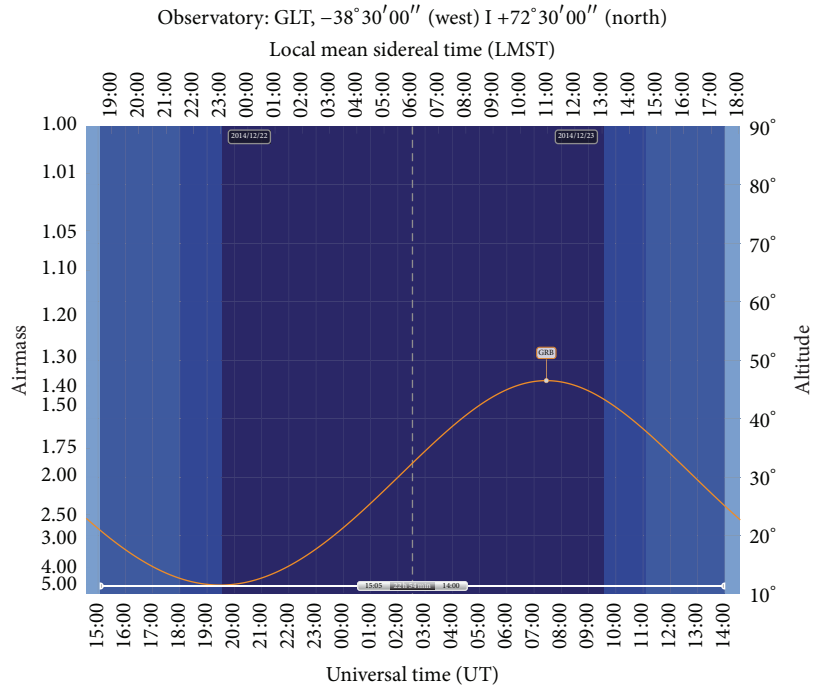

FIGURE 5: An example of visibility plot in winter for the GRB that declination is 29 deg. Hatchs indicate the sun altitude lower than −18 (dark blue), −12 (blue), −6 (dark cyan), and 0 (cyan) deg., respectively.

5.2. Characterization of Forward and Reverse Shock Emissions. The spectral characteristics of FS and RS synchrotron emissions are related as follows: $\nu_{m,\mathrm{FS}} \sim \mathcal{R}_B^{1/2}\mathcal{R}_M^2\nu_{m,\mathrm{RS}}$, and $F_{\max,\mathrm{RS}} \sim \mathcal{R}_M\mathcal{R}_B^{-1/2}F_{\max,\mathrm{FS}}$ (e.g., [70]), where $\mathcal{R}_M$ $(= \Gamma_d^2/\Gamma_0)$ and $\mathcal{R}_B$ $(= \epsilon_{B,\mathrm{FS}}/\epsilon_{B,\mathrm{RS}})$ denote the mass and magnetization ratio parameters, respectively. Here, Γ_d, $\epsilon_{B,\mathrm{FS}}$, and $\epsilon_{B,\mathrm{RS}}$ are the Lorentz factors at the deceleration time, the fractions of magnetic energy of RS and FS, respectively. RS emission is typically expected to be considerably brighter (~100 times) than FS emission as shown in Figure 7. Therefore, the emission from RSs is sensitive to the properties of the fireball, and the broadband spectrum and light curve evolutions of FS/RS can provide critical clues to understanding GRBs.

Regarding FSs, afterglows can be described by synchrotron emissions from a decelerating relativistic shell that collides with an external medium. According to the FS synchrotron model, both the spectrum and light curve consist of several power-law segments with related indices (e.g., [78, 79]). The broadband spectrum is characterized according to the synchrotron peak frequency $\nu_{m,\mathrm{FS}}$ and the peak spectrum flux density $F_{\max,\mathrm{FS}}$. The peak spectrum flux is expected to occur at low frequencies (from X-ray to radio) over time (from minutes to several weeks) as $\nu_{m,\mathrm{FS}} \propto t^{-3/2}$. The peak spectrum flux density $F_{\max,\mathrm{FS}}$ is predicted to remain constant in the circumburst model, whereas it decreases as $F_{\max,\mathrm{FS}} \propto t^{-1/2}$ in the wind model. Therefore, determining the characterizing frequencies and peak fluxes by using temporal and spectrum observations provides direct evidence of the FS/RS shock synchrotron model and typical (or average) physical conditions of a fireball.

Snapshots of the broadband spectrum and continuous monitoring of light curves in the submm bands are essential to characterizing the radiation of afterglow by decoding each component. Figure 8 shows the expected light curve in the 230 GHz band at $z = 0.3$, 0.5, and 0.7. We fix the rest of parameters as explosion energy $E = 3\times10^{52}$ erg, circumburst number density $n = 1\,\mathrm{cm}^{-3}$, the electron spectral index $p = 2.1$, the electron energy density $\epsilon_e = 0.3$, and the magnetic energy density of FS $\epsilon_{B,\mathrm{FS}} = 0.01$. The brightening caused by the passing of the synchrotron peak frequency ν_m can be detected to determine the FS component in light curves. The GLT has also enough sensitivities to detect FS component for nearby ($z \lesssim 0.7$) events and the monitoring determines their $\nu_{m,\mathrm{FS}}$. The expected $\nu_{m,\mathrm{FS}}$ passing through time across the 230 GHz band is several $\times10^5$ s (Figure 8). Therefore, the submm band is suitable for decoding both RS and FS components. Some of closure relations for FS and RS [79] will also constrain components even if the light curve or spectrum observations are sparsely performed. For X-ray and OIR cases, the expected timescale is between several minutes and ~2 hours after the burst. In this time range, detecting the peak frequency directly is difficult because several additional components (e.g., long-lasting prompt emission, X-ray flares, etc.) characterize this phase. For the MIR case, observations fully rely on the satellite-based instruments. In this case, timely follow-ups are difficult because of operation confinement and limitation of number of resources. Furthermore, the slow temporal evolution in the radio band makes it difficult to obtain simultaneous optical and X-ray segments. This creates uncertainty regarding whether we observe the same synchrotron components or not. Hence, the GLT will

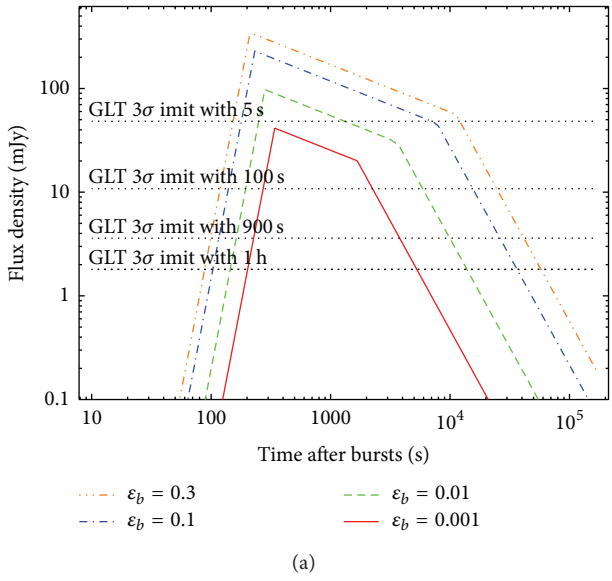

FIGURE 6: (a) Expected RS light curves in the 230 GHz band with various $\epsilon_{B,\mathrm{RS}}$ (0.001, 0.01, 0.1, and 0.3). Other physical parameters are fixed as $z = 1$, $E = 3 \times 10^{52}$, $\Gamma = 80$, $n = 1$, $\epsilon_e = 0.3$, and $\epsilon_{B,\mathrm{FS}} = 0.01$. (b) Expected RS light curves in the 230 GHz band with various initial Lorentz factor Γ_0. Other physical parameters are $z = 1$, $E = 3 \times 10^{52}$, $n = 1$, $\epsilon_e = 0.3$, $\epsilon_{B,\mathrm{RS}} = 0.03$, and $\epsilon_{B,\mathrm{FS}} = 0.01$. The expected GLT 3-$\sigma$ limits with 900 s and 1 h exposure are indicated with dotted lines in both panels.

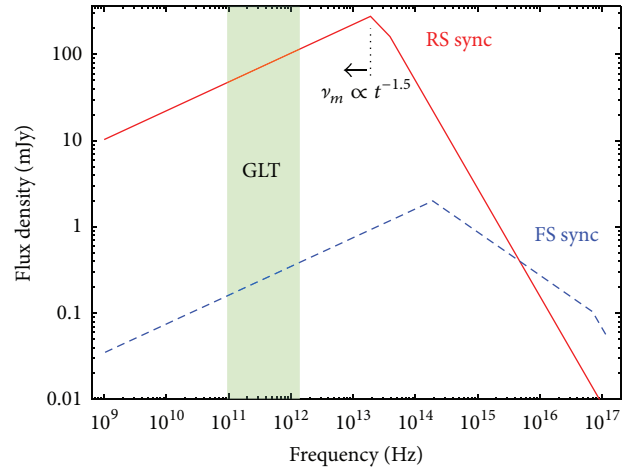

FIGURE 7: Expected spectrum at the deceleration time with $z = 1$, $E = 1 \times 10^{52}$, $\Gamma = 80$, $n = 1$, $\epsilon_e = 0.3$, $\epsilon_{B,\mathrm{RS}} = 0.03$, and $\epsilon_{B,\mathrm{FS}} = 0.01$. Synchrotron radiations from reverse and forward shock are indicated by red solid and blue dashed lines, respectively. A green hatched box indicates the frequency coverage of GLT.

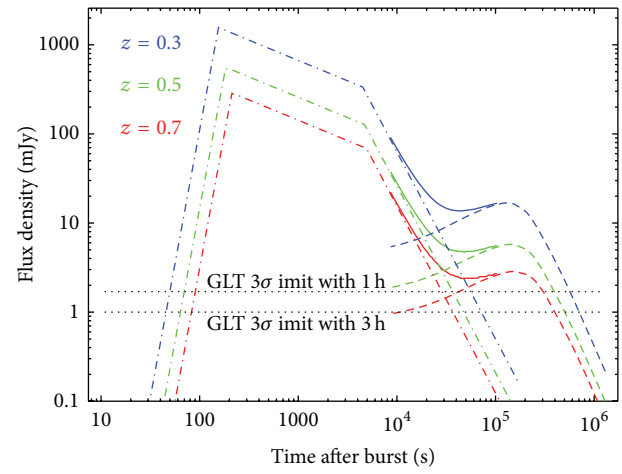

FIGURE 8: Expected RS (dashed-dot) and FS (dashed) light curves in the 230 GHz band at $z = 0.3$, 0.5, and 0.7 with $E = 3 \times 10^{52}$ erg, $n = 1\ \mathrm{cm}^{-3}$, $p = 2.1$, $\epsilon_e = 0.3$, and $\epsilon_{B,\mathrm{FS}} = 0.01$. Solid lines indicate the total of RS and FS. GLT has also enough sensitivity to characterize the FS components for nearby ($z \lesssim 0.7$) GRBs. The expected GLT 3-σ limits with 1 h and 3 h exposure are indicated with dotted lines.

provide unique results for nearby events ($z \lesssim 0.7$) by facilitating continuous monitoring.

Optical monitoring combined with the GLT will be required. As we describe above, RS components will be caught by submm observations. For characterizing FS components, multicolor optical monitoring is suitable because the temporal evolution and spectrum of optical afterglow around 1 day after bursts are well consistent with the expectation of the FS model. Figure 3 shows one of the most appropriate examples of the earliest submm afterglow detection procedures performed using the SMA and related optical monitoring [18]. Because of the rapid submm monitoring, the FS and RS components were separated. Conducting multifrequency monitoring by using the GLT requires rapid optical follow-ups, which will be conducted using our own optical network EAFON [80–82] and other ground-based optical telescopes, as numerous observations have been conducted.

5.3. Discovering of First-Star Explosions by Using GRBs. The findings regarding a high-redshift GRB at $z = 8.2$ [1] indicated the possibility of using GRBs to probe the processes and environments of star formation as far back in time as the earliest cosmic epochs. Numerous theoretical models (e.g., [83–85]) show that some POP-III stars generate GRBs as

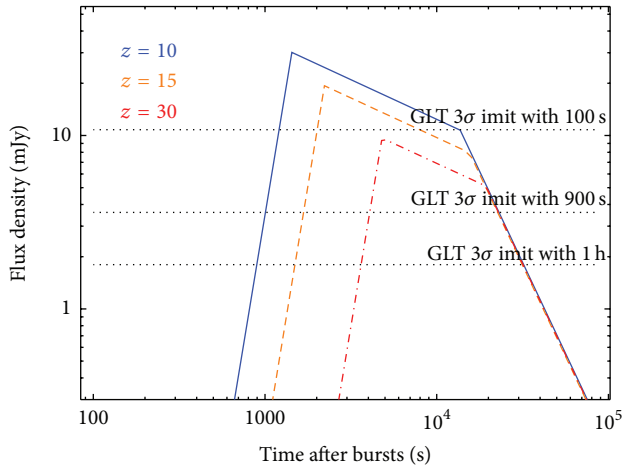

FIGURE 9: Expected light curves of GRB afterglows at $z = 10, 15$, and 30 at 230 GHz. Other physical parameters are fixed as $E = 1 \times 10^{53}$, $\Gamma = 80$, $n = 1$, $\epsilon_e = 0.3$, $\epsilon_{B,\mathrm{RS}} = 0.03$, and $\epsilon_{B,\mathrm{FS}} = 0.01$. The expected GLT 3-$\sigma$ limits with 900 s and 1 h exposure are indicated with dotted lines. GLT with rapid follow-ups has sufficient potential to detect these higher-z events.

an end product. Hence, detecting the signals of high-z GRBs has been a recent prominent objective in modern astrophysics.

One of the prospective methods of identifying POP-III GRBs is to detect RS components in the submm bands. Unlike OIR observations, submm observations provide clean measurements of the source intensity, unaffected by extinction. Because of the intense luminosity of the RSs, it is expected that the radiation from high-z GRBs ($z > 10$–30) can be observed if the GLT is used with the rapid response system. Inoue et al. [86] showed that the RS component of POP-III GRBs at $z = 15$ and 30 in the 300 GHz band is substantially brighter than 1 mJy, and these bright RS components will be detectable by using the GLT. In addition, we simulated the expected RS light curves at $z = 10$, 15, and 30 based on Kobayashi [69] and Kobayashi et al. [72]. For this calculation, we assumed that $E = 1 \times 10^{53}$ because the progenitor stars might be considerably more massive than nearby events (e.g., [83]). Other physical parameters are fixed as $\Gamma = 80$, $n = 1$, $\epsilon_e = 0.3$, $\epsilon_{B,\mathrm{RS}} = 0.03$, and $\epsilon_{B,\mathrm{FS}} = 0.01$. As shown in Figure 9, the GLT has great potential to detect the high-z GRBs even those at $z = 30$ with the rapid responding, shorter exposure cycle, and continuous dense monitoring. These initial detections of the GLT in the early phase will provide the opportunity to conduct additional follow-ups using 30-m class telescopes such as the TMT. Because these large telescopes typically enable conducting follow-ups for a limited number of events, the target selections of the GLT observations will be critical.

The event rate of high-z GRBs, which may be connected to the star-formation rate in the early universe, is not known. Wanderman and Piran [87] estimated that the event rate of high-z ($z > 7$) GRBs might be ~10 events per year per steradian on the basis of limited ~100 *Swift*-detected long GRBs with known redshift and measured peak flux. Their estimation showed that *Swift*/BAT exhibited substantially high redshift fractions (~3.4% at $z > 7$), whereas *Swift* and related follow-ups detected only a few $z > 7$ events. Hence, uncertainty exists regarding the number of higher-z events that *Swift* has detected; thus, the frequency of such events is not thoroughly understood because appropriate follow-ups in long wavelength (e.g., IR, submm) have not been conducted. Actually, $z \sim 9$ GRB candidate [88] was also detected through *Swift*. Therefore, a continuous effort is required in this field of research, despite a success rate that is typically low. In addition, Wanderman and Piran [87] expected that *SVOM* will detect 0.1–7 events per year at $z > 10$. To detect these events, rapid follow-up coordination with submm instruments will be crucial, because it is impossible to identify higher-z candidates within hours from bursts with limited observational information. Therefore, the installing of a rapid responding system in the GLT will enable us to perform high-z GRB observations.

6. Summary

We briefly summarized the current achievements of submm follow-up observations of GRBs. Although submm afterglow observations are critical to understanding the nature of GRBs (e.g., GRB030329 and GRB120326A), the number of successful observations has been limited. This is because of the lack of dedicated submm telescopes that has made it difficult to perform rapid follow-up.

Furthermore, we introduced the single-dish mode of GLT. The development is ongoing and the expected first light of the GLT will be made in 2017/18. The first light instrument will be the VLBI receivers at 86, 230, and 345 GHz. The expected sensitivities of the receivers are 36 and 88 mJy in 1 s integration at 230 and 345 GHz, respectively. The GLT enables rapid and continuous submm monitoring of GRB submm counterparts in the prompt phase.

According to the aforementioned situations and expected capabilities of the GLT, we established the following three key scientific goals regarding GRB studies: (1) systematic detection of bright submm emissions originating from RS in the early afterglow phase by conducting rapid follow-ups, (2) characterization of FS and RS emissions by capturing their peak flux and frequencies through continuous monitoring, and (3) detection of the first star explosions as a result of GRBs at a high redshift through systematic rapid follow-ups.

Detecting RS emissions and monitoring light curves in the submm band could lead to constraints on several crucial parameters of the GRB ejecta, such as the initial Lorentz factor and magnetization. We calculated the expected RS light curves by using various initial Lorentz factors Γ_0 and the magnetic energy densities of RS $\epsilon_{B,\mathrm{RS}}$ and showed that these light curves could be characterized through rapid follow-ups of the GLT. Determining the origins of XRRs and XRFs will also be a major focus of the GLT together with the *SVOM* mission.

In addition to characterizing RS components, the GLT will be able to detect FS components of nearby ($z \lesssim 0.7$) GRBs. Because the spectral characteristics of the FS and RS

synchrotron emissions are related, characterizing both FS and RS components provides critical insights into GRBs. We generated an expected submm light curve at $z = 0.3$, 0.5, and 0.7 and showed that the GLT can separate RS and FS components through long-term and continuous monitoring, because RS and FS components dominate earlier than $\sim 4 \times 10^4$ s and later than $\sim 10^5$ s, respectively.

These two RS science topics will enhance the GRB studies as the probe of a high-z universe. Because of the existence of RS and its extreme luminosity, it is expected that the radiation from high-z GRB ($z > 10$–30) can be observed if the GLT is used with a rapid (hours scale) response system. We simulated the expected RS light curves at $z = 10$, 15, and 30. These light curves showed that the GLT has sufficient sensitivity to detect and characterize these events. The future *SVOM* mission may provide the capability to detect GRBs at $z > 10$; the establishment of close coordination using longer wavelength (e.g., infrared, submm) instruments will be crucial. Because the rapid identification of counterparts at long wavelengths is crucial for conducting additional further follow-ups using 30-m class telescopes such as the TMT will be used. Therefore, the GLT could play a crucial role in detecting high-z GRBs.

Conflict of Interests

The authors declare that there is no conflict of interests regarding the publication of this paper.

Acknowledgments

The Greenland Telescope (GLT) Project is a collaborative project between Academia Sinica Institute of Astronomy and Astrophysics, Smithsonian Astrophysical Observatory, MIT Haystack Observatory, and National Radio Astronomy Observatory. The authors would like to thank Shiho Kobayashi for the useful comments. The authors would also like to thank all members of the GLT single-dish science team organized at ASIAA. This work is partly supported by the Ministry of Science and Technology of Taiwan Grants MOST 103-2112-M-008-021- (Yuji Urata), 103-2112-M-001-038-MY2 (Keiichi Asada), and 102-2119-M-001-006-MY3 (Hiroyuki Hirashita).

References

[1] N. R. Tanvir, D. B. Fox, A. J. Levan et al., "A γ-ray burst at a redshift of z ≈ 8.2," *Nature*, vol. 461, no. 7268, pp. 1254–1257, 2009.

[2] J. S. Bloom, D. A. Perley, W. Li et al., "Observations of the naked-eye GRB 080319B: implications of nature's brightest explosion," *Astrophysical Journal*, vol. 691, no. 1, pp. 723–737, 2009.

[3] K. Z. Stanek, T. Matheson, P. M. Garnavich et al., "Spectroscopic discovery of the supernova 2003dh associated with GRB 030329," *Astrophysical Journal Letters*, vol. 591, no. 1, pp. L17–L20, 2003.

[4] P. Mészáros and M. J. Rees, "Optical and long-wavelength afterglow from gamma-ray bursts," *The Astrophysical Journal*, vol. 476, no. 1, pp. 232–237, 1997.

[5] N. Gehrels, G. Chincarini, P. Giommi et al., "The *Swift* gamma-ray burst mission," *The Astrophysical Journal*, vol. 611, no. 2, p. 1005, 2004.

[6] I. A. Steele, "The Liverpool robotic telescope," *New Astronomy Reviews*, vol. 45, no. 1-2, pp. 45–47, 2001.

[7] C. W. Akerlof, R. L. Kehoe, T. A. McKay et al., "The ROTSE-III robotic telescope system," *Publications of the Astronomical Society of the Pacific*, vol. 115, no. 803, pp. 132–140, 2003.

[8] W. T. Vestrand, K. N. Borozdin, S. P. Brumby et al., "The RAPTOR experiment: a system for monitoring the optical sky in real time," in *2nd Advanced Global Communications Technologies for Astronomy*, vol. 4845 of *Proceedings of SPIE*, pp. 126–136, Waikoloa, Hawaii, USA, November 2002.

[9] A. Burd, M. Cwiok, H. Czyrkowski et al., "Pi of the sky—all-sky, real-time search for fast optical transients," *New Astronomy*, vol. 10, no. 5, pp. 409–416, 2005.

[10] A. Klotz, M. Boër, J. L. Atteia, and B. Gendre, "Early optical observations of gamma-ray bursts by the TAROT telescopes: period 2001–2008," *Astronomical Journal*, vol. 137, no. 5, pp. 4100–4108, 2009.

[11] A. Ferrero, L. Hanlon, R. Felletti et al., "The photometry pipeline of the watcher robotic telescope," *Advances in Astronomy*, vol. 2010, Article ID 715237, 5 pages, 2010.

[12] Y. Urata, M. S. Tashiro, T. Tamagawa et al., "WIDGET: system performance and GRB prompt optical observations," *Publications of the Astronomical Society of Japan*, vol. 63, no. 1, pp. 137–146, 2011.

[13] C. Akerlof, R. Balsano, S. Barthelmy et al., "Observation of contemporaneous optical radiation from a γ-ray burst," *Nature*, vol. 398, no. 6726, pp. 400–402, 1999.

[14] W. T. Vestrand, P. R. Wozniak, J. A. Wren et al., "A link between prompt optical and prompt γ-ray emission in γ-ray bursts," *Nature*, vol. 435, no. 7039, pp. 178–180, 2005.

[15] W. T. Vestrand, J. A. Wren, P. R. Wozniak et al., "Energy input and response from prompt and early optical afterglow emission in γ-ray bursts," *Nature*, vol. 442, no. 7099, pp. 172–175, 2006.

[16] J. L. Racusin, S. V. Karpov, M. Sokolowski et al., "Broadband observations of the naked-eye γ-ray burst GRB 080319B," *Nature*, vol. 455, pp. 183–188, 2008.

[17] P. Chandra and D. A. Frail, "A radio-selected sample of gamma-ray burst afterglows," *The Astrophysical Journal*, vol. 746, no. 2, p. 156, 2012.

[18] Y. Urata, K. Huang, S. Takahashi et al., "Synchrotron self-inverse compton radiation from reverse shock on GRB 120326A," *The Astrophysical Journal*, vol. 789, p. 146, 2014.

[19] D. A. Smith, E. S. Rykoff, C. W. Akerlof et al., "ROTSE-III observations of the early afterglow from GRB 030329," *Astrophysical Journal Letters*, vol. 596, no. 2, pp. L151–L154, 2003.

[20] A. Tiengo, S. Mereghetti, G. Ghisellini, E. Rossi, G. Ghirlanda, and N. Schartel, "The X-ray afterglow of GRB 030329," *Astronomy and Astrophysics*, vol. 409, no. 3, pp. 983–987, 2003.

[21] S. Klose, E. Palazzi, N. Masetti et al., "Prospects for multiwavelength polarization observations of GRB afterglows and the case GRB 030329," *Astronomy & Astrophysics*, vol. 420, no. 3, pp. 899–903, 2004.

[22] G. Kosugi, Y. Mizumoto, N. Kawai et al., "Spectral evolution of the GRB 030329 afterglow: detection of the supernova nebular phase emissions," *Publications of the Astronomical Society of Japan*, vol. 56, no. 1, pp. 61–68, 2004.

[23] Y. Urata, T. Miyata, S. Nishiura et al., "Early (<0.3 days) *R*-band light curve of the optical afterglow of GRB 030329," *Astrophysical Journal Letters*, vol. 601, no. 1, pp. L17–L19, 2004.

[24] A. Tiengo, S. Mereghetti, G. Ghisellini, F. Tavecchio, and G. Ghirlanda, "Late evolution of the X-ray afterglow of GRB 030329," *Astronomy and Astrophysics*, vol. 423, no. 3, pp. 861–865, 2004.

[25] N. Kuno, N. Sato, H. Nakanishi et al., "Radio observations of the afterglow of GRB 030329," *Publications of the Astronomical Society of Japan*, vol. 56, pp. L1–L4, 2004.

[26] V. Šimon, R. Hudec, and G. Pizzichini, "The color evolution of the optical afterglow of GRB 030329 and the implications for the underlying supernova SN 2003dh," *Astronomy and Astrophysics*, vol. 427, no. 3, pp. 901–905, 2004.

[27] D. A. Frail, A. M. Soderberg, S. R. Kulkarni et al., "Accurate calorimetry of GRB 030329," *The Astrophysical Journal*, vol. 619, no. 2, pp. 994–998, 2005.

[28] K. Kohno, T. Tosaki, T. Okuda et al., "Nobeyama millimeter array observations of GRB 030329: a decay of afterglow with bumps and molecular gas in the host galaxy," *Publications of the Astronomical Society of Japan*, vol. 57, no. 1, pp. 147–153, 2005.

[29] I. A. Smith, R. P. J. Tilanus, N. Tanvir et al., "SCUBA sub-millimeter observations of gamma-ray bursts: III. GRB 030329: the brightest sub-millimeter afterglow to date," *Astronomy and Astrophysics*, vol. 439, no. 3, pp. 981–986, 2005.

[30] J. Gorosabel, D. Pérez-Ramírez, J. Sollerman et al., "The GRB 030329 host: a blue low metallicity subluminous galaxy with intense star formation," *Astronomy & Astrophysics*, vol. 444, no. 3, pp. 711–721, 2005.

[31] J. Van Der Horst, A. Kamble, L. Resmi et al., "Detailed study of the GRB 030329 radio afterglow deep into the non-relativistic phase," *Astronomy and Astrophysics*, vol. 480, no. 1, pp. 35–43, 2008.

[32] K. Sheth, D. A. Frail, S. White et al., "Millimeter observations of GRB 030329: continued evidence for a two-component jet," *Astrophysical Journal Letters*, vol. 595, no. 1, pp. L33–L36, 2003.

[33] L. Resmi, C. H. Ishwara-Chandra, A. J. Castro-Tirado et al., "Radio, millimeter and optical monitoring of GRB 030329 afterglow: constraining the double jet model," *Astronomy and Astrophysics*, vol. 440, no. 2, pp. 477–485, 2005.

[34] P. A. Price, D. W. Fox, S. R. Kulkarni et al., "The bright optical afterglow of the nearby γ-ray burst of 29 March 2003," *Nature*, vol. 423, no. 6942, pp. 844–847, 2003.

[35] E. Berger, S. R. Kulkarni, G. Pooley et al., "A common origin for cosmic explosions inferred from calorimetry of GRB030329," *Nature*, vol. 426, no. 6963, pp. 154–157, 2003.

[36] P. T. P. Ho, J. M. Moran, and K. Y. Lo, "The submillimeter array," *The Astrophysical Journal*, vol. 616, no. 1, article L1, 2004.

[37] A. de Ugarte Postigo, A. Lundgren, S. Martín et al., "Pre-ALMA observations of GRBs in the mm/submm range," *Astronomy & Astrophysics*, vol. 538, article A44, 23 pages, 2012.

[38] F. E. Marshall, L. A. Antonelli, D. N. Burrows et al., "The late peaking afterglow of GRB 100418A," *The Astrophysical Journal*, vol. 727, article 132, 2011.

[39] A. Panaitescu, P. Mészáros, D. Burrows et al., "Evidence for chromatic X-ray light-curve breaks in Swift gamma-ray burst afterglows and their theoretical implications," *Monthly Notices of the Royal Astronomical Society*, vol. 369, no. 4, pp. 2059–2064, 2006.

[40] K. Y. Huang, Y. Urata, P. H. Kuo et al., "Multicolor shallow decay and chromatic breaks in the GRB 050319 optical afterglow," *The Astrophysical Journal Letters*, vol. 654, no. 1, pp. L25–L28, 2007.

[41] Y. Urata, R. Yamazaki, T. Sakamoto et al., "Testing the external-shock model of gamma-ray bursts using the late-time simultaneous optical and X-ray afterglows," *The Astrophysical Journal Letters*, vol. 668, no. 2, pp. L95–L98, 2007.

[42] T. Laskar, E. Berger, B. A. Zauderer et al., "A reverse shock in GRB 130427A," *Astrophysical Journal*, vol. 776, no. 2, article 119, 2013.

[43] D. A. Perley, S. B. Cenko, A. Corsi et al., "The afterglow of GRB 130427A from 1 to 1016 GHz," *The Astrophysical Journal*, vol. 781, no. 1, article 37, 2014.

[44] A. J. van der Horst, Z. Paragi, A. G. de Bruyn et al., "A comprehensive radio view of the extremely bright gamma-ray burst 130427A," *Monthly Notices of the Royal Astronomical Society*, vol. 444, no. 4, pp. 3151–3163, 2014.

[45] I. A. Smith, R. P. J. Tilanus, N. R. Tanvir, and D. A. Frail, "GRB 120404A: JCMT SCUBA-2 sub-mm observation," *GRB Coordinates Network*, vol. 13233, p. 1, 2012.

[46] I. A. Smith, R. P. J. Tilanus, N. R. Tanvir, and D. A. Frail, "GRB 130131A: JCMT SCUBA-2 sub-mm observations," *GRB Coordinates Network*, vol. 13259, p. 1, 2012.

[47] I. A. Smith, R. P. J. Tilanus, N. R. Tanvir, and D. A. Frail, "GRB 120724A: JCMT SCUBA-2 sub-mm observation," *GRB Coordinates Network*, vol. 13519, p. 1, 2012.

[48] I. A. Smith, R. P. J. Tilanus, N. R. Tanvir, and D. A. Frail, "GRB 120729A: JCMT SCUBA-2 sub-mm observation," *GRB Coordinates Network*, vol. 13554, p. 1, 2012.

[49] I. A. Smith, R. P. J. Tilanus, N. R. Tanvir, and D. A. Frail, "GRB 120422A: JCMT SCUBA-2 sub-mm observation," *GRB Coordinates Network*, vol. 14281, p. 1, 2013.

[50] I. A. Smith, R. P. J. Tilanus, N. R. Tanvir, and D. A. Frail, "GRB 130831A: JCMT SCUBA-2 sub-mm observation," *GRB Coordinates Network*, vol. 15174, p. 1, 2013.

[51] M. Inoue, J. C. Algaba-Marcos, K. Asada et al., "Greenland telescope project: direct confirmation of black hole with sub-millimeter VLBI," *Radio Science*, vol. 49, no. 7, pp. 564–571, 2014.

[52] H. Hirashita, P. M. Koch, S. Matsushita et al., "First-generation science cases for ground-based Terahertz telescopes," *Publications of the Astronomical Society of the Pacific*. Submitted.

[53] P. L. Martin-Cocher, K. Asada, S. Matsushita, M.-T. Chen, P. T. P. Ho, and C.-P. Chen, "225 GHz opacity measurements at Summit camp, Greenland, for the GreenLand Telescope (GLT) site testing," in *5th Ground-based and Airborne Instrumentation for Astronomy*, vol. 9147 of *Proceedings of SPIE*, p. 91473N, Montréal, Canada, July 2014.

[54] P. K. Grimes, K. Asada, R. Blundell et al., "Instrumentation for single-dish observations with The Greenland Telescope," in *Millimeter, Submillimeter, and Far-Infrared Detectors and Instrumentation for Astronomy VII*, vol. 9153 of *Proceedings of SPIE*, Montreal, Canada, June 2014.

[55] O. Godet, J. Paul, J. Y. Wei et al., "The Chinese-French SVOM mission: studying the brightest astronomical explosions," in *Space Telescopes and Instrumentation 2012: Ultraviolet to Gamma Ray*, Proceedings of SPIE, 84431O, September 2012.

[56] T. Sakamoto and N. Gehrels, "Review the anti-sun pointing operation of Swift," in *Proceedings of the Swift Mission Conference: Celebrating 5 Years*, State College, Pa, USA, November 2009.

[57] D. Götz, J. Osborne, B. Cordier et al., "The microchannel X-ray telescope for the gamma-ray burst mission SVOM," in *Space Telescopes and Instrumentation 2014: Ultraviolet to Gamma Ray*, vol. 9144 of *Proceedings of SPIE*, p. 914423, Montréal, Canada, July 2014.

[58] T. Sakamoto, D. Q. Lamb, N. Kawai et al., "Global characteristics of X-ray flashes and X-ray-rich gamma-ray bursts observed by *HETE-2*," *The Astrophysical Journal*, vol. 629, p. 311, 2005.

[59] K. Yamaoka, A. Endo, T. Enoto et al., "Design and in-orbit performance of the Suzaku wide-band all-sky monitor," *Publications of the Astronomical Society of Japan*, vol. 61, supplement 1, pp. S35–S53, 2009.

[60] R. L. C. Starling, P. T. O'Brien, R. Willingale et al., "Swift captures the spectrally evolving prompt emission of GRB 070616," *Monthly Notices of the Royal Astronomical Society*, vol. 384, no. 2, pp. 504–514, 2008.

[61] H. A. Krimm, K. Yamaoka, S. Sugita et al., "Testing the EpeakE iso relation for GRBs detected by Swift and Suzaku-WAM," *Astrophysical Journal Letters*, vol. 704, no. 2, pp. 1405–1432, 2009.

[62] S. Sugita, K. Yamaoka, M. Ohno et al., "Suzaku-WAM, Konus-Wind, and Swift-BAT observations of prompt emission of the high-redshift GRB 050904," *Publications of the Astronomical Society of Japan*, vol. 61, no. 3, pp. 521–527, 2009.

[63] Y. Urata, K. Huang, M. Im et al., "*Swift* GRB GRB071010B: outlier of the E^{src}_{peak}–E_{γ} and E_{iso}–E^{src}_{peak}–t^{src}_{jet} correlations," *The Astrophysical Journal*, vol. 706, no. 7, p. L183, 2009.

[64] Y. Urata, K. Huang, K. Yamaoka, P. P. Tsai, and M. S. Tashiro, "Energetic Fermi/LAT GRB100414A: energetic and correlations," *Astrophysical Journal Letters*, vol. 748, no. 1, article L4, 2012.

[65] O. Godet, G. Nasser, J. Atteia et al., "The X-/gamma-ray camera ECLAIRs for the gamma-ray burst mission SVOM," in *Space Telescopes and Instrumentation 2014: Ultraviolet to Gamma Ray*, vol. 9144 of *Proceedings of SPIE*, p. 914424, Montréal, Canada, July 2014.

[66] Y. Dong, B. Wu, Y. Li, Y. Zhang, and S. Zhang, "SVOM gamma ray monitor," *Science China Physics, Mechanics and Astronomy*, vol. 53, no. 1, supplement, pp. 40–42, 2010.

[67] Y. Shirasaki, N. Kawai, A. Yoshida et al., "Design and performance of the wide-field X-ray monitor on board the high-energy transient explorer 2," *Publications of the Astronomical Society of Japan*, vol. 55, pp. 1033–1049, 2003.

[68] S. R. Kulkarni, D. A. Frail, R. Sari et al., "Discovery of a radio flare from GRB 990123," *Astrophysical Journal Letters*, vol. 522, no. 2, pp. L97–L100, 1999.

[69] S. Kobayashi, "Light curves of gamma-ray burst optical flashes," *The Astrophysical Journal*, vol. 545, no. 2, pp. 807–812, 2000.

[70] B. Zhang, S. Kobayashi, and P. Mészáros, "Gamma-ray burst early optical afterglows: implications for the initial Lorentz factor and the central engine," *The Astrophysical Journal*, vol. 595, no. 2, pp. 950–954, 2003.

[71] A. Melandri, S. Kobayashi, C. G. Mundell et al., "GRB 090313 and the origin of optical peaks in gamma-ray burst light curves: implications for Lorentz factors and radio flares," *Astrophysical Journal Letters*, vol. 723, no. 2, pp. 1331–1342, 2010.

[72] S. Kobayashi, B. Zhang, P. Mészáros, and D. Burrows, "Inverse compton X-ray flare from gamma-ray burst reverse shock," *The Astrophysical Journal*, vol. 655, no. 1, p. 391, 2007.

[73] P. Veres, A. Corsi, D. A. Frail, S. B. Cenko, and D. A. Perley, "Early-time VLA observations and broad-band afterglow analysis of the Fermi-LAT detected GRB 130907A," http://arxiv.org/abs/1411.7368.

[74] Y. F. Huang, Z. G. Dai, and T. Lu, "Failed gamma-ray bursts and orphan afterglows," *Monthly Notices of the Royal Astronomical Society*, vol. 332, no. 3, pp. 735–740, 2002.

[75] R. Yamazaki, K. Ioka, and T. Nakamura, "X-ray flashes from off-axis gamma-ray bursts," *Astrophysical Journal Letters*, vol. 571, no. 1, pp. L31–L35, 2002.

[76] E. Nakar and T. Piran, "On-axis orphan afterglows," *New Astronomy*, vol. 8, no. 2, pp. 141–153, 2003.

[77] Y. Urata, K. Huang, R. Yamazaki, and T. Sakamoto, "Extremely soft X-ray flash as the indicator of off-axis orphan GRB afterglow," *The Astrophysical Journal*. In press.

[78] R. Sari, T. Piran, and J. P. Halpern, "Jets in gamma-ray bursts," *Astrophysical Journal Letters*, vol. 519, no. 1, pp. L17–L20, 1999.

[79] H. Gao, W.-H. Lei, Y.-C. Zou, X.-F. Wu, and B. Zhang, "A complete reference of the analytical synchrotron external shock models of gamma-ray bursts," *New Astronomy Reviews*, vol. 57, no. 6, pp. 141–190, 2013.

[80] K. Y. Huang, Y. Urata, A. V. Filippenko et al., "Optical afterglow observations of the unusual short-duration gamma-ray burst GRB 040924," *Astrophysical Journal Letters*, vol. 628, no. 2, pp. L93–L96, 2005.

[81] I. Lee, M. Im, and Y. Urata, "First Korean observations of gamma-ray burst afterglows AT MT. Lemmon optical astronomy observatory (LOAO)," *Journal of the Korean Astronomical Society*, vol. 43, no. 3, pp. 95–104, 2010.

[82] Y. Urata, S. Nishiura, T. Miyata et al., "Multiband optical follow-up observations of GRB 020813 at the Kiso and Bisei observatories," *The Astrophysical Journal*, vol. 595, no. 1, pp. L21–L24, 2003.

[83] R. S. De Souza, N. Yoshida, and K. Ioka, "Populations III.1 and III.2 gamma-ray bursts: constraints on the event rate for future radio and X-ray surveys," *Astronomy and Astrophysics*, vol. 533, article A32, 2011.

[84] H. Nagakura, Y. Suwa, and K. Ioka, "Population III gamma-ray bursts and breakout criteria for accretion-powered jets," *The Astrophysical Journal*, vol. 754, no. 2, article 85, 2012.

[85] D. Nakauchi, Y. Suwa, T. Sakamoto, K. Kashiyama, and T. Nakamura, "Long-duration X-ray flash and X-ray-rich gamma-ray bursts from low-mass population III stars," *Astrophysical Journal*, vol. 759, no. 2, article 9, 2012.

[86] S. Inoue, K. Omukai, and B. Ciardi, "The radio to infrared emission of very high redshift gamma-ray bursts: probing early star formation through molecular and atomic absorption lines," *Monthly Notices of the Royal Astronomical Society*, vol. 380, no. 4, pp. 1715–1728, 2007.

[87] D. Wanderman and T. Piran, "The luminosity function and the rate of Swift's gamma-ray bursts," *Monthly Notices of the Royal Astronomical Society*, vol. 406, no. 3, pp. 1944–1958, 2010.

[88] A. Cucchiara, A. J. Levan, D. B. Fox et al., "A photometric redshift of $z \sim 9.4$ for GRB 090429B," *The Astrophysical Journal*, vol. 736, no. 1, article 7, 2011.

[89] H. van Eerten, A. van der Horst, and A. MacFadyen, "Gamma-ray burst afterglow broadband fitting based directly on hydrodynamics simulations," *The Astrophysical Journal*, vol. 749, no. 1, article 44, 2012.

Hindawi Publishing Corporation
Advances in Astronomy
Volume 2015, Article ID 568516, 10 pages
http://dx.doi.org/10.1155/2015/568516

Review Article

Gamma-Ray Bursts as Multienergy Neutrino Sources

Katsuaki Asano[1] and Kohta Murase[2]

[1]*Institute for Cosmic Ray Research, The University of Tokyo, 5-1-5 Kashiwanoha, Kashiwa, Chiba 277-8582, Japan*
[2]*Institute for Advanced Study, Einstein Drive, Princeton, NJ 08540, USA*

Correspondence should be addressed to Katsuaki Asano; asanok@icrr.u-tokyo.ac.jp

Received 23 December 2014; Accepted 23 March 2015

Academic Editor: Valery Nakariakov

We review theoretical models for nonelectromagnetic emission, mainly neutrinos and cosmic rays, from gamma-ray bursts (GRBs). In various stages of the relativistic jet propagation, cosmic-ray ion acceleration and subsequent neutrino emission are expected. GRBs are popular candidate sources of the highest-energy cosmic rays, and their prompt phase has been most widely discussed. IceCube nondetection of PeV neutrinos coincident with GRBs has put interesting constraints on the standard theoretical prediction. The GRB-UHECR hypothesis can critically be tested by future observations. We also emphasize the importance of searches for GeV-TeV neutrinos, which are expected in the precursor/orphan or prompt phase, and lower-energy neutrinos would be more guaranteed and their detections even allow us to probe physics inside a progenitor star. Not only classical GRBs but also low-power GRBs and transrelativistic supernovae can be promising sources of TeV-PeV neutrinos, and we briefly discuss implications for the cumulative neutrino background discovered by IceCube.

1. Introduction

The most luminous explosions in the universe, gamma-ray bursts (GRBs), are characterized by nonthermal photon emission in both the prompt and afterglow phases. In such extreme phenomena, nonleptonic emissions, such as cosmic rays and neutrinos, have been suggested. Waxman [1] and Vietri [2] pointed out GRBs as possible sources of ultrahigh-energy cosmic rays (UHECRs). Then, associated neutrino emission was predicted [3, 4].

The GRB jets have several candidate sites where nonthermal particles are accelerated. First, the energetic jet launched from the central engine may generate a jet's head-cocoon structure (e.g., [5, 6]) in the progenitor star. Then, the shock wave reaches the stellar surface (shock breakout, e.g., [7–9], for the supernova case), and the jet propagates in the interstellar medium (ISM) or the wind material from the progenitor. In the classical internal shock model, the prompt gamma-ray emission is attributed to internal shocks due to the inhomogeneity in the jet or the temporal variability of the engine activity. At $\sim 10^{16}$–10^{17} cm from the central engine, the jet starts deceleration via interactions with the external medium. The external shock in this stage corresponds to the afterglow observed at optical, X, and radio wavelengths. In those various stages of the jet evolution, we can expect particle acceleration, which may result in not only photon emission but also neutrino and cosmic-ray emissions.

In this paper, we review studies on neutrino and cosmic-ray emission from GRBs. The multimessenger astronomy is an important subject, the present day is just at the dawn of neutrino astrophysics, since IceCube recently detected astrophysical neutrinos [10–13]. The detected PeV neutrino flux is compatible with various upper bounds based on the UHECR production rate [14–16], which may suggest some connection between UHECRs and PeV neutrinos. In the next decade, the connection between neutrinos and high-energy celestial objects may be revealed by not only IceCube but also other neutrino detectors [17–21].

GRBs will be detected with also gravitational wave (GW) detectors [22] such as aLIGO [23], aVirgo [24], and KAGRA [25]. The promising candidate of short GRB sources especially is a binary neutron star merger, which is the primary target for GW detectors. The recent claim of detection of a "kilonova," infrared transient about ~10 days after the burst, from short GRB 130603B [26] is encouragingly consistent with the binary merger models, in which r-process nuclei

produced in the neutron rich ejecta provide the infrared energy via their radioactive decays (e.g., [27, 28] and the references therein). Therefore, GW observations of GRBs will be one of the hottest research areas in the next decade. Taking into account qualitative difference between GW and neutrinos, we omit this topic in this paper. However, we should notice the importance of the future correlation study between GW and neutrino detectors (e.g., [29–33]).

2. GeV-TeV Neutrinos in the Precursor/Orphan Stage

In the most widely accepted scenario for long GRBs, a relativistic jet is launched from a black hole-accretion disk system in a core collapse of a massive star. Alternatively, the central engine may be a fast-rotating, highly magnetized neutron star. The classical fireball scenario [34] supposes that a radiation-dominated electron-positron pair plasma is formed just above the accretion disk. The accretion disk may emit copious thermal MeV neutrinos, which may generate the fireball via neutrino pair annihilation [35–37]. However, the contribution of the GRB thermal neutrinos would be negligible compared to the diffuse supernova neutrino background [38]. Here, we discuss high-energy neutrinos produced in the early stage of the fireball.

The bulk Lorentz factor of the fireball evolves with radius R as $\Gamma \sim R/R_0$, where R_0 is the initial size of the fireball. The acceleration saturates at $R \sim \eta R_0$, where $\eta \equiv (L_{\rm jet}/\dot{M}c^2)$. At the base of the fireball, a significant fraction of baryons may be in the form of neutrons. Initially p and n components are tightly coupled via nuclear elastic scattering with the cross-section of $\langle \sigma_{\rm el} v_{\rm rel} \rangle \sim \sigma_{\rm pp} c$, where the cross-section for pion production via pp-collision is $\sigma_{\rm pp} \sim 3 \times 10^{-26}$ cm^2. When the scattering timescale $(n'_p \langle \sigma_{\rm el} v_{\rm rel} \rangle)^{-1}$ becomes longer than the dynamical timescale $R/(c\Gamma)$, p and n components decouple. Defining the density ratio $f_n \equiv n'_n/n'_p$, the proton density in the comoving frame can be written as

$$n'_p = \frac{1}{1+f_n} \frac{\dot{M}}{4\pi R^2 m_p c \Gamma}. \quad (1)$$

If the decouple occurs during the acceleration period, only the p component can be accelerated by the radiation pressure. Then, the relative velocity between p and n flows can be high enough to produce pions via np collision. Then, we can expect neutrino emissions at an energy of a few GeV from pion and muon decays [39, 40]. If the decouple occurs later, internal shocks should also play a role in dissipation. If we adopt the Poynting flux dissipation model as an alternative acceleration mechanism, the jet may initially evolve as $\Gamma \sim (R/R_0)^{1/3}$ [41], depending on the dissipation mechanism. Koers and Giannios [42] and Gao and Mészáros [43] calculated the neutrino flux for such models.

This compound-flow model has been considered in the context of the photospheric scenario for prompt emission, in which the origin of gamma-ray photons is mainly thermal rather than synchrotron. The injection of secondary electron-positron pairs via inelastic np collisions leads to a nonthermal component in the photon spectrum [44]. Such models inevitably predict quasithermal neutrino emission in the 10–100 GeV range [45–47]. However, detecting neutrinos from a single GRB is challenging. Murase et al. [45] showed that ~10 yr stacking analyses will be needed to find quasithermal neutrino signatures (see Figure 1).

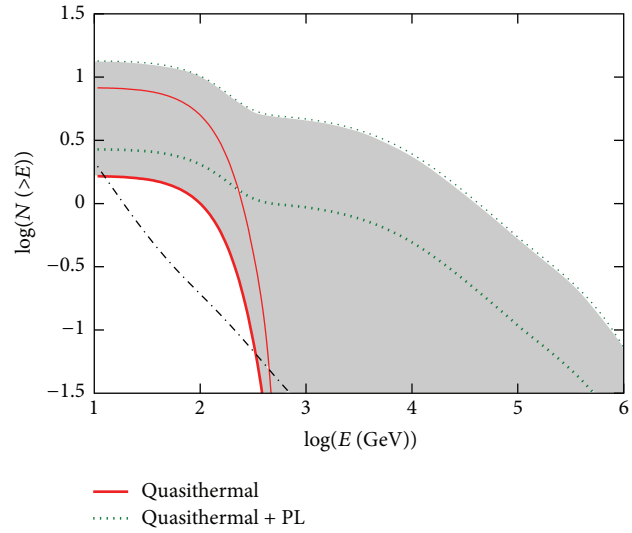

Figure 1: The expected number of subphotospheric $\nu_\mu + \bar{\nu}_\mu$ for 3250 GRB stacking analyses with DeepCore + IceCube from Murase et al. [45].

The jet inside a progenitor star can be the site where precursor and orphan neutrinos are produced [48–51]. A significant fraction of the jets originated from core collapse of massive stars may fail to break through the stellar envelope. The shock-accelerated protons can produce pions via interactions with thermal photons and thermal nucleons. If cosmic-ray acceleration occurs in the high density plasma, cooling effects of pions can strongly limit neutrino energies, and contributions from kaons can be dominant at higher energies [52–54]. Neutrinos from choked jets can also be expected for massive progenitors in the first generation of stars (Pop. III stars [55]).

However, particle acceleration postulated in choked jets and subphotospheric GRB emission models is inefficient in high-power jets [51]. The high radiation pressure inside the progenitors deforms the shock structure [56], where the shock transition layer becomes thicker than the collisionless mean-free path of particles, so that particles cannot be efficiently accelerated to very high energies. Murase and Ioka [51] derives radiation constraints on high-energy neutrino production, taking into account the fact that the jet is collimated and becomes cylindrical rather than conical. Although high-power GRB jets cannot be good neutrino emitters, interestingly, it is shown that low-power GRB jets are more promising sources of TeV neutrinos. Low-power jets are more difficult to penetrate the star, so that "choked jets" or "failed GRBs" may be better neutrino sources. If the fraction of the choked GRBs is high enough, this greatly enhances the neutrino background flux compared to the estimate according to only the observed GRB rate [51].

Then, can we still expect nonthermal neutrinos from high-power GRBs? An interesting idea to overcome this difficulty is to invoke the neutron-proton-converter (NPC) acceleration mechanism [57, 58], and Murase et al. [45] pointed out that this mechanism naturally occurs in GRB jets as long as neutrons are loaded. When compound flows cause internal shocks, neutrons from the upstream can easily cross the shock transition layer and may be converted again into protons in the downstream. Then, such protons are easily isotropized by magnetic fields, and some of them can go back to the upstream as neutrons. Kashiyama et al. [58] first performed numerical simulations and showed that a good fraction of the incoming neutron energy is converted into high-energy nucleons. Since the neutrino-nucleon cross-section increases as energy, the NPC acceleration mechanism enhances the detectability of neutrinos.

Detections of high-energy neutrinos produced in jets inside a star will bring to us precious information about the progenitor stars from the energy-dependent onset time of the neutrinos and cutoff energy in the neutrino spectrum [59]. One would be able to study neutrino oscillation including matter effects [60, 61], and flavor measurements could allow us to probe magnetic fields [62] or other new physics effects such as neutrino decay or quantum decoherence [63].

3. PeV Neutrinos and UHECRs in the Prompt Emission Stage

The internal shock in the prompt emission stage is one of the candidates of UHECR acceleration site. Using the conventional energy fraction parameters ϵ_e and ϵ_B, the magnetic field in the jet frame is written as

$$B' = \sqrt{\frac{2\epsilon_B L_\gamma}{\epsilon_e c R^2 \Gamma^2}} \sim 10^5 \left(\frac{\epsilon_e}{0.5}\right)^{-1/2} \left(\frac{\epsilon_B}{0.1}\right)^{1/2} \left(\frac{\Gamma}{300}\right)^{-1} \left(\frac{R}{10^{13}\,\mathrm{cm}}\right)^{-1} \cdot \left(\frac{L_\gamma}{10^{52}\,\mathrm{erg\,s^{-1}}}\right)^{1/2} \mathrm{G}. \quad (2)$$

Although synchrotron cooling often limits the maximum energy of accelerated protons, if not, equating the dynamical timescale and acceleration timescale $\xi\varepsilon_p'/ceB'$ leads to

$$\varepsilon_{p,\max} \sim 4\times 10^{20}\xi^{-1} \left(\frac{\epsilon_e}{0.5}\right)^{-1/2} \left(\frac{\epsilon_B}{0.1}\right)^{1/2} \left(\frac{\Gamma}{300}\right)^{-1} \cdot \left(\frac{L_\gamma}{10^{52}\,\mathrm{erg\,s^{-1}}}\right)^{1/2} \mathrm{eV}, \quad (3)$$

where $\xi > 1$ is the effective Bohm factor. According to the local GRB rate of 0.1–1 $\mathrm{Gpc^{-3}\,yr^{-1}}$ (e.g., [64]), the required energy of accelerated protons to explain local UHECR flux (integrated from the minimum proton energy to the maximum proton energy) is 10–100 times the gamma-ray energy released in the prompt phase (e.g., [65]). Although the GRB rate in our Galaxy may be very low, a possible past GRB could contribute to the observed flux and composition of cosmic rays [66, 67]. However, the required baryon loading factor has to be quite large.

If cosmological GRBs are sources of UHECRs, the arrival time is energy-dependent owing to intergalactic and galactic magnetic fields, so that individual sources could show a narrow spectral feature, depending on the apparent source number density [68–70]. Although a point source or striking anisotropy in the arrival directions of UHECRs has not been found yet [71], the UHECR constraints are still consistent with the GRB-UHECR scenario [70, 72].

Results of the Pierre Auger Collaboration claimed on depths of shower maximum for UHECRs suggest an increasing fraction of heavy nuclei [73, 74], while the data of the Telescope Array Team can still be interpreted as a proton dominated composition [75]. If the GRB jet is magnetically dominated, heavy nuclei may be synthesized because of its low entropy [76]. The survival of UHE nuclei in emission regions has been shown to be possible [65, 77, 78].

The timescale of photomeson production is calculated by

$$t_{p\gamma}'^{-1} = \frac{c}{2}\int d\varepsilon' \int_{-1}^{1} d\mu' \left(1-\mu'\right) n_\gamma'\left(\varepsilon'\right)\sigma_{p\gamma}K_{p\gamma}, \quad (4)$$

where μ is the cosine of the photon incident angle and $K_{p\gamma}$ is the proton inelasticity. If we adopt the rectangular approximation for pion production around the Δ-resonance (however see [79] for importance of multipion production), $\sigma_{p\gamma} \sim 5\times 10^{-28}\,\mathrm{cm^2}$ for 200 MeV $< \varepsilon'' <$ 400 MeV, where ε'' is the photon energy in the proton rest frame. the photomeson production efficiency $f_{p\gamma} \equiv t_{\mathrm{dyn}}'/t_{p\gamma}'$ is estimated to be

$$f_{p\gamma} \simeq \frac{2K_\Delta\sigma_\Delta}{1+\alpha}\frac{\Delta\bar{\varepsilon}_\Delta}{\bar{\varepsilon}_\Delta}\frac{L_\gamma^b}{4\pi R\Gamma^2 c\varepsilon_\gamma^b}\left(\frac{\varepsilon_p}{\varepsilon_p^b}\right)^{\beta-1}, \quad (5)$$

where $t_{\mathrm{dyn}}' \approx r/\Gamma_j c$ is the dynamical time, $K_\Delta \sim 0.2$, $\bar{\varepsilon}_\Delta \sim 0.3$ GeV, $\Delta\bar{\varepsilon}_\Delta \sim 0.2$ GeV, L_γ^b is the luminosity at ε_γ^b, β is the photon index, R is the emission radius, and Γ is the bulk Lorentz factor of jets. The typical neutrino energy is given by

$$\varepsilon_\nu^b \sim 0.02\Gamma_j^2 m_p c^2 \bar{\varepsilon}_\Delta \left[\varepsilon_\gamma^b\right]^{-1}. \quad (6)$$

For a low-energy portion ($\varepsilon_p < \varepsilon_p^b$), the photomeson production efficiency decreases as $t_{p\gamma}'^{-1} \propto \varepsilon_p'^{-(1+\beta)}$. For a high-energy portion, if $\beta \sim 1$, the timescale does not depend on proton energy.

The cumulative neutrino background intensity is obtained by integrating the comoving GRB rate, $R_{\mathrm{GRB}}(z)$, into (e.g., [80])

$$\Phi_\nu\left(E_\nu\right) = \frac{c}{4\pi}\int_0^{z_{\max}} dz\,(1+z)\,R_{\mathrm{GRB}}\left(z\right)N_\nu\left((1+z)\,E_\nu\right)\left|\frac{dt}{dz}\right|, \quad (7)$$

where

$$\left|\frac{dt}{dz}\right| = \frac{1}{(1+z)\,H_0\sqrt{\Omega_m\left(1+z\right)^3+\Omega_\Lambda}}, \quad (8)$$

and $N_\nu(\varepsilon_\nu)$ (neutrinos GeV^{-1}) is the average neutrino spectrum per burst.

Several authors have estimated the cumulative neutrino flux from GRBs [79, 81–87]. The IceCube Collaboration has put interesting constraints on theoretical predictions [88]. However, their theoretical model used for interpretations has several caveats that do not exist in earlier theoretical papers (e.g., [79, 86]). The predicted flux based on the original paper [4] is actually lower than that shown by Abbasi et al. [88]. Note that this difference does not arise from astrophysical uncertainty, so it should be properly taken into account [89–92]. As a result, only optimistic models such as the ones with large baryon loading factors have been ruled out by observations. Furthermore, nondetections of neutrinos from the nearby bright burst GRB 130427A [93] severely constrain the neutrino production efficiency [94].

In addition, several sophisticated developments have been made (e.g., [92, 95–100]). Asano and Mészáros [95] carried out time-dependent numerical simulations of hadronic cascades for a wide range of parameter sets, adopting the luminosity function in the work of Wanderman and Piran [64] and a log-normal distribution of variability timescale ($\delta t \sim R/\Gamma^2 c$). The diffuse neutrino intensity is well below the experimental limit by IceCube indicated by Abbasi et al. [88] (see Figure 2) and the latest result shown by Aartsen et al. [101], while UHECRs released by GRBs contribute to only above $10^{19.5}$ eV in this parameter set. The neutrino production efficiency should be suppressed by larger Γ or smaller f_p at least for bright GRBs. We should also notice that, depending on models, the neutrino intensity can be dominated by contributions from a few very bright GRBs, while most UHECRs are released from relatively less luminous GRBs. Bustamante et al. [97] performed simulations of internal shocks and first calculated neutrino, gamma-ray, and UHECR emission from multiple emission regions. They took into account all the detailed microphysics, including multipion production and neutrino mixing. They found that the neutrino emission is dominated by contributions around the photosphere, while UHECRs and gamma rays come from larger radii. Interestingly, it is shown that the minimum diffuse neutrino is pretty robust, which is $\sim 10^{-11}$ GeV cm^{-2} s^{-1} sr^{-1}. This implies that, in the internal shock model, the GRB-UHECR hypothesis can be more robustly tested by next-generation neutrino detectors.

Large nonthermal baryon loading factors have been challenged by gamma rays as well as neutrinos. If protons are efficiently accelerated in the prompt phase as assumed in the above models, electromagnetic cascades triggered by pionic gamma rays and/or proton synchrotron emission may generate GeV-TeV photons [102–108]. Actually *Fermi* has found extra spectral components in the GeV energy range, which are possible signatures of the hadronic cascades [109–112]. However, other interpretations exist, including leptonic models [113–117] and early afterglow models [118–120]. In hadronic models, the required energy of protons to agree with the observed GeV flux is 10–100 times the gamma-ray energy itself [121–123], which is consistent with the GRB-UHECR scenario. If all GRBs have such a large proton luminosity,

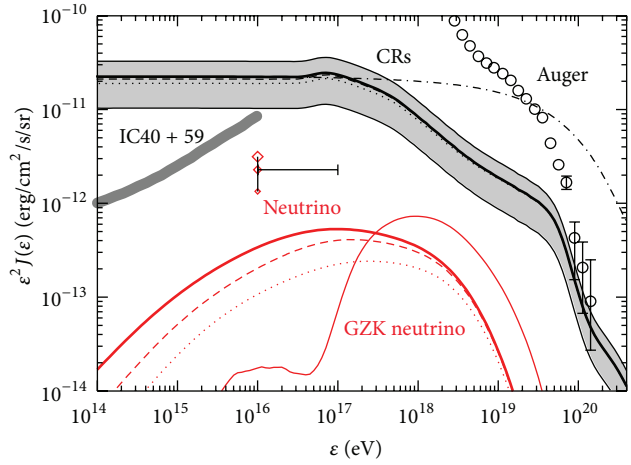

Figure 2: CR (black) and neutrino diffuse intensities in the model calculation in the work of Asano and Mészáros [95].

hadronic cascade emission should overwhelm the original leptonic component and distort the gamma-ray spectrum [124]. Most GRBs do not have strong evidence of the extra spectral components in the GeV range [125, 126], which implies that the neutrino production efficiency should not be high either [127].

There are alternative models of the prompt emission, in which hadronic cascades play a crucial role. The leptonic stochastic acceleration model (e.g., [128]) assumes a narrow energy distribution of electrons due to the balance of acceleration and cooling. While such an energy distribution can naturally reproduce the hard spectral index in the low-energy portion, a high-energy component is needed to be explained. Murase et al. [129] considered hadronic cascade processes as an efficient electron injection mechanism, and the synchrotron spectrum is shown to be very hard. The combination of thermal and synchrotron spectra can explain spectra of various GRBs. In the model of Petropoulou et al. [130], the secondary photons produced via hadronic cascades are scattered by secondary electron-positron pairs. This comptonization makes a band-like spectrum. Such models always accompany some neutrino emission, so that constraints by IceCube should be taken into account.

Although the internal shock model can reproduce the observed light curves and gamma-ray spectra qualitatively, there are several quantitative difficulties such as the emission efficiency, low-energy spectral index, and the narrow distribution of the spectral peak energies. An alternative model is the dissipative photosphere model [44, 47, 131–135], in which some fraction of the jet energy is dissipated into nonthermal electrons near the photosphere. In such models, the dissipation radius, where particle acceleration is expected, is much smaller than that in the internal shock model. As a result, the $p\gamma$ and pp efficiency becomes higher, while the cooling effect on pions/muons softens the neutrino spectrum [136, 137]. For Poynting flux dominated jets, they have a relatively larger photosphere and magnetic field. Such differences in model characteristics lead to some variety in neutrino spectra [65, 91, 138, 139].

TeV gamma-ray observations in the CTA era will also be relevant. If CTA detects a GRB, its huge photon statistics provide dedicated light curves. The correlation study between TeV and MeV light curves allows us to determine the emission mechanism of GeV-TeV photons. If the GeV-TeV photons are secondary photons from hadronic cascades, GeV-TeV light curves will correlate with MeV gamma-ray variability but would show broader pulse profiles reflecting the longer timescale of the photomeson production than the electron cooling [140].

The dominant contributions to the UHECRs and cumulative neutrino background may come from another population of GRBs, such as low-luminosity GRBs (LL GRBs [142–144]). Though the gamma-ray energy, $E_{\rm iso} \lesssim 10^{51}$ erg, is much lower, its higher event rate makes LL GRBs candidate sources of UHECRs and neutrinos [65, 141, 145, 146]. As shown in Figure 3, one of the model spectra in the works of Murase et al. [141] and Murase and Ioka [51] is interestingly close to the observed diffuse PeV neutrino intensity ($\sim 10^{-8}$ GeV cm^{-2} s^{-1} sr^{-1} [11]).

So far, all LL GRBs are accompanied by broad-line-type Ic supernovae with mildly relativistic ejecta [147, 148]. The UHECR production and neutrinos from such a mildly relativistic shock [65, 149] and shock breakout [58] have been discussed as well. The shock breakout model of Kashiyama et al. [58] predicts TeV gamma rays as well as high-energy neutrinos, so future TeV gamma-ray observations such as CTA will be important although the detection possibility with CTA may be <~0.1 yr^{-1} [150, 151].

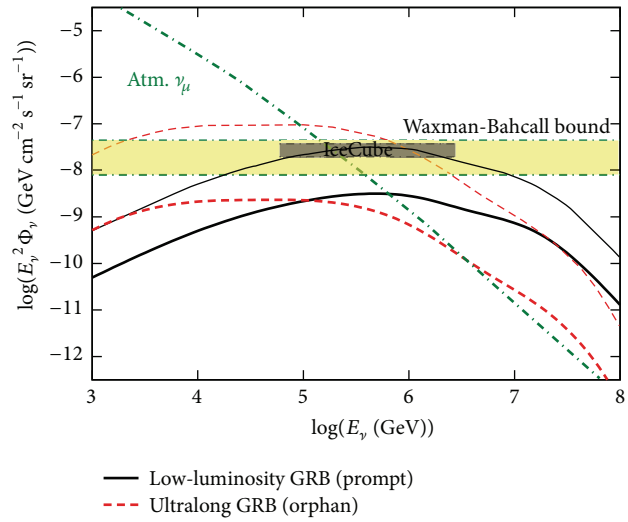

Figure 3: The neutrino background from LL GRBs in the works of Murase et al. [141] and Murase and Ioka [51]. The optimistic case agrees with the observed neutrino intensity reported by Aartsen et al. [11].

4. EeV Neutrinos and UHECRs in the Afterglow Phase

Afterglow emission is caused by external shocks propagating the ISM or wind material. The external-forward shock has been considered as the site of UHECR and EeV neutrino production [152–154]. The long-lasting GeV emissions from several GRBs detected with *Fermi* can be interpreted as afterglows [118, 119], in which a significant fraction of the bulk energy is dissipated into electrons, unless only a fraction of the particles are injected into nonthermal acceleration. Note that the spectral peak is in the EeV range; this model cannot explain the cumulative neutrino background detected by IceCube. We should also notice the theoretical difficulty of particle acceleration to ultrahigh energies at the forward shock (see, e.g., [155] and the references therein). The relativistic shock often becomes superluminal, where particle acceleration is inefficient at very high energies. It has been thought that UHECRs cannot be generated by the shock acceleration mechanism at the forward shock, but other possibilities such as stochastic acceleration have also been invoked [152].

On the other hand, the external-reverse shock has been one of the good sites of UHECR production and EeV neutrino production, since it is mildly relativistic or nonrelativistic [156]. The low photon density in the afterglow phase typically implies a moderate efficiency of photomeson production. The afterglow picture is now rich in the *Swift* era, and

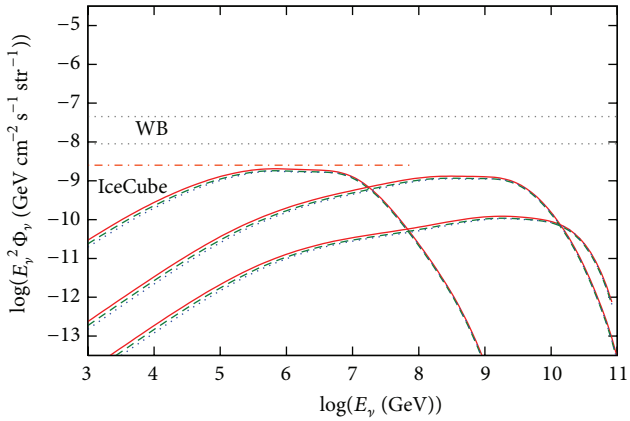

Figure 4: Afterglow neutrino fluxes shown by Murase [80].

many models have been proposed. UHECRs accelerated at the reverse shock can interact with photons produced by both forward and reverse shocks. Murase [80] investigated various possibilities and showed that it is possible to detect EeV neutrinos by next-generation neutrino detectors such as Askaryan Radio Array (see Figure 4).

In addition, afterglow emission may include components coming from internal dissipation. A famous example is X-ray flare emission. Although high-energy gamma-ray emission from flares is typically discussed in view of leptonic models [157], it is possible to expect hadronic emission as well [158]. Since the photomeson production efficiency is likely to be higher than that in the prompt phase, neutrinos coincident with flares and afterglow emission (caused by internal dissipation) can be as much important as prompt neutrino emission [80, 158].

5. Summary

The multimessenger era of GRBs is now coming. In particular, the IceCube Collaboration has discovered high-energy neutrinos, and neutrino astrophysics has now started. Although GRB neutrinos have not been found yet, detecting GRB neutrinos is still one of the appealing possibilities to identify neutrino sources. Even with nondetections, the latest constraints are important to test the connection between GRBs and UHECRs. Gamma-ray observations by *Fermi* have also provided complementary information, and CTA may enable us to detect TeV gamma rays from GRBs with high statistics.

CTA should also be powerful to study afterglow mechanisms. So far, there has been no indication of hadronic emission in the afterglow phase, but it is possible to expect associated UHECR and EeV neutrino emission. Searches for extremely high-energy neutrinos from afterglows will also be improved in the future; next-generation detectors such as Askaryan Radio Array may enable us to test the GRB-UHECR hypothesis even in afterglow models.

In addition, GeV-TeV neutrino detections are also promising, and analyses for such low-energy neutrinos from choked jets and GRBs before jet breakouts should be important to reveal the jet physics and relationship between GRBs and supernovae. In this case, gamma rays cannot escape directly, so neutrinos provide us with a unique opportunity.

Conflict of Interests

The authors declare that there is no conflict of interests regarding the publication of this paper.

Acknowledgment

This paper is partially supported by Grants-in-Aid for Scientific Research no. 25400227 from the Ministry of Education, Culture, Sports, Science and Technology (MEXT) of Japan.

References

[1] E. Waxman, "Cosmological Gamma-Ray Bursts and the Highest Energy Cosmic Rays," *Physical Review Letters*, vol. 75, no. 3, pp. 386–389, 1995.

[2] M. Vietri, "The acceleration of ultra-high-energy cosmic rays in gamma-ray bursts," *Astrophysical Journal Letters*, vol. 453, no. 2, pp. 883–889, 1995.

[3] B. Paczynski and G. Xu, "Neutrino bursts from gamma-ray bursts," *The Astrophysical Journal*, vol. 427, no. 2, pp. 708–713, 1994.

[4] E. Waxman and J. Bahcall, "High energy neutrinos from cosmological gamma-ray burst fireballs," *Physical Review Letters*, vol. 78, no. 12, pp. 2292–2295, 1997.

[5] C. D. Matzner, "Supernova hosts for gamma-ray burst jets: dynamical constraints," *Monthly Notices of the Royal Astronomical Society*, vol. 345, no. 2, pp. 575–589, 2003.

[6] O. Bromberg, E. Nakar, T. Piran, and R. Sari, "The propagation of relativistic jets in external media," *Astrophysical Journal*, vol. 740, no. 2, article 100, 2011.

[7] S. A. Colgate, "The prompt effects of supernovae," *Annals of the New York Academy of Sciences*, vol. 262, pp. 34–46, 1975.

[8] R. I. Klein and R. A. Chevalier, "X-ray bursts from type II supernovae," *The Astrophysical Journal*, vol. 223, pp. L109–L112, 1978.

[9] A. M. Soderberg, E. Berger, K. L. Page et al., "An extremely luminous X-ray outburst at the birth of a supernova," *Nature*, vol. 453, no. 7194, pp. 469–474, 2008.

[10] M. G. Aartsen, R. Abbasi, Y. Abdou et al., "First observation of PeV-energy neutrinos with IceCube," *Physical Review Letters*, vol. 111, Article ID 021103, 2013.

[11] M. G. Aartsen, R. Abbasi, and Y. Abdou, "Evidence for high-energy extraterrestrial neutrinos at the IceCube detector," *Science*, vol. 342, no. 6161, Article ID 1242856, 2013.

[12] M. G. Aartsen, M. Ackermann, J. Adams et al., "Observation of high-energy astrophysical neutrinos in three years of icecube data," *Physical Review Letters*, vol. 113, Article ID 101101, 2014.

[13] M. Aartsen, R. Abbasi, M. Ackermann et al., "Search for a diffuse flux of astrophysical muon neutrinos with the IceCube 59-string configuration," *Physical Review D*, vol. 89, no. 6, Article ID 062007, 19 pages, 2007.

[14] E. Waxman and J. Bahcall, "High energy neutrinos from astrophysical sources: an upper bound," *Physical Review D*, vol. 59, no. 2, Article ID 023002, 8 pages, 1998.

[15] K. Mannheim, R. J. Protheroe, and J. P. Rachen, "Cosmic ray bound for models of extragalactic neutrino production," *Physical Review D*, vol. 63, no. 2, Article ID 023003, 2001.

[16] K. Murase and J. F. Beacom, "Neutrino background flux from sources of ultrahigh-energy cosmic-ray nuclei," *Physical Review D*, vol. 81, Article ID 123001, 2010.

[17] U. F. Katz, "KM3NeT: towards a km3 Mediterranean neutrino telescope," *Nuclear Instruments and Methods in Physics Research A: Accelerators, Spectrometers, Detectors and Associated Equipment*, vol. 567, no. 2, pp. 457–461, 2006.

[18] P. Allison, J. Auffenberg, R. Bard et al., "Design and initial performance of the Askaryan radio array prototype EeV neutrino detector at the south pole," *Astroparticle Physics*, vol. 35, no. 7, pp. 457–477, 2012.

[19] S. W. Barwick, "ARIANNA: a new concept for UHE neutrino detection," *Journal of Physics: Conference Series*, vol. 60, pp. 276–283, 2007.

[20] P. W. Gorham, P. Allison, S. W. Barwick et al., "The antarctic impulsive transient antenna ultra-high energy neutrino detector: design, performance, and sensitivity for the 2006-2007 balloon flight," *Astroparticle Physics*, vol. 32, no. 1, pp. 10–41, 2009.

[21] P. W. Gorham, F. E. Baginski, P. Allison et al., "The ExaVolt antenna: a large-aperture, balloon-embedded antenna for ultra-high energy particle detection," *Astroparticle Physics*, vol. 35, no. 5, pp. 242–256, 2011.

[22] I. Bartos, P. Brady, and S. Márka, "How gravitational-wave observations can shape the gamma-ray burst paradigm," *Classical and Quantum Gravity*, vol. 30, no. 12, Article ID 123001, 2013.

[23] G. M. Harry, "Advanced LIGO: the next generation of gravitational wave detectors," *Classical and Quantum Gravity*, vol. 27, Article ID 084006, 2010.

[24] F. Acernese, M. Agathos, K. Agatsuma et al., "Advanced virgo: a 2nd generation interferometric gravitational wave detector," *Classical and Quantum Gravity*, vol. 32, no. 2, Article ID 024001, 2014.

[25] K. Somiya, "Detector configuration of KAGRA—the Japanese cryogenic gravitational-wave detector," *Classical and Quantum Gravity*, vol. 29, no. 12, Article ID 124007, 2012.

[26] N. R. Tanvir, A. J. Levan, A. S. Fruchter et al., "A 'kilonova' associated with the short-duration γ-ray burst GRB 130603B," *Nature*, vol. 500, no. 7464, pp. 547–549, 2013.

[27] L.-X. Li and B. Paczynski, "Transient events from neutron star mergers," *The Astrophysical Journal*, vol. 507, no. 1, p. L59, 1998.

[28] K. Hotokezaka, K. Kyutoku, M. Tanaka et al., "Progenitor models of the electromagnetic transient associated with the short gamma ray burst 130603B," *The Astrophysical Journal*, vol. 778, no. 1, article L16, 2013.

[29] V. van Elewyck, S. Ando, B. Baret et al., "Joint searches between gravitational-wave interferometers and high-energy neutrino telescopes: science reach and analysis strategies," *International Journal of Modern Physics D*, vol. 18, no. 10, p. 1655, 2009.

[30] I. Bartos, C. Finley, A. Corsi, and S. Márka, "Observational constraints on multimessenger sources of gravitational waves and high-energy neutrinos," *Physical Review Letters*, vol. 107, no. 4, Article ID 251101, 2011.

[31] B. Baret, I. Bartos, B. Bouhou et al., "Multimessenger science reach and analysis method for common sources of gravitational waves and high-energy neutrinos," *Physical Review D*, vol. 85, Article ID 103004, 2012.

[32] S. Ando, B. Baret, I. Bartos et al., "*Colloquium*: multimessenger astronomy with gravitational waves and high-energy neutrinos," *Reviews of Modern Physics*, vol. 85, no. 4, pp. 1401–1420, 2013.

[33] S. Adrián-Martínez, I. Al Samarai, A. Albert et al., "A first search for coincident gravitational waves and high energy neutrinos using LIGO, virgo and ANTARES data from 2007," http://arxiv.org/abs/1205.3018.

[34] M. J. Rees and P. Mészáros, "Relativistic fireballs: energy conversion and time-scales," *Monthly Notices of the Royal Astronomical Society*, vol. 258, article 41P, 1992.

[35] D. Eichler, M. Livio, T. Piran, and D. N. Schramm, "Nucleosynthesis, neutrino bursts and γ-rays from coalescing neutron stars," *Nature*, vol. 340, no. 6229, pp. 126–128, 1989.

[36] K. Asano and T. Fukuyama, "Relativistic effects on neutrino pair annihilation above a Kerr black holewith the accretion disk," *The Astrophysical Journal*, vol. 546, no. 2, pp. 1019–1026, 2001.

[37] I. Zalama and A. M. Beloborodov, "Neutrino heating near hyper-accreting black holes," *Monthly Notices of the Royal Astronomical Society*, vol. 410, no. 4, pp. 2302–2308, 2011.

[38] J. F. Beacom, "The diffuse supernova neutrino background," *Annual Review of Nuclear and Particle Science*, vol. 60, no. 1, pp. 439–462, 2010.

[39] J. N. Bahcall and P. Mészáros, "5–10 GeV neutrinos from gamma-ray burst fireballs," *Physical Review Letters*, vol. 85, no. 7, pp. 1362–1365, 2000.

[40] M. J. Rees and P. Mészáros, "Dissipative photosphere models of gamma-ray bursts and X-ray flashes," *The Astrophysical Journal*, vol. 628, no. 2, p. 847, 2005.

[41] G. Drenkhahn, "Acceleration of GRB outflows by Poynting flux dissipation," *Astronomy and Astrophysics*, vol. 387, no. 2, pp. 714–724, 2002.

[42] H. B. J. Koers and D. Giannios, "Neutron-rich gamma-ray burst flows: dynamics and particle creation in neutron-proton collisions," *Astronomy & Astrophysics*, vol. 471, no. 2, pp. 395–408, 2007.

[43] S. Gao and P. Mészáros, "Multi-GeV neutrino emission from magnetized gamma-ray bursts," *Physical Review D*, vol. 85, Article ID 103009, 2012.

[44] A. M. Beloborodov, "Collisional mechanism for gamma-ray burst emission," *Monthly Notices of the Royal Astronomical Society*, vol. 407, no. 2, pp. 1033–1047, 2010.

[45] K. Murase, K. Kashiyama, and P. Mészáros, "Subphotospheric neutrinos from gamma-ray bursts: the role of neutrons," *Physical Review Letters*, vol. 111, no. 13, Article ID 131102, 2013.

[46] I. Bartos, A. M. Beloborodov, K. Hurley, and S. Márka, "Detection prospects for GeV neutrinos from collisionally heated gamma-ray bursts with IceCube/DeepCore," *Physical Review Letters*, vol. 110, no. 24, 2013.

[47] K. Asano and P. Mészáros, "Photon and neutrino spectra of time-dependent photospheric models of gamma-ray bursts," *Journal of Cosmology and Astroparticle Physics*, vol. 2013, no. 9, article 008, 2013.

[48] P. Mészáros and E. Waxman, "TeV neutrinos from successful and choked gamma-ray bursts," *Physical Review Letters*, vol. 87, Article ID 171102, 2001.

[49] S. Razzaque, P. Mészáros, and E. Waxman, "Neutrino tomography of gamma ray bursts and massive stellar collapses," *Physical Review D*, vol. 68, Article ID 083001, 2003.

[50] S. Razzaque, P. Mészáros, and E. Waxman, "TeV neutrinos from core collapse supernovae and hypernovae," *Physical Review Letters*, vol. 93, no. 18, Article ID 181101, 4 pages, 2004.

[51] K. Murase and K. Ioka, "TeV-PeV neutrinos from low-power gamma-ray burst jets inside stars," *Physical Review Letters*, vol. 111, Article ID 121102, 2013.

[52] S. Ando and J. F. Beacom, "Revealing the supernova-gamma-ray burst connection with TeV neutrinos," *Physical Review Letters*, vol. 95, Article ID 061103, 2005.

[53] S. Horiuchi and S. Ando, "High-energy neutrinos from reverse shocks in choked and successful relativistic jets," *Physical Review D*, vol. 77, Article ID 063007, 2008.

[54] R. Enberg, M. H. Reno, and I. Sarcevic, "High energy neutrinos from charm in astrophysical sources," *Physical Review D*, vol. 79, no. 5, Article ID 053006, 6 pages, 2009.

[55] F. Iocco, K. Murase, S. Nagataki, and P. D. Serpico, "High-energy neutrino signals from the epoch of reionization," *The Astrophysical Journal*, vol. 675, no. 2, pp. 937–945, 2008.

[56] A. Levinson and O. Bromberg, "Relativistic photon mediated shocks," *Physical Review Letters*, vol. 100, Article ID 131101, 2008.

[57] E. V. Derishev, F. A. Aharonian, and V. V. Kocharovsky, "Particle acceleration through multiple conversions from a charged into a neutral state and back," *Physical Review D*, vol. 68, no. 4, Article ID 043003, 2003.

[58] K. Kashiyama, K. Murase, and P. Mészáros, "Neutron-proton-conversion acceleration at subphotospheres of relativistic outflows," *Physical Review Letters*, vol. 111, Article ID 131103, 2011.

[59] I. Bartos, B. Dasgupta, and S. Márka, "Probing the structure of jet-driven core-collapse supernova and long gamma-ray burst progenitors with high-energy neutrinos," *Physical Review D*, vol. 86, Article ID 083007, 2012.

[60] O. Mena, I. Mocioiu, and S. Razzaque, "Oscillation effects on high-energy neutrino fluxes from astrophysical hidden sources," *Physical Review D*, vol. 75, Article ID 063003, 2007.

[61] S. Razzaque and A. Y. Smirnov, "Flavor conversion of cosmic neutrinos from hidden jets," *Journal of High Energy Physics*, vol. 2010, no. 3, article 31, 2010.

[62] Y. Farzan and A. Y. Smirnov, "Coherence and oscillations of cosmic neutrinos," *Nuclear Physics B*, vol. 805, no. 1-2, pp. 356–376, 2008.

[63] P. Mehta and W. Winter, "Interplay of energy dependent astrophysical neutrino flavor ratios and new physics effects," *Journal of Cosmology and Astroparticle Physics*, vol. 2011, no. 3, article 41, 2011.

[64] D. Wanderman and T. Piran, "The luminosity function and the rate of Swift's gamma-ray bursts," *Monthly Notices of the Royal Astronomical Society*, vol. 406, no. 3, pp. 1944–1958, 2010.

[65] K. Murase, K. Ioka, S. Nagataki, and T. Nakamura, "High-energy cosmic-ray nuclei from high- and low-luminosity gamma-ray bursts and implications for multimessenger astronomy," *Physical Review D*, vol. 78, Article ID 023005, 2008.

[66] S. D. Wick, C. D. Dermer, and A. Atoyan, "High-energy cosmic rays from gamma-ray bursts," *Astroparticle Physics*, vol. 21, no. 2, pp. 125–148, 2004.

[67] A. Calvez, A. Kusenko, and S. Nagataki, "Role of galactic sources and magnetic fields in forming the observed energy-dependent composition of ultrahigh-energy cosmic rays," *Physical Review Letters*, vol. 105, Article ID 091101, 2010.

[68] J. Miralda-Escudé and E. Waxman, "Signatures of the origin of high-energy cosmic rays in cosmological gamma-ray bursts," *Astrophysical Journal Letters*, vol. 462, no. 2, pp. L59–L62, 1996.

[69] E. Waxman and J. Miralda-Escudé, "Images of bursting sources of high-energy cosmic rays: effects of magnetic fields," *Astrophysical Journal Letters*, vol. 472, no. 2, pp. L89–L92, 1996.

[70] H. Takami and K. Murase, "The role of structured magnetic fields on constraining properties of transient sources of ultra-high-energy cosmic rays," *The Astrophysical Journal*, vol. 748, no. 1, p. 9, 2012.

[71] A. Aab, P. Abreu, M. Aglietta et al., "Searches for anisotropies in the arrival directions of the highest energy cosmic rays detected by the Pierre Auger observatory," http://jp.arxiv.org/pdf/1411.6111v2.

[72] K. Murase and H. Takami, "Implications of ultra-high-energy cosmic rays for transient sources in the auger era," *The Astrophysical Journal Letters*, vol. 690, no. 1, pp. L14–L17, 2009.

[73] A. Aab, P. Abreu, M. Aglietta et al., "Depth of maximum of air-shower profiles at the Pierre Auger observatory. I. Measurements at energies above $10^{17.8}$ eV," *Physical Review D*, vol. 90, Article ID 122005, 2014.

[74] A. Aab, P. Abreu, M. Aglietta et al., "Depth of maximum of air-shower profiles at the Pierre Auger observatory. I. Measurements at energies above $10^{17.8}$ eV," *Physical Review D*, vol. 90, no. 12, Article ID 122005, 25 pages, 2014.

[75] R. U. Abbasi, M. Abe, T. Abu-Zayyad et al., "Study of ultra-high energy cosmic ray composition using telescope array's middle drum detector and surface array in hybrid mode," *Astroparticle Physics*, vol. 64, pp. 49–62, 2015.

[76] B. D. Metzger, D. Giannios, and S. Horiuchi, "Heavy nuclei synthesized in gamma-ray burst outflows as the source of ultrahigh energy cosmic rays," *Monthly Notices of the Royal Astronomical Society*, vol. 415, no. 3, pp. 2495–2504, 2011.

[77] X.-Y. Wang, S. Razzaque, and P. Mészáros, "On the origin and survival of ultra-high-energy cosmic-ray nuclei in gamma-ray bursts and hypernovae," *The Astrophysical Journal*, vol. 677, no. 1, pp. 432–440, 2008.

[78] S. Horiuchi, K. Murase, K. Ioka, and P. Mészáros, "The survival of nuclei in jets associated with core-collapse supernovae and gamma-ray bursts," *The Astrophysical Journal*, vol. 753, no. 1, p. 69, 2012.

[79] K. Murase and S. Nagataki, "High energy neutrino emission and neutrino background from gamma-ray bursts in the internal shock model," *Physical Review D*, vol. 73, no. 6, Article ID 063002, 14 pages, 2006.

[80] K. Murase, "High energy neutrino early afterglows from gamma-ray bursts revisited," *Physical Review D*, vol. 76, Article ID 123001, 2007.

[81] J. P. Rachen and P. Mészáros, "Photohadronic neutrinos from transients in astrophysical sources," *Physical Review D*, vol. 58, Article ID 123005, 1998.

[82] C. D. Dermer and A. Atoyan, "High-energy neutrinos from gamma ray bursts," *Physical Review Letters*, vol. 91, Article ID 071102, 2011.

[83] D. Guetta, D. Hooper, J. Alvarez-Muñiz, F. Halzen, and E. Reuveni, "Neutrinos from individual gamma-ray bursts in the BATSE catalog," *Astroparticle Physics*, vol. 20, no. 4, pp. 429–455, 2004.

[84] K. Asano, "Cooling of accelerated nucleons and neutrino emission in gamma-ray bursts," *Astrophysical Journal Letters*, vol. 623, no. 2, pp. 967–972, 2005.

[85] K. Asano and S. Nagataki, "Very high energy neutrinos originating from Kaons in gamma-ray bursts," *The Astrophysical Journal Letters*, vol. 640, no. 1, p. L9, 2006.

[86] P. Baerwald, S. Hummer, and W. Winter, "Magnetic field and flavor effects on the gamma-ray burst neutrino flux," *Physical Review D*, vol. 83, Article ID 067303, 2011.

[87] M. Ahlers, M. C. Gonzalez-Garcia, and F. Halzen, "GRBs on probation: testing the UHE CR paradigm with IceCube," *Astroparticle Physics*, vol. 35, no. 2, pp. 87–94, 2011.

[88] R. Abbasi, Y. Abdou, T. Abu-Zayyad et al., "An absence of neutrinos associated with cosmic-ray acceleration in γ-ray bursts," *Nature*, vol. 484, pp. 351–354, 2012.

[89] Z. Li, "Note on the normalization of predicted gamma-ray burst neutrino flux," *Physical Review D*, vol. 85, no. 2, Article ID 027301, 3 pages, 2012.

[90] S. Hümmer, P. Baerwald, and W. Winter, "Neutrino emission from gamma-ray burst fireballs, revised," *Physical Review Letters*, vol. 108, no. 23, Article ID 231101, 5 pages, 2012.

[91] H.-N. He, R.-Y. Liu, X.-Y. Wang, S. Nagataki, K. Murase, and Z.-G. Dai, "Icecube nondetection of gamma-ray bursts: constraints on the fireball properties," *Astrophysical Journal*, vol. 752, no. 1, article 29, 2012.

[92] R.-Y. Liu and X.-Y. Wang, "Diffuse PeV neutrinos from gamma-ray bursts," *The Astrophysical Journal*, vol. 766, no. 2, article 73, 2013.

[93] M. Ackermann, M. Ajello, K. Asano et al., "Fermi-LAT observations of the gamma-ray burst GRB 130427A," *Science*, vol. 343, no. 6166, pp. 42–47, 2013.

[94] S. Gao, K. Kashiyama, and P. Mészáros, "On the neutrino non-detection of GRB 130427A," *Astrophysical Journal Letters*, vol. 772, no. 1, article L4, 2013.

[95] K. Asano and P. Mészáros, "Neutrino and cosmic-ray release from gamma-ray bursts: time-dependent simulations," *The Astrophysical Journal*, vol. 785, no. 1, p. 54, 2014.

[96] P. Baerwald, M. Bustamante, and W. Winter, "Are gamma-ray bursts the sources of ultra-high energy cosmic rays?" *Astroparticle Physics*, vol. 62, p. 66, 2015.

[97] M. Bustamante, P. Baerwald, K. Murase, and W. Winter, "Neutrino and cosmic-ray emission from multiple internal shocks in gamma-ray bursts," http://arxiv.org/abs/1409.2874.

[98] W. Winter, J. B. Tjus, and S. R. Klein, "Impact of secondary acceleration on the neutrino spectra in gamma-ray bursts," *Astronomy & Astrophysics*, vol. 569, article A58, 11 pages, 2014.

[99] M. Petropoulou, D. Giannios, and S. Dimitrakoudis, "Implications of a PeV neutrino spectral cut-off in gamma-ray burst models," *Monthly Notices of the Royal Astronomical Society*, vol. 445, no. 1, pp. 570–580, 2014.

[100] N. Globus, D. Allard, R. Mochkovitch, and E. Parizot, "UHECR acceleration at GRB internal shocks," http://arxiv.org/abs/1409.1271.

[101] M. G. Aartsen, M. Ackermann, J. Adams et al., "Search for prompt neutrino emission from gamma-ray bursts with IceCube," http://arxiv.org/abs/1412.6510.

[102] M. Vietri, "GeV photons from ultrahigh energy cosmic rays accelerated in gamma ray bursts," *Physical Review Letters*, vol. 78, no. 23, pp. 4328–4331, 1997.

[103] M. Bottcher and C. D. Dermer, "High-energy gamma rays from ultra-high-energy cosmic-ray protons in gamma-ray bursts," *The Astrophysical Journal*, vol. 499, no. 2, article L131, 1998.

[104] T. Totani, "TeV burst of gamma-ray bursts and ultra-high-energy cosmic rays," *The Astrophysical Journal*, vol. 509, no. 2, pp. L81–L84, 1998.

[105] K. Asano and F. Takahara, "Photon emission in a cascade from relativistic protons initiated by residual thermal photons in gamma-ray bursts," *Publications of the Astronomical Society of Japan*, vol. 55, no. 2, pp. 433–444, 2003.

[106] C. D. Dermer and A. Atoyan, "Ultra-high energy cosmic rays, cascade gamma rays, and high-energy neutrinos from gamma-ray bursts," *New Journal of Physics*, vol. 8, article 122, 2006.

[107] K. Asano and S. Inoue, "Prompt GeV-TeV emission of gamma-ray bursts due to high-energy protons, muons, and electron-positron pairs," *The Astrophysical Journal*, vol. 671, no. 1, pp. 645–655, 2007.

[108] N. Gupta and B. Zhang, "Prompt emission of high-energy photons from gamma ray bursts," *Monthly Notices of the Royal Astronomical Society*, vol. 380, no. 1, pp. 78–92, 2007.

[109] A. A. Abdo, M. Ackermann, M. Ajello et al., "A limit on the variation of the speed of light arising from quantum gravity effects," *Nature*, vol. 462, pp. 331–334, 2009.

[110] A. A. Abdo, M. Ackermann, M. Ajello et al., "*FERMI* observations of GRB 090902B: a distinct spectral component in the prompt and delayed emission," *The Astrophysical Journal*, vol. 706, no. 1, article L138, 2009.

[111] M. Ackermann, K. Asano, W. B. Atwood et al., "Fermi observations of GRB 090510: a short hard gamma-ray burst with an additional, hard power-law component from 10 keV to GeV energies," *The Astrophysical Journal*, vol. 716, no. 2, pp. 1178–1190, 2010.

[112] M. Ackermann, M. Ajello, K. Asano et al., "Detection of a spectral break in the extra hard component of GRB 090926A," *The Astrophysical Journal*, vol. 729, no. 2, p. 114, 2011.

[113] K. Toma, X.-F. Wu, and P. Mészáros, "An up-scattered cocoon emission model of gamma-ray burst high-energy lags," *The Astrophysical Journal*, vol. 707, no. 2, article 1404, 2009.

[114] K. Toma, X.-F. Wu, and P. Mészáros, "Photosphere-internal shock model of gamma-ray bursts: case studies of Fermi/LAT bursts," *Monthly Notices of the Royal Astronomical Society*, vol. 415, no. 2, pp. 1663–1680, 2011.

[115] A. Corsi, D. Guetta, and L. Piro, "GeV emission from short gamma-ray bursts: the case of GRB 081024B," *Astronomy and Astrophysics*, vol. 524, no. 4, article 92, 2010.

[116] K. Asano and P. Mészáros, "Spectral–temporal simulations of internal dissipation models of gamma-ray bursts," *The Astrophysical Journal*, vol. 739, no. 2, p. 103, 2011.

[117] A. M. Beloborodov, R. Hascoët, and I. Vurm, "On the origin of GeV emission in gamma-ray bursts," *The Astrophysical Journal*, vol. 788, no. 1, article 36, 2014.

[118] G. Ghisellini, G. Ghirlanda, L. Nava1, and A. Celotti, "GeV emission from gamma-ray bursts: a radiative fireball?" *Monthly Notices of the Royal Astronomical Society*, vol. 403, no. 2, pp. 926–937, 2010.

[119] P. Kumar and R. Barniol Duran, "External forward shock origin of high-energy emission for three gamma-ray bursts detected by *Fermi*," *Monthly Notices of the Royal Astronomical Society*, vol. 409, no. 1, pp. 226–236, 2010.

[120] K. Murase, K. Toma, R. Yamazaki, S. Nagataki, and K. Ioka, "High-energy emission as a test of the prior emission model for gamma-ray burst afterglows," *Monthly Notices of the Royal Astronomical Society: Letters*, vol. 402, no. 1, pp. L54–L58, 2010.

[121] K. Asano, S. Guiriec, and P. Mészros, "Hadronic models for the extra spectral component in the short GRB 090510," *Astrophysical Journal Letters*, vol. 705, no. 2, pp. L191–L194, 2009.

[122] K. Asano, S. Inoue, and P. Mészáros, "Prompt X-ray and optical excess emission due to hadronic cascades in gamma-ray bursts," *Astrophysical Journal Letters*, vol. 725, no. 2, pp. L121–L125, 2010.

[123] S. Razzaque, C. D. Dermer, and J. D. Finke, "Synchrotron radiation from ultra-high energy protons and the fermi observations of GRB 080916C," *The Open Astronomy Journal*, vol. 3, pp. 150–155, 2010.

[124] K. Asano, S. Inoue, and P. Mészáros, "Prompt high-energy emission from proton-dominated gamma-ray bursts," *The Astrophysical Journal*, vol. 699, no. 2, article 953, 2009.

[125] P. Beniamini, D. Guetta, E. Nakar, and T. Piran, "Limits on the GeV emission from gamma-ray bursts," *Monthly Notices of the Royal Astronomical Society*, vol. 416, no. 4, pp. 3089–3097, 2011.

[126] M. Ackermann, M. Ajello, L. Baldini et al., "Constraining the high-energy emission from gamma-ray bursts with Fermi," *The Astrophysical Journal*, vol. 754, no. 2, article 121, 2012.

[127] L. Yacobi, D. Guetta, and E. Behar, "Constraints on the hadronic content of gamma ray bursts," *The Astrophysical Journal*, vol. 793, no. 1, p. 48, 2014.

[128] K. Asano and T. Terasawa, "Slow heating model of gamma-ray burst: photon spectrum and delayed emission," *Astrophysical Journal Letters*, vol. 705, no. 2, pp. 1714–1720, 2009.

[129] K. Murase, K. Asano, T. Terasawa, and P. Mészáros, "The role of stochastic acceleration in the prompt emission of gamma-ray bursts: application to hadronic injection," *The Astrophysical Journal*, vol. 746, no. 2, article 164, 2012.

[130] M. Petropoulou, S. Dimitrakoudis, A. Mastichiadis, and D. Giannios, "Hadronic supercriticality as a trigger for γ-ray burst emission," *Monthly Notices of the Royal Astronomical Society*, vol. 444, no. 3, pp. 2186–2199, 2014.

[131] P. Mészáros and M. J. Rees, "Steep slopes and preferred breaks in gamma-ray burst spectra: the role of photospheres and comptonization," *Astrophysical Journal Letters*, vol. 530, no. 1, pp. 292–298, 2000.

[132] D. Giannios, "Prompt emission spectra from the photosphere of a GRB," *Astronomy & Astrophysics*, vol. 457, no. 3, pp. 763–770, 2006.

[133] A. Pe'er, P. Mészáros, and M. J. Rees, "The observable effects of a photospheric component on GRB and XRF prompt emission spectrum," *The Astrophysical Journal*, vol. 642, no. 2, p. 995, 2006.

[134] K. Ioka, K. Murase, K. Toma, S. Nagataki, and T. Nakamura, "Unstable GRB photospheres and $e^{\pm}$ annihilation lines," *The Astrophysical Journal*, vol. 670, no. 2, pp. L77–L80, 2007.

[135] D. Lazzati and M. C. Begelman, "Non-thermal emission from the photospheres of gamma-ray burst outflows. I. high-frequency tails," *The Astrophysical Journal Letters*, vol. 725, no. 1, pp. 1137–1145, 2010.

[136] K. Murase, "Prompt high-energy neutrinos from gamma-ray bursts in photospheric and synchrotron self-Compton scenarios," *Physical Review D*, vol. 78, no. 10, Article ID 101302, 5 pages, 2008.

[137] X.-Y. Wang and Z.-G. Dai, "Prompt TeV neutrinos from the dissipative photospheres of gamma-ray bursts," *The Astrophysical Journal Letters*, vol. 691, p. L67, 2009.

[138] S. Gao, K. Asano, and P. Mészáros, "High energy neutrinos from dissipative photospheric models of gamma ray bursts," *Journal of Cosmology and Astroparticle Physics*, vol. 2012, no. 11, article 58, 2012.

[139] B. Zhang and P. Kumar, "Model-dependent high-energy neutrino flux from gamma-ray bursts," *Physical Review Letters*, vol. 110, no. 12, Article ID 121101, 5 pages, 2013.

[140] K. Asano and P. Mészáros, "Delayed onset of high-energy emissions in leptonic and hadronic models of gamma-ray bursts," *The Astrophysical Journal*, vol. 757, no. 2, p. 115, 2012.

[141] K. Murase, K. Ioka, S. Nagataki, and T. Nakamura, "High-energy neutrinos and cosmic rays from low-luminosity gamma-ray bursts?" *The Astrophysical Journal Letters*, vol. 651, no. 1, p. L5, 2006.

[142] A. M. Soderberg, S. R. Kulkarni, E. Nakar et al., "Relativistic ejecta from X-ray flash XRF 060218 and the rate of cosmic explosions," *Nature*, vol. 442, no. 7106, pp. 1014–1017, 2006.

[143] K. Toma, K. Ioka, T. Sakamoto, and T. Nakamura, "Low-luminosity GRB 060218: a collapsar jet from a neutron star, leaving a magnetar as a remnant?" *Astrophysical Journal*, vol. 659, no. 2 I, pp. 1420–1430, 2007.

[144] E. Liang, B. Zhang, F. Virgili, and Z. G. Dai, "Low-luminosity gamma-ray bursts as a unique population: luminosity function, local rate, and beaming factor," *The Astrophysical Journal*, vol. 662, no. 2, pp. 1111–1118, 2007.

[145] N. Gupta and B. Zhang, "Neutrino spectra from low and high luminosity populations of gamma ray bursts," *Astroparticle Physics*, vol. 27, no. 5, pp. 386–391, 2007.

[146] R.-Y. Liu, X.-Y. Wang, and Z.-G. Dai, "Nearby low-luminosity gamma-ray bursts as the sources of ultra-high-energy cosmic rays revisited," *Monthly Notices of the Royal Astronomical Society*, vol. 418, no. 2, pp. 1382–1391, 2011.

[147] A. M. Soderberg, S. Chakraborti, G. Pignata et al., "A relativistic type Ibc supernova without a detected γ-ray burst," *Nature*, vol. 463, no. 7280, pp. 513–515, 2010.

[148] N. Smith, S. B. Cenko, N. Butler et al., "SN 2010jp (PTF10aaxi): a jet in a type II supernova," *Monthly Notices of the Royal Astronomical Society*, vol. 420, no. 2, pp. 1135–1144, 2012.

[149] X.-Y. Wang, S. Razzaque, P. Mészáros, and Z.-G. Dai, "High-energy cosmic rays and neutrinos from semirelativistic hypernovae," *Physical Review D*, vol. 76, Article ID 083009, 2007.

[150] J. Kakuwa, K. Murase, K. Toma, S. Inoue, R. Yamazaki, and K. Ioka, "Prospects for detecting gamma-ray bursts at very high energies with the Cherenkov Telescope Array," *Monthly Notices of the Royal Astronomical Society*, vol. 425, no. 1, pp. 514–526, 2012.

[151] S. Inoue, J. Granot, P. T. O'Brien et al., "Gamma-ray burst science in the era of the Cherenkov telescope array," *Astroparticle Physics*, vol. 43, pp. 252–275, 2012.

[152] C. D. Dermer, "Neutrino, neutron, and cosmic-ray production in the external shock model of gamma-ray bursts," *Astrophysical Journal Letters*, vol. 574, no. 1, pp. 65–87, 2002.

[153] Z. G. Dai and T. Lu, "Neutrino afterglows and progenitors of gamma-ray bursts," *The Astrophysical Journal*, vol. 551, no. 1, article 249, 2001.

[154] S. Razzaque, "Long-lived PeV-EeV neutrinos from gamma-ray burst blastwave," *Physical Review D*, vol. 88, no. 10, Article ID 103003, 11 pages, 2013.

[155] L. Sironi, A. Spitkovsky, and J. Arons, "The maximum energy of accelerated particles in relativistic collisionless shocks," *The Astrophysical Journal*, vol. 771, no. 1, article 54, 2013.

[156] E. Waxman and J. N. Bahcall, "Neutrino afterglow from gamma-ray bursts: $\sim 10^{18}$ eV," *Astrophysical Journal Letters*, vol. 541, article 707, 2000.

[157] X.-Y. Wang, Z. Li, and P. Mészáros, "GeV-TeV and X-ray flares from gamma-ray bursts," *The Astrophysical Journal*, vol. 641, pp. L89–L92, 2006.

[158] K. Murase and S. Nagataki, "High energy neutrino flashes from far-ultraviolet and X-ray flares in gamma-ray bursts," *Physical Review Letters*, vol. 97, Article ID 051101, 2006.